University of Nevada, Reno

Igneous Geology of the Keystone Window, Simpson Park Mountains, Eureka County, Nevada:

Age, Distribution, Composition, and Relationship to Carlin-style Gold Mineralization

A thesis submitted in partial fulfillment of the

requirements for the degree of Master of Science in

Geology

by

Gabriel E. Aliaga

Dr. Michael W. Ressel/Thesis Advisor

December 2018

THE GRADUATE SCHOOL

We recommend that the thesis
prepared under our supervision by

GABRIEL E. ALIAGA

Entitled

**Igneous Geology Of The Keystone Window, Simpson Park Mountains,
Eureka County, Nevada: Age, Distribution, Composition,
And Relationship To Carlin-Style Gold Mineralization**

be accepted in partial fulfillment of the
requirements for the degree of

MASTER OF SCIENCE

Michael W. Ressel, Ph.D., Advisor

Philipp Ruprecht, Ph.D., Committee Member

Dhanesh Chandra, Ph.D., Graduate School Representative

David W. Zeh, Ph.D., Dean, Graduate School

December, 2018

Abstract

Keystone is an early-stage gold exploration project operated by U.S. Gold Corp. located in the northern Simpson Park Mountains, in the Battle Mountain-Eureka mineral belt of north-central Nevada. Dating of ore-stage minerals and cross-cutting relationships between mineralization and dikes elsewhere in Nevada shows that most Carlin-type gold deposits (CTDs) formed over a short interval in the Eocene (~42-35 Ma), coeval with a distinct pulse of arc magmatism that supplied heat and permissively, metals for CTDs. The on-trend location of Keystone, 25 km south of the giant Cortez Hills and Goldrush CTDs, together with widespread alteration of a domed lower plate structural window in the Roberts Mountains allochthon (RMA) that is cored by an Eocene intermediate pluton, make it ideal for the study of proximal to distal styles of Eocene mineralization, including CTDs. U-Pb zircon and $^{40}Ar/^{39}Ar$ dating in conjunction with mapping of igneous rocks and alteration provide constraints on the timing and style of magmatism and mineralization.

A major normal fault along Keystone's west flank tilted units moderately east, exposing a 2 km thick crustal section that includes Eocene volcanic rocks, the RMA, lower plate carbonates, and abundant intrusions. Eocene igneous rocks comprise the 4.1 km^2 intermediate composite Walti pluton, which domed surrounding wall rocks, and abundant porphyritic, intermediate to silicic stocks, dikes, lavas, and tuffs. All Eocene rocks are shoshonitic to high-K calc-alkaline, metaluminous to weakly peraluminous, and were emplaced from ~36-34.5 Ma. A ~25 km^2 magnetic anomaly coincides with the Walti pluton and indicates much larger intrusions at depth. The anomaly is of similar size to the magnetic anomaly associated with the Eocene Bullion intrusion (22 km^2) in the southern Carlin trend and the Copper Canyon stock (11 km^2), which is associated with the Phoenix-Fortitude gold skarns. Trace-element geochemistry, petrography, crosscutting relations, and isotopic dating of Eocene igneous rocks at Keystone support a complex magmatic evolution with likely varied sources. Older andesite of McClusky Creek, Mud Springs diorite and Gund diorite are interpreted as a separate magmatic system from the later Walti granodiorite to diorite intrusion and its related rocks.

The composition and timing of igneous rocks at Keystone are consistent with the last stages of mid-Cenozoic, dominantly intermediate composition magmatism in northeast Nevada, which was active

from ~44 to 34 Ma and migrated rapidly southwestward. This Eocene magmatism was characterized by shallow intrusion and mostly effusive volcanism. After ~34 Ma and generally at or immediately south of Keystone, magmatism became dominantly silicic and pyroclastic, part of the Oligocene ignimbrite flare-up of central Nevada (e.g. the nearby ~34 Ma Caetano and Hall Creek calderas). The change in style and composition of mid-Cenozoic magmatism at this latitude coincides with a change in the distribution of Eocene Carlin-type gold deposits from major deposits (+5 Moz contained Au) to the north, to relatively smaller deposits to the south. Whether the change in the magnitude of Carlin-type gold mineralization is directly or indirectly related to changes in mid-Cenozoic magmatism is uncertain and an area of future research.

$^{40}Ar/^{39}Ar$ dating of biotite from an alkaline basalt in the Valmy Formation yielded a plateau age of 466.1±0.7 Ma, which is Middle Ordovician. This age is consistent with biostratigraphic ages from conodonts and radiolaria at Keystone. Alkaline mafic rocks at Keystone solely occur in the Ordovician Valmy and Cambrian-Ordovician Comus formations as sills, volcanogenic debris flows, and pillows, typically intercalated with limestone. These rocks, in addition to unusual mineralogy, have distinctive and unusually high concentrations of both compatible and incompatible trace elements consistent with ocean island basalts (OIB) and unlike depleted mid-ocean ridge basalts (MORB) or arc-related basalts. OIBs likely reflect intraplate or hotspot-related magmatism that developed as a series of seamounts during deposition of rocks of the Valmy and Comus formations and which were later tectonically transported eastward to the Keystone area during Late Devonian/Early Mississippian Antler thrusting. The age, lithologic, and geochemical similarities of these rocks to the Comus Formation in the Osgood Mountains is permissive for their correlation and is particularly important, since the Comus is the principal host unit in the Getchell trend Carlin-type gold deposits.

U-Pb zircon dating of conglomerate resting on Paleozoic rocks of the RMA yielded a maximum depositional age of 35.62±0.32 Ma. Conglomeratic rocks elsewhere are commonly correlated with the Paleozoic Antler overlap sequence based on the abundance of RMA-derived chert and quartzite clasts. The recognition of this Eocene conglomerate is important not only for regional mapping but also for understanding the development of Eocene basins, some of which are hydrocarbon-bearing, and for

characterizing the switch from late Cretaceous Sevier contraction to an early Cenozoic extensional regime. The basal Eocene conglomerate is the oldest exposed Cenozoic unit at Keystone and is used to constrain the Eocene paleosurface and estimate the depth that Eocene intrusions were emplaced and that mineralization occurred.

Hydrothermal activity at Keystone was constrained by field relations and $^{40}Ar/^{39}Ar$ of illite in altered igneous rocks. The Walti pluton is associated with proximal Pb-Zn-Cu skarn, at the site of the historic Keystone mine. Distal epithermal and Carlin-style mineralization occurs outboard of hornfels halos in overlying and adjacent strata. Drilling by U.S. Gold Corp. commonly intercepted mineralized breccia and jasperoid at the Paleozoic upper- to lower-plate transition, and argillized dikes adjacent to decarbonatized Paleozoic lower-plate carbonate rocks, both of which contain strongly anomalous gold and high concentrations of As, Sb, Hg, Bi, W, Se, and/or Tl. Illite from two samples of altered andesite dikes of McClusky Creek did not yield $^{40}Ar/^{39}Ar$ plateaus but nonetheless produced geologically reasonable weighted mean ages of 35.71±0.12 Ma and 35.54±0.06 Ma, which are slightly younger than the ~35.99 to 35.85 Ma $^{40}Ar/^{39}Ar$ igneous hornblende ages. Thus, the illite ages from the altered andesite dikes are considered the best approximate for the age of Carlin-type gold mineralization in the northeastern area of Keystone. A rhyolite porphyry intrusion exhibited the most sericitic and argillic alteration after the altered dikes, and $^{40}Ar/^{39}Ar$ dating of sanidine from the unaltered core of the rhyolite yielded an age of 35.43±0.06 Ma. This rhyolite porphyry is possibly the youngest intrusion at Keystone, and is preferentially altered over adjacent intrusions. This suggests the rhyolite intruded an extensional structure that also controlled hydrothermal fluids. Abundant quartz porphyry rhyolite dikes at the nearby Cortez Hills CTD have been interpreted as syn-mineralization because they are altered and locally mineralized; these pre-Caetano caldera dikes are of similar age and composition to the rhyolite porphyry at Keystone.

Acknowledgements

I would first like to sincerely thank Dr. Mike Ressel who gave me my shot at changing careers. I was living and working in Chicago, IL, heading down a path of clinical laboratory management and FDA regulation. I knew in my heart I wanted to instead be a geologist, to be outdoors, to study the Earth, to make maps! I chose economic geology so I could learn applicable skills and contribute to an exciting industry. I'm happy and grateful that Mike chose me. Thank you for your guidance, patience, and your trust.

I thank my committee members Dr. Philipp Ruprecht and Dr. Dhanesh Chandra for their incredible patience and willingness to meet during their summers. This project was a bit of a scramble to get started and I am appreciative of your time.

Several thanks to the people who helped with the extensive geochronology this thesis required. Chris Henry and Dr. Matt Heizler, for your time and assistance with my $^{40}Ar/^{39}Ar$ mineral separation, analysis, and interpretation. It was a pleasure to visit New Mexico Tech and I am grateful for the invitation, Chris. Dr. Stacia Gordon, who saved me from nearly panicking when the bureau's lab needed maintenance. Thank you for generously offering your zircon separation lab and your time. And thanks to the scientists at University of Arizona's Laserchron Center. I did not know a lab visit could be that streamlined and luxurious, and I have always recommended it to others thereafter.

I am incredibly grateful to Dave Mathewson and U.S. Gold Corp., who have provided financial support and data for this thesis. Many thanks to Dave and the rest of the geologists, Tom Chapin, Brion Theriault, Ken Coleman, and Neil Whitmer, who demonstrated the excitement of exploration. Tom Chapin was a phenomenal mentor and I really wish I could have spent more days with you in the field to learn from your expertise.

Thank you, Dr. John Muntean and students of the CREG program, for always making me feel welcome even though I wasn't technically "one of you"! Moving into the CREG office no doubt saved me from becoming a hermit as I finished my thesis. It has been a blast being part of SEG and seeing Finland and Japan with you guys, and I look forward to working with you all in the future. Thank you, Heather

Winslow and Michelle Dunn for your friendship since the first day I came to Reno and for loving my dog Terra! Special thanks to Elizabeth Hollingsworth for being an awesome officemate, an incredibly knowledgeable scientist who always answered my questions, and a great friend.

I thank my family for their love and support. It wasn't that long ago when I doubted applying to school and my sister Yana *yelled* at me to just go for it and how of course I'll succeed, and I thank her for the encouragement. Thank you, mom, for letting me follow my dreams. Thank you, Naseem, for loving me, marrying me, and following me all the way to Nevada so I could look at rocks. It is a change neither of us expected, and I can't wait for the many more surprises the future holds for us. You are the best and you are my favorite person.

Table of Contents

List of Tables

List of Figures

List of Plates

Introduction

Carlin-type gold deposits of Nevada

Gold constituted 84% of Nevada's mineral and energy production in 2016, with 5.47 million ounces (Moz) produced in that year amounting to $6.84 billion (Muntean et al., 2017). In 2014, Nevada alone accounted for 5.5% of world production of gold. Much of this gold is produced from sediment-hosted gold deposits known as Carlin-type gold deposits (CTD). Several >5 Moz Au CTDs occur in linear trends in Nevada, and collectively CTDs are estimated to have pre-mining reserves of over 200 Moz Au (Cline et al., 2005; Sillitoe, 2010). The Carlin trend of northern Nevada alone accounts for 1.5% of all the gold ever mined in the world. CTDs are sought by major mining companies for their large endowments and for the size and shape of orebodies that make bulk-mining methods feasible. Extensive research into CTDs since the Carlin deposit discovery in 1961 have clarified their depositional controls, hydrothermal processes, and age. However, a widely accepted genetic model explaining the source of heat, fluids, and metals, has yet to emerge.

Unoxidized Carlin-type gold ore is characterized by disseminated Au-bearing pyrite, arsenian pyrite, and/or arsenopyrite, typically in carbonate or partly calcareous host rocks. Ore-stage hydrothermal fluids were acidic and relatively low temperature (180-240°C), low salinity (≤6 wt% NaCl equiv), and weakly CO_2- and H_2S-bearing (Bakken, 1990; Kuehn and Rose, 1992; Cline and Hofstra, 2000). Fluids decarbonatized carbonate host rocks, commonly intense enough to produce collapse breccias, and argillize igneous rocks where encountered. The distribution of alteration commonly follows structures and zones of inherent permeability such as bedding, but decarbonatization of host carbonate rocks by fluids significantly enhanced porosity and permeability, producing orebodies with a variety of asymmetrical shapes and sizes. Where argillized, wall rocks contain assemblages of kaolinite, dickite, and/or illite. Silicification accompanied other late-stage alteration and commonly converted decarbonatized carbonate rocks to jasperoid. Deposition of Au was likely by sulfidation of Fe in the host rocks: Au-sulfide complexes in the fluid were destabilized as sulfur reacted with Fe^{2+} to form pyrite, resulting in incorporation of Au and other trace metals in the pyrite as micrometer-size grains or as rims on pre-existing pyrite. These trace metals and

semi-metals include As, Hg, Cu, Sb, Tl, and Te (Longo et al., 2009b). CTDs often have orpiment, realgar, and stibnite as late-stage minerals, which contain little to no Au.

One important aspect of CTD genesis is the widely agreed age of these deposits. Most or all CTDs in Nevada formed during the Eocene, from 42 to 34 Ma (Groff et al., 1997; Hofstra et al., 1999; Hall et al., 2000; Tretbar et al., 2000; Ressel et al., 2000a, b; Hollingsworth et al., 2017). Research has yet to definitively show what caused the regional hydrothermal events, although hydrothermal activity was coincident in time and space with a southwestward sweep of magmatism through Nevada immediately prior to the ignimbrite flareup of southwestern North America (Henry and Ressel, 2000). Despite the conspicuous timing of mineralization, many important structural controls on the distribution, style, and grade of CTDs were established in the Paleozoic and Mesozoic (e.g., Teal and Jackson, 1997; Rhys et al., 2015).

Nevada Geology - Paleozoic

The oldest widely exposed rocks of north-central Nevada are marine sedimentary rocks that were deposited along the western passive margin of Laurentia, beginning in the Late Proterozoic after the rifting of Rodinia (Dickinson, 2006; Cook, 2015). Shales and sandstones were initially deposited across Utah and Nevada until the middle Cambrian, when carbonate depositional environments were established. In Nevada, the broad Paleozoic depositional environments or domains are the continental shelf, slope, and basin (Crafford, 2008). The shallow water carbonate shelf and reef deposits of eastern Nevada transition to silty and muddy carbonate slope deposits and debris flows of north-central Nevada, and are historically termed the eastern assemblage. Siliceous and siliciclastic deposits of the deep ocean basin distal to the continental margin are termed the western assemblage. These styles of deposition continued through the Late Devonian with intermittent sea level rise and fall (Cook and Corboy, 2004), which resulted in E-W oscillation of major facies through the middle Paleozoic.

In the Late Devonian to Early Mississippian, passive margin carbonate deposition was interrupted by the Antler orogeny (Roberts et al., 1958; Crafford, 2008). The Antler orogenic highlands, originally described in the Roberts Mountains (Roberts et al., 1958), stretched north-south, approximately coincident

with the slope-basin interface. Chert and other siliceous, primarily Paleozoic basinal sedimentary rocks including shale to sandstone were eroded and redeposited in basins to the east and west of the highlands during the Mississippian and Pennsylvanian. Thin-skinned Antler thrusting is interpreted to have formed the Antler orogenic highlands, originally described in the Roberts Mountains (Roberts et al., 1958). Many locations in north-central Nevada expose Late Devonian slope-facies rocks (herein termed lower plate) structurally beneath Cambrian through late Devonian basinal- and lesser slope-facies rocks, the latter comprising the Roberts Mountains allochthon (herein termed the RMA, or also the "upper plate"; Ketner, 2013). The RMA stratigraphy is relatively complex due to imbricated thrust sheets containing deformed rocks, varied sources of sediments including the western continental margin rifted from Rodinia and locally, the Comus carbonate-basalt sequence (Cook, 2015; Linde et al., 2017)

By Late Mississippian to Permian, the passive margin architecture was partly reestablished and short-lived shelf deposition resumed in eastern Nevada. However, investigations have shown that some Antler eastward thrusting continued into the late Pennsylvanian and even early Permian (Trexler et al., 2004; Arney, 2013; Holm-Denoma et al., 2017), although others (e.g. Ketner and Alpha, 1992) counter that some of this deformation postdates Triassic rocks. The manner of Antler thrusting and origin of the RMA are still debated, and new mapping and geochronology permit alternate tectonic models (Linde et al., 2016; Linde et al., 2017).

Carbonate slope-facies rocks commonly host major Carlin-type deposits (Cline et al., 2005 and references therein). Rocks are typically thin- to medium-bedded, carbonaceous, pyritic, silty limestone and limestone breccia or conglomerate, which have high initial porosity. These host rocks are commonly interpreted to have resulted from gravity-driven flow from the slope topography, i.e., turbidite flow. Rheologic and hydrologic contrasts between these lower-plate slope-facies carbonates and overlying tectonically emplaced, upper-plate siliciclastic rocks as well as overprinting Mesozoic folds and thrusts, are important controls for Carlin-type gold deposits (Rhys et al., 2015). The tops of most giant Carlin-type deposits lie within about 100 m vertically of major thrust faults most commonly interpreted as Antler faults. Siliceous allochthonous rocks that overlie host carbonates may have formed a non-reactive, much less

permeable layer that impeded upward flow of hydrothermal fluids, thus promoting mineralization in the underlying carbonates (Cline et al., 2005 and references therein).

Nevada Geology - Eocene

Subduction of the Farallon plate beneath the North America plate is widely thought to be responsible for Jurassic to Cretaceous arc magmatism over a broad area of the Cordillera, including the Great Basin and the Sierra Nevada batholith. Post-Sierra Nevada batholith crustal shortening associated with flat-slab subduction in the late Cretaceous to Paleocene likely contributed to thrusting far inboard of the continental margin during the Sevier orogeny (Dickinson, 2006), the low-angle of subduction eventually shutting off arc magmatism entirely from about 80 to 44 Ma at the latitude of the Great Basin. By the Eocene, the Farallon slab, perhaps cooler and less buoyant, may have started to sink, in the process removing or delaminating lithospheric mantle from the crust (Humphreys, 1995). Delamination and slab roll back is thought to have resulted in widespread and voluminous potassium-rich arc-type magmatism in the Eocene as the Farallon slab began to steepen to the southwest (Humphreys, 1995). Magmatism started in southern British Columbia around 55 Ma, rapidly migrated into eastern Washington, Idaho, and western Montana from about 53-43 Ma, then reached northernmost Nevada and Utah by about 44 Ma (Christiansen and Yeats, 1992; Henry, 2008). Curiously, the wave of Eocene magmatism was broadly coeval with a tectonic change from compression to extension that occurred in the Paleogene in northern Nevada. This tectonic transition approximately coincided with the start of metamorphic core complex exhumation and with lacustrine deposition of the Eocene Elko Formation and similar units, which were deposited in paleovalleys and small basins (Henry 2008; Cassel et al., 2014; Smith et al., 2017). Eventually, voluminous arc magmatism at~44 Ma in the north and ~38 Ma at the latitude of Carlin, Nevada, inundated early sedimentary basins with volcanic and volcaniclastic rocks. Abundant calc-alkalic, mostly intermediate lavas and domes and associated plutons and batholiths, and a few ash-flow-forming rhyolitic calderas formed in northern Nevada from 42 to 34 Ma, over the same time and space that CTDs formed (Figure 1; Henry and Ressel, 2001; Ressel and Henry, 2006). Magmatism continued to track southward into central Nevada. By 34 or 33 Ma, magmatism became dominantly silicic and pyroclastic, thus defining the major pulse of caldera volcanism in the Great Basin and other regions of southwest North America called the

ignimbrite flare-up, which lasted until ~19 Ma and migrated from central Nevada to west-central and southwest Nevada. (Henry and John, 2013).

The relationship between giant Carlin-type gold deposits and arc magmatism, mid-Cenozoic extension, and lacustrine basin development is uncertain, although there is a curious temporal and spatial tie between all processes. Altered Eocene felsic dikes are encountered in many CTDs and have been used to constrain the timing of both magmatism, and alteration and gold mineralization of CTDs (Ressel and Henry, 2006). Although larger Eocene intrusions such as stocks do not occur within major CTDs, mapping of spatially related Eocene igneous centers and aeromagnetic data support the existence of large composite plutons or batholiths at greater modern depths between ~3 and 10 km. Eocene intrusions have been cited as potential sources of doming and related structures that controlled hydrothermal fluids (Mathewson, 2001). The 33.9 Ma Caetano tuff, adjacent to the Cortez district and only 19 km northwest of the thesis study area, erupted from a caldera-forming magma chamber that measured ~300 km^2 at a depth of 8-10 km (John et al., 2008). The Cortez Hills CTD, located on the east margin of the Caetano caldera, contains abundant rhyolite quartz porphyry dikes associated with the late stages of Carlin-type gold mineralization that have $^{40}Ar/^{39}Ar$ ages of about 35.46 ± 0.05 Ma (Arbonies et al., 2011; Colgan et al., 2011). These and other relatively tight age relationships have stimulated research into the role of Eocene magmatism for Carlin-type hydrothermal systems and suggest magma bodies at ~10 km provided heat, and possibly fluid, and/or metals (Henry and Boden, 1998; Ressel et al., 2000a, b; Henry and Ressel, 2001; Muntean et al., 2011). Extensional structures active during the Eocene likely played a role for Carlin-type mineralization, but Eocene near-surface expression of extension was relatively minor compared to major extension that postdates Eocene-Oligocene magmatism (Henry et al., 2001; Cline et al., 2005 and references therein; Colgan and Henry, 2009).
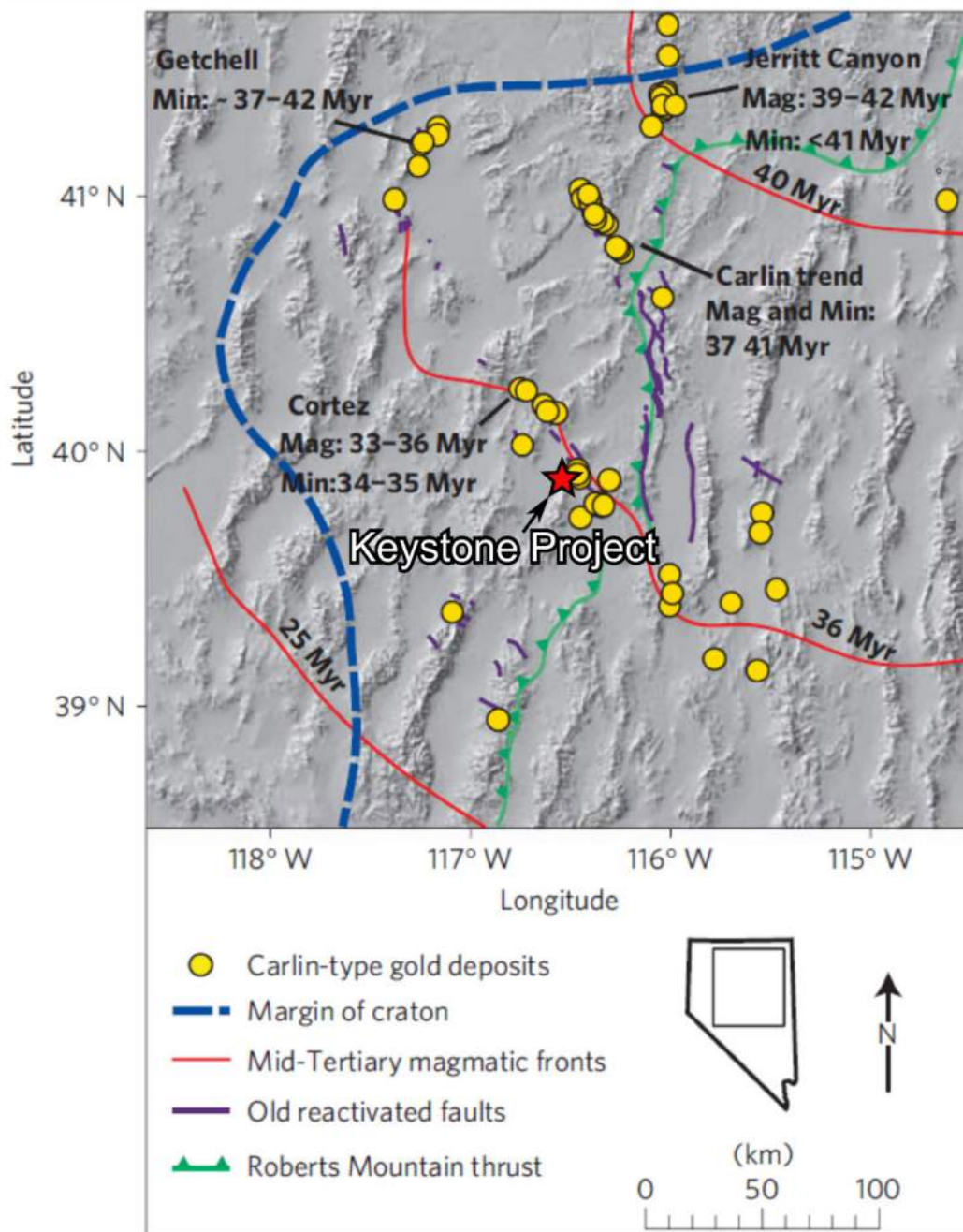
Figure 1. Locations of Carlin-type gold deposits and their estimated age of mineralization (Min) and age of associated magmatism (Mag). The dashed blue line represents the craton margin based on Sr isotopes, which controlled passive margin deposition from the Late Proterozoic through Early Mississippian. The red lines mark the limits of the advancing magmatic arc at indicated times. Purple lines mark old reactivated fault systems. Green line marks the easternmost extent of the Roberts Mountains allochthon during the Late Devonian-Early Mississippian Antler orogeny. Red star marks location of Keystone. Modified from Muntean et al. (2011). Age data for magmatism and mineralization are: Getchell (Groff et al., 1997; Hall et al., 2000; Tretbar et al., 2003), Jerritt Canyon (Hofstra et al., 1999), Carlin (Ressel et al., 2000a, b; Ressel and Henry, 2006), and Cortez (Colgan et al., 2011; Arbonies et al., 2011).

Keystone Project

The Keystone project is an early-stage gold exploration project operated by U.S. Gold Corp. and is located in northern Simpson Park Mountains, in the Battle Mountain-Eureka mineral belt of north-central Nevada (Figure 2). No mineral resources currently exist at Keystone, but the historic Keystone mine in the Roberts mining district was periodically exploited for base metals in skarn from its discovery in 1870 until 1962 (Roberts et al., 1967). Mineralization at Keystone occurred along the contact of the Walti granodiorite intrusion and metasomatized Devonian carbonates of the Keystone window; reported primary ore minerals include sphalerite, galena, chalcopyrite, and pyrite.

Keystone has many features relevant to CTDs. It exposes lower-plate carbonate strata in the Keystone window (Plate 1), which is surrounded by allochthonous, or upper-plate, chert, siltstone, sandstone, basalt, and mudstone. In addition, the Keystone window and immediately flanking area are cored by four Eocene intermediate to silicic stocks (Walti, Mud Springs, Gund, and rhyolite porphyry) and numerous sills and dikes emanate from them; coeval andesite through rhyolite lavas are widespread and flank intrusions. Hydrothermal alteration commonly associated with Carlin-type deposits, including decarbonatization of limestone, and silicification and argillization of siliciclastic rocks, are recorded in surface exposures and drill core. Although no gold resource currently exists at Keystone, nearby sedimentary rock-hosted gold deposits include those at Tonkin Springs, Gold Bar, and Cortez (Figure 2), which are from 5 km to 20 km away. The on-trend location of Keystone, 25 km south of the giant Cortez Hills and Goldrush CTDs of the Cortez district, make it ideal for the study of proximal to distal styles of Eocene mineralization. Characterization of wall rock alteration and igneous rocks, including their age, composition, and depth of emplacement, serve as the basis to explore the relationship between Eocene magmatism and CTDs.

Few publications on the geology of Keystone exist beyond regional mapping (Roberts et al., 1967). Biotite from the Walti pluton gave a K-Ar age of 34.2±0.7 Ma (Silberman and McKee, 1971; recalculated to decay constants and isotopic abundances of Steiger and Jäger (1977)). The nearest studies were focused on stratigraphy and structures of either the northern Simpson Park Mountains (Johnson, 1959;

McKee and Conrad, 1994; Arney, 2013) or of the Roberts Mountains (McKee, 1986; McKee et al., 1986; Fair, 2012; Arney, 2013; Finney et al., 2015). Publications on the nearby Tonkin Springs and Gold Bar districts include Mehrtens (1987), Espell and Rich (1991), and Yigit et al. (2006), respectively. This thesis is therefore the first detailed geologic study at Keystone and most of it focuses on mapping and characterization of Keystone's igneous rocks and their age relationships to hydrothermal alteration and mineralization. Detailed stratigraphy and structural geology are beyond the scope of this thesis. It is the author's hope that future work at the Keystone window will be aided by the context and timing of Eocene magmatism this thesis provides.
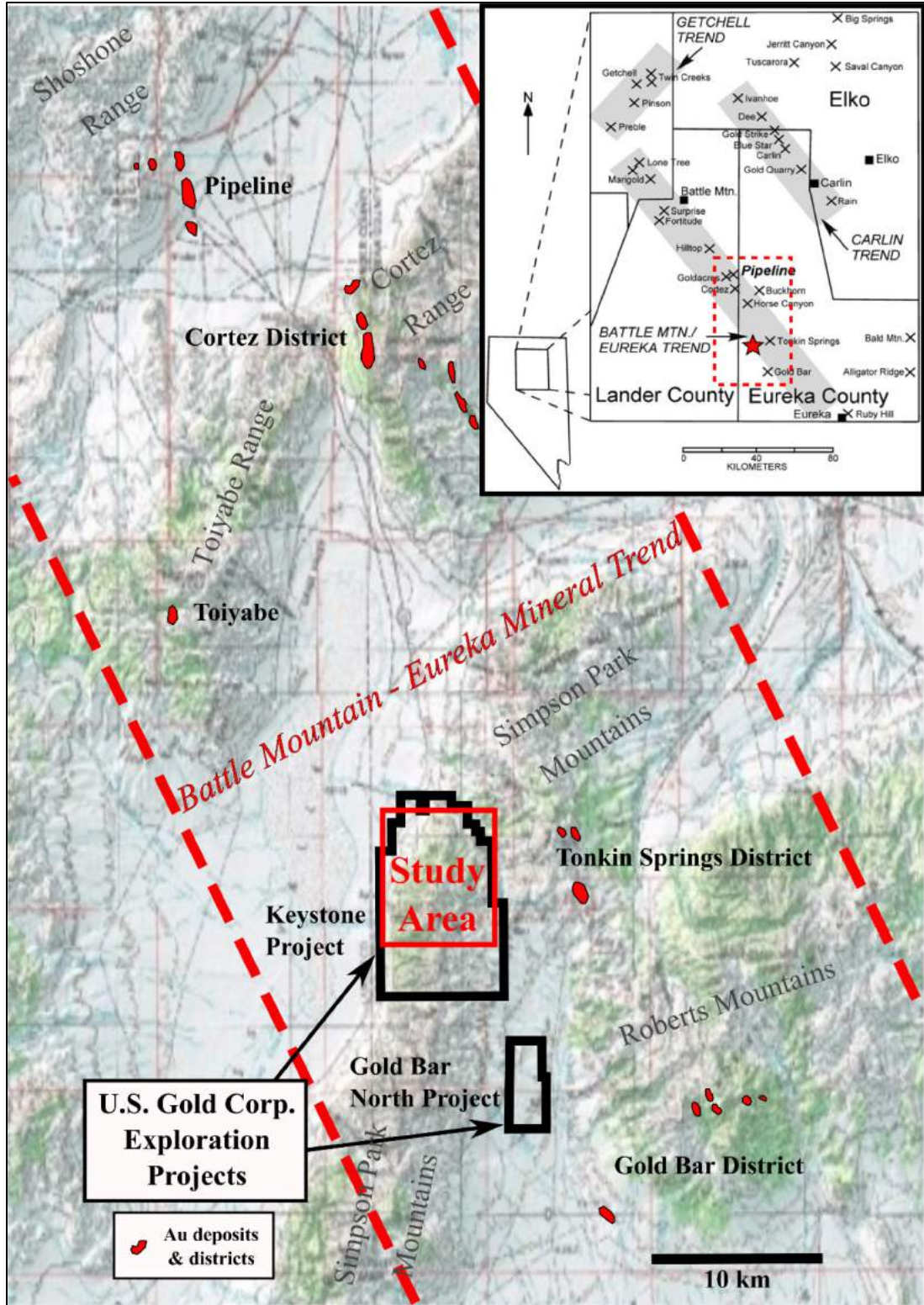
Figure 2. Location map of the Keystone project and this study area with nearby gold deposits (red polygons) and districts. Inset shows location within Nevada and within the Battle Mountain-Eureka trend. Red star in the inset figure marks Keystone.

Methods

Field Methods

Field work was conducted by the author in the summers of 2017 and 2018 and incorporated detailed outcrop-style mapping at 1:2000- and 1:5000-scale on paper using a detailed NAIP color photo base; mapping focused on igneous lithologies and hydrothermal alteration. Geology was later digitized in ArcGIS from Esri. Detailed mapping and stratigraphy by U.S Gold Corp. geologist Thomas Chapin supported final map products of this thesis, as have published maps by Roberts et al. (1967). Aeromagnetic, resistivity, and gravity survey data provided by U.S. Gold Corp. also supported the final map product.

Sampling

For this study, 143 rock-chip samples were collected from outcrops and from drill core provided by U.S. Gold Corp. Igneous rocks with the least amount of alteration as well as those possessing different alteration assemblages were sampled and later analyzed for geochemistry and petrography. Sampling was also undertaken to assess a sample's appropriateness for isotopic dating; criteria for dating included the importance of a given map unit and/or its alteration in addressing questions of magmatism and mineralization. Potassium-bearing igneous minerals such as hornblende, biotite, sanidine, and plagioclase were sought for $^{40}Ar/^{39}Ar$ analyses, whereas zircon was appropriate for acquiring igneous ages in highly altered igneous rocks using U/Pb methods. Dating of K-bearing clays, particularly illite, was accomplished by sampling pervasive alteration of feldspar in altered and/or mineralized dikes.

Petrography

Rock samples were sawed at the University of Nevada, Reno (UNR) and slabs were sent to Wagner Petrographic in Lyndon, Utah for thin-section preparation. A total of 114 30-μm-thick standard and polished thin sections were made. Thin sections were inspected by petrographic microscope under transmitted and reflected light, and by scanning electron microscope (SEM) at UNR, under secondary electron and backscatter electron (BSE) imaging modes using a JEOL JSM-6010LA instrument. The JEOL SEM is equipped with an energy-dispersive X-ray spectrometer (EDS), which is useful for the semi-

quantitative determination of elements. Plagioclase compositions were determined semi-quantitatively by SEM-EDS, and by the Michel-Levy and Carlsbad-albite method using the petrographic microscope.

Geochemistry

Fresh and slightly weathered samples were coarse-crushed using jaw and cone crushers at UNR to gravel-sized fractions, hand-picked for chips having only fresh surfaces, and then sent to ALS Global for major- and trace-element analysis using the ME-MS81 package. The samples were pulped, then fused in a resistance furnace using a lithium borate flux. The resultant glass beads were then completely dissolved in a 4-acid digestion and analyzed using ICP-AES and ICP-MS. Sulfur and carbon were determined using Leco analysis, and fire assay using an aqua regia digestion was used for gold determinations. Additional ICP and fire-assay data from rock chip, stream sediment, soil, and drill core samples were provided by U.S. Gold Corp. Geochemical interpretations and plots were assembled with ioGAS from REFLEX.

U-Pb Zircon Dating

Whole-rock samples were crushed using a jaw crusher and disk mill, rinsed in water, dried, and sieved to below 100-mesh at UNR. A non-magnetic fraction was then separated from the sample using a Frantz Isodynamic Magnetic Separator (side slope 15°, tilt 25°, 1.7 amperes). Zircons were separated from the non-magnetic fraction using methylene iodide as a high-density liquid. After final rinsing in acetone, zircon separates were sent to the Arizona Laserchron Center (ALC) in Tucson, AZ for mounting, imaging, and analysis.

Cathodoluminescence (SEM-CL) images were taken of the mounted zircons to examine growth zonation and verify locations of spot analyses. Zircons were analyzed by laser ablation inductively coupled plasma mass spectrometry (LA-ICP-MS), using a Teledyne Analyte G2 Excimer laser attached to a Thermo Fisher Scientific Element2 ICP-MS. Laser spot sizes were set to 20µm diameter. Zircon standards used during analysis included FC-1 from the Duluth gabbro complex (1099.5±1.9 Ma), SL-Mix from Sri Lanka (563.2±4.8 Ma), and R-33 from the Ecstall pluton from the Coast Range, of British Columbia. (419.3±0.4 Ma) (Pullen et al., 2018; for further details on analytical procedures refer to ALC's website (https://sites.google.com/a/laserchron.org/laserchron).

^{40}Ar/^{39}Ar Dating

Thin sections were reviewed for viable K-bearing minerals for igneous crystallization and alteration dating. Rock samples were crushed and sieved to fractions between 20-60 and 60-80 standard mesh at the University of Nevada, Reno. Both magnetic and non-magnetic fractions were then separated from the sample using a Frantz Model LB-1 Isodynamic magnetic separator. Biotite and hornblende were handpicked from magnetic fractions. Potassium feldspars were separated from the non-magnetic fraction using deionized water-diluted lithium metatungstate as a high-density liquid, and handpicked from the float fraction. Plagioclase crystals were handpicked from the sink fraction. Mineral separates had a final rinsing in acetone. Samples with pervasively sericitized feldspar phenocrysts were selected for ^{40}Ar/^{39}Ar illite dating of the hydrothermal event. Selected samples were analyzed by short-wave infrared spectroscopy (SWIR) using the ASD Terraspec to differentiate white clay minerals such as kaolinite and illite. Thin sections of selected samples were also reviewed to evaluate the crystallinity and size of illite grains and to verify there was no remnant feldspar. Altered phenocryst sites were plucked directly from the hand sample without crushing. Mineral separates were sent to the New Mexico Geochronology Research Laboratory in Socorro, NM, for irradiation and ^{40}Ar/^{39}Ar analysis.

Local Geology

Paleozoic allochthonous rocks of the basin domain

Mapping by Thomas Chapin and supporting biostratigraphy and basalt geochemistry identified Upper Cambrian-Early Ordovician Comus Formation, Ordovician Valmy Formation, Silurian Elder Sandstone, and Devonian Slaven Chert comprising the Roberts Mountains allochthon at Keystone (Figure 3; T. Chapin, 2017, unpublished report for U.S. Gold Corp.; P. Zippi, 2016-2018, unpublished reports for U.S. Gold Corp.). These upper-plate rocks cover over 15 km^2 within the study area (Plate 1). The lens-shaped north-northeast trending Keystone lower-plate window through the upper plate exposes the underlying younger Early Silurian through Late Devonian lower-plate carbonate rocks. Ordovician Valmy comprises most of the upper plate and overlies upper-plate Comus as well as lower-plate Late Devonian Horse Canyon and Wenban formations along the margins of the window. Biostratigraphy shows upper-plate rocks decrease in age from Late Cambrian to Silurian south and southeastward, and to Late Devonian beyond the study area. (Figure 3; Table 1; P. Zippi, 2016-2018, unpublished reports for U.S. Gold Corp.).

Cambrian-Ordovician Comus Formation (COc)

In the northeastern part of the study area are outcrops of dark silty limestone with mudstone and intercalated alkalic greenstone debris flows and mafic sills (Plate 1). Dating of conodonts returned ages of latest Cambrian or Ibexian to Early Ordovician or lowest Whiterockian (Table 1). Both the lithology and age identify these rocks as equivalent to the Late Cambrian Comus Formation, described in the Osgood Mountains 150 km north-northwest of Keystone and along the Getchell mineral trend (Hotz and Willden, 1964; Breit et al., 2005; Cook, 2015).
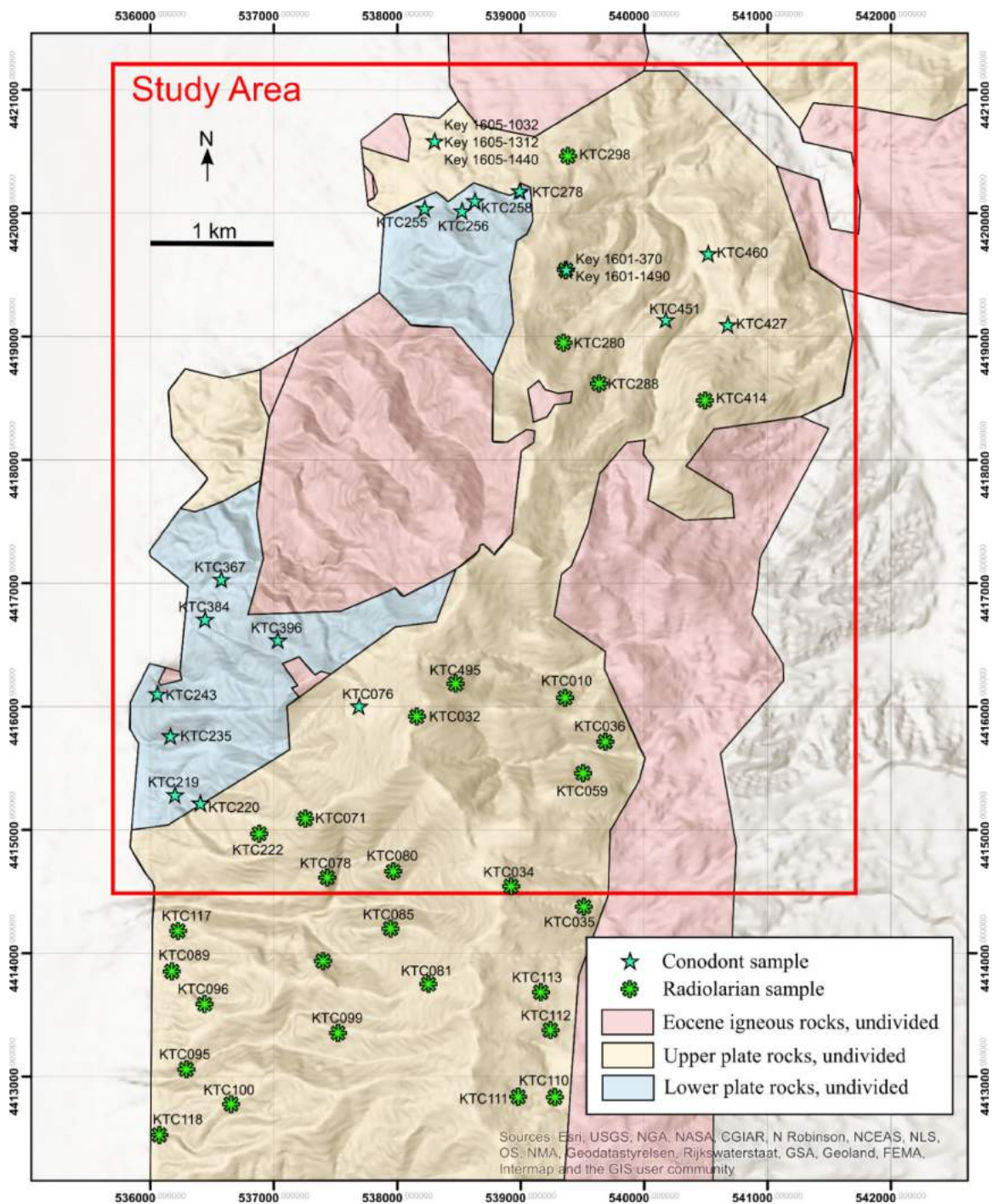
Figure 3. Generalized geologic map showing locations of samples collected by Tom Chapin and submitted for conodont and radiolaria analysis. Biostratigraphy results are summarized in Table 1.

Table 1. Summary of conodont and radiolaria fossil ages from limestone and chert strata. From P. Zippi, 2016-2018, unpublished reports for U.S. Gold Corp. Locations shown in Figure 3.

Sample ID	UTM NAD27 North	UTM NAD27 East	Sample type	Fossil Type	Age Period	Age Epoch/Stage	Formation	Tectonic plate
Key 1601-1490	4419541	539367	drill core @1490'	cono	early Late Devonian	Early Frasnian	Wenban	Lower
Key 1601-370	4419541	539367	drill core @370'	rad	Late Ordovician	Katian	Valmy	Upper
Key 1605-1032	4420589	538304	drill core @1032'	cono	early Late Devonian	Frasnian	Wenban	Lower
Key 1605-1312	4420589	538304	drill core @1312'	cono	Early Ordovician	Late Ibexian	Comus	Upper
Key 1605-1440	4420589	538304	drill core @1440'	cono	Early Ordovician	Late Ibexian	Comus	Upper
KTC010	4416073	539365	Outcrop	rad	Late Ordovician to Late Silurian	n/a	Cherry Spring	Upper
KTC032	4415919	538156	Outcrop	rad	Late Ordovician to Early Silurian	Katian to Wenlock	Cherry Spring	Upper
KTC034	4414542	538922	Outcrop	rad	late Early Silurian	late Llandovery Early Wenlock	Cherry Spring	Upper
KTC035	4414379	539514	Outcrop	rad	late Early Silurian	late Llandovery Early Wenlock	Cherry Spring	Upper
KTC036	4415711	539688	Outcrop	rad	Late Ordovician to Early Silurian	Katian to Wenlock	Cherry Spring	Upper
KTC059	4415463	539503	Outcrop	rad	Early Silurian	late Llandovery Early Wenlock	Cherry Spring	Upper
KTC071	4415094	537256	Outcrop	rad	Late Ordovician to Early Silurian	Katian to mid-Wenlock	Cherry Spring	Upper
KTC076	4416004	537690	Outcrop	cono	Middle Ordovician to Silurian	n/a	Valmy	Upper
KTC078	4414611	537433	Outcrop	rad	Early Silurian	late Llandovery to Early Wenlock	Cherry Spring	Upper
KTC080	4414668	537969	Outcrop	rad	Late Ordovician to Early Silurian	Katian to late-Wenlock	Cherry Spring	Upper
KTC081	4413745	538255	Outcrop	rad	Early Silurian	mid-Llandovery	Cherry Spring	Upper
KTC085	4414202	537949	Outcrop	rad	Early Devonian or younger	n/a	Slaven	Upper
KTC089	4413853	536175	Outcrop	rad	Early Devonian or younger	n/a	Slaven	Upper
KTC095	4413059	536288	Outcrop	rad	Late Devonian	Frasnian	Slaven	Upper
KTC096	4413587	536436	Outcrop	rad	Early Devonian or younger	n/a	Slaven	Upper
KTC099	4413353	537521	Outcrop	rad	Early Devonian or younger	n/a	Slaven	Upper
KTC100	4412775	536654	Outcrop	rad	Late Devonian	Frasnian	Slaven	Upper
KTC110	4412850	539272	Outcrop	rad	Late Devonian	Middle Famennian	Slaven	Upper
KTC111	4412851	538979	Outcrop	rad	Late Devonian	Middle Famennian	Slaven	Upper
KTC112	4413393	539232	Outcrop	rad	Late Devonian	Middle Famennian	Slaven	Upper
KTC113	4413693	539136	Outcrop	rad	Late Devonian	Middle Famennian?	Slaven	Upper
KTC116	4413946	537392	Outcrop	rad	Late Devonian to Early Carboniferous	n/a	Slaven	Upper
KTC117	4414188	536225	Outcrop	rad	Silurian to Early Carboniferous	n/a	Slaven	Upper
KTC118	4412537	536073	Outcrop	rad	Late Devonian to Early Carboniferous	n/a	Slaven	Upper
KTC122	4420478	540545	Outcrop	cono	Late Devonian to Early Carboniferous	Emsian	Slaven	Lower
KTC219	4415284	536198	Outcrop	cono	Early Devonian	late Frasnian	Wenban	Lower
KTC220	4415222	536407	Outcrop	cono	Late Devonian	late Darriwilian to Katian	Horse Canyon	Lower
KTC222	4414972	536881	Outcrop	rad	Middle to Late Ordovician	latest Lochkovian to Pragian	Valmy	Upper
KTC235	4415758	536165	Outcrop	cono	Early Devonian	late Lochkovian	Wenban	Lower
KTC243	4416102	536057	Outcrop	cono	Early Devonian	Early Frasnian	Wenban	Lower
KTC255	4420042	538222	Outcrop	cono	early Late Devonian	Middle Frasnian	Wenban	Lower
KTC256	4420017	538524	Outcrop	cono	early Late Devonian	n/a	Wenban	Lower
KTC258	4420101	538631	Outcrop	cono	Silurian-Devonian	n/a	Wenban	Lower
KTC278	4420172	539003	Outcrop	cono	Devonian?	n/a	Horse Canyon	Lower
KTC280	4418950	539348	Outcrop	rad	Late Ordovician	Katian	Valmy	Upper
KTC288	4418622	539635	Outcrop	rad	Late Ordovician	Katian	Valmy	Upper

Sample ID	UTM NAD27		Sample type	Fossil Type	Age		Formation	Tectonic plate
	North	East			Period	Epoch/Stage		
KTC298	4420467	539384	Outcrop	rad	Late Ordovician	Katian	Valmy	Upper
KTC367	4417026	536578	Outcrop	cono	Devonian	n/a	Wenban	Lower
KTC384	4416702	536446	Outcrop	cono	Devonian	n/a	Wenban	Lower
KTC396	4416534	537036	Outcrop	cono	Devonian	n/a	Wenban	Lower
KTC414	4418486	540495	Outcrop	rad	Late Ordovician	Katian/Hirnantian	Valmy	Upper
KTC427	4419092	540682	Outcrop	cono	Latest Cambrian	IX, Cambrian	Comus	Upper
KTC451	4419139	540180	Outcrop	cono	Early to Middle Ordovician	upper Ibexian to lowest Whiterockian	Comus	Upper
KTC460	4419674	540526	Outcrop	cono	Latest Cambrian	Latest Cambrian	Comus	Upper
KTC495	4416185	538475	Outcrop	rad+cono	Early Silurian	mid-Llandovery	Cherry Spring	Upper

Although the Comus was originally described in the Battle Mountain district by Ferguson et al. (1952) and Roberts (1951) in the Golconda and Antler Peak quadrangles, respectively, there have been revisions to its age and lithology since (Roberts, 1964; Hotz and Willden, 1964; Cook, 2015). Along the east side of the Osgood Mountains, the Comus is predominantly alternating dolomite, limestone, and shale, with lesser chert, siltstone, and tuffaceous material. Contrasting with the structurally overlying Valmy, sandstone and quartzite are rare or absent in the Comus. Twin Creeks is a +16 Moz Au CTD in the Getchell trend east of the Osgood Mountains, and its main hosts are carbonate rocks of the Comus Formation. As described at Twin Creeks, the Comus is a distal slope to basinal plain facies unit composed of laminated and thin-bedded black shale, siltstone, and silty carbonate rocks with basaltic debris flows and abundant mafic and ultramafic alkalic sills (Breit et al., 2005). Bloomstein et al. (1991) provided a depositional model of the Comus Formation involving a Late Cambrian to Early Ordovician carbonate-capped seamount that evolved on an isolated structural block following the Late Proterozoic rifting of Rodinia. Carbonate debris flows, turbidites, and fine-grained black carbonate ooze were transported westward from the seamount, whereas siliciclastic mudstones and siltstones were transported eastward from a subaerial island arc(?) source to the west of the seamount. Isolated submarine volcanism associated with the seamount accounts for the local abundance of mafic sills and basalts, as well as their alkalic composition, which is similar to ocean island basalts or intraplate basalts and contrasts with the depleted chemical character of mid-ocean ridge basalts. Geochemistry and composition of Comus mafic rocks at Keystone is discussed in greater detail on page 78.

Drill holes at Keystone have intercepted 150 to 300 m thickness of mixed greenstone and limestone underlying siliciclastic sedimentary rocks of the Ordovician Valmy Formation, with contacts between the two units described as faulted. At Twin Creeks and regionally, the Comus is interpreted as autochthonous or parautochthonous, with the overlying, highly deformed Valmy rocks transported from farther west via a low-angle thrust fault, possibly during the Late Mississippian Antler orogeny (Hotz and Willden, 1964; Breit et al., 2005). The presence and proximity of underlying, younger lower plate and therefore, autochthonous, Devonian carbonate rocks at Keystone indicate that the Comus rocks at Keystone did not form in situ but were instead transported some distance, likely during the Antler orogeny.

Occurrences of the Comus Formation have not yet been described in the Simpson Park Mountains or nearby ranges, but it is possible similar lithologies of the appropriate age received different nomenclature. Only 5 km east of Keystone is the Tonkin Springs mining district, which features numerous small gold deposits with typical Carlin-type gold alteration and mineral assemblages. One of the hosts at Tonkin Springs is the Cambrian-Ordovician Hales Formation comprised of sandy limestones, calcareous siltstones, shales, mafic tuffs, mafic sills, and minor chert (Alan Noble, 2008, Technical Report on the Tonkin Project, prepared for the former US Gold Corporation, now McEwen Mining, and different from the U.S. Gold Corp. that sponsored this project); http://s21.q4cdn.com/390685383/files/doc_downloads/governance/reserves-and-resources/technical-report.pdf). The Hales at Tonkin Springs was noted to be a time-equivalent to the Comus at Twin Creeks and was mapped as autochthonous, with rocks of the Ordovician Vinini Formation thrusted above it.

Ordovician Valmy Formation (Ov)

The Ordovician Valmy Formation was first described at North Peak in the Antler Peak quadrangle of the Battle Mountain district, 90 km northwest of Keystone (Roberts, 1964) and subsequently many other localities in northern Nevada including the Cortez Mountains north of Keystone. The Valmy comprises a substantial part of the Roberts Mountains allochthon (Roberts, 1964; Gilluly and Masursky, 1965; Madrid, 1987). Indeed, the Valmy makes up most of the upper plate outcrops in the study area. Lithologies of the Valmy at Keystone are heterogeneous and include calcareous mudstone locally intercalated with greenstone, but the unit is dominated by mudstone, siltstone, and sandy siltstone, bedded chert, and quartzite.

Lithologically, the Ordovician Vinini Formation is similar to the Valmy and is mapped in the Roberts Mountains to the east of Keystone as well as the Cortez Mountains to the north. The two units have been interpreted as lateral and/or transitional equivalents, the Vinini having more carbonate and shale, and the Valmy more quartzite and greenstone (Gilluly and Masursky, 1965; Madrid, 1987). Visits to the type locality at Vinini Creek in the Roberts Mountains by the author and U.S. Gold Corp. geologists support the presence of more Valmy-like upper-plate lithologies at Keystone.

Detailed mapping at Keystone (T. Chapin, 2017, unpublished report for U.S. Gold Corp.) divided the Valmy Formation into three informal subunits. The lower Valmy member is an Early to Middle Ordovician unit about 60 m thick that rests conformably on the Late Cambrian to Early Ordovician Comus Formation, and is dominated by well-sorted and well-rounded quartz grains in quartzite and yellow sandstone. The middle Valmy is about 180 m thick and is from Late Darriwilian to Katian (Middle to Late Ordovician) and comprises a submarine fan delta sequence with sandstone, siltstone, mudstone, chert, and minor pillow basalt and hyaloclastite. The upper Valmy is about 90 m thick and consists of polymict siltstone with minor chert and continues into the Early Silurian. At the top of the Valmy is the Cherry Spring Chert from Llandovery to early Wenlock (Early to Middle Silurian) comprised of thick chert beds that may have a distinctive strong green color (Table 1).

Valmy rocks generally dip 30-50 degrees to the east in the eastern half of the study area, with topography less than but generally reflecting this eastward dip (Plate 1). To the north and west of the Walti pluton, beds are either flat or dip gently north and west. Such opposing dips form a dome around the Keystone window and Walti pluton that was subsequently tilted east by young normal faults on the west flank of the range. Alkalic mafic sills and greenstone of the Valmy are similar to those of the Comus and form a semi-continuous trend along the southeast margin of the window. Contact metamorphism surrounding the Walti pluton caused hornfels metamorphism and makes differentiating siltstone, mudstone, and chert difficult. Chaotic folding and displacement of chert beds along minor faults occur along the eastern margin of the Walti pluton (Figure 4), whereas Valmy rocks to the west of the pluton are not affected by strong deformation and recrystallization. Hydrothermal alteration and mineralization of upper plate rocks are widespread throughout the Keystone property; alteration includes bleaching, brecciation, silicification, and local gossan of red-yellow limonite after primary sulfides.

Figure 4. Photo of chaotically folded chert beds of the Valmy Formation east of the Walti pluton. Hammer is 28 cm long.

Valmy Quartzite in the Mud Springs Pluton (Ovq)

Resting on top of the Mud Springs pluton in the east-central part of the study are isolated 100-1000 m^2 outcrops of marble (ODul) and quartzite (Ovq) (Plate 1) that appear conspicuously out of place. Quartzite outcrops are contained entirely within the Mud Springs pluton. These outcrops are interpreted as stoped blocks of upper plate rocks incorporated during the rise and emplacement of the magma that formed the Mud Springs pluton. The quartzite closely resembles quartzite of the Valmy, with nearly 100% coarse (1-2mm) sub-rounded interlocking quartz grains.

Basalts of the Valmy and Comus (Ovb and COcb)

Several outcrops of mafic sills, pillow basalts, and greenstones are found in the upper plate rocks in both the Comus and Valmy formations (Plate 1). The mafic rocks partly follow specific stratigraphic horizons, most notably along the southern contact of the Keystone window (Figure 5). Outcrops are relatively isolated and discontinuous, typically spanning <50 m. Compositions range from basalt to mafic/ultramafic picrite containing abundant olivine. Basalts were not found cutting any other igneous units nor lower-plate carbonates.

Textures in basalts range from fine-grained to very fine-grained hypidiomorphic equigranular to seriate (Figure 6). Porphyritic textures with an aphanitic or glassy matrix were not observed, although this may be due to pervasive weathering and/or alteration to clay that obscure original textures in some cases. The most common primary mineral assemblage includes elongate plagioclase, olivine altered to iddingsite or serpentine minerals, acicular apatite, ilmenite, magnetite, and interestingly, biotite (Figure 7). Biotite is locally so abundant that the rock shimmers black. In one sample, hornblende was also observed. Calcite is commonly present, and the basalts commonly occur either next to or even intercalated with very dark micritic limestone; the Comus at Twin Creeks similarly has basalts associated with limestone. The basalt commonly displays breccia or hyaloclastite textures and associated round cm-size pillow-like forms. The presence of biotite in mafic and ultramafic rocks is unusual and indicates alkaline compositions such as those associated with ocean-island basalts (OIBs).

Outcrops of basalt near the eastern margin of the Walti pluton are hornfels altered and superficially resemble a pale-green to gray fine-grained quartzite to silicified limestone. In spite of alteration, identification of these outcrops is possible using lithogeochemistry, discussed later.

Figure 5. Oblique 3D view to the east from the Keystone lower-plate window generated in ArcGlobe. Valmy basalts (Ovb) comprise discontinuous outcrops that follow stratigraphic horizons within the Valmy Formation (Ov). The Gund diorite (Tgd) is a lopolith-shaped intrusion that is roofed by Late Devonian Horse Canyon (Dhc) just below the Roberts Mountains allochthon.

Figure 6. Representative micrographs and photographs of basalts of the Valmy (Ovb). Textures are generally seriate and fine grained, and minerals are generally altered to serpentine, chlorite, and calcite. A) Micrograph of sample KS024 in cross-polarized light. B) Photograph of sample KS024. C) Micrograph of sample KS063 in cross-polarized light. D) Photograph of sample KS063. E) Micrograph of sample KS143 in cross-polarized light. F) Photograph of sample KS143.
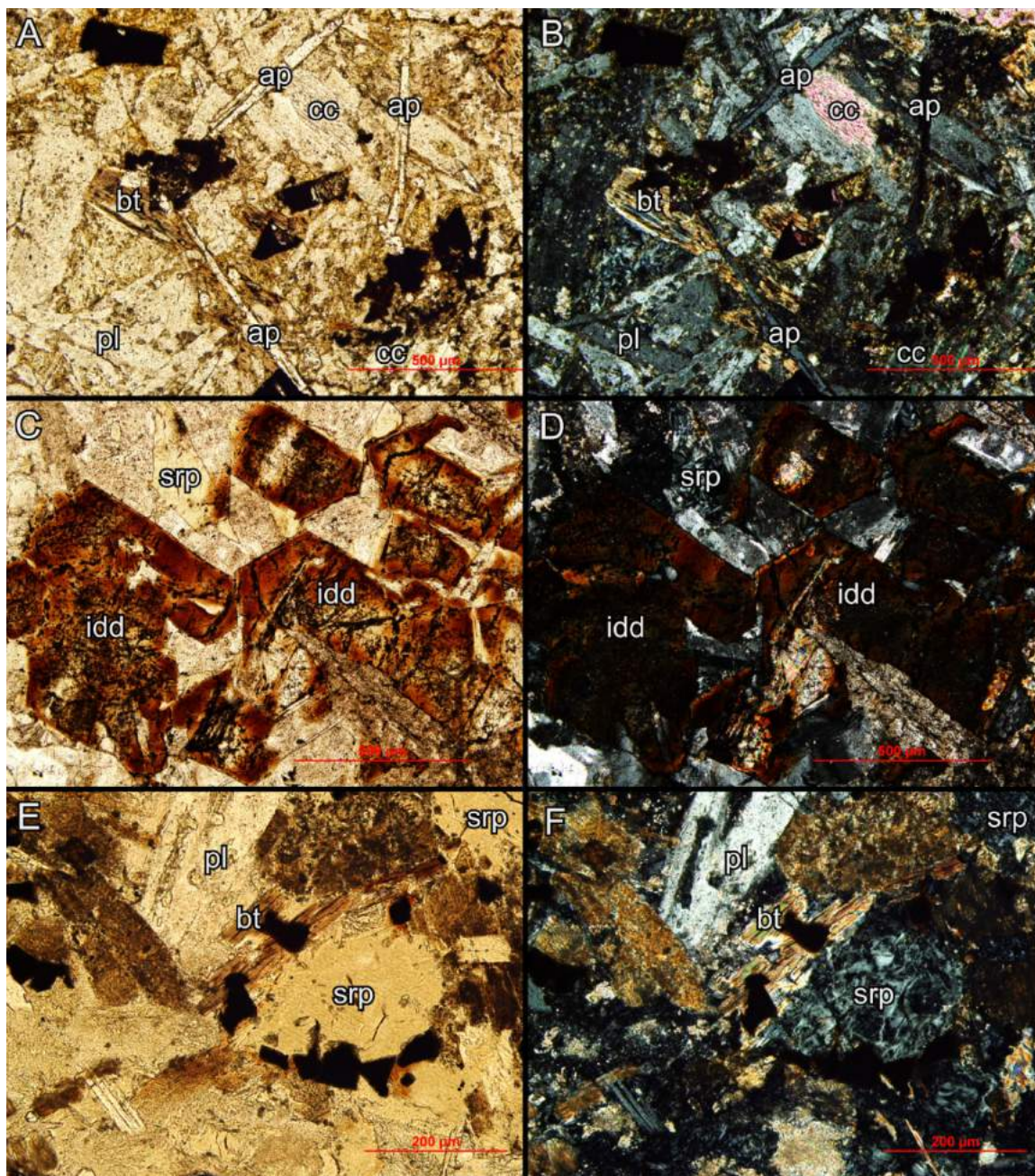
Figure 7. Representative micrographs of basalts of the Valmy Formation, in plane- and cross-polarized light. A-B) Sample KS024 showing acicular apatite and biotite in a groundmass of plagioclase with calcite. C-D) Sample KS063 showing olivine altered to iddingsite, a mixture of clay and iron oxides. E-F) Sample KS143 showing biotite and olivine altered to serpentine minerals in a clay-altered groundmass. Abbreviations: ap=apatite, bt=biotite, pl=plagioclase, cc=calcite, srp=serpentine, idd=iddingsite.

Silurian Elder Sandstone (Se)

Resting on the Valmy to the south of the Keystone window is the Silurian Elder Sandstone, an age supported by underlying cherts containing Llandovery to early Wenlock radiolaria (Table 1). The Elder Sandstone is part of the Roberts Mountains allochthon and is mapped in the Cortez Mountains to the north and at the Robert Mountains to the east (Gilluly and Masursky, 1965; Finney et al., 2000). Regionally, the Elder is quartz-rich but also contains local arkosic and micaceous yellow-brown sandstone and siltstone that grades into chert and argillite. At Keystone, the Elder is about 60 m thick and is a yellow quartz sandstone with minor feldspar grains and some white mica, with scattered calcareous beds.

The Lower Silurian Cherry Spring Chert is commonly used as a distinctive regional marker unit due its deep green color and phosphatic nodules (Holm-Denoma et al., 2011). At Keystone however the Silurian chert underlying the Elder is discontinuous and may or may not have a green color. The Cherry Spring Chert has therefore not been differentiated from the Valmy Formation. The Elder occurs on a topographic high where it rests on Valmy in the southern part of the study area (Plate 1).

Paleozoic autochthonous rocks of the slope domain

Silurian-Early Devonian Roberts Mountains Formation (Srm)

The Roberts Mountains Formation of Silurian to Early Devonian age was first described by Merriam (1940) at its type locality in the Roberts Mountains 20 km to the east of Keystone. This unit was also described by Gilluly and Masursky (1965) in the Cortez Mountains 25 km to the north of Keystone. Merriam and McKee (1976) provide a detailed review of the variety and extent of the Roberts Mountains Formation, including another occurrence on the northern slopes of the Simpson Park Mountains at Coal Canyon, only 17 km north-northeast of Keystone. The Roberts Mountains is considered a transition between the western assemblage siliciclastic sedimentary rocks and contemporaneous eastern assemblage dolomitic shelf rocks. It has similarities to the Elder Sandstone to the west but with a higher clastic calcite component, forming a north-south slope-to-basin facies limestone belt that extends over 500 km (Gilluly and Masursky, 1965; Merriam and McKee, 1976; Cook and Corboy, 2004).

At Keystone, the Roberts Mountains Formation is found on the west side of the range in the southwestern part of the lower plate window (Plate 1). It crops out as a band about 700 meters long, striking east-northeast and dipping 30 degrees southeast. Its upper 60 meters is well exposed and has a gradational contact with the base of the Wenban Formation. Conodont fossil dating of the overlying lowermost Wenban returned an Early Devonian, Late Lockhovian age (Table 1). This date agrees with the upper part of the Roberts Mountains encompassing the Silurian-Devonian boundary (Merriam and McKee, 1976). In the southwest part of the study area, the Late Devonian Horse Canyon unit and the western extension of the Gund stock are found below the Roberts Mountains Formation, and therefore an obvious fault relationship. The low-angle trace of the contact between the Horse Canyon and Roberts Mountains, in conjunction with parallel bedding, indicate a thrust fault caused the juxtaposition. Rocks of the Roberts Mountains Formation are truncated to the northeast by the same thrust fault, which continues northeast and juxtaposes rocks of the Horse Canyon unit beneath limestone of the Wenban Formation. To the southwest the Roberts Mountains Formation is buried by Quaternary alluvium.

A sill related to the Gund stock intrudes the thrust fault described above, and metamorphosed the surrounding wall rock, including silty limestone of the overlying Roberts Mountains Formation. The Roberts Mountains here is bleached to white marble, but retains plane laminar bedding, typically 2-10 mm thick, and altered phosphate lenses. Away from the Gund sill and towards its upper contact with the Wenban, the Roberts Mountains Formation is typically composed of platy, dark gray silty limestone with common black phosphate lenses.

Wenban Formation

The Wenban Formation, first described by Gilluly and Masursky (1965), includes limestone of Early, Middle, and Late Devonian age, and is age correlative with parts of the Nevada Formation, Guilmette Limestone, and Devils Gate Limestone. Its type locality is at Wenban Peak in the Cortez Mountains, 25 km north of Keystone. Other formations such as the Denay, McColley, and Popovich are also partly correlative with the Wenban. As such, the Wenban has been subdivided into 8 units (Cook and Corboy, 2004; Jackson et al., 2010). Although it also represents a slope facies, the Wenban contains proportionally more carbonate and bioclastic material than the underlying Roberts Mountains Formation,

suggesting its relative proximity to the Devonian-Silurian platform margin to the east (Cook and Corboy, 2004).

Detailed mapping (T. Chapin, 2017, unpublished report for U.S. Gold Corp.) identified all 8 informal units of the Wenban described for nearby Cortez (Jackson et al. 2010) at Keystone. At Keystone, the Wenban is approximately 730 m thick, which includes its unfaulted lower and upper contacts. Conodont fossil ages of the Wenban at Keystone span the Devonian from Late Lockhovian to Middle Frasnian (Table 1). The Wenban has a debris flow boundary with the underlying Roberts Mountains, mapped in the southwestern part of the Keystone window. The nature of the upper Wenban contact with the Horse Canyon unit is uncertain because of later faulting and folding, but it is likely an erosional contact, as it appears to be at least at the Cortez mine (Jackson et al., 2010). Mapping at Keystone suggests the presence of both erosional and fault contacts for the Wenban. The Wenban comprises most of the surface exposures of the 4 km^2 lower-plate Keystone window; the Horse Canyon is exposed along the window's perimeter and lesser parts of the interior (Plate 1) and the Roberts Mountains Formation occupies a small area in the southwest corner of the window. Bedding attitudes are strongly affected by intrusions, and bedding generally dips away from the Walti pluton creating a dome shape. Outcrops farthest from the Walti in the southern part of the window dip 20-30 degrees to the southeast.

Lithologies of the Wenban Formation are diverse across its members. It is most commonly a dark- to medium-gray thick- to thin-bedded carbonaceous silty micrite. Bioturbation textures, bioclastic debris flows, and soft-sediment slumps, are more prominent in certain subunits by varying degrees. Proximal to the Walti pluton and Gund stock, the Wenban is contact metamorphosed to marble, skarnoid (metamorphism of impure limestone), and skarn (metamorphism and metasomatism by magmatic-hydrothermal fluids). Marbled Wenban is commonly white with light-gray wavy foliations, and has a sugary to medium-grained crystalline texture. Skarnoid in Wenban is typically fine-grained and composed of forest green diopside and/or amber-colored fine-grained garnet. Base-metal skarn mineralization occurs in the historic Keystone mine (Figure 8) along the northern margin of the Walti pluton, and features coarser and darker brown to black garnet, and sulfides, including pyrite, chalcopyrite, bornite, covellite, cuprite, and galena (Figure 9). Historic workings are also found in roof pendants of mineralized Wenban in the

northwest parts of the Walti pluton. A <1 m rind of magnetite skarn is found at the southwest contact

between the Walti and the Wenban (Figure 10). The Wenban also has black to red jasperoid alteration

typically along contacts with the Horse Canyon or along interpreted faults, with transitions to partly

decarbonatized, or sanded, pink to brown limestone.

Figure 8. Photo of collapsed shaft of the Keystone mine and oxidized skarn mineralization. Photo taken where near sample KS035 of skarn mineralization. Hammer is 28 cm long.
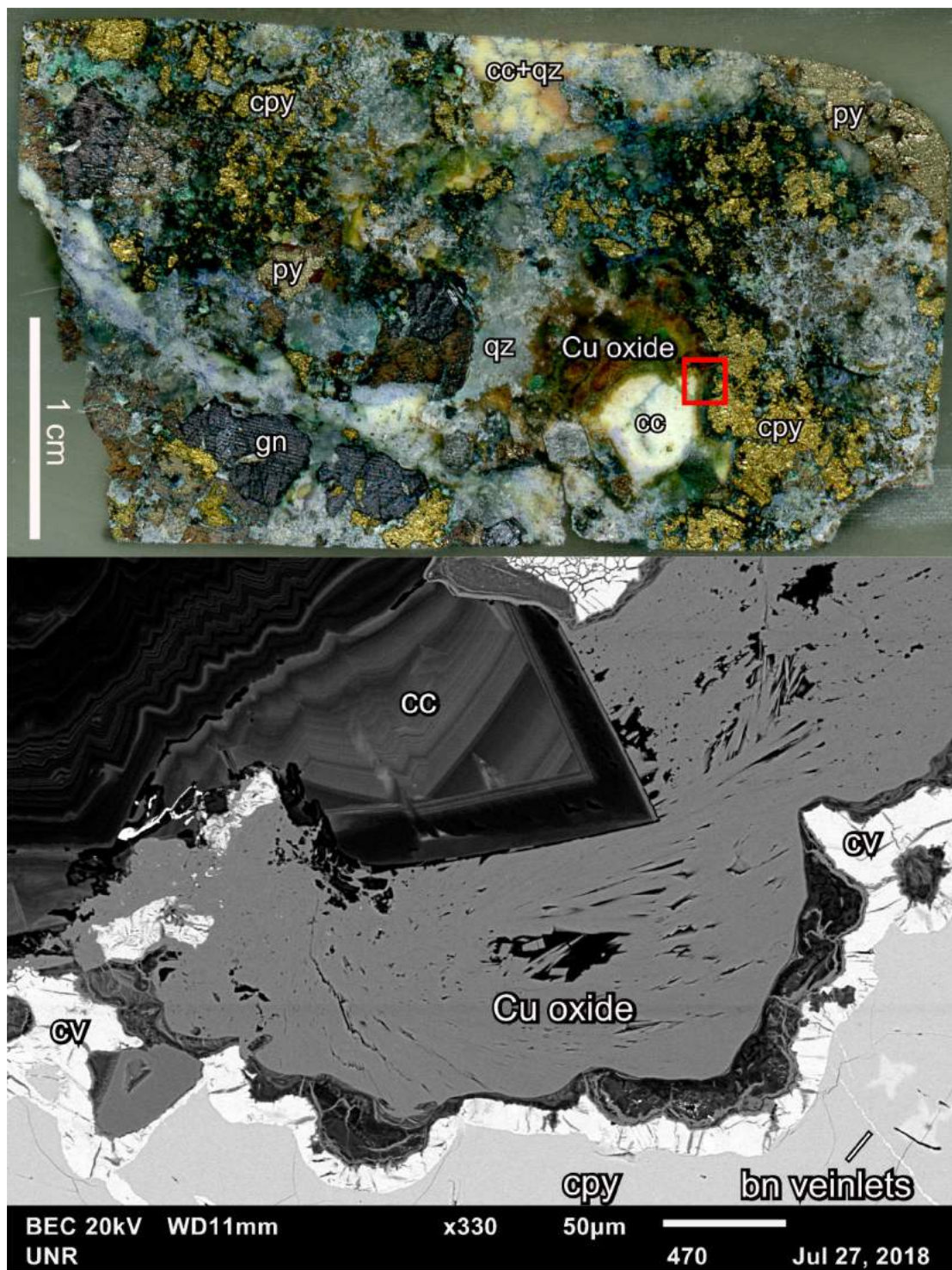
Figure 9. Photo and SEM backscattered electron image of sample KS035 from skarn mineralization at the Keystone mine. Red square indicates field of view for SEM image. Abbreviations: cc=calcite, qz=quartz, py=pyrite, cpy=chalcopyrite, bn=bornite, cv=covellite, gn=galena.
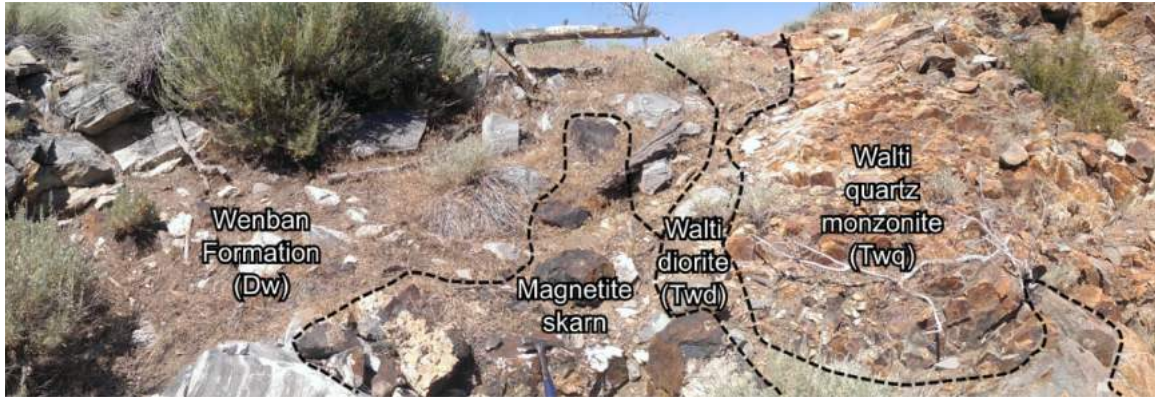
Figure 10. View south towards the Walti pluton's southwest contact with the Wenban Formation. Magnetite skarn occurs at the Wenban contact with the Walti diorite phase mingled with the Walti quartz monzonite phase. Photo taken near sample KS017 of mingled Walti diorite. Hammer is 28 cm long.

Undifferentiated Limestone/Marble in the Mud Springs Pluton (ODul)

Resting on top of the Mud Springs pluton in the east-central part of the study area are isolated 100-1000 m^2 outcrops of marble (ODul) and quartzite (Ovq) (Plate 1). Marble forms prominent outcrops, with the largest covering ~0.15 km^2. These outcrops are contained entirely within the Mud Springs pluton and are interpreted as stoped blocks of marble during the rise and emplacement of magma that formed the Mud Springs pluton. The marble is white to lightly buff-colored and coarsely crystalline. A likely candidate for the marble protolith is limestone of the Wenban, or potentially older Silurian or Ordovician carbonate such as the Lone Mountain Dolomite mapped in the Roberts Mountains to the east (Roberts et al., 1967). The quartzite is possibly derived from similar lithologies in the Valmy Quartzite.

Horse Canyon Unit (Dhc)

The Horse Canyon unit of Late Devonian age was first described by Harry Cook in the Cortez Mountains, with subdivisions detailed along the Cortez mine haul road (Cook, 2015). The Horse Canyon is temporally and lithologically correlative to the Rodeo Creek unit of the Carlin trend gold belt. The Fammenian depositional setting of the Horse Canyon is likely a marine basin that received siliciclastic material from the west (the onset of the Antler orogenic highlands) and carbonate material from the east (the drowned carbonate shelf margin; Cook, 2015). At Cortez and Keystone, the Horse Canyon transitions

from basal debris flows to interbedded carbonate and quartz turbidites. The upper parts of the Horse Canyon unit, with black siltstone, claystone, and buff-colored mudstone, represent a definitive end to the Devonian carbonate deposition, after which slope-to-basin carbonate facies no longer occurred. The top of the Horse Canyon is faulted and not exposed at Keystone because of presumed Antler deformation.

The Horse Canyon unit occurs in several locations in the Keystone window. Detailed mapping (T. Chapin, 2017, unpublished report for U.S. Gold Corp.) shows both depositional and thrust contacts between the Horse Canyon and underlying Wenban. Mapping at Keystone suggests the thickness of the Horse Canyon unit is between 40 and 100 meters, similar to its ~75-meter thickness at Cortez (Cook, 2015). The Horse Canyon unit typically crops out along the perimeter of the Keystone window and in thrust-fault contact with rocks of the overlying and allochthonous Valmy Formation (Plate 1). Bedding attitudes are generally conformable with the underlying Wenban and the overlying rocks of the Roberts Mountains allochthon. Conodonts yield Late Frasnian ages, suggesting the Horse Canyon at Keystone represents the last passive margin depositional event before Late Devonian to Early Mississippian eastward thrusting during the Antler orogeny (Table 1).

Plane laminar, interbedded black chert with calcareous gray to black siltstone are typical lithologies of the Horse Canyon unit at Keystone. Contact metamorphism is widespread and altered the unit to a hard, white siliceous hornfels characterized by conchoidal fracturing. More calcareous layers alter to fine-grained, layered, lime-green calc-silicate hornfels found both above the Gund stock and the Walti pluton. Away from intrusions, fresh and non-metamorphosed Horse Canyon siltstone is pink to buff-colored. In these distal locations, the Horse Canyon fine clastic units are locally altered to jasperoid, especially along contacts with thrust faults and with the underlying Wenban.

Cenozoic rocks

Eocene conglomerates, volcaniclastic rocks, and lavas rest on the Ordovician rocks of the upper plate both to the west and east of the Keystone window (Plate 1). These Cenozoic rocks define the Paleozoic-Cenozoic unconformity in this area. The Pennsylvanian-Permian Antler overlap assemblage consisting of conglomerate and sandstone that resemble some of the Cenozoic conglomerate at Keystone

do not crop out in the study area, but have been extensively mapped in the Simpson Park Mountains 10 km to the northeast and 20 km to the south (Roberts et al., 1967; Stewart and Carlson, 1976).

Tertiary Conglomerate (Tcg)

Along two ridges east of the Walti pluton and north of the Mud Springs pluton are massive outcrops of coarse pebbly sandstone and pebble to cobble conglomerate (Tcg) (Plate 1), which contain both angular and subround clasts. Clasts include chert, siltstone, sandstone, and quartzite as well as locally abundant clay-altered or silicified felsic volcanic rocks. Clasts along the western and topographically higher ridge are generally coarser and dominated by cobble-sized cherts and sandstones; on the eastern ridge clasts are gravel-sized and have a greater proportion of altered volcanic material. The eastern ridge also shows more hydrothermal alteration with limonite and clay.

The Tcg conglomerate rests on upper plate rocks, although the contact between it and diorite of the Walti pluton on the western ridge is under cover. Bedding attitudes are unclear on the western ridge because of strong orthogonal jointing and silicification. Resting on the conglomerate to the east are rhyolitic tuff and volcaniclastics, and aphyric rhyolite lava (Tvc). Here, rocks dip east but with angular unconformity on the southeast-dipping beds of underlying Paleozoic siltstone of the upper plate (Figure 11). The Tcg conglomerate is dated using LA-ICP-MS U-Pb methods on detrital zircons, with the greatest proportion and youngest population of zircons yielding an Eocene age as discussed in detail in the Geochronology section.

Figure 11. Photograph of outcrop of altered Tertiary conglomerate (Tcg), viewing north. Beds of moderately-sorted subrounded cobble conglomerate dip east and contain a mixture of siltstone, chert, and volcanic clasts. Photo taken near sample KS079 of Tertiary conglomerate. Angular unconformity with underlying Valmy is west of the photo. Hammer is 28 cm long.

Intrusive rocks

The abundant intrusive rocks mapped at Keystone are entirely of Eocene age. They include four high-level stocks (Walti, Mud Springs, Gund, and rhyolite porphyry) of intermediate to silicic composition along with abundant intermediate to silicic dikes (Plate 1). The only mafic rocks in the study area are Lower Paleozoic basalt lava and sills of the Valmy and Comus formations. A summary of igneous textures and mineral assemblages is provided in Table 2. Representative examples of intrusive rocks are provided in Figure 12 and Figure 13. Plagioclase compositions determined semi-quantitatively by SEM-EDS are provided in Figure 14.

Table 2. Summary of igneous textures and mineral assemblages

Code	Unit	Texture	Primary mineralogy (vol%)
Tmd	Mud Springs diorite	Seriate to porphyritic with >50% phenocrysts in a very fine-grained groundmass (0.05-0.1 mm)	40-50% plag (1-3 mm), 20-30% gm (0.05-0.1 mm, ksp >> plag + qz), 15-20% mafics (<1 mm, cpx > hbl + bt), 2-3% mt (<0.1 mm), 2-3% py (<0.1 mm), local miarolitic cavities (1-3 mm, <0.5 mm qz > ep > ksp) acc. ap, zir, ep
Tmp	Mud Springs pegmatite	Hypidiomorphic, very coarse, pegmatitic	70-80% ksp (>5 mm), 20-30% qz (>2 mm)
Tgd	Gund diorite	Hypidiomorphic equigranular to seriate, medium- to fine-grained	50-60% plag (<1 mm), 20-30% mafics (<0.5 mm, bt > hbl > cpx), 5-10% ksp (<0.3 mm), 3-5% mt (<0.05 mm), 1-5% qz (<0.3 mm), 1-2% py (<0.05 mm), acc. ap, zir
Trp	Rhyolite porphyry	Porphyritic with 15-25% phenocrysts in micro- to cryptocrystalline groundmass	70-80% gm (<0.05 mm, ksp > qz), 10% plag (1-4 mm), 3-4% qz (1-2 mm), 3-6% san (0.5-2 mm), 2-5% mafics (<1 mm, bt > hbl), acc. mt, zir
Twq	Walti quartz monzonite	Hypidiomorphic equigranular to seriate to porphyritic with >60% phenocrysts in fine-grained to aplitic groundmass	20-40% plag (2-5 mm), 30-45% ksp (<2 mm), 10-20% qz (<1 mm), 5-10% bt (<1mm), 5-10% hbl + cpx + mt (<0.5 mm in 1-2 mm glomerocrysts), 0-30% fine-grained to aplitic gm (0.01 to 0.2 mm) acc. ap, zir, tit, ep
Twd	Walti diorite	Porphyritic with 15-35% phenocrysts in a very fine-grained groundmass (0.01-0.1 mm), variable due to mixing and disequilibrium	65-85% fine-grained gm (0.01-0.1 mm plag > bt > hbl > mt) 20-25% plag (1-5 mm), 5-10% hbl + cpx + mt (<0.5 mm in 1-2 mm glomerocrysts), 1-2% bt (<1 mm), 1-2% mt (<0.1 mm), acc. ap, zir
Twp	Walti intermediate porphyritic dikes	Porphyritic with 20-40% phenocrysts in aplitic to microcrystalline groundmass (<0.05 mm), variable due to mixing and disequilibrium	60-80% gm, 5-15% plag (1-4 mm), 5-10% ksp (0.5-4 mm), 1-5% qz (<1 mm), 1-3% hbl (<1 mm), 1-3% bt (<1 mm) 1-5% glomerocrysts (bt + hbl + cpx + mt, <0.5 mm in 1-5 mm clumps), acc. mt, ap, ep, zir
Tta	Trachyandesite dikes	Porphyritic with 10-15% phenocrysts in micro- to cryptocrystalline groundmass	85-90% gm, 5-10% plag (1-2 mm and microlites), 3-4% oxidized and altered mafics (<0.2 mm), 1% mt (<0.2 mm), acc. ap, zir
Tvc	Volcaniclastics and aphyric rhyolite	Pyroclastic (polymict) to aphyric to sparsely porphyritic with <5% phenocrysts in micro- to cryptocrystalline groundmass	>90% clay-altered to silicified gm, <5% clay-altered fsp + bt (<0.5 mm), <1 mm qz veins, local chert and quartzite subangular pebble clasts
Ta, Tad	Andesite lavas of McClusky Creek, and dikes	Porphyritic with 40-45% phenocrysts in cryptocrystalline to locally glassy groundmass	55-60% gm, 30-35% plag (bimodal, 0.5-2 mm phenocrysts, 0.01-0.1 mm microlites), 4-7 % opx > cpx (0.5-1 mm), 1-5% hbl (0.2-1 mm), 1% mt (<0.5 mm), acc. ap
Tda, Tdad	Dacite agglomerate and dikes	Porphyritic with 25-30% phenocrysts in cryptocrystalline groundmass	70-75% gm, 25-30% plag (<1 mm), 1-3% mafics (<0.5 mm, cpx > hbl), 1% mt (<0.2 mm), acc. ap, zir
COcb, Ovb	Basalts of the Comus and Valmy formations	Hypidiomorphic equigranular to seriate, medium- to very fine-grained, breccias, hyaloclastites, pillows	30-50% plag (<1 mm), 20-30% altered olivine (<0.5 mm), 10-30% mt + ilm (<0.5 mm), 1-5% bt (<0.3 mm), 5-10% acicular ap (<1 mm length), 0-20% calcite (speckled to coarse/massive)

Abbreviations: gm=groundmass, fsp=feldspar, plag=plagioclase, ksp=K-feldspar, san=sanidine, qz=quartz, cpx=clinopyroxene, opx=orthopyroxene, hbl=hornblende, bt=biotite, ap=apatite, zir=zircon, ep=epidote, mt=magnetite, ilm=ilmenite
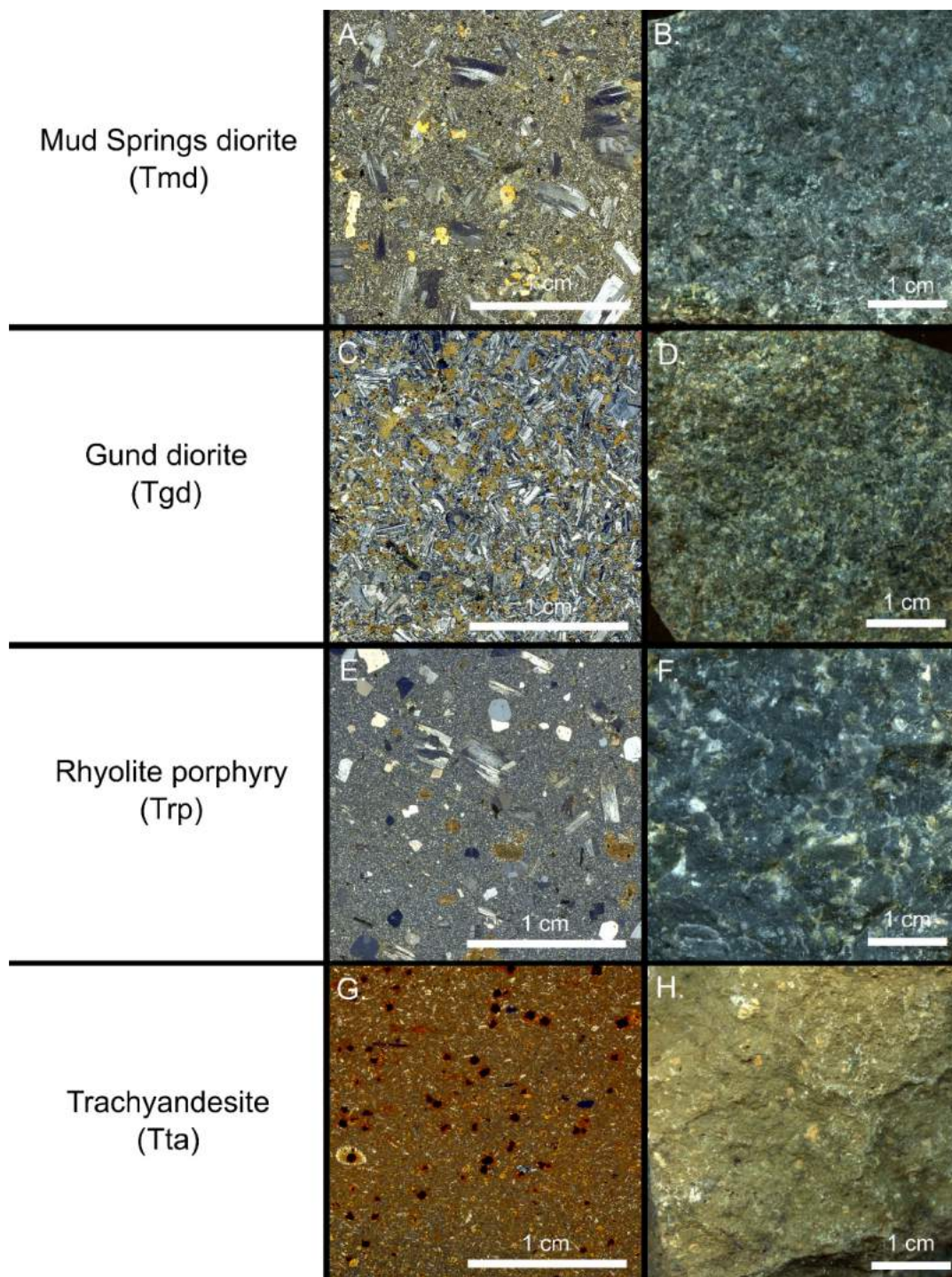
Figure 12. Representative micrographs and photographs of Eocene intrusive units, excluding the Walti pluton. A) Micrograph of the Mud Springs diorite (sample KS003) in cross-polarized light. B) Photograph of the Mud Springs diorite (sample KS003). C) Micrograph of the Gund diorite (sample KS079) in cross-polarized light. D) Photograph of the Gund diorite (sample KS079). E) Micrograph of the rhyolite porphyry (sample KS097) in cross-polarized light. F) Photograph of the rhyolite porphyry (sample KS098). G) Micrograph of the trachyandesite (sample KS025) n cross-polarized light. H) Photograph of the trachyandesite (sample KS021).
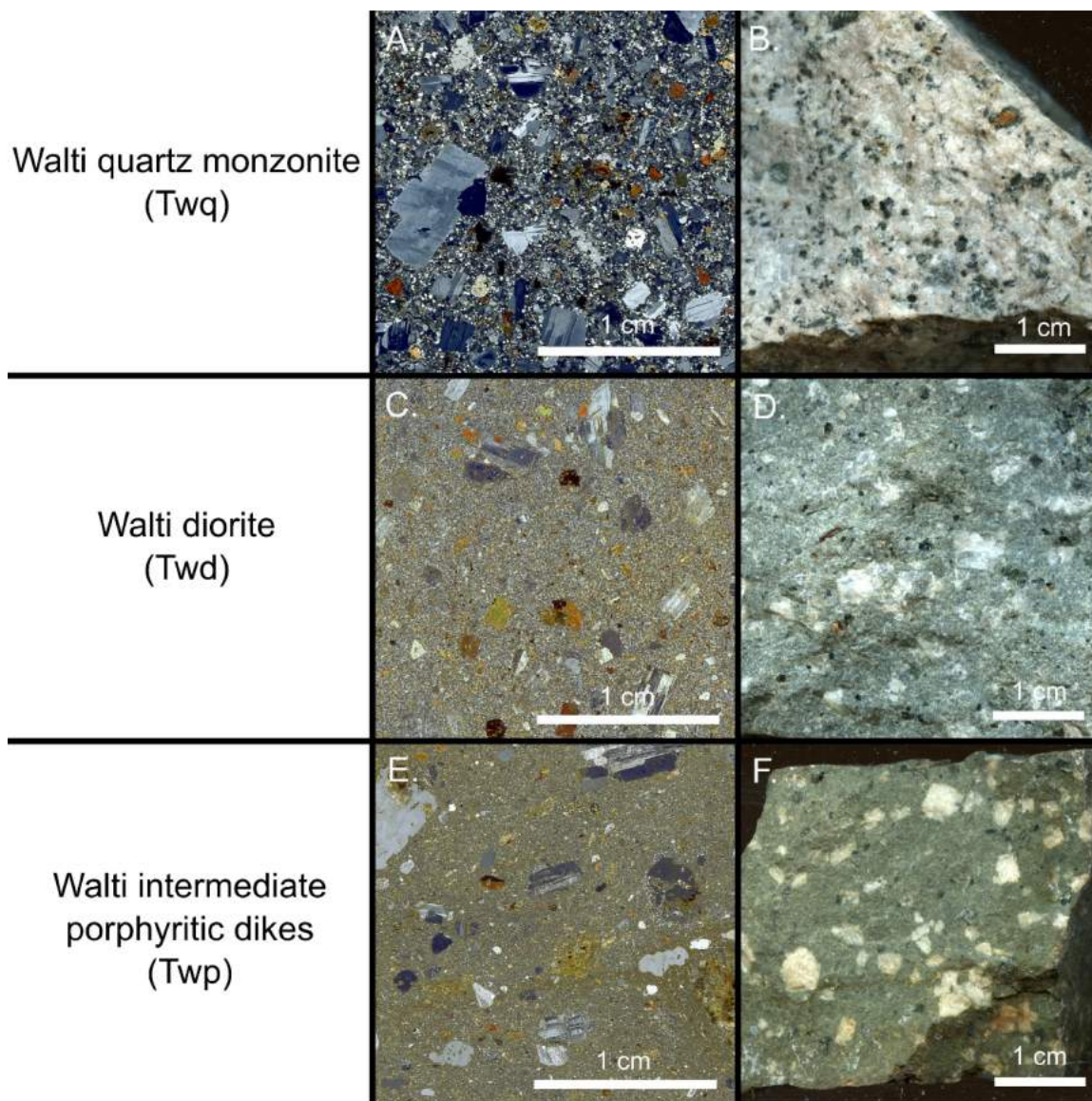
Figure 13. Representative micrographs and photographs of intrusive units of the Walti. A) Micrograph of the Walti quartz monzonite (sample KS007) in cross-polarized light. B) Photograph of the Walti quartz monzonite (sample KS007). C) Micrograph of the Walti diorite (sample KS086) in cross-polarized light. D) Photograph of the Walti diorite (sample KS068). E) Micrograph of the Walti intermediate porphyritic dikes (sample KS095) in cross-polarized light. F) Photograph of the Walti intermediate porphyritic dikes (sample KS115).
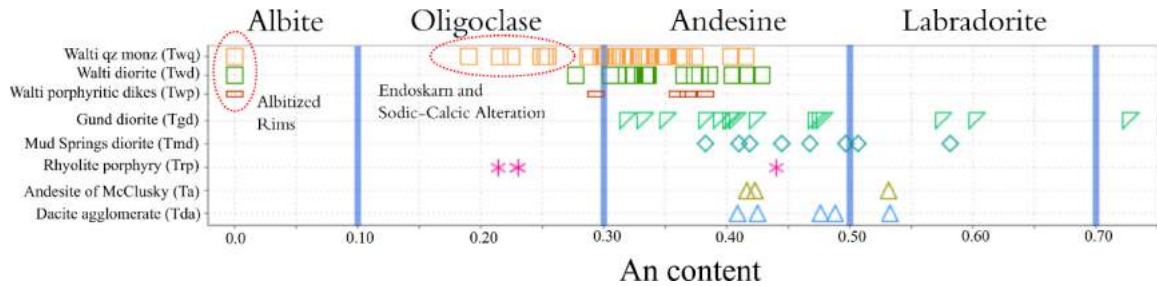
Figure 14. Anorthite compositions of plagioclase phenocrysts determined using semi-quantitative SEM-EDS. See text for discussion.

Mud Springs diorite (Tmd)

The 1 km² Mud Springs diorite pluton (Tmd) is located in the east-central part of Keystone (Plate 1). Fault-bounded to the west by upper-plate rocks, the Mud Springs pluton is sill-like and forms an E-W oval map pattern that mimics the gently east-dipping topography. A rhyolite porphyry plug (Trp) cuts the Mud Springs pluton's northwest corner. The east-west striking Walti porphyritic intermediate dikes (Twp) also cut the pluton. Resting on the diorite are the aphyric rhyolite and volcaniclastics unit (Tvc) and dacite agglomerate (Tda). Also resting on top of or within the pluton are several large isolated xenoliths of marble (ODul) and quartzite (Ovq).

The Mud Springs pluton is hypidiomorphic seriate to weakly porphyritic with >50% phenocrysts in a very fine-grained gray to dark green groundmass (Figure 12A-B). Its phenocryst assemblage includes 1-3 mm plagioclase, <1 mm clinopyroxene, hornblende, and biotite (Table 2). Plagioclase compositions determined by SEM-EDS are andesine to labradorite (An_{38-58}), similar to compositions from the Gund diorite but differing from diorite of the Walti pluton (Figure 14). Where the texture is more porphyritic, the very fine-grained groundmass tends to be K-feldspar-rich with lesser amounts of quartz and plagioclase. Groundmass crystals are generally 0.01-0.3 mm. Phenocrysts of K-feldspar are rare and no larger than 1 mm. Fine-grained magnetite and cubic pyrite are common in the pluton, and primary pyrite is generally more prevalent (1-2%) in less-altered rocks.

Mafic minerals occur as phenocrysts and in clumps or 1-2 mm glomerocrysts. Glomerocrysts consist of pyroxene cores mantled by biotite and as unoriented aggregates of pyroxene, amphibole, biotite,

and plagioclase. Millimeter- to centimeter-size miarolitic cavities are found throughout the Mud Springs pluton and typically contain intergrowths of quartz and epidote with minor orthoclase, as well as open space (Figure 15A-B).
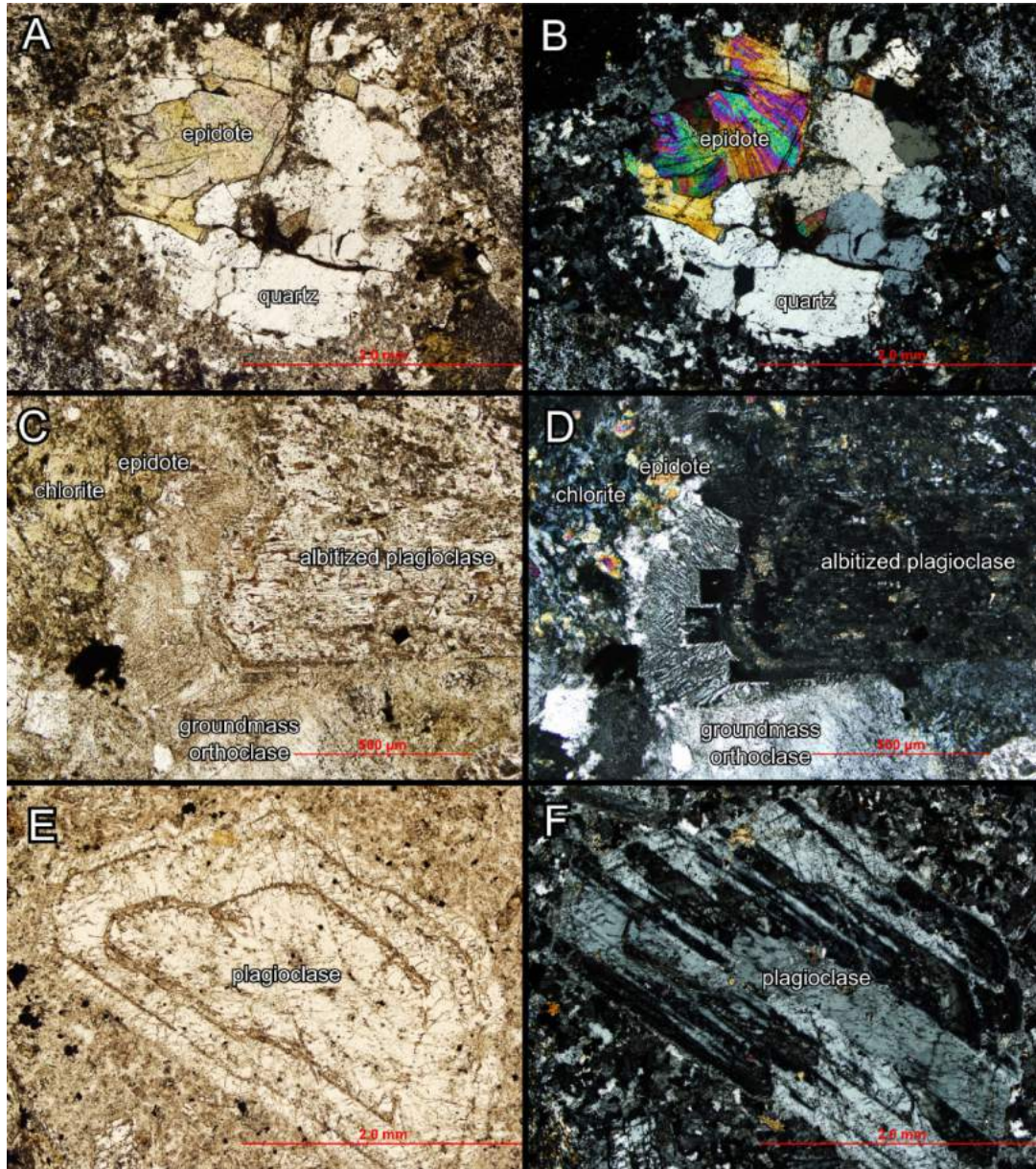
Figure 15. Micrographs of the Mud Springs diorite in plane- and cross-polarized light. A-B) Sample KS102. Miarolitic cavities with quartz and epidote are locally abundant in the Mud Springs pluton. C-D) Sample KS104. Plagioclase is altered to sericite, epidote, and albite, and has an albitized rim which has rectangular growths into groundmass orthoclase. The orthoclase displays an unusual myrmekitic or vermicular intergrowth texture with quartz. E-F) Plagioclase phenocryst showing three events producing sieve-textured rims (the outer rim and two inner layers). Plagioclase is locally altered to sericite.

Unaltered hornblende or biotite was not found in the Mud Springs pluton. In the least-altered samples, these mafic minerals are typically completely altered to chlorite, with or without epidote. Identification of hornblende is possible where vestiges of unaltered hornblende remain. Biotite is identified by its typical form and cleavage. Clinopyroxene is generally unaltered but can be weathered and fragmented as well as oxidized.

Plagioclase phenocrysts in the Mud Springs pluton show varying degrees of alteration to albite, sericite, calcite, and epidote. Intensely altered plagioclase is albitized and has patches of calcite with fine-grained epidote. These features combined with alteration of mafic minerals to chlorite and calcite indicate propylitic alteration. Intense albitization of plagioclase is also accompanied by recrystallization of the groundmass to interlocking and interstitial orthoclase. In these samples, the groundmass shows angular, skeletal quartz textures within orthoclase. The orthoclase also displays a myrmekitic texture (Figure 15C-D). Plagioclase phenocrysts commonly have sieve-textured rims, suggesting magma disequilibrium and/or resorption during the crystallization history (Figure 15E-F). The abundance of orthoclase in the groundmass further supports the possibility of disequilibrium between calcic plagioclase phenocrysts and more evolved potassium-rich late melt.

Mud Springs pegmatite (Tmp)

Throughout the Mud Springs pluton are coarse-grained pegmatites (Tmp) as centimeter to meter size inclusions, as well as outcrops that span tens of meters along strike (Figure 16). The largest outcrops of pegmatite are located on the west side of the exposed pluton (Plate 1). Inclusions of pegmatite decrease in size and abundance away from the large outcrops, although they occur sporadically throughout the pluton. Pegmatite mineral assemblages are typically restricted to graphic-textured intergrowths of quartz (2-5 mm) and orthoclase (>1 cm). Quartz crystals are elongated and sinuous in a matrix of coarse orthoclase crystals (Figure 17).
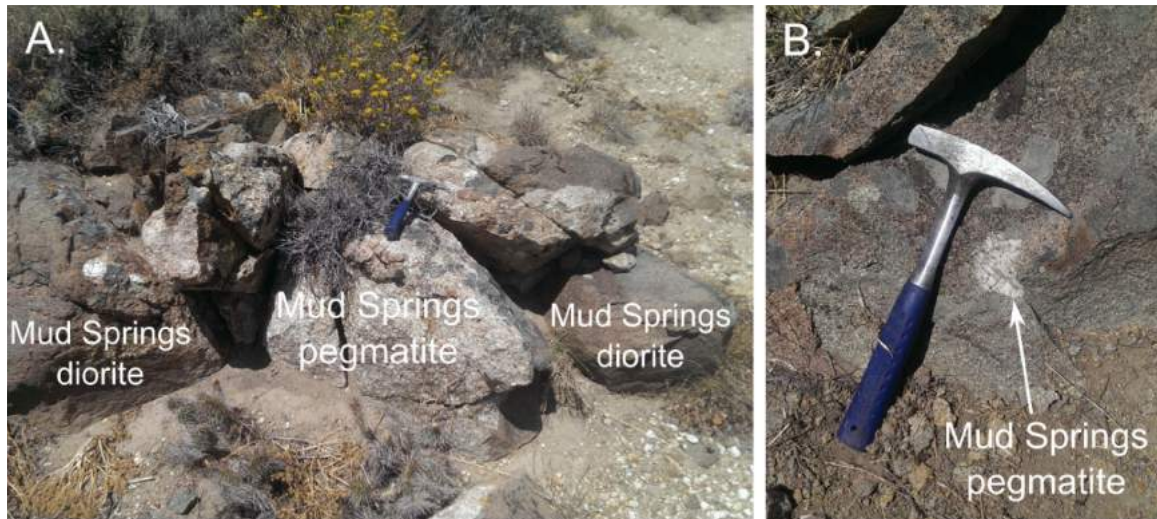
Figure 16. Photos of outcrops of the Mud Springs pegmatite. A. Example of a larger outcrop surrounded by diorite. B. Example of a smaller pegmatite inclusion in the diorite, which are common throughout the Mud Springs pluton. Hammer is 28 cm long.
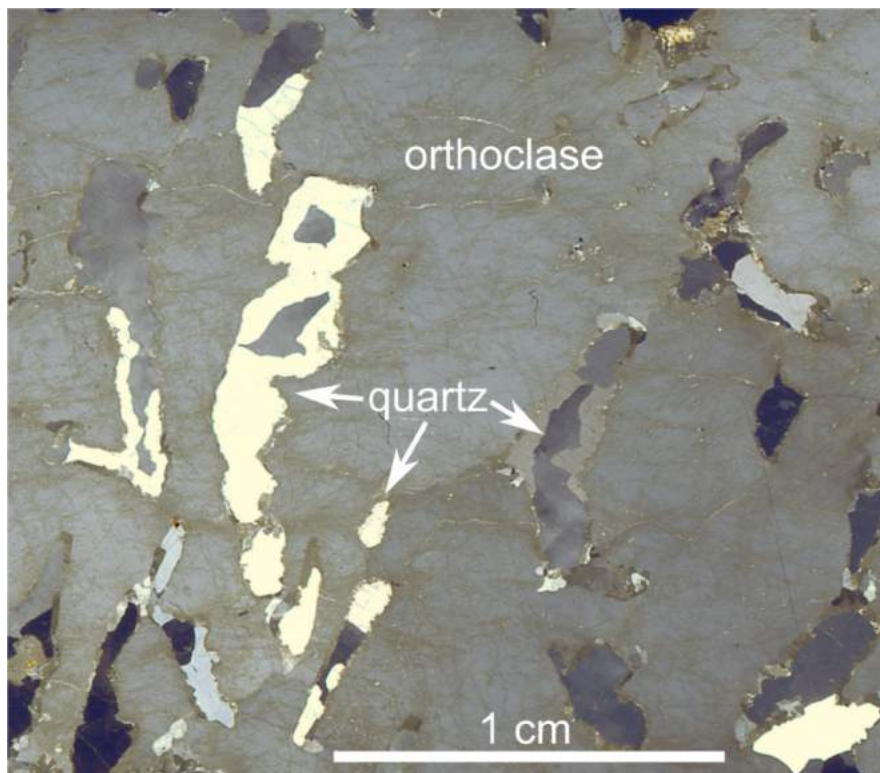
Figure 17. Micrograph of the Mud Springs pegmatite (sample KS110) in cross-polarized light. Coarse elongate quartz grains are in a matrix of very coarse orthoclase.

Gund diorite (Tgd)

About 500 m to the south of the Walti pluton is the Gund stock (Tgd), which is compositionally a diorite and has an outcrop exposure of about 0.36 km^2 (Plate 1; Figure 18). The Gund has primary intrusive contacts with the Wenban and Horse Canyon formations. A small (<0.02 km^2) sill-like extension of the Gund stock is well exposed along the western range front fault about 1 km to the west, just east of the Gund Ranch (Plate 1). The Gund stock generally has a lopolith shape with a concave-upward roof where it intruded rocks of the Horse Canyon unit. A thrust separating rocks of the Roberts Mountains allochthon (RMA) is exposed immediately above rocks of the Horse Canyon unit, less than 50 m above the upper contact of the Gund; here, the RMA features cataclasized chert and siltstone (Figure 19). Outcrops of calcareous siltstone and mudstone of the Horse Canyon unit adjacent to the Gund are recrystallized to calc-silicate and siliceous hornfels. The Wenban adjacent to the Gund is recrystallized to marble and contains fine-grained green calcic garnet, but no mineralized skarn was found in this area.

Figure 18. Labeled photograph of the Keystone window looking southeast across the Walti pluton toward the Gund diorite, lower-plate carbonates, and along the skyline, upper-plate rocks of the Valmy Formation. Labels are same as map units.

Figure 19. Photograph of cataclasized and sheared chert and siltstone along the thrust fault separating Devonian Horse Canyon (Dhc) and overlying Ordovician Valmy (Ov). Sample was taken <50 m from the upper contact of the Gund stock (Tgd).

The Gund diorite is hypidiomorphic equigranular to seriate, and medium to fine grained (Figure 12C-D). The finer-grained groundmass texture, with minerals rarely exceeding 1 mm, and a lack of phenocrysts in the Gund diorite readily differentiate it from the Walti diorites (Table 2). Plagioclase is the most abundant mineral, and it is generally ≤1 mm, with a few grains as large as 2 mm. Plagioclase compositions determined by SEM-EDS are andesine to labradorite (An_{32-73}), a departure from the strictly andesine compositions of plagioclase in rocks of the Walti pluton (Figure 14) and consistent with a relatively more mafic composition. Mafic minerals include biotite, hornblende, and clinopyroxene, all ≤0.5 mm. Interstitial quartz and orthoclase <0.3 mm form the fine-grained groundmass, which makes up <15% of the rock. Local clumps of epidote and quartz are also common. Magnetite is common in the groundmass and associated with other mafic minerals. Outcrops with little oxidation have as much as 1-2% disseminated pyrite.

Alteration of mafic minerals to chlorite is common throughout the Gund stock, and biotite and hornblende generally alter more readily than clinopyroxene (Figure 20A-B). Plagioclase is commonly dusted with sericite and clay. Pervasive alteration of mafic minerals to actinolite is common along margins of the stock adjacent to marble of the Wenban (Figure 20C-D). Intense endoskarn alteration occurs at the southern margin of the Gund towards its upper contact adjacent to hornfels of the Horse Canyon unit (Figure 21). The mineral assemblage of the endoskarn is simplified here and consists of bleached feldspars, abundant fine-grained diopside, and titanite. At the eastern margin of the Gund is an outcrop with clay-altered mafic minerals, heavily sericitized plagioclase, and intense oxidation.
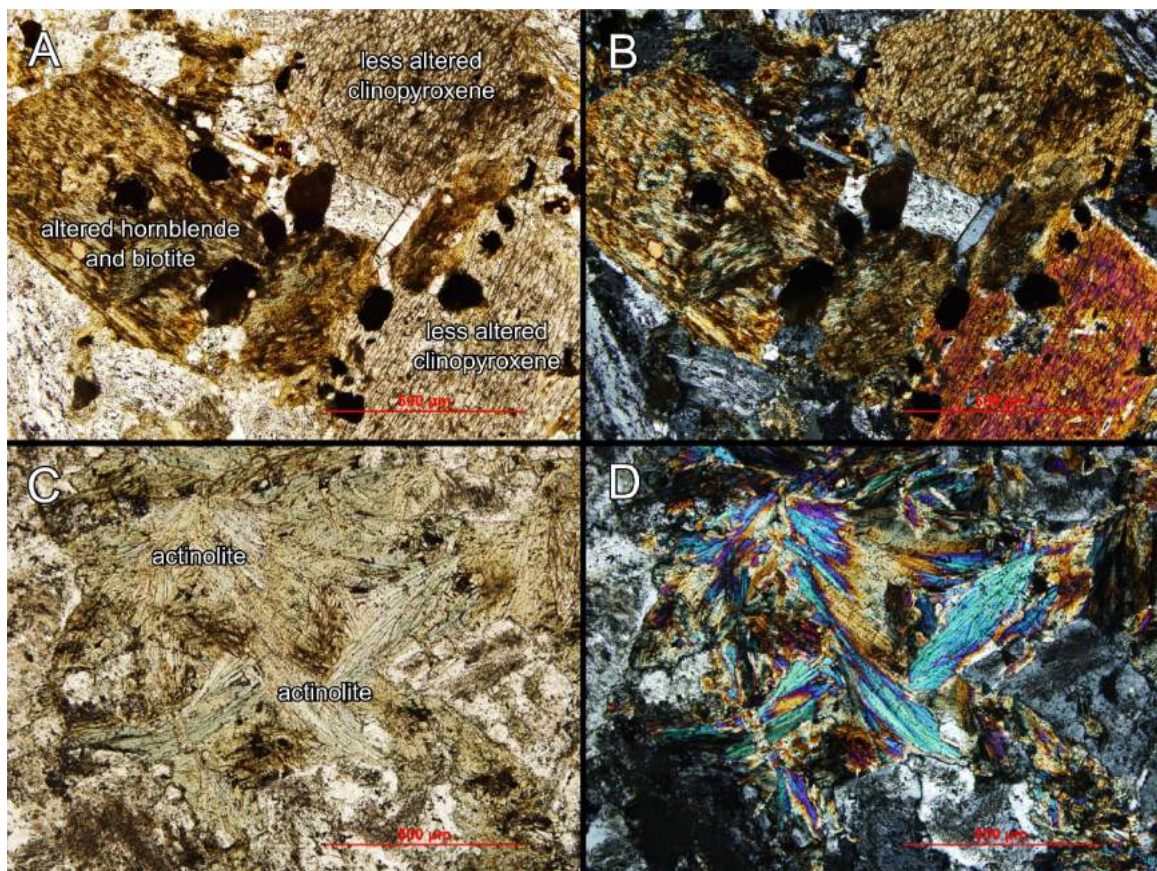
Figure 20. Micrographs of the Gund diorite in plane- and cross-polarized light. A-B) Sample KS076. Typical alteration observed in the Gund, featuring hydrous mafic minerals hornblende and biotite altering to chlorite while clinopyroxene is relatively unaltered. Opaques are oxidized pyrite and magnetite. C-D) Sample KS075. Mafic minerals have altered to acicular actinolite and local tremolite in an outcrop adjacent to marbled Wenban.
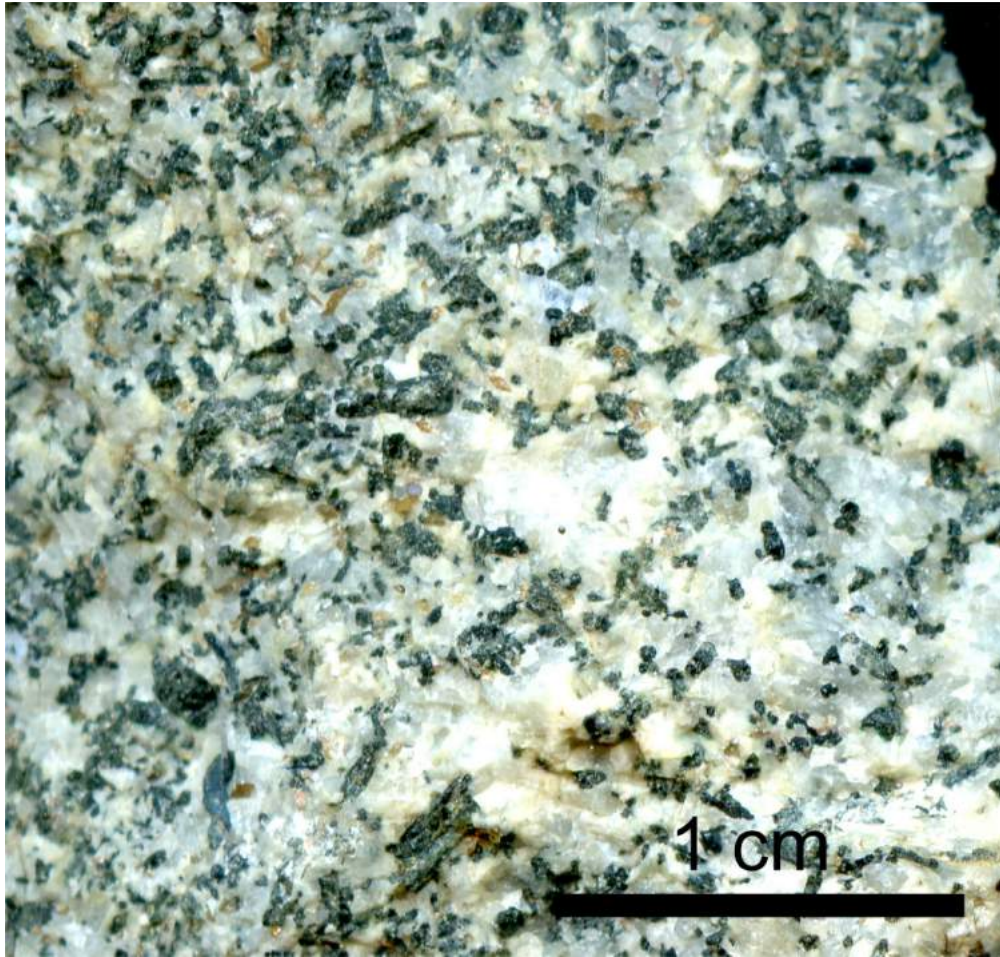
Figure 21. Photograph of the Gund diorite (sample KS072) with endoskarn alteration. Light gray crystals are plagioclase, dark green are diopside, amber-colored are titanite.

Walti pluton – quartz monzonite (Twq)

The Walti pluton is the largest intrusive body at Keystone, covering approximately 4.1 km^2 and

having ~600 m of exposed vertical extent (Plate 1). The Walti pluton was compositionally subdivided for

mapping purposes into a light to medium gray quartz monzonite to granodiorite (Twq) (Figure 13A-B), and

a dark gray diorite (Twd) (Figure 13C-D), the latter discussed later. The two main subtypes along with

other more localized compositions indicate that the Walti is a composite pluton of intermediate to felsic

composition. Textures of the quartz monzonite range from strongly porphyritic with phenocrysts >5 mm in

a fine- to medium-grained matrix, to coarse-grained hypidiomorphic equigranular textures at greater depth

(Figure 22; Table 2). The Walti pluton intrudes Devonian calcareous sedimentary rocks of the Wenban and

Horse Canyon formations, thus forming the core of the Keystone carbonate window. The pluton is roofed

by chert, mudstone, and siltstone of the Roberts Mountains allochthon (RMA) on its eastern margin.

Northeast-striking high-angle normal faults down dropped the Walti towards the northwest, in a stepped

fashion. The geomorphology associated with the Walti pluton is strongly influenced by the NE normal

faults as well as by high-temperature sodic-calcic hydrothermal alteration, which made the rock more

resistive to weathering. Major, young, range-bounding NNE-striking, WNW-dipping normal faults place

the RMA and Eocene volcaniclastics against the Walti pluton along its northwestern margin. Isolated roof

pendants of Wenban-derived marble and skarn rest on the northwestern part of the pluton, whereas the

historic Keystone mine copper skarn occurs along the steep northern contact between the Walti and the

Wenban Limestone.
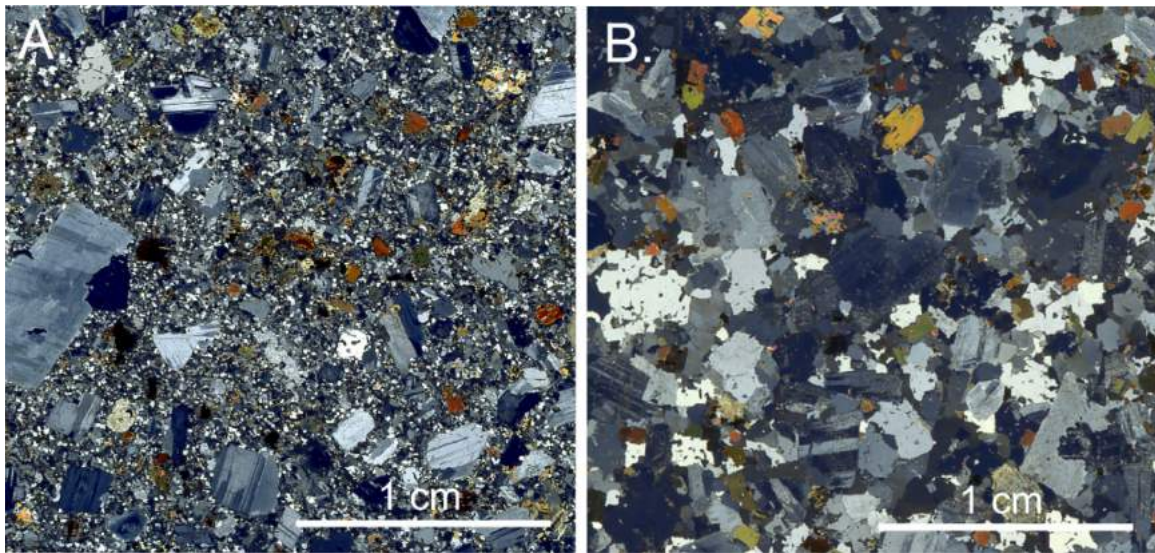
Figure 22. Micrographs of the Walti quartz monzonite, in cross-polarized light. A) Sample KS007 from outcrop has typical porphyritic texture found across all outcrops of the Walti quartz monzonite phase. B) Sample KS137 from drill core at 530 m depth has coarse-grained hypidiomorphic texture.

The most common phenocryst assemblage in the Walti pluton quartz monzonite (Twq) consists of

3-5 mm plagioclase, ≤1 mm biotite, and either ≤1 mm clinopyroxene as augite or ≤1mm green hornblende,

rarely both. Magnetite occurs only with mafic phenocrysts and not in the groundmass. Accessory phases

include zircon, apatite, and titanite. Medium- to fine-grained quartz and orthoclase make up the

groundmass and may occur as ≤1 mm phenocrysts. Plagioclase phenocrysts typically have oscillatory zoning. Semi-quantitative feldspar compositions were determined by SEM-EDS are dominantly andesine as An_{30-41} excluding samples affected by albite, endoskarn, or sodic-calcic alteration (Figure 14).

Different phases within the quartz monzonite can be identified based the presence, size, and abundance of mafic minerals, such as those with or without coarse biotite phenocrysts, and those with only hornblende or pyroxene. Variations in texture also distinguish different phases of Twq. A hornblende-rich phase tends to occur towards the northwest, and a fine-grained biotite phase occurs only in the southeast near the inferred contact with the RMA, the latter representing the uppermost part of the quartz monzonite. All outcrops of the Walti are porphyritic with notably larger plagioclase phenocrysts than other phenocrysts, but a sample collected from drill core at 530 m depth was coarse-grained and equigranular.

Mafic, 1-2 mm glomerocrysts or autoliths regularly appear within the quartz monzonite (Figure 23A-B). Glomerocrysts typically have a core of clinopyroxene, granular magnetite, and apatite, and are mantled by biotite and rarely by patchy hornblende. Anhedral titanite occasionally occurs in the glomerocrysts. The clinopyroxene in the glomerocrysts tended to alter, oxidize, and/or weather more commonly than phenocrystic clinopyroxene, suggesting differing compositions and crystallization histories between the two. Other less common styles of glomerocrysts are mixed aggregates of hornblende and clinopyroxene, less commonly with biotite.
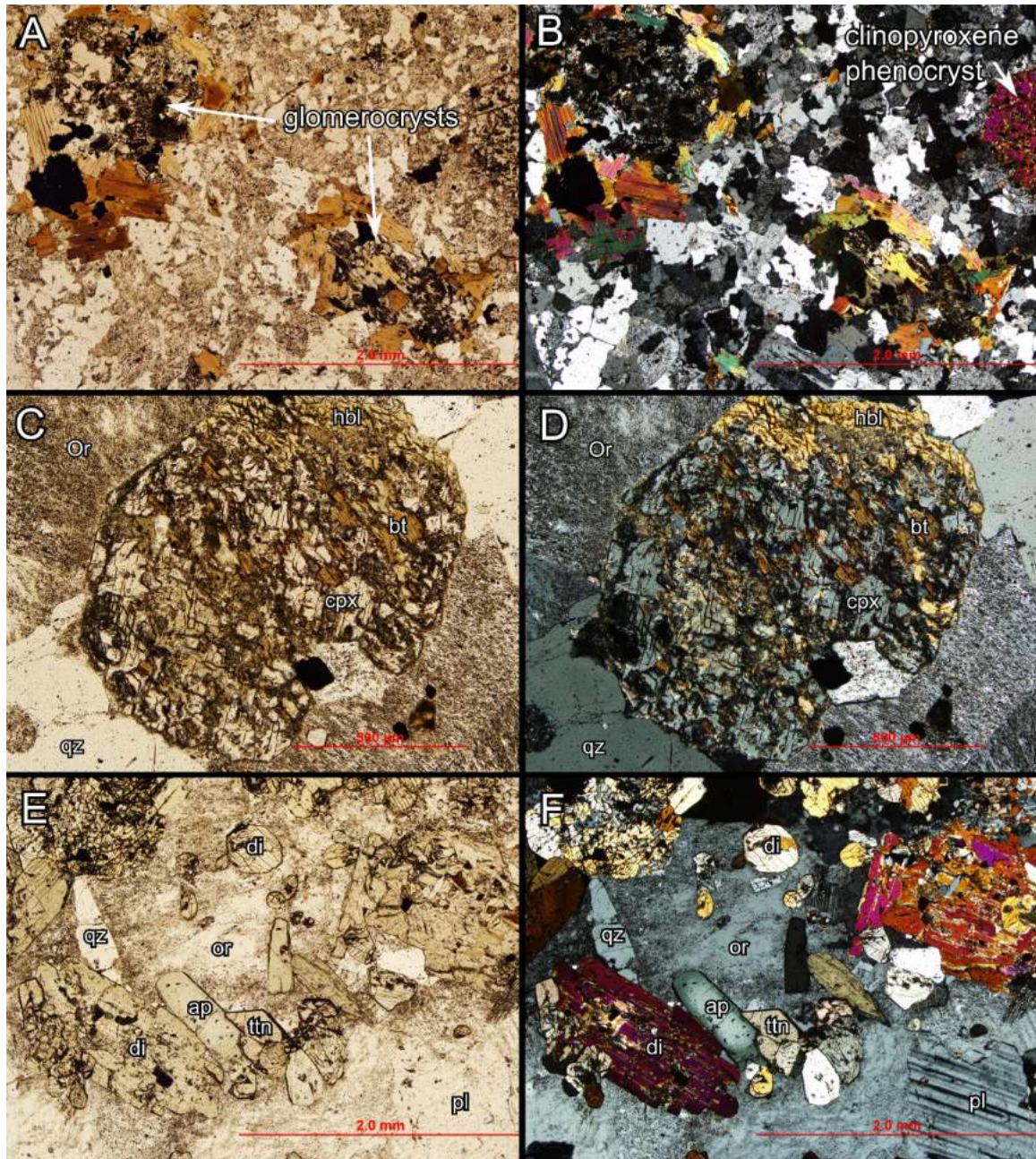
Figure 23. Micrographs of the Walti quartz monzonite in plane- and cross-polarized light. A-B) Sample KS060. Glomerocrysts in the Walti quartz monzonite are common and cored by clinopyroxene with magnetite and apatite, mantled by biotite. Clinopyroxene in the core commonly was oxidized and altered before other mafic minerals. Also shown is a clinopyroxene phenocryst that shares no features with the glomerocryst, suggesting it had a different crystallization history. C-D) Sample KS137. Clinopyroxene has altered to patchy hornblende and biotite, possibly due to late magmatic volatile exsolution causing deuteric alteration. E-F) Sample KS010. Endoskarn alteration of the Walti quartz monzonite features diopside, titanite, and apatite. Coarse and interstitial orthoclase, plagioclase, with lesser quartz make up the matrix. Abbreviations: qz=quartz, or=orthoclase, hbl=hornblende, bt=biotite, cpx=clinopyroxene, di=diopside, ap=apatite, ttn=titanite, pl=plagioclase.

The most common alteration style of the Walti quartz monzonite and granodiorite consists of chlorite and minor epidote replacement of primary mafic minerals combined with minor sericite dusting of plagioclase and albitization of plagioclase rims. Interstitial 1 mm clusters, likely filled or partly filled miaroles, are common and not associated with a specific alteration assemblage. The clusters are comprised of euhedral quartz, epidote, and rarely with titanite. Clinopyroxene may show deuteric alteration to patchy light-green amphibole, but the distribution across samples or even within a single sample does not appear to follow a pattern (Figure 23C-D). More intense sodic-calcic alteration occurs in the Walti, with pyroxene altered to epidote and calcite, andesine altered to oligoclase, and an increase in titanite in the groundmass.

A few outcrops of Twq in contact with marble exhibit endoskarn alteration, with a simplified mineral assemblage of diopside, titanite, apatite, and coarse interlocking plagioclase and orthoclase (Figure 23E-F). Inboard of the southeast margin of the pluton are abundant 1-10 mm sheeted garnet veins striking N-S and dipping west (Figure 24). Diopside also occurs in these veins and as disseminated fine-grained crystals in the groundmass. The contact with wall rock here is obscured by talus in a steep drainage. Two localities in the northwest part of the pluton show intense acidic hydrothermal alteration, wherein feldspars are altered to illite and/or kaolinite with a silicified groundmass. The locality southwest of the Keystone mine has quartz veins with weak mineralization including galena but is generally oxidized (Figure 25).
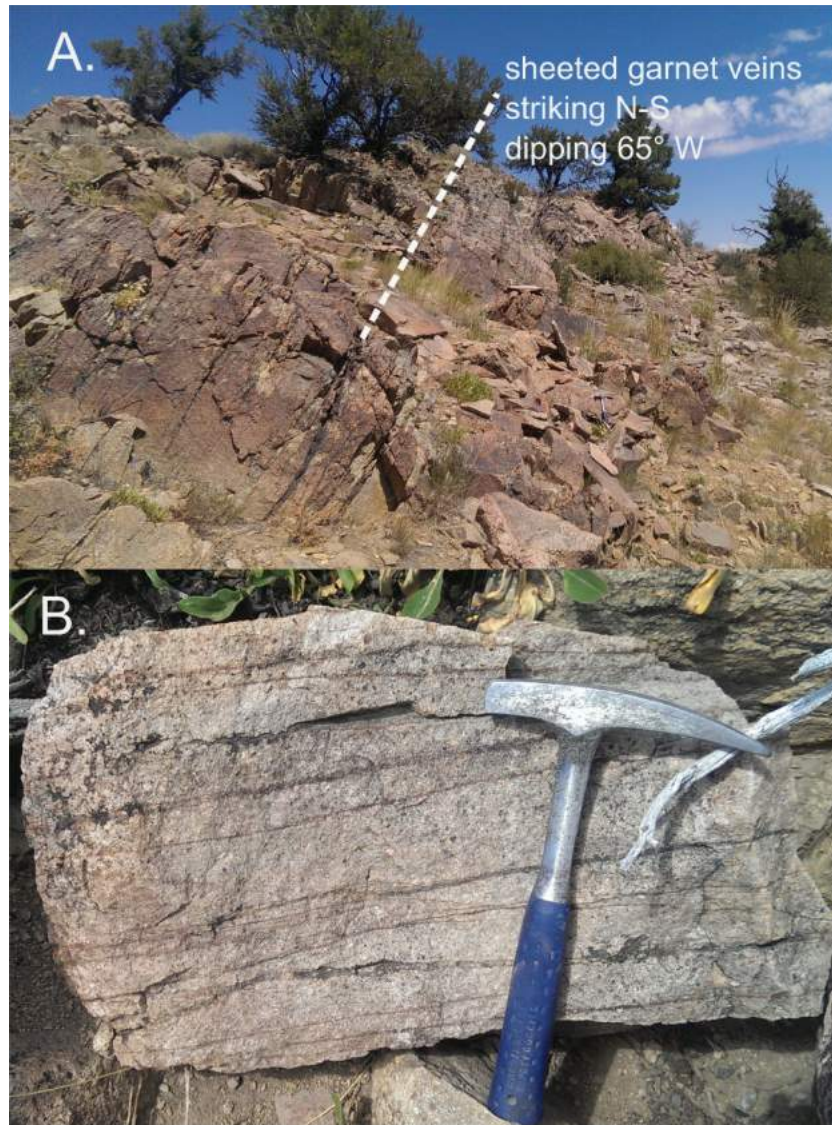
Figure 24. A) Photograph of sheeted garnet veins in the Walti quartz monzonite with N-S orientation and dipping 65° west. Photo taken near sample KS059, viewing north. B) Closer view of garnet veins, typically 1-10 mm wide. Hammer is 28 cm long.

Figure 25. Photograph of hydrothermally altered and bleached Walti quartz monzonite (sample KS030). Feldspars have been altered to illite and kaolinite and groundmass partly silicified. Vein has euhedral comb quartz with weak local sulfide mineralization such as galena (not shown) that is now mostly oxidized.

Walti pluton – diorite (Twd)

A slightly more mafic quartz diorite to monzonite phase (Twd) crops out in irregular zones within the interior of the Walti pluton and as larger bodies on the pluton's eastern and uppermost margin (Plate 1). This diorite appears as outcrops surrounded by quartz monzonite with soft and partly mingled contacts (Figure 26), and as a border phase in contact with Paleozoic sedimentary rocks. Small, round diorite enclaves from 5 to 10 cm diameter commonly occur within the quartz monzonite (Figure 27). At the eastern margin, the diorite phase extends past the thrust fault bounding the lower plate and intrudes rocks recrystallized to hornfels in the Roberts Mountains allochthon.

The Walti diorite is typically finer grained and darker in color than the quartz monzonite and it contains sparse and smaller phenocrysts (Figure 13C-D). Its mineral assemblage includes 3-5 mm plagioclase, ≤ 1 mm pyroxene, ≤ 1 mm biotite, in a fine-grained groundmass of plagioclase and lesser biotite, pyroxene, orthoclase, magnetite, and rare quartz (Table 2). Plagioclase composition by SEM-EDS is andesine, typically An_{30-42}, overlapping with plagioclase compositions from the quartz monzonite phase

(Figure 14). Differing texture, color, and amount of quartz reliably distinguish the Walti quartz monzonite and the Walti diorite. Another key difference between the two units is the presence of magnetite in the diorite's groundmass, which is lacking in the quartz monzonite groundmass.

Figure 26. Photograph of typical mingled contact between the Walti diorite and Walti quartz monzonite. Patterns of mingling suggest the lighter and more felsic magma intruded and fragmented the darker more mafic magma. Contacts are diffusive and rounded, indicating the mafic magma was still partly molten when intruded by quartz monzonite magma. Hammer is 28 cm long.
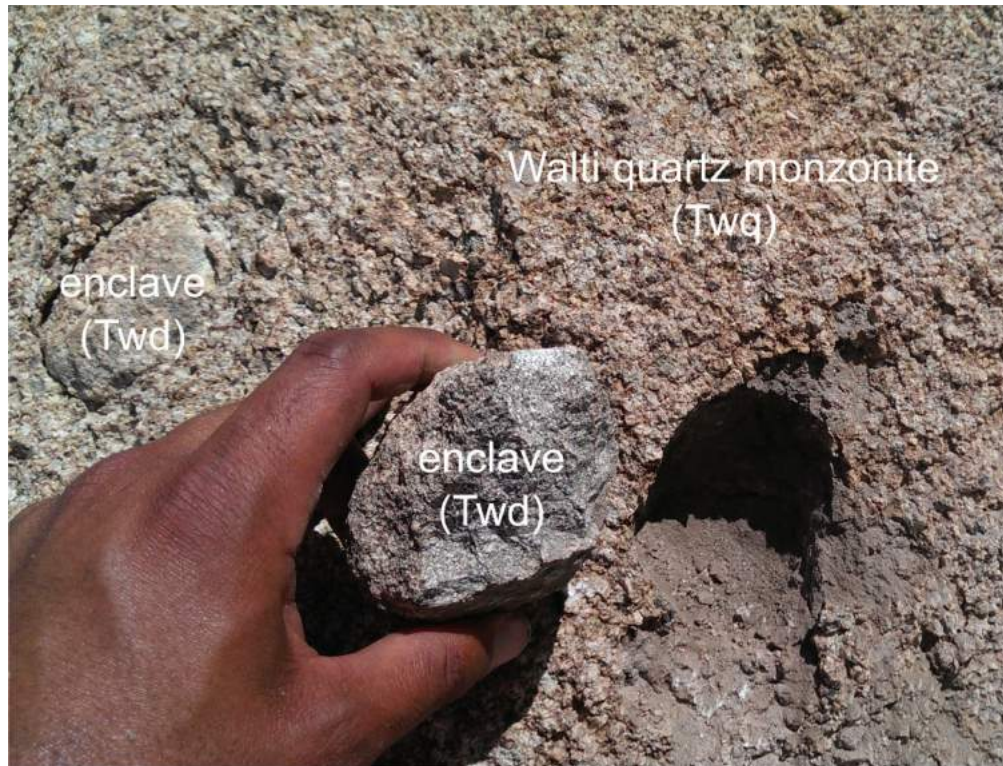
Figure 27. Photograph of example of the Walti diorite occurring as a hand-sized enclave within the Walti quartz monzonite, plucked from the outcrop. Another enclave is visible in the upper left

Discontinuous diorite bodies on the eastern margin of the Walti pluton crop out in patches that are generally >0.2 km^2 and are, to some extent, variable in terms of mineralogy, texture, and alteration. These differences suggest slight variation in their crystallization histories and/or variable amounts of magma mixing/mingling and disequilibrium. In particular, the diorite closest to McClusky Peak along the north-south ridge features >1 cm orthoclase megacrysts (Figure 28) not observed in other diorite bodies.

Glomerocrysts typical of the quartz monzonite (i.e. composed of clinopyroxene, magnetite, and apatite, mantled by biotite), appear less commonly in the diorite. A diorite enclave in the pluton's southeast side has orthopyroxene mantled by clinopyroxene, plagioclase, and biotite. The same sample also has intensely resorbed quartz phenocrysts (Figure 29A) suggesting disequilibrium and mingling with the quartz monzonite phase. More common are randomly oriented aggregates of mafic minerals. Rarely, xenocrystic quartz is mantled by mafic minerals like biotite and hornblende (Figure 29).
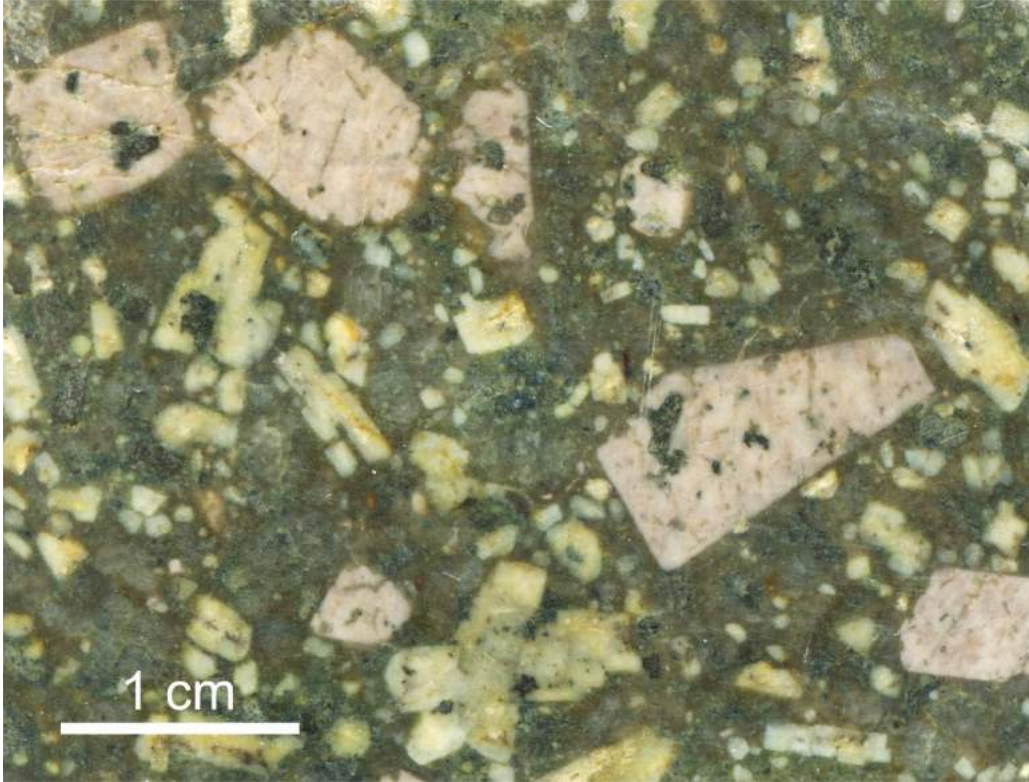
Figure 28. Photograph of the Walti diorite (sample KS087, slabbed) from an outcrop with unusual pink orthoclase megacrysts. White-tan phenocrysts are plagioclase, smaller gray round phenocrysts are quartz. Dark inclusions in the orthoclase are chloritized biotite.
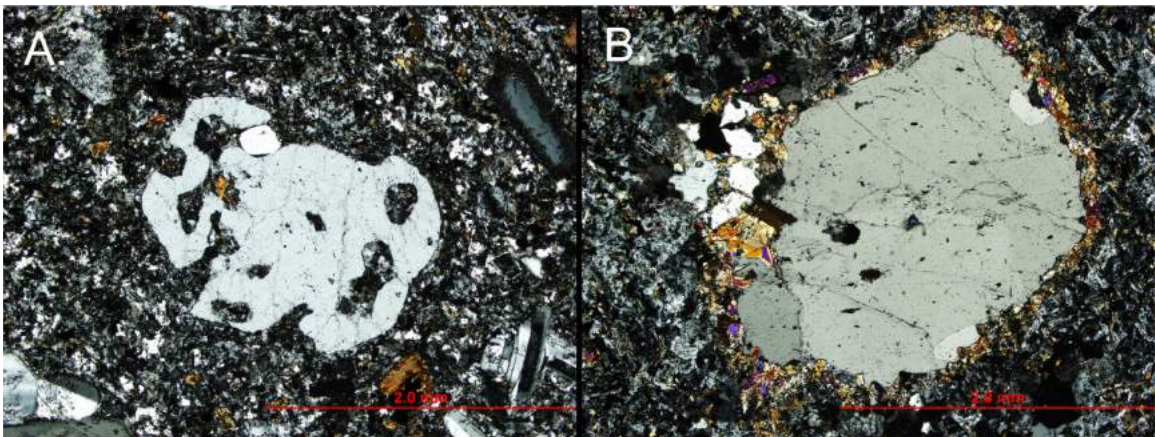
Figure 29. Micrographs of the Walti diorite in cross-polarized light showing textures compatible with magma mixing and disequilibrium. A) Sample KS068, quartz phenocryst with poor integrity and embayments. B) Sample KS067, quartz phenocryst mantled by fine-grained mafic minerals including clinopyroxene, hornblende, and biotite.

Alteration of the Walti diorite matches that of adjacent quartz monzonite. Hornblende and biotite commonly are altered to chlorite, and pyroxene was altered to epidote and actinolite. More calcic and/or endoskarn alteration proximal to marble resulted in high-temperature assemblages containing epidote, diopside, titanite, calcite, and garnet, including rare vesuvianite.

Walti porphyritic intermediate dikes (Twp)

East of the Walti pluton are intermediate porphyritic dacite and andesite dikes (Twp) that cut Paleozoic allochthonous rocks and continue farther east where they cut the Mud Springs pluton (Plate 1). Outcrops are relatively isolated, and dikes are highly variable in terms of their phenocryst assemblage. Generally, outcrops of dikes are traced for only a few 10s of meters along strike. Dikes are generally more altered than their surrounding wall rocks and weather recessively, thus the nature and geometry of their contacts are typically obscure. One dike that cuts the west flank of the Mud Springs pluton is oriented east-west and contains flow features expressed by phenocryst-poor margins and a phenocryst-rich center.

The mineral assemblages in Walti porphyritic dikes are highly variable, but they all share a similar texture of relatively sparse (20-40%) and coarse (1-4 mm) phenocrysts set in an aplitic to microcrystalline groundmass (Figure 13E-F). Phenocryst assemblages generally include plagioclase, orthoclase, quartz, hornblende, and/or biotite in varying amounts and sizes (Table 2). Plagioclase compositions approximated by SEM-EDS are andesine (An_{29-38}), overlapping with compositions from the Walti pluton (Figure 14). Relatively mafic glomerocrysts as 1-5 mm clumps of biotite, hornblende, clinopyroxene, and magnetite are common. Accessory minerals include magnetite, apatite, epidote, and zircon.

Alteration is typically intense across all dike outcrops, bleaching rocks to a tan color and causing them to crop out poorly. Only one occurrence had relatively fresh hornblende. Otherwise, biotite and hornblende are oxidized and altered to chlorite, epidote, and/or calcite. Clinopyroxene where present is typically unaltered. Feldspars can be sericite dusted but are commonly altered to calcite and epidote. Quartz and feldspar phenocrysts commonly have embayments and resorbed rims with sieve textures or alteration to mafic minerals (Figure 30), respectively, suggesting magmatic disequilibrium.
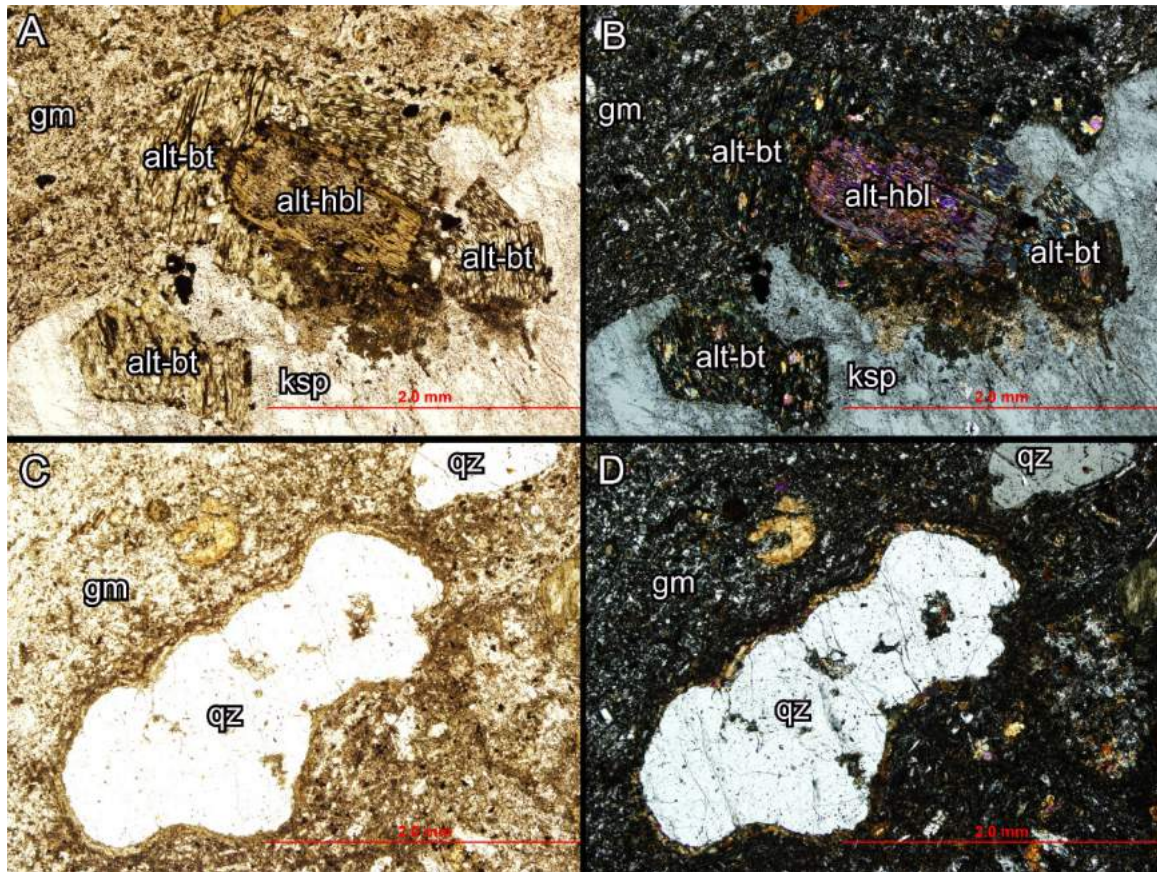
Figure 30. Micrographs of the Walti intermediate porphyritic dikes. A-B) Sample KS095 in plane- and cross-polarized light. The rim of a K-feldspar megacryst is resorbed and altered to mafic minerals biotite and hornblende, which are now mostly altered to chlorite and sericite. C-D) Sample KS095 in plane- and cross-polarized light. Quartz phenocryst rims are resorbed and altered to clinopyroxene and chlorite. The textures in (A-D) are compatible with magma disequilibrium, and suggest the phenocrysts were transported in a relatively mafic melt.

The nomenclature of "Walti porphyritic intermediate dikes" was assigned because of the similarities in texture and phenocryst assemblage with the Walti pluton. Textures are porphyritic with phenocrysts in an aplitic to microcrystalline groundmass. Plagioclase phenocrysts are sparse and typically 1-5 mm, a similar size and distribution of plagioclase in the Walti pluton, in contrast with the smaller and crowded plagioclase phenocrysts of the Mud Springs pluton and nearby andesite and dacite lavas. Another set of dikes 1 km to the north that cut the Valmy and Comus formations feature smaller and abundant feldspar phenocrysts very similar to the andesite lavas of McClusky Creek. Plagioclase compositions in the Walti porphyritic intermediate dikes determined by SEM-EDS are andesine (An_{29-38}), similar to those of the

Walti and unlike the more anorthitic plagioclase of the Mud Springs pluton or adjacent andesite lavas. Quartz (<1 mm) and K-feldspar (0.5-4 mm) phenocrysts, are present in the Walti porphyritic intermediate dikes and are not observed as phenocrysts in the Mud Springs pluton or adjacent andesite and dacite lavas. Finally, the outcrops of dikes with these characteristics only occur east of the Walti pluton and therefore, above it, however they do not cut any of the phases of the Walti pluton itself. These factors suggest the Walti porphyritic intermediate dikes are related to the magmatic system of the Walti pluton.

Rhyolite porphyry (Trp)

In the central part of the study area is a rhyolite porphyry (Trp) exposed over 0.2 km^2. The rhyolite porphyry cuts the Mud Springs pluton to the south and upper plate Paleozoic sedimentary rocks to the north (Plate 1). Prominent joints in the rhyolite strike east-west and are near vertical. Flow-banding and interstitial glass were not observed. The restricted extent, lack of obvious flow lobes and other lava features, and relatively round profile suggest this rhyolite is a steep-sided plug-shaped intrusion and not a lava flow or flow dome.

The Trp rhyolite is porphyritic with 15-25% phenocrysts in a micro- to cryptocrystalline groundmass (Figure 12E-F). Phenocrysts include 1-4 mm plagioclase, 1-2 mm quartz, 0.5-2 mm sanidine, and <1 mm hornblende and biotite (Table 2). Plagioclase composition data by SEM-EDS is sparse but ranged from oligoclase to andesine (Figure 14). Where identifiable, the groundmass is dominantly composed of K-feldspar with less abundant quartz. Less altered rhyolite has a dark gray to black holocrystalline groundmass, while hydrothermally altered rhyolite is bleached white due to sericitic alteration.

Even in the least-altered Trp rhyolite, biotite and hornblende phenocrysts are mostly altered to chlorite and calcite. Identification of biotite and hornblende is possible by habit and presence of vestiges of the original mineral (Figure 31). Plagioclase and sanidine are locally unaffected by alteration. However, pervasive sericite and quartz-sericite alteration is widespread, commonly resulting in nearly complete alteration of feldspar and biotite to sericite. Altered rhyolite porphyry is easily identified as a strongly porphyritic white rock with sericitized feldspars and clear rounded quartz phenocrysts (Figure 32).
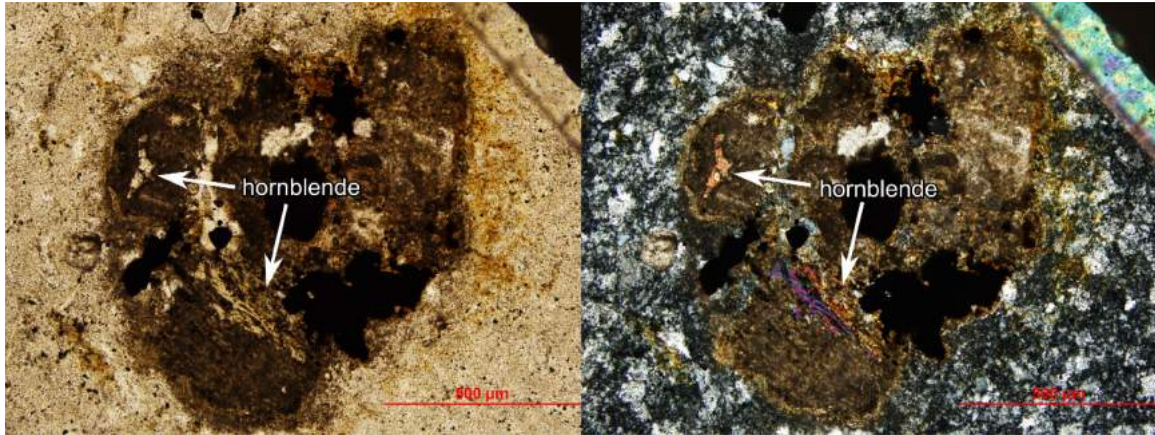
Figure 31. Micrograph of the rhyolite porphyry (sample KS097) in plane- and cross-polarized light. Clump of mafic minerals pervasively altered to clay and calcite. Two fragments of unaltered hornblende remain.
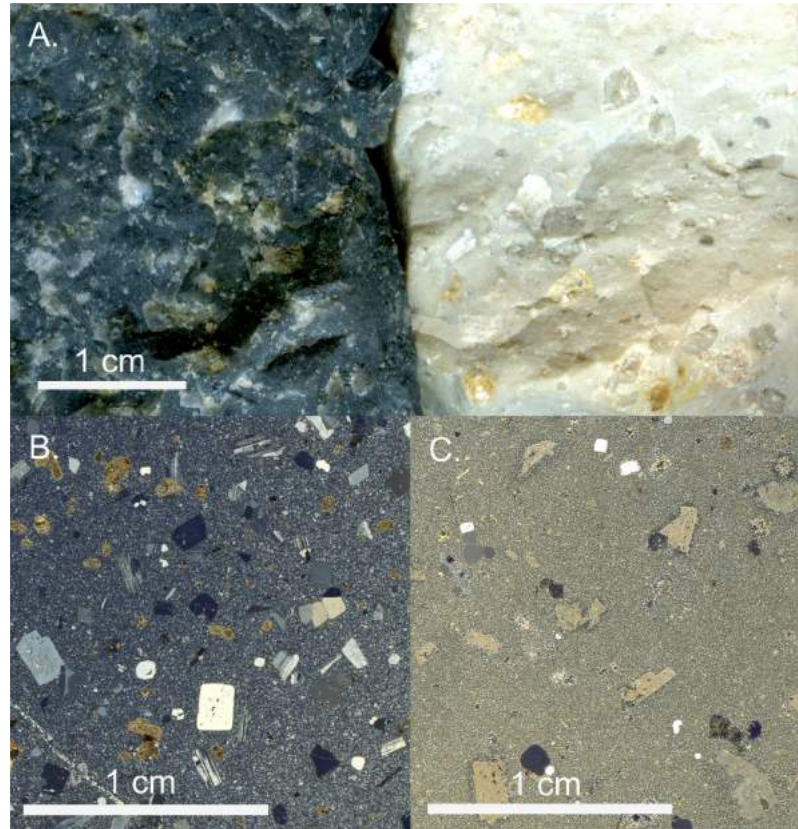
Figure 32. A) Photograph of rhyolite porphyry samples comparing alteration. Left: Sample KS098 has unaltered sanidine and plagioclase, but mafics are chloritized. Right: Sample KS099 is bleached and feldspars are sericitized. Only quartz remains unaffected. B) Micrograph of sample KS98 in cross-polarized light. C) Micrograph of sample KS099 in cross-polarized light.

Trachyandesite dikes (Tta)

To the northwest of the Walti pluton are distinctive, dark green-yellow andesite dikes that cut allochthonous rocks (Plate 1). Outcrops of this andesite were not found elsewhere in the study area. These dikes strike E to NNE, and the longest exposure is approximately 100 meters long.

The andesite is sparsely porphyritic with 10-15% phenocrysts in a micro- to cryptocrystalline groundmass (Figure 12G-H). Its mineral assemblage includes plagioclase as 1-2 mm phenocrysts and as abundant microlites (Table 2). Plagioclase is mostly altered to sericite and clay in all outcrops; composition of plagioclase by EDS was therefore not possible. Mafic minerals are <0.2 mm but completely oxidized and/or chloritized and therefore unidentifiable (Figure 33). The groundmass is heavily altered to chlorite and clay. Geochemistry shows relatively high concentrations of potassium, and on a total alkalis-silica diagram, these dikes plot as trachyandesites as discussed in the geochemistry section. Overall the texture is preserved despite alteration and the Tta unit is distinguished by the paucity of whitened clay-altered plagioclase phenocrysts in a yellow-green aphanitic groundmass.
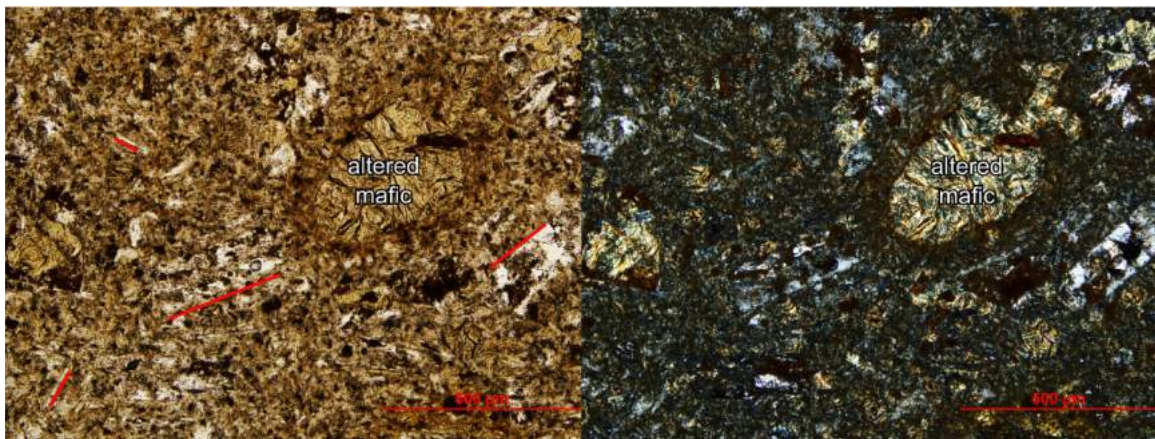
Figure 33. Micrograph of the trachyandesite dikes unit (sample KS025) in plane- and cross-polarized light. All mafic minerals are oxidized and altered to chlorite and clay minerals. Groundmass shows traces of microlitic plagioclase, marked by red lines.

Volcanic rocks

Eocene volcanic rocks crop out mostly on the north and east sides of the study area (Plate 1) and range in composition from intermediate to silicic. Most volcanic rocks are lavas, but some are tuffaceous and/or volcaniclastic in origin. A summary of textures and mineral assemblages is provided in Table 2. Representative examples of volcanics are provided in Figure 34.
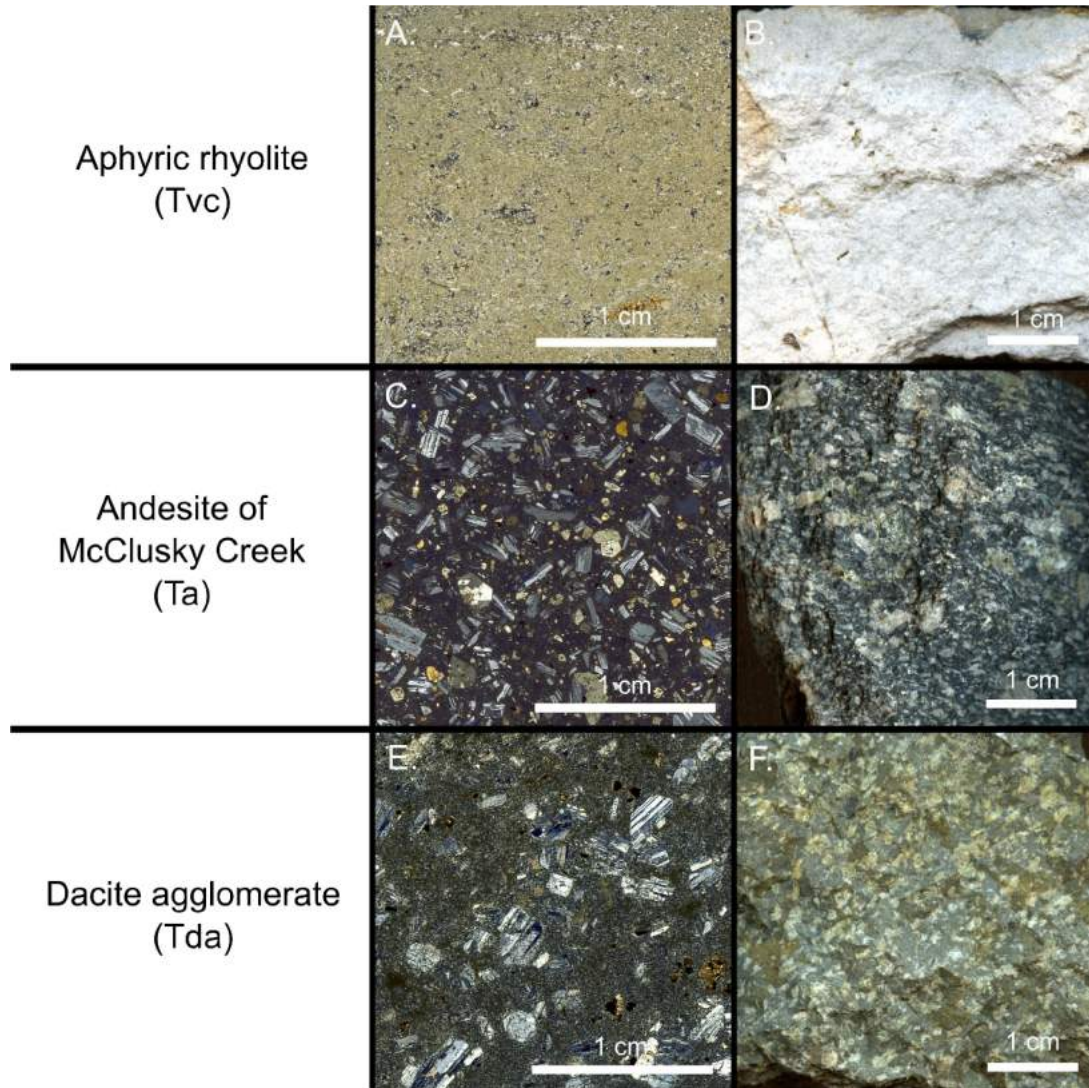
Figure 34. Representative micrographs and photographs of volcanic units. A) Micrograph of the aphyric rhyolite (sample KS050) in cross-polarized light. B) Photograph of the aphyric rhyolite (sample KS050). C) Micrograph of the andesite of McClusky Creek (sample KS144) in cross-polarized light. D) Photograph of the andesite of McClusky Creek (sample KS144). E) Micrograph of the dacite agglomerate (sample KS051) in cross-polarized light. F) Photograph of the dacite agglomerate (sample KS051).

Volcaniclastics and aphyric rhyolite flows (Tvc)

On the low hills west of McClusky Creek are white outcrops of aphyric rhyolite, tuffaceous volcaniclastic rocks, and conglomerate exposed over 0.5 km^2 (Plate 1). Outcrops are generally bleached entirely white with few features to distinguish composition or crystallinity (Figure 34A-B). Some outcrops display chaotic flow-banding indicative of lava flows (Figure 35), whereas others resemble conglomerate or lithic tuff. In the eastern part of the study area, this unit rests on upper plate chert and siltstone, Eocene conglomerate (Tcg), and partly the Mud Springs pluton (Tmd). The volcaniclastics also crop out as probable fault slivers juxtaposed against the northwest margin of the Walti pluton, and farther north, where Tvc rests on upper plate rocks. Outcrops to the northwest do not include aphyric rhyolite but rather consist of poorly sorted, nearly clast-supported, subangular pebble to cobble conglomerate containing clasts of volcanic material as well as chert and quartzite.

Figure 35. Photograph of aphyric rhyolite outcrop with flow banding, suggestive of a lava flow. Hammer is 28 cm long.

Where rhyolite lava, unit Tvc is generally aphyric or has rare fine-grained feldspar and/or biotite phenocrysts that are completely sericitized (Figure 36). No quartz phenocrysts were found, distinguishing this unit from the rhyolite porphyry (Trp). Alteration is pervasive, commonly consisting of a combination of sericitization and silicification; irregular and discontinuous <1 mm quartz veinlets are present as are leached cavities containing euhedral quartz infilling (Figure 36).
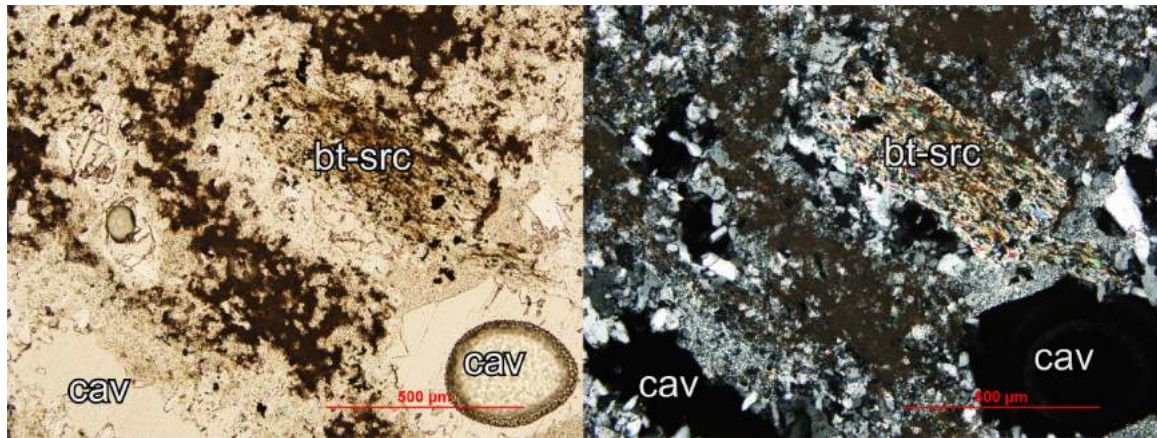
Figure 36. Micrograph of the aphyric rhyolite (sample KS050) in plane- and cross-polarized light. Rare phenocrysts have either been altered to sericite and clay or leached completely. Abbreviations: bt-src=biotite altered to sericite, cav=leached cavity.

Andesite lavas and dikes of McClusky Creek (Ta and Tad)

The andesite lavas of McClusky Creek (Ta and Tad) are exposed from east of the Mud Springs pluton to the northern perimeter of the study area along McClusky Creek (Plate 1). The unit is extensive, covering over 5 km^2, and likely continues for several kilometers to the north and south as suggested by regional mapping and aeromagnetic surveys. The andesite lavas rest on allochthonous Paleozoic sedimentary rocks to the north. Andesite outcrops east of the Mud Springs pluton are in drainage exposures otherwise covered in alluvium (QToa) and hence its contacts are obscured. South of the Mud Springs diorite, the andesite lavas of McClusky Creek rest on the dacite agglomerate (Tda and Tdad). Only Quaternary alluvium rests on the andesite of McClusky Creek in the map area. Some outcrops of the andesite display foliation or local flow banding.

Lavas typically weather maroon brown with platy partings and are porphyritic with ~40 percent phenocrysts in a cryptocrystalline, locally glassy, groundmass (Figure 34C-D). Crystals are fine-grained (mostly <1 mm) and abundant, in contrast with the Walti porphyritic intermediate dikes (Twp) that have larger (up to 4 mm) and fewer phenocrysts (Table 2). Andesite lavas of McClusky Creek have a consistent mineral assemblage that includes plagioclase as both 0.5-2 mm phenocrysts and <0.1 mm microlites. Plagioclase phenocryst composition approximated by SEM-EDS are andesine to labradorite (An$_{42-53}$)

(Figure 14). No quartz or K-feldspar was observed. Mafic minerals include orthopyroxene, clinopyroxene, hornblende, magnetite, and rare biotite. Andesite lavas are largely unaltered and typically have pristine plagioclase and hornblende phenocrysts, although some variability in mineral assemblages exists between flows. Sample KS135 represents an oxidized lava flow with intensely oxidized and weathered orthopyroxene phenocrysts and groundmass minerals. Sample KS144 to the far south has a partly glassy groundmass with local flow banding and abundant <1 mm vesicles.

To the north of the Mud Springs pluton and rhyolite porphyry are several dikes (Tad) that cut rocks of the allochthon. Although all are intensely hydrothermally altered with varying levels of texture destruction, many of the dikes are related to the andesite lavas of McClusky Creek based on lithogeochemistry, discussed later. Those with the least texture destruction are porphyritic in a cryptocrystalline groundmass. Their alteration includes intense to complete sericitization of plagioclase, quartz- and clay-alteration of mafic minerals, and up to 2% disseminated pyrite (<0.3 mm), representing quartz-sericite-pyrite (QSP) alteration assemblage (Figure 37). The sericitized feldspars in the dikes have similar size, shape, and abundance as McClusky andesite lavas and are thus correlated with this unit.
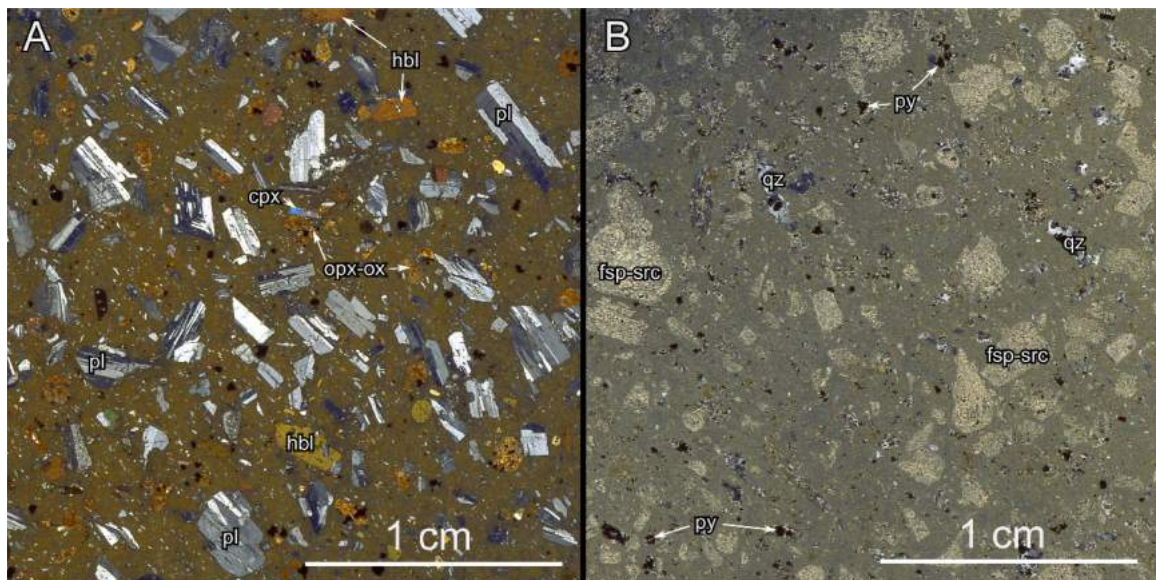
Figure 37. Micrographs of the andesite of McClusky Creek in cross-polarized light. A) Sample KS135 of an oxidized lava. Plagioclase and hornblende remain unaltered, but clinopyroxene and especially orthopyroxene phenocrysts are oxidized. B) Sample KS139 from drill core. Abbreviations: hbl=hornblende, pl=plagioclase, cpx=clinopyroxene, opx-ox=oxidized orthopyroxene, fsp-src=sericitized feldspar (typically illite).

Dacite agglomerate and dikes (Tda and Tdad)

The dacite agglomerate unit (Tda and Tdad) comprises shattered and/or fragmented volcanic material including lavas and breccias that surround the Mud Springs pluton (Plate 1). Their surface exposure is <1 km^2, much smaller than the area underlain by the andesite of McClusky Creek, and agglomerate is restricted to the Mud Springs area. The agglomerate rests on the Mud Springs pluton as well as outcrops of volcaniclastic tuff (Tvc) and upper plate rocks to the west. Both the andesite lavas of McClusky Creek (Ta) and alluvium (QToa) rest on the agglomerate. Drilling adjacent to the rhyolite porphyry intercepted altered dacite agglomerate (Sample KS141) within ~17 m of the surface, which rests on siltstone of the allochthon.

Lava clasts within the agglomerate are porphyritic dacite with 25-30% phenocrysts in a cryptocrystalline groundmass (Figure 34E-F). Phenocrysts are fine-grained (<1 mm) like the McClusky andesite lavas, but sparser. Clast mineral assemblages include plagioclase, clinopyroxene, hornblende, and magnetite. One distinction of the agglomerate from the McClusky andesite is a smaller amount of mafic phenocrysts (<4%) and absence of orthopyroxene (Table 2). Plagioclase phenocrysts tend be rounded with a shattered appearance, suggesting an explosive history (Figure 38). Their composition determined by EDS is andesine to labradorite (An_{41-53}) (Figure 14). Plagioclase microlites were not observed, however alteration may have masked their presence in the groundmass. The agglomerate is locally oxidized and weakly altered to sericite, chlorite, and clay, although most outcrops are strongly affected by weathering to clay. The only intense quartz-sericite-pyrite alteration of the agglomerate was observed in drill 1701C, which intercepted it near the surface.

Dacite agglomerate is also distinguished from McClusky andesite lavas by lithogeochemistry, discussed later. Altered dacite dikes (Tdad) that cut the Valmy and Comus formations to the north, in the vicinity of McClusky andesite dikes (Tad), are correlated with dacite agglomerate using lithogeochemistry and mineralogy.
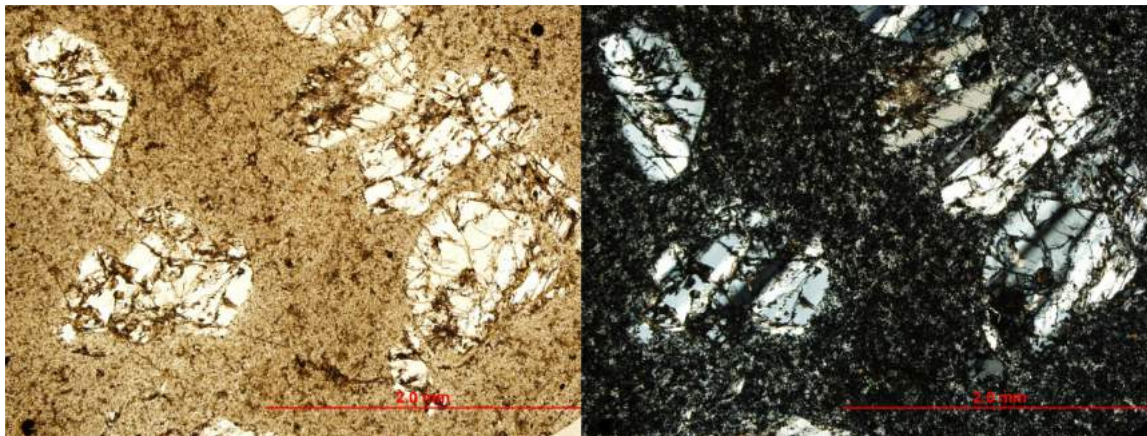
Figure 38. Micrograph of the dacite agglomerate (sample KS051) in plane- and cross-polarized light. Plagioclase phenocrysts are rounded and shattered in the agglomerate.

Quaternary units

Quaternary and Tertiary alluvium (QToa, Qaf, Qal)

On the eastern side of the study area are older, possibly Tertiary, weakly consolidated gravels (QToa; Plate 1) comprised of upper plate siliceous rocks, igneous rocks resembling the Mud Springs pluton, andesite lava, and conglomerates. This older alluvium is incised by modern drainages at the headwaters of McClusky Creek. One drainage has andesite lava of McClusky Creek beneath the old alluvium. The northern and western parts of the study area are covered by Quaternary alluvial fans and alluvium that lead into the Grass Valley alkali flats west of the study area (Plate 1).

Geochemistry

Major elements

Igneous samples were initially separated into altered and unaltered categories based on the presence or not of visible pervasive hydrothermal alteration of primary minerals in both hand samples and in thin section. Primary alteration criteria were based on presence of clay, leaching, and/or silicification of feldspars and matrix. Samples of the intrusive igneous rocks were further distinguished based on the presence of low-temperature acidic hydrothermal alteration versus those with high-temperature sodic-calcic and endoskarn alteration. Furthermore, many Walti pluton samples (including unaltered samples) indicated some level of magma mixing or mingling between different phases and/or some degree of magma disequilibrium supported by the presence of resorbed and unstable primary minerals. These samples were categorized separately from the rest of the groups because of their geochemical variability, which commonly was not related to hydrothermal alteration. A summary table with representative analyses of the least altered rocks is provided in Table 3 and the full dataset is provided in Appendix A.

Major-element geochemistry shows that all unaltered Eocene rocks fall in the high-K calc-alkaline magma series, except the Walti and Mud Springs plutons, which extend into the shoshonite series (Figure 39). Barring a couple of samples, the Gund diorite and andesite lavas of McClusky Creek have lower K_2O and form a separate group, but are still high-K calc-alkaline. Eocene rocks differ substantially in silica and alkali contents from the Ordovician alkaline mafic rocks of the Comus and Valmy formations. The Comus and Valmy basalts are the only mafic rocks at Keystone, whereas the Eocene calc-alkaline rocks all have SiO_2 >59 wt. %. Exceptions to this rule are the trachyandesite dikes (Tta), which are altered and enriched in K_2O (8-11%) and have SiO_2 contents as low as 53 wt. %. In a total alkalis-silica (TAS) diagram, they plot as a trachyandesite (Figure 40). All Eocene igneous rocks plot as metaluminous to weakly peraluminous (Figure 41). The dacite agglomerate is strongly peraluminous compared to other Eocene rocks. Samples of the trachyandesite and silicic volcaniclastic rocks are altered and likely not representative.

Table 3. Representative geochemical analyses of igneous units. Full dataset provided in Table A1.

Sample ID	KS111	KTC 426	KS078	KS098	KS137	KS041	KS105	KTC 344	KS047	KS052	KS051	KS022
Abb.	Tmd	Tmp	Tgd	Trp	Twq	Twd	Twp	Tta	Tvc	Ta	Tda	Ovb
Unit	Mud Springs diorite	Mud Springs peg.	Gund diorite	Rhyolite porphyry	Walti quartz monz.	Walti diorite	Walti int. porph. Dikes	Trachy-andesite dikes	Aphyric rhyolite	Andesite of McClusky Creek	Dacite agglom.	Valmy basalt
SiO_2	62.21	75.51	61.90	71.93	68.12	61.75	64.73	53.64	82.86	64.44	67.54	48.90
Al_2O_3	15.97	14.11	17.04	13.99	15.25	17.20	15.89	18.97	11.75	16.44	16.68	16.44
$FeO*$	5.63	0.74	5.57	2.62	3.49	5.74	4.59	9.26	2.04	4.65	3.04	9.99
CaO	5.29	1.05	4.49	2.01	2.75	4.90	4.06	1.41	0.24	4.70	3.34	8.14
MgO	3.00	0.10	2.79	0.75	1.63	2.23	2.06	4.94	0.38	1.98	0.82	6.47
Na_2O	2.53	3.49	2.90	3.34	3.34	3.37	3.01	0.21	0.07	3.49	3.46	4.48
K_2O	3.80	4.74	3.66	4.78	4.46	3.18	4.37	9.44	2.38	3.03	4.23	1.26
Cr_2O_3	0.01	0.01	0.01	0.01	0.01	0.01	0.01	0.01	0.01	0.01	0.01	0.02
TiO_2	0.93	0.05	0.88	0.29	0.55	0.91	0.78	1.23	0.12	0.70	0.41	2.96
MnO	0.10	0.04	0.10	0.07	0.07	0.11	0.08	0.09	0.01	0.08	0.07	0.14
P_2O_5	0.30	0.09	0.34	0.10	0.15	0.36	0.21	0.43	0.07	0.26	0.15	0.81
SrO	0.07	0.02	0.09	0.03	0.05	0.08	0.06	0.02	0.01	0.07	0.06	0.14
BaO	0.16	0.05	0.23	0.09	0.13	0.15	0.14	0.36	0.05	0.14	0.19	0.26
LOI	1.58	0.82	2.08	0.79	0.84	1.24	3.2	6.62	3.62	2.86	2.07	3
Total	98.64	100.49	100.1	100.76	99.28	100.97	98.69	99.28	98.68	101.28	101.3	99.56
C %	0.02		0.01	0.06	0.05	0.04	0.25		0.08	0.27	0.11	0.02
S %	0.09		0.07	0.02	0.03	<0.01	0.01		0.01	<0.01	<0.01	0.01
Ag	<0.5	0.25	<0.5	<0.5	<0.5	<0.5	<0.5	<0.5	<0.5	<0.5	<0.5	<0.5
As	21.8	5	6.3	2	0.9	2	2	26	53.5	0.4	0.9	8.1
Ba	1280	432	2060	707	1275	1360	1145	2960	401	1135	1560	2260
Bi	0.2		0.02	0.09	0.02	0.03	0.02		0.09	0.01	0.02	0.01
Cd	<0.5	0.25	<0.5	<0.5	<0.5	<0.5	<0.5	0.5	<0.5	<0.5	<0.5	0.7
Ce	100.5	27.9	83.9	59.1	106.5	96.7	102	63.6	75.3	79.2	108.5	113.5
Co	15	0.5	10	4	9	10	11	18	2	9	4	34
Cr	60	10	20	30	30	10	30	20	10	10	20	130
Cs	1.92	0.83	22.5	3.36	8.52	5.85	2.29	1.86	4.71	1.64	1.68	2.04
Cu	8	2	8	9	6	6	12	10	5	8	5	35
Dy	4.26	1.96	3.74	3.1	3.28	4.56	3.48	5.02	2.52	3.05	4.12	5.82
Er	2.3	1.63	1.88	1.69	1.62	2.52	1.94	2.95	1.43	1.76	2.2	2.55
Eu	1.6	0.5	1.65	0.8	1.35	1.65	1.37	1.42	0.96	1.36	1.66	3.03
Ga	20.5	28.1	21.7	18.7	21.7	25.2	19.9	20.1	14.8	19.7	21.4	23.5
Gd	5.72	1.96	5.54	3.67	4.37	6.16	4.78	5.45	3.25	4.16	5.22	8.52
Ge	<5		<5	<5	<5	<5	<5		<5	<5	<5	<5
Hf	7.2	2.3	5.8	3.9	5.6	6.6	6.3	4.5	3.6	5.5	8.3	7.4

Sample ID	KS111	KTC 426	KS078	KS098	KS137	KS041	KS105	KTC 344	KS047	KS052	KS051	KS022
Abb.	T md	T mp	T gd	T rp	T wq	T wd	T wp	T ta	T vc	T a	T da	Ovb
Unit	Mud Springs diorite	Mud Springs peg.	Gund diorite	Rhyolite porphyry	Walti quartz monz.	Walti diorite	Walti int. porph. Dikes	Trachy-andesite dikes	Aphyric rhyolite	Andesite of McClusky Creek	Dacite agglom.	Valmy basalt
Hg	<0.005		0.01	<0.005	0.005	0.009	<0.005		0.024	0.04	0.006	0.02
Ho	0.82	0.45	0.77	0.61	0.6	0.88	0.7	1.03	0.5	0.6	0.79	1.04
In	0.014		0.014	0.021	0.022	0.021	0.02		0.008	0.033	0.028	0.043
La	51.7	14.8	45.4	30.7	62.2	50.9	55.5	31.3	38.9	42.4	58	57.1
Li	10	10	20	10	30	10	20	20	20	10	10	40
Lu	0.32	0.35	0.25	0.25	0.26	0.32	0.29	0.44	0.25	0.27	0.3	0.32
Mo	1	0.5	2	3	4	1	1	3	2	2	2	2
Nb	16.4	4.5	12.4	16.1	17.3	16.1	15.5	10.9	13	10.6	13.7	54
Nd	40.4	11.7	38.9	23.7	38.8	42.7	37.3	32.9	28.4	29.8	41.3	53.4
Ni	8	1	2	2	7	1	9	8	5	1	2	67
Pb	13	22	18	23	23	16	14	9	9	22	21	4
Pr	11.7	3.14	10.5	6.63	11.4	11.4	11.3	8.37	8.56	8.87	12.25	13.5
Rb	104	124	120	168.5	172.5	99.4	149	206	82.9	80.6	124	23.1
Re	<0.001		<0.001	<0.001	<0.001	<0.001	<0.001		<0.001	<0.001	<0.001	<0.001
Sb	1.24		0.73	0.23	0.12	0.17	0.22		1.06	0.05	0.07	0.62
Sc	11	1	11	5	6	10	8	19	3	8	4	17
Se	<0.2		<0.2	0.3	<0.2	<0.2	0.2		0.8	<0.2	0.2	0.8
Sm	7.6	2.42	6.8	4.9	6.66	7.8	6.41	6.78	5.3	5.43	7.38	10.55
Sn	1	1	2	3	2	2	2	1	1	1	2	4
Sr	581	257	755	260	514	719	501	201	50.4	593	543	1095
Ta	0.9	0.2	0.8	1.3	1.3	1	1.2	0.5	0.8	0.6	0.9	3.4
Tb	0.79	0.29	0.72	0.59	0.59	0.86	0.62	0.83	0.45	0.57	0.74	1.12
Te	<0.01		<0.01	<0.01	<0.01	<0.01	<0.01		0.03	<0.01	<0.01	0.04
Th	17.15	4.06	12.65	16.3	27.7	16.85	22.8	7.73	11.8	11.25	18.2	6.96
Tl	0.05	5	0.15	0.21	0.28	0.34	0.06	<10	0.39	<0.02	0.04	0.08
Tm	0.37	0.26	0.28	0.24	0.25	0.37	0.28	0.44	0.23	0.27	0.32	0.37
U	3.64	5.54	3.02	5.34	5.71	3.18	4.46	4.31	3.27	2.32	3.31	1.9
V	118	6	122	33	67	113	95	225	6	99	32	219
W	1	1	1	1	1	1	2	18	1	1	1	1
Y	23.8	13.2	20.2	17.5	18.2	24.6	19.9	28.5	14.7	17.8	22.6	26.5
Yb	2.22	2.2	1.83	1.68	1.77	2.4	1.95	2.86	1.53	1.76	2.05	2.1
Zn	48	34	58	62	69	99	68	89	58	85	71	112
Zr	288	55	227	134	213	261	241	181	117	225	345	321

Major oxides are reported in weight percent normalized to 100% anhydrous. "Total" field refers to original analysis. Trace elements contents are in parts per million.
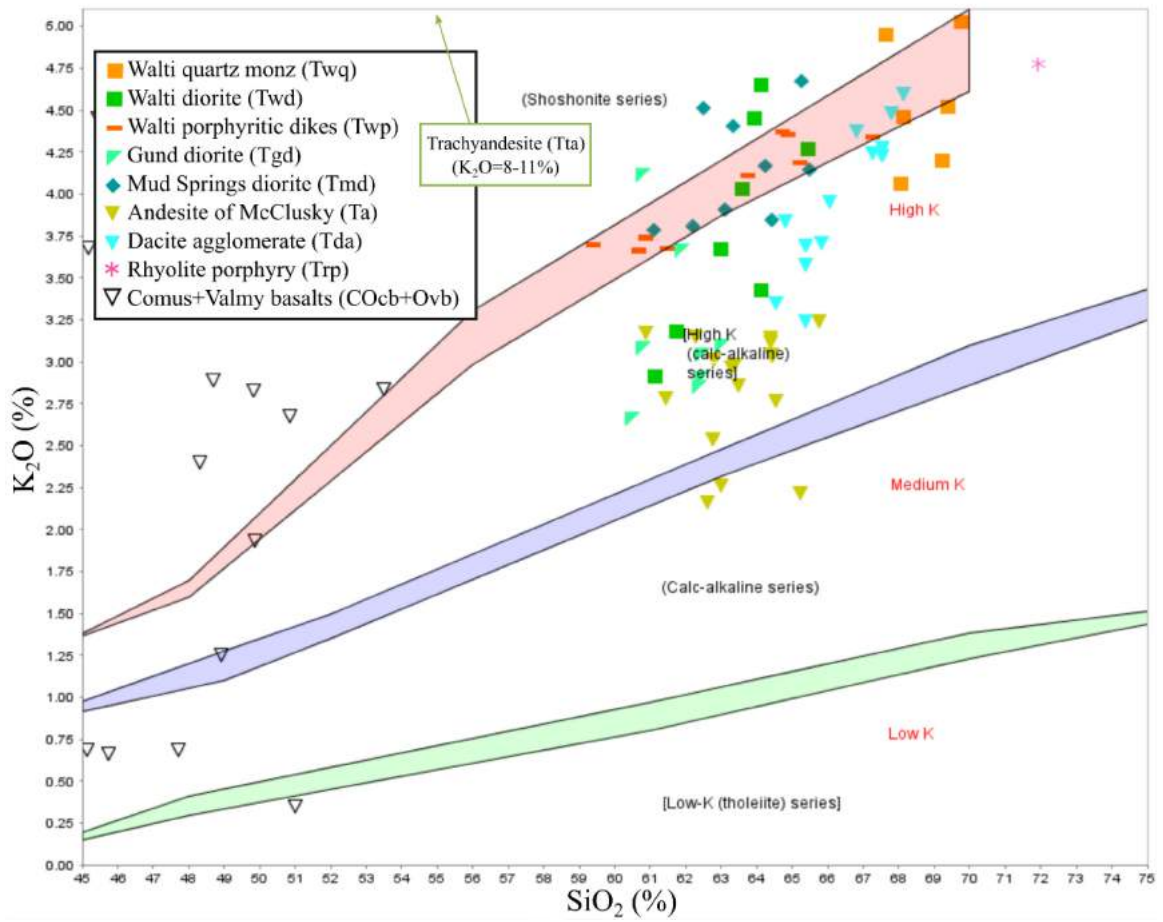
Figure 39. K$_2$O vs SiO$_2$ plot from Le Maitre et al. (1989). Altered samples omitted for clarity. A very large compositional gap is present between Paleozoic basalts and Eocene rocks, which are intermediate to felsic and plot as high-K calc-alkaline to shoshonitic magma series. The trachyandesite dikes (Tta) are more mafic than other Eocene rocks but highly altered with enriched K$_2$O, plotting outside the diagram.
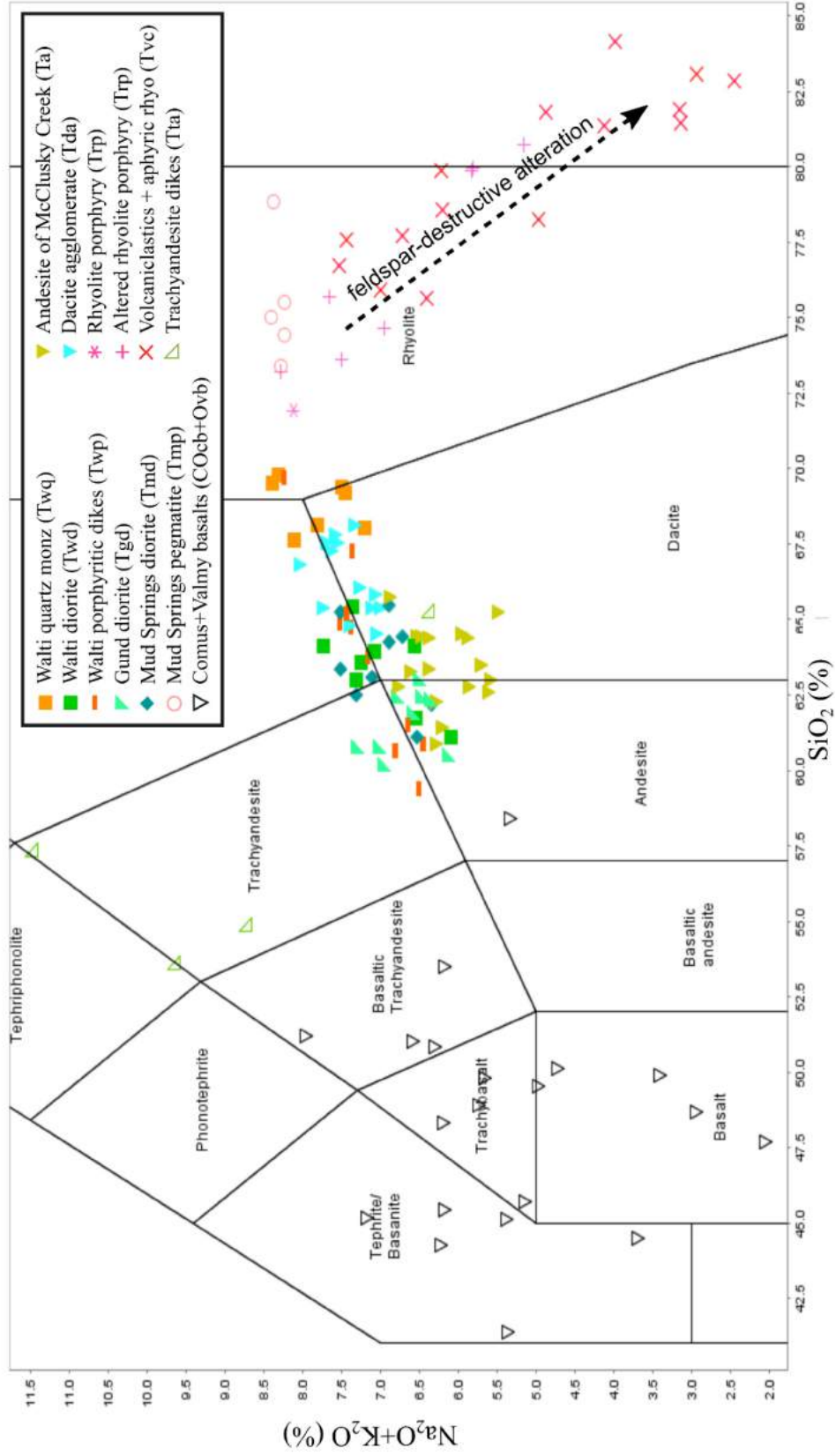
Figure 40. Total alkalis-silica diagram (Le Bas et al., 1986). Most altered rocks omitted for clarity. Altered samples of the rhyolite porphyry unit (Trp) and the volcaniclastics unit (Tvc) are included to show spread of silica content and differentiation trend. Early Paleozoic basalts of the Comus and Valmy formations show variability due partly to spilitization. Samples of trachyandesite dikes are Eocene but fall off the calc-alkaline differentiation trend due to intense alteration and enrichment in K_2O.
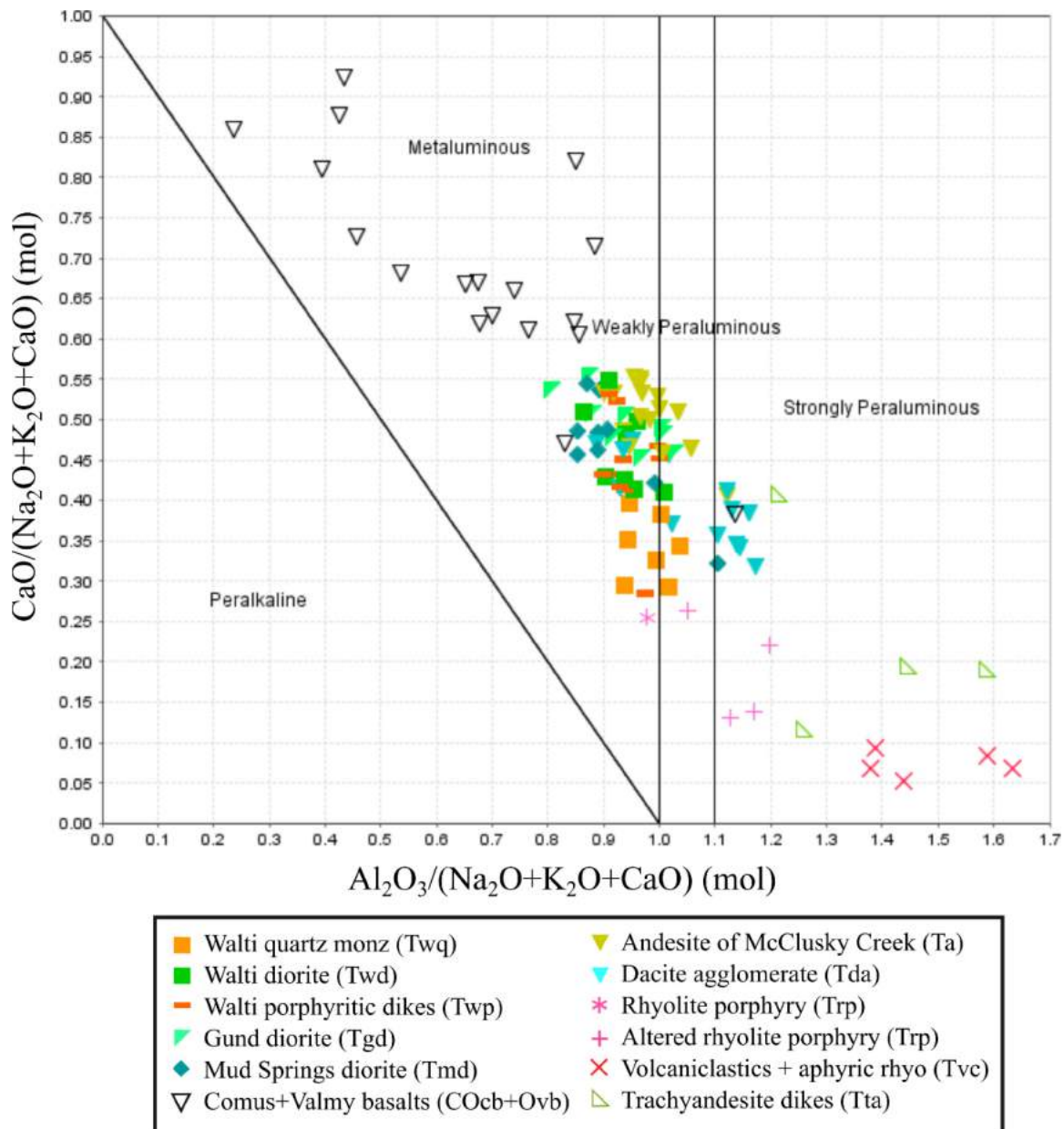
Figure 41. Plot of alumina saturation index (Frost and Frost, 2008) using molar CaO/(Na$_2$OK$_2$O+Cao) vs. Al$_2$O$_3$/(Na$_2$O+K$_2$O+CaO). Eocene igneous rocks are metaluminous to weakly peraluminous. Dacite agglomerate (Tda) is distinctly peraluminous. Samples of the rhyolite porphyry (Trp altered), volcaniclastics (Tvc) and trachyandesite (Tta) units are altered and have lost Na, Ca, ± K relative to alumina and are thus, are not represented correctly.

Aside from the Ordovician Comus basalts and probable Eocene trachyandesite, the remaining

igneous rocks at Keystone, which are all Eocene and locally sourced, show relatively tight differentiation

trends in TAS and other variation diagrams of major elements, especially for Ti, Ca, and P (Figure 42). The

most siliceous rocks are pegmatites within the Mud Springs pluton (Tmd) and the volcaniclastics and aphyric rhyolite of unit Tvc. The volcaniclastics have >75 wt. % SiO_2, however all samples of volcaniclastics show intense clay and silica alteration, which is demonstrated by the decreasing alkali content with higher silica content. The rhyolite porphyry is also mostly altered and shows the same silica enrichment pattern, however one relatively unaltered sample (KS098) shows it is likely the most felsic unit at Keystone with 72 wt. % SiO_2.
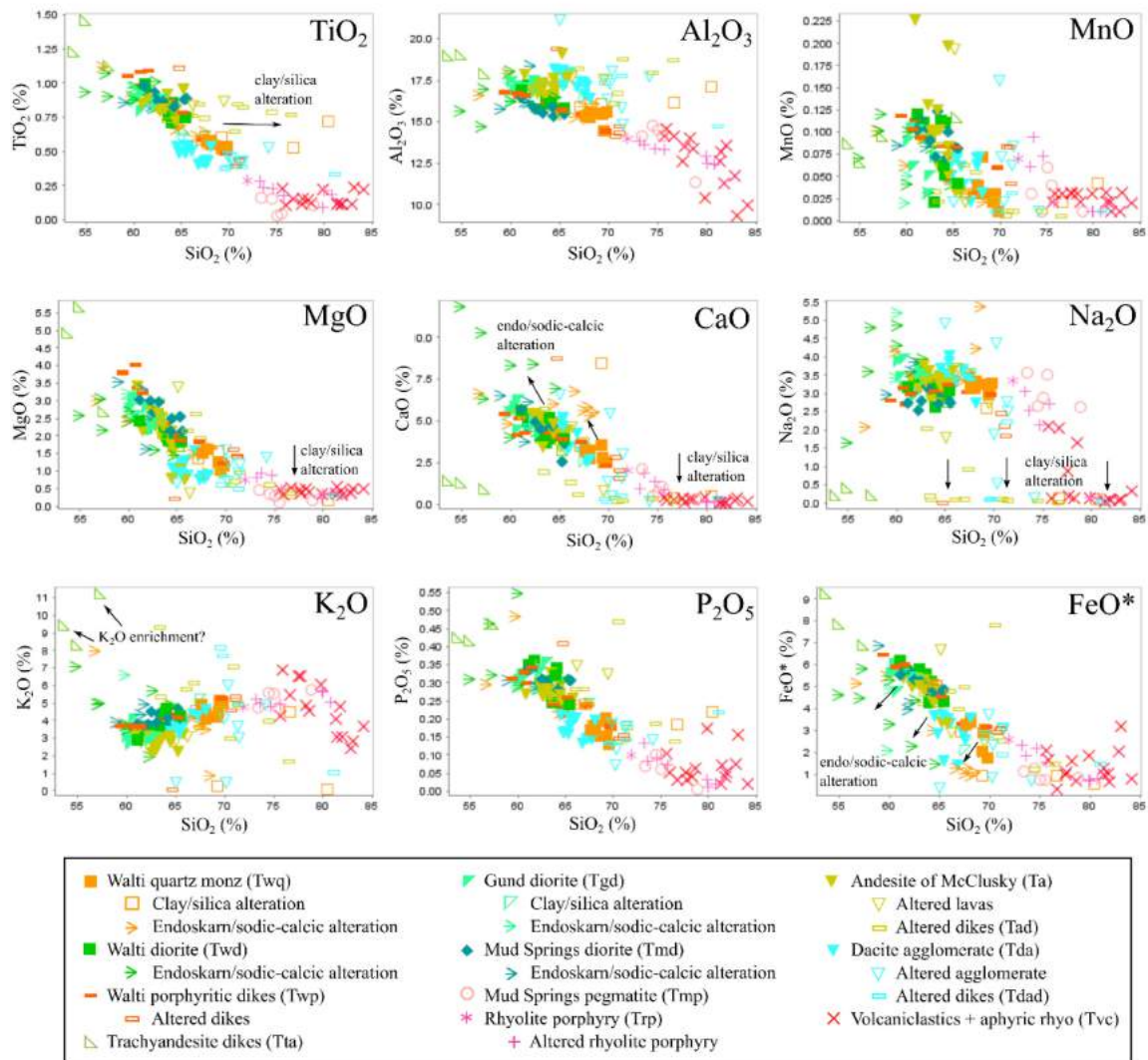
Figure 42. Major elements vs. SiO_2 plots for unaltered Eocene rocks at Keystone; patterns generally follow a differentiation trend across all elements. Rocks affected by low-temperature clay/silica alteration show depletion in alkalis and relative enrichment in SiO_2. Rocks affected by high-temperature endoskarn/sodic-calcic alteration show relative depletion in SiO_2 and FeO and enrichment in CaO. Trachyandesite dikes show unusual geochemical alteration with depletion in alkalis CaO and Na_2O, but relatively high MgO and K_2O.

The Walti pluton has quartz monzonitic to granodioritic phases (Twp) that range from 67-70 wt. % SiO_2, whereas the dioritic phases (Twd) range from 61-65 wt. % SiO_2. There is no chemical composition overlap or gradation between the intermediate and felsic phases of the Walti pluton, however samples with mixing or mingling textures fill this gap (Figure 43). The Walti intermediate porphyritic dikes (Twp) have a wide range of SiO_2 content (59-70 wt. %) which reflects their variable phenocryst assemblage and petrographic evidence of magma disequilibrium. The Mud Springs diorite overlaps with the Walti diorite chemically, and the Gund diorite is the most mafic pluton with 60-63 wt. % SiO_2. Magma mixing, mingling, and disequilibrium affected many Walti pluton samples, and thus their geochemistry is highly variable and difficult to characterize. Sodic-calcic and endoskarn alterations are common in the Walti and Gund plutons, and are expressed as enrichment in Na, Ca, P, and K, with depletion in Si and Fe. This alteration can also cause an apparent alkaline and slightly more mafic character with SiO_2 as low as 54.8 wt. % (Figure 43).
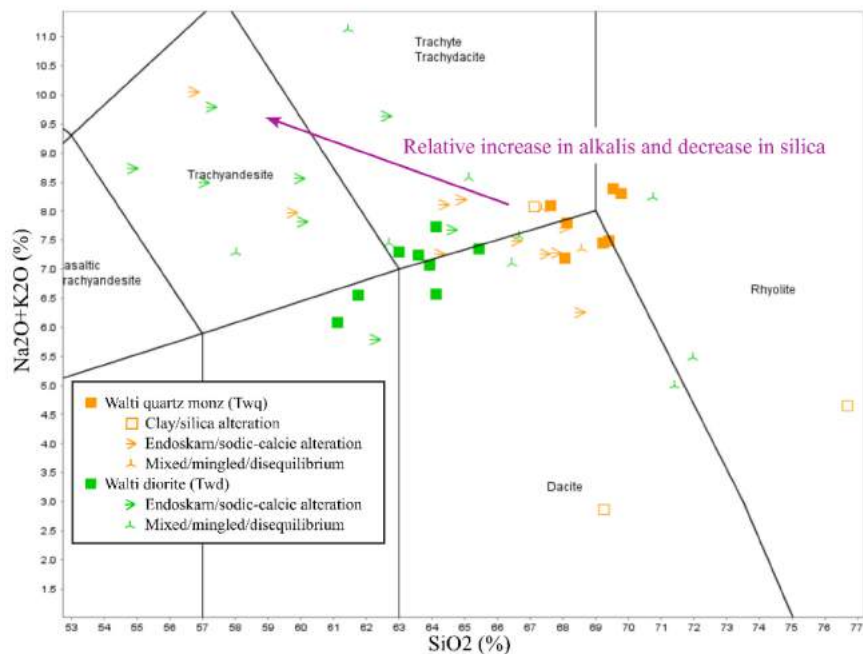
Figure 43. Total alkalis-silica diagram of Walti pluton samples only. Included are samples affected by low-temperature clay/silica alteration and high-temperature endoskarn/sodic-calcic alteration. Also included are samples with petrographic evidence of magma mixing/mingling and/or magma disequilibrium, resulting in variable geochemistry. Samples affected by endoskarn or sodic-calcic alteration show a relative increase in alkalis and decrease in silica.

Andesite lavas of McClusky Creek are relatively unaltered and range from 59-65 wt. % SiO_2. Although their geochemical composition ranges from andesite to dacite, their phenocryst assemblage of orthopyroxene, clinopyroxene, and plagioclase would classify them more appropriately as andesite. Much of the silica and alkalis are therefore likely in the groundmass. The dacite agglomerate is notably more felsic than the lavas of McClusky Creek and ranges from 64-68 wt. % SiO_2.

Hydrothermal alteration of igneous rocks is commonly expressed by partial removal of Na, Mg, and Ca; removal of K is less common. Alteration can also cause apparent enrichment in SiO_2, best shown in TiO_2 and Al_2O_3 variation diagrams where leached samples that have undergone feldspar-destructive alteration have shifted to the right of their respective unit's cluster (Figure 42). Intense low-temperature acidic alteration affected all samples of the volcaniclastics and aphyric rhyolite unit (Tvc) as well as most samples of the rhyolite porphyry (Trp). Dikes of andesite of McClusky Creek (Tad) and the dacite agglomerate (Tdad) are similarly intensely altered and show pervasive sodium removal, but the Walti intermediate porphyritic dikes (Twp) are relatively less altered. Pervasive chlorite and clay alteration of the trachyandesite (Tta) was observed in every sample and is reflected by depletion in sodium. However, these rocks also have the highest K_2O, suggesting they may have originally been more alkaline than other Eocene rocks at Keystone, or underwent a unique magmatic and/or alteration history.

Trace and immobile elements

Although alkalis can be added or removed depending on the style of alteration, other elements such as high-field strength elements (HFSE; e.g. Zr, Ti, Hf, Nb, Th) are rarely added during hydrothermal transport. HFSEs tend to resist mobilization by hydrothermal activity, because they are contained in resistive minerals such as zircon, rutile, and apatite. Such HFSEs are therefore considered immobile (Cann, 1970; Pearce, 1996; Pearce, 2014). With leaching and mass loss, however, relatively immobile elements become enriched from their primary concentrations and are thus important in assessing mass balance. Variation diagrams of HFSE can be useful for identifying cogenetic igneous rocks that share magmatic geochemical differentiation trends (Figure 44). Although all Eocene rocks appear to roughly follow the same differentiation trend in terms of SiO_2 and P_2O_5, plots of other elements reveal certain units have

separate trends or clusters and therefore, indicate rocks that are not cogenetic; such geochemical disparity is supported by field relations, petrography, and geochronology that indicate complex variability in composition and age. For example, the dacite agglomerate unit is off the main differentiation trend in an Al_2O_3 vs. TiO_2 plot, and is also distinctly different than the andesite lavas of McClusky Creek and the Walti quartz monzonite phase. The geochemical distinction of the dacite agglomerate is also strongly apparent in Hf and Zr. The Mud Springs diorite also shows trends inconsistent with cogenetic magmas, best demonstrated in Hf, Nb, and Zr (Figure 44). A general lack of linear differentiation trends likely reflects the complex open-system nature of magmatism that involved episodic intrusion, variable storage, and extensive hybridization. Another interesting feature in these plots is the repeated overlap between the Gund diorite and andesite lavas of McClusky Creek, allowing for a possible cogenetic relationship. The Walti intermediate porphyritic dikes show a spread of compositions across different trace elements, which likely reflects their variable phenocryst assemblage and petrographic evidence of magma disequilibrium. An inset plot of Al_2O_3 vs. TiO_2 that includes the Comus and Valmy basalts shows they do not share any differentiation trend with Eocene rocks (Figure 44). The lack of any geochemical relationship between the basalts and all other Eocene rocks attests to their unique magmatic history unrelated to Eocene arc magmatism as supported by field relations, biostratigraphy, and isotopic dating.

Geochemical fingerprints can be further explored by considering a Nb/Zr vs. SiO_2 plot (Figure 45). As mafic to intermediate magmas fractionate during crystallization the Nb/Zr ratio will generally not change. The mutual incompatibility of Nb and Zr is therefore useful for the identification of distinct magma sources. Furthermore, hydrothermal alteration will have little impact on the Nb/Zr ratio because of their relative immobility. However, sequestration of zirconium by crystallization of zircon can have a significant impact on the Nb/Zr ratio of felsic rocks. This is shown by increased Nb/Zr in rocks with SiO_2 >68%. The Walti quartz monzonite, Walti intermediate porphyritic dikes, Mud Springs pegmatite, rhyolite porphyry, and volcaniclastics units, show progressive increase in Nb/Zr with SiO_2. Altered andesitic lavas and dikes that are silicified and therefore have higher SiO_2 than corresponding fresh rocks do not show this behavior and preserve their "andesitic" Nb/Zr ratio.
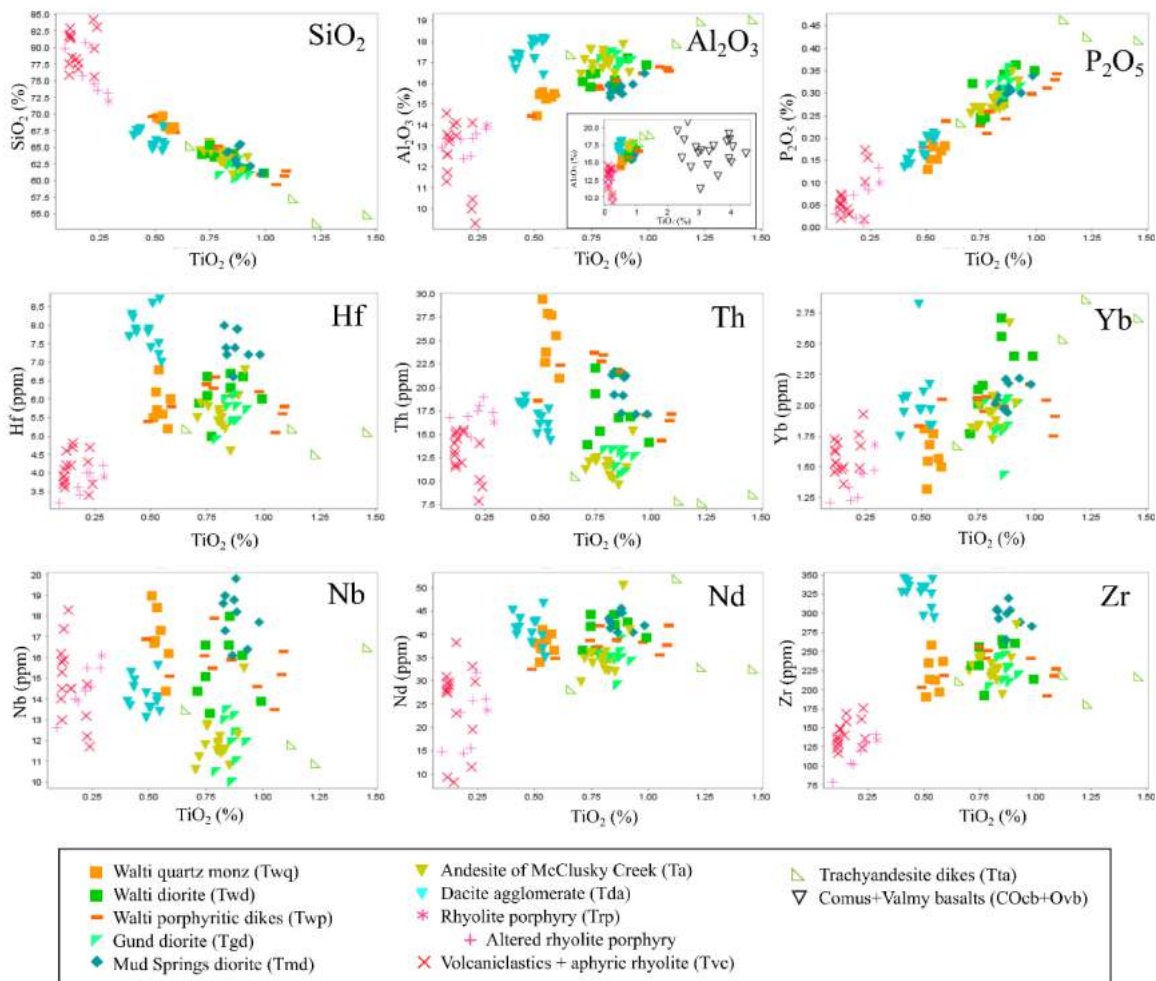
Figure 44. Select major and trace elements vs. TiO$_2$. Unaltered Eocene rocks at Keystone generally follow a differentiation trend for only SiO$_2$ and P$_2$O$_5$. All others show deviations or separate clusters. The dacite agglomerate (Tda) and Mud Springs diorite (Tmd) best show their separation in Hf, Nb, and Zr. The Gund diorite (Tgd) and andesite lavas of McClusky Creek (Ta) tend to overlap and form a cluster. The Walti intermediate porphyritic dikes (Twp) show a spread of compositions that follow a trend, likely reflecting their variable phenocryst assemblage and magma disequilibrium by mixing. Comus and Valmy basalts do not share any differentiation trend with Eocene rocks and were omitted for clarity. An example of their composition is shown as an inset plot of Al$_2$O$_3$ vs. TiO$_2$.
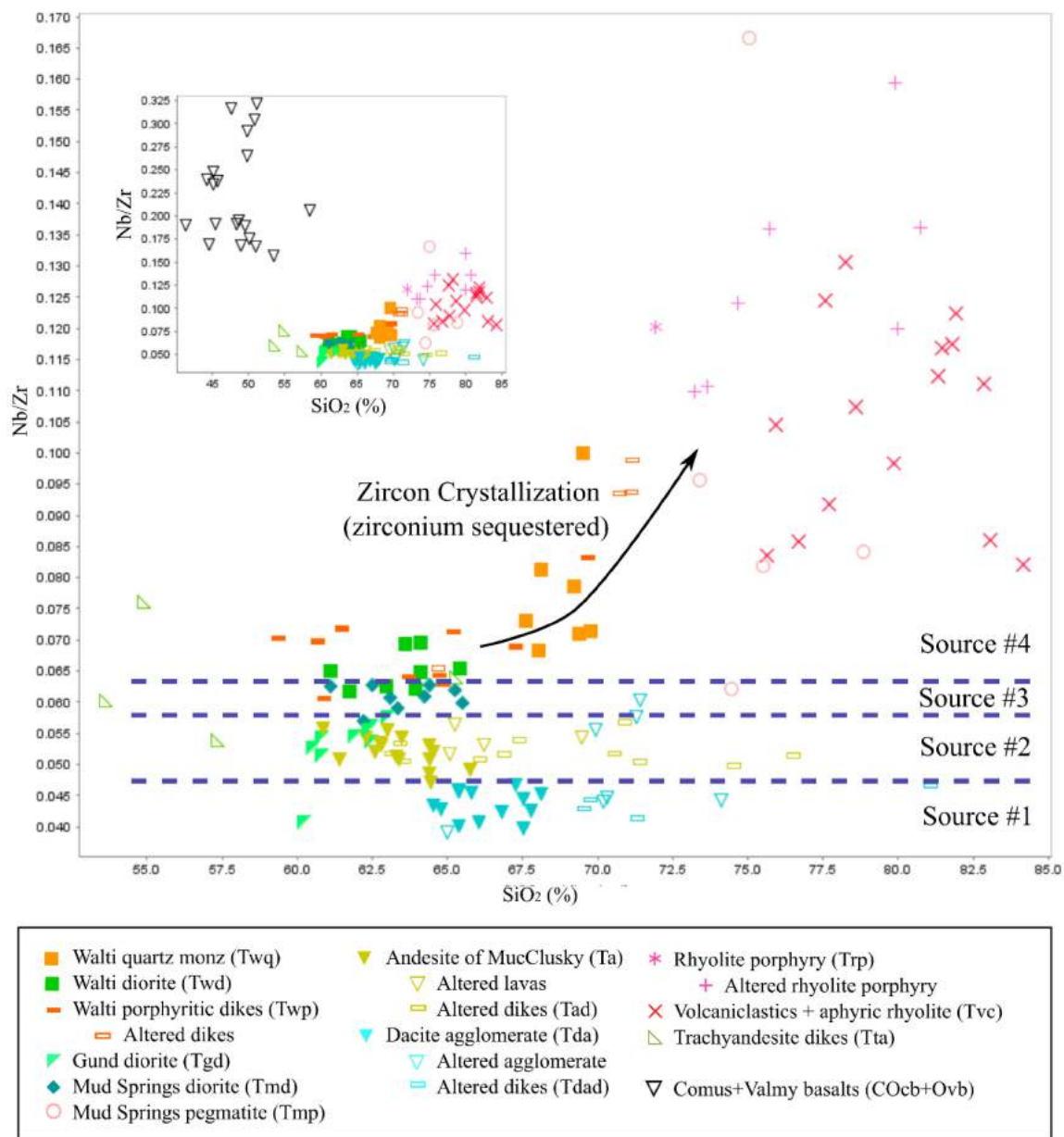
Figure 45. Plot of Nb/Zr vs SiO₂. Inset figure shows distribution of Comus and Valmy basalts. Felsic rocks show increasing Nb/Zr ratio because of sequestration of Zr by crystallization of zircons. Otherwise, Nb/Zr ratios of units are relatively stable as varying degrees of partial melting of a source of magmatic differentiation will affect both Nb and Zr equally. Furthermore, hydrothermal alteration tends to not affect the Nb/Zr ratio. To investigate the diverse magmatic history of Eocene igneous rocks at Keystone, possible magmatic sources are outlined by dashed lines. See text for further explanation.

The dacite agglomerate unit has Nb/Zr ratios <0.047 which distinguish it from the lavas of McClusky Creek unit (Figure 45, "Source #1"). Exceptions to this are three samples with Nb/Zr ratios of 0.055-0.060 (samples KTC012, KTC013, KTC051). These samples were collected by Tom Chapin from two outcrops not visited by the author. One outcrop was interpreted as a separate tuff unit underlying the dacite agglomerate, and the other is an isolated outcrop of lava resting on the Mud Springs diorite. Explanations for their unique Nb/Zr ratio include incorporation of material from wall rocks or other volcanics, or they could represent a separate flow or eruption that is difficult to resolve from the dacite agglomerate from hand sample or petrography. Aside from these three samples, the Nb/Zr ratio was useful for classifying altered dikes and their volcanic counterparts. Lavas of the dacite agglomerate can appear similar to andesite lavas of McClusky Creek in hand sample, although differences between the two are immediately apparent under petrographic microscope, such as the shattered and rounded nature of plagioclase in the dacite. To the north of the rhyolite porphyry are intensely altered dikes that cut the Comus and Valmy formations. These dikes were also intercepted by drilling and are pervasively altered to sericite and/or clay, prohibiting identification of primary mineral assemblages. Their textures resemble both the dacite agglomerate and andesite lavas. The Nb/Zr ratio of these altered dikes was therefore used to associate them with either the dacite agglomerate or the andesite lavas of McClusky Creek. Furthermore, the Nb/Zr ratios are unlike those of the Walti intermediate porphyritic dikes, which have a Nb/Zr ratio closer to the Walti pluton.

Similar to observed overlapping trace-element compositions (Figure 44), the Gund diorite and andesite of McClusky Creek overlap in Nb/Zr ratios from 0.047 to 0.057 (Figure 45, "Source #2"), suggesting a shared source and/or magmatic history. One exception is sample KS114B, which has a much lower Nb/Zr ratio of 0.040. This sample came from an outcrop of the Gund diorite adjacent to marble and with a coarser texture and greater abundance of biotite phenocrysts. The unique Nb/Zr suggests this outcrop is separate from the Gund diorite, and is unlike other igneous rocks at Keystone; it may also have undergone metasomatic exchange with marble. Samples of the Mud Springs diorite have Nb/Zr ratios of 0.057 to 0.063 and have little overlap with samples from the Gund or Walti plutons (Figure 45, "Source #3"). The Walti pluton and Walti intermediate porphyritic dikes have the highest Nb/Zr ratios before being

affected by zirconium sequestration at SiO_2 >68% (Figure 45, "Source #4"). Samples of the trachyandesite dikes have scattered Nb/Zr ratios and do not fall into any single outlined "source".

A plot of Zr/Ti vs. Nb/Y from Pearce (1996) can offer insight into the trachyandesite dikes unit (Figure 46). This discrimination diagram was modified from the original diagram by Winchester and Floyd (1977) and intended for discrimination of unknown basalts affected by weathering or metamorphism. The Zr/Ti ratio is steady during crystallization of mafic magmas until magnetite, titanite, or hornblende fractionate, thereby sequestering Ti while Zr continues to increase in the melt. Thus, felsic rocks will have a higher Zr/Ti ratio than mafic rocks, demonstrated by the upward trend from andesites and diorites to the rhyolite porphyry. The trachyandesite dikes have relatively low Zr/Ti and could therefore be considered basalt or basaltic andesite.

Higher Nb/Y ratios are commonly interpreted to reflect lower mantle partial melt fractions and/or source enrichment, resulting in a more alkaline character. The Ordovician Comus and Valmy basalts are indeed alkaline as supported by the presence of biotite. All other igneous rocks at Keystone, which are Eocene, are high-K calc-alkaline to shoshonitic. However, the trachyandesite dikes are sub-alkaline in this plot, providing further evidence their high K_2O is a product of alteration and that they may have a separate history from other Eocene igneous rocks at Keystone. An interesting observation in this plot is the dacite agglomerate, which has considerably lower Nb/Y than other Eocene rocks. Pearce (1996) notes that low Nb/Y ratios may represent greater contributions from crustal material with less fractionation (instead of evolved from a mafic melt) The relatively high alumina saturation index of dacite agglomerate, which places it within the peraluminous field, supports it having a greater crustal component relative to other Eocene igneous rocks.
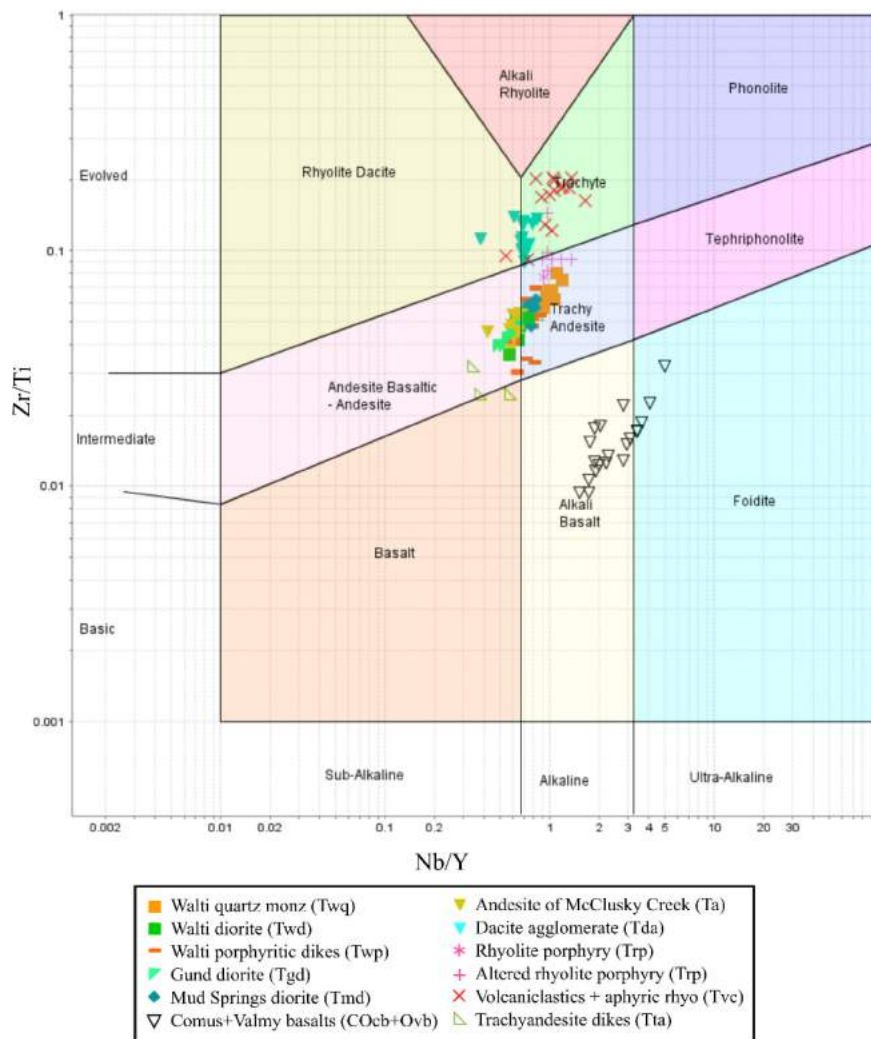
Figure 46. Zr/Ti vs. Nb/Y rock classification plot from Pearce (1996), after Winchester and Floyd (1977). Samples of trachyandesite dikes (Tta) are relatively mafic and sub-alkaline compared to the rest of Eocene igneous rocks at Keystone. The dacite agglomerate (Tda) is relatively evolved and sub-alkaline. See text for further explanation. Note the strong alkaline character of Early Paleozoic Comus and Valmy basalt.

Basalts

A Th/Yb vs. Nb/Yb plot from Pearce (2014), designed for use with basaltic rocks, highlights the different tectonic setting of Ordovician Comus and Valmy basalts from Eocene igneous rocks at Keystone (Figure 47). Although both Th and Nb are incompatible elements and behave similarly during melting, Th contents are higher in arc-related rocks possibly because of its hypothesized stronger partitioning into subduction-derived aqueous fluids, whereas Nb is not partitioned into subduction fluids. Thus, assessing

relative Th and Nb concentration is one way to potentially distinguish rocks derived from arc magmatism

versus those derived from non-subduction settings. Crustal contamination can also increase the Th/Nb ratio.

Ocean island basalts (OIB), or intraplate basalts, are alkalic and have higher Nb/Yb than tholeiitic basalts

of mid ocean ridges (MORB). All basalts of the Comus and Valmy formations plot in the OIB area. As they

only occur within these Paleozoic rocks and are typically intercalated with shales and limestones, they

likely represent syn-depositional intraplate magmatism, possibly in a seamount setting as suggested by

Bloomstein et al. (1991) for the Twin Creeks area, 155 km to the NNW.
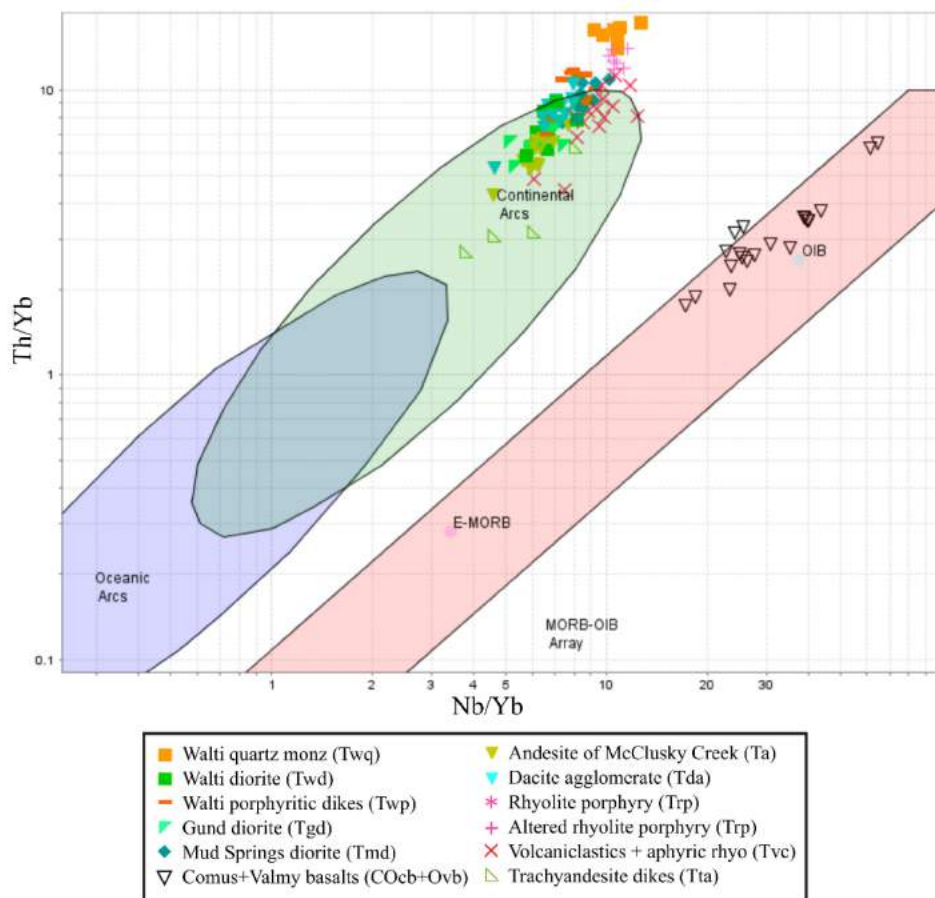
Figure 47. Th/Yb vs. Nb/Yb tectonic discriminant plot from Pearce (2014). Igneous rocks are separated by tectonic setting, with all basalts of the Comus and Valmy formations being distinctly ocean island basalts (OIB). All other rocks originate from the Eocene continental arc. Note that the diagram is designed for use with basaltic rocks, thus the differentiated Eocene rocks from Keystone partly lie outboard of the arc field.

Rare earth elements

All rocks except for the Walti quartz monzonite, rhyolite porphyry, volcaniclastics and aphyric rhyolite, trachyandesite, and basalts of the Comus and Valmy, have overlapping rare-earth element compositions (Figure 48). The Walti quartz monzonite deviates from the cluster of other Eocene rocks by having higher light rare-earth element contents (LREE) and relatively lower concentrations of heavy rare earth elements (HREE), thus making steeper overall normalized patterns. Apatite and titanite incorporate LREEs, both of which are present as accessory phases in the Walti quartz monzonite. The rhyolite porphyry and volcaniclastics unit have the lowest REE concentrations and strongest negative Eu anomalies. The wide spread of data for the volcaniclastics unit reflects its variability and difficulty to differentiate distinct rock types within it with the exception of the aphyric rhyolite; some variability is due to dilution by upper-plate quartzite and chert clasts. The data spread of the basalts may reflect variations across mafic sills or between the Comus and Valmy formations, as well as alteration to greenstone.

All Eocene rocks show a strong Eu anomaly, the largest found in the rhyolite porphyry. Sequestration of Eu^{2+} into plagioclase early in a magma's history can cause an Eu anomaly; such anomalies are characteristic of arc magmas and may bear on aspects such as their water contents. Interestingly, the dacite agglomerate, albeit relatively felsic, lacks the large negative Eu anomaly of the Walti quartz monzonite, rhyolite porphyry, and volcaniclastics units. The dacite may therefore have formed from processes that suppressed major plagioclase crystallization, perhaps because of a different magma composition and/or higher water content. Based on high ASI, Nb/Y, and lack of an Eu anomaly, it is possible the dacite magma represents a higher percentage of crustal melt than other Eocene igneous rocks. The Comus and Valmy basalts do not have an Eu anomaly, further evidence they do not originate from arc magmatism.
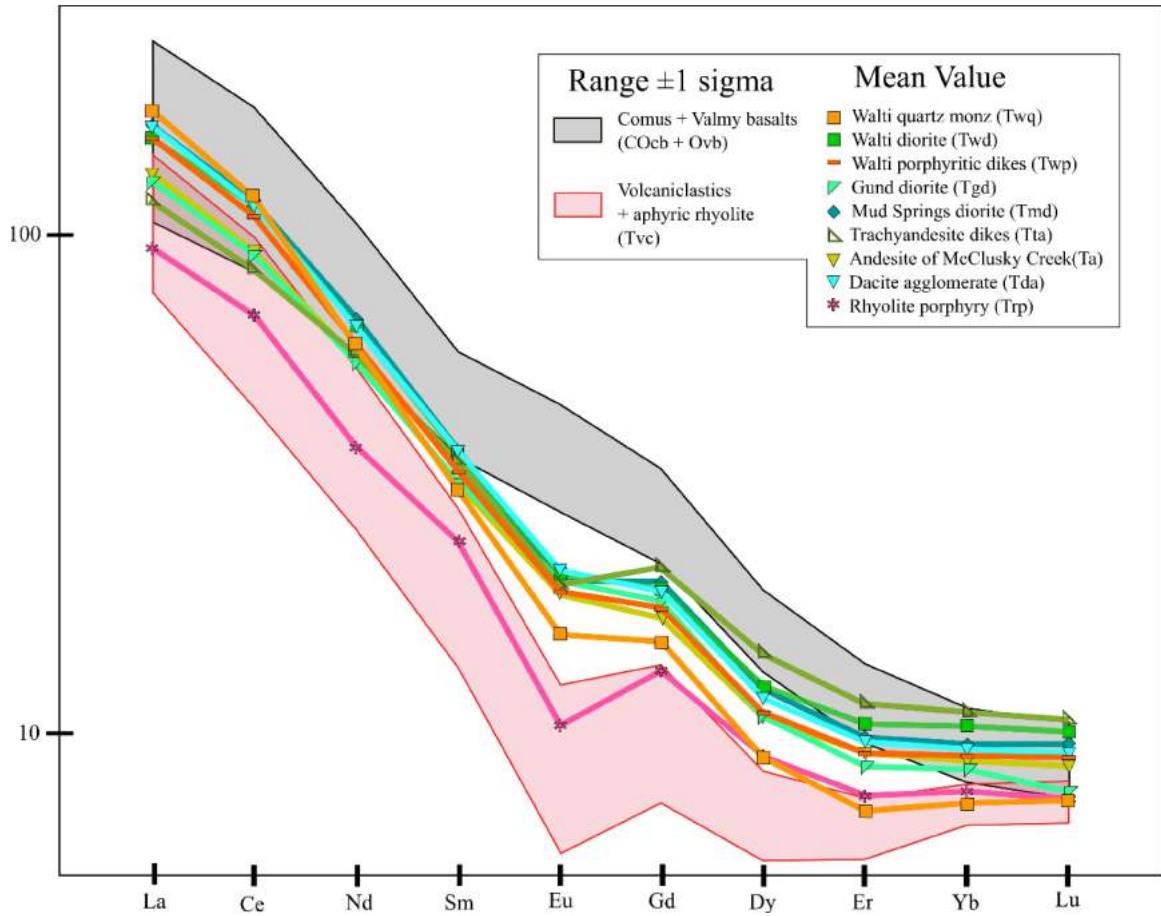
Figure 48. Chondrite-normalized rare-earth element spider plot (Nakamura, 1974). Mean values are shown for indicated units, and shaded areas for basalts and volcaniclastics units show variation of compositions.

Geochronology

U-Pb zircon results

Six igneous samples representing the Walti pluton and various volcanic units, as well as one sedimentary sample representing the basal conglomerate at the Tertiary unconformity were selected for U-Pb zircon dating. All samples had variable amounts of chlorite and sericite alteration and were unsuitable for $^{40}Ar/^{39}Ar$ analysis of primary minerals. U-Pb zircon crystallization ages for all six igneous samples are Eocene, between 34 and 37 Ma, and summarized in Table 4, and Figures 49 and 50. Full U-Pb zircon results are provided in Appendix B.

Two samples from the rhyolite porphyry and Walti intermediate porphyry dikes reported very high U concentrations (thousands of ppm), whereas the rest reported typical U (hundreds of ppm) (Figure 49A). High U results in higher decay and possible damage to the crystal lattice, which can contribute to radiogenic Pb loss and make the sample appear younger. Results for sample KS126 (Twp) suggest Pb loss due to high U, and analyses with >4000 ppm were omitted from the weighted mean age calculation. KS044 (Trp) also had high U but did not show compelling evidence of Pb loss.

Scanning electron microscope cathodoluminescence (SEM-CL) images of zircons were viewed for morphology and to target growth rims for analysis (Corfu et al., 2003). Although many grains showed complex zoning patterns under cathodoluminescence, inherited cores were rarely observed and where present, were avoided. The Walti quartz monzonite (Twq), dacite agglomerate (Tda), and aphyric rhyolite (Tvc) were the only rocks to have a few individual zircon rims dated at >40 Ma. Two zircons from sample KS014 (Twq) yielded dates of 41.9±0.8 and 46.3±0.8 Ma, and both analyses were rims of igneous zircons that appear no different from other zircons. Three zircons from sample KS051 (Tda) yielded dates of 50.1±1.9, 52.2±2.1, and 55.3±1.8 Ma, all on rims of zircons with no visual CL differences. Sample KS050 (Tvc) had three pre-Eocene zircons, at 81.7±0.7, 318.3±10.7, and 1642.8±21.1 Ma. Zircons of this sample range from acicular to stubby and weathered, and the three older zircons also show typical euhedral igneous morphologies. KS050 is a tuffaceous volcaniclastic rock that likely incorporates older zircons contained in exotic clasts and transported from elsewhere.

Table 4. Summary of isotopic dating results

Sample	Location, Type	Age (Ma)	±2σ	MSWD	n¹	Method	Method	Mineral	Age type	UTM NAD27 East	North	Comment
Tmd	**Mud Spring diorite**											
KS003	E margin of pluton	35.87	0.06	0.21	6	$^{40}Ar/^{39}Ar$	Single crystal step-heating	plagioclase	igneous	540682	4417021	2 age clusters, considered older
Tmp	**Mud Springs pegmatite**											
KS110	W margin of pluton	n/a	n/a	n/a	2	$^{40}Ar/^{39}Ar$	Single crystal step-heating	orthoclase	igneous	539514	4417280	poor spectra, no meaningful age
Tgd	**Gund diorite**											
KS114A	W sill	35.82	0.08	0.71	6	$^{40}Ar/^{39}Ar$	Bulk grain step-heating	hornblende	igneous	536139	4416180	
KS023	W dike cutting RMA	34.8	0.3	70.51	6	$^{40}Ar/^{39}Ar$	Bulk grain step-heating	hornblende	igneous	536466	4417671	wide error, poor spectra
KS079	main stock	32.48	0.61	116	11	$^{40}Ar/^{39}Ar$	Single crystal step-heating	plagioclase	igneous	537214	4416387	spread of ages, no meaningful age
Trp	**Rhyolite porphyry**											
KS044	E margin, altered, qz veins	36.17	0.33	3.6	33	U-Pb	LA-ICP-MS	zircon	igneous	539997	4417710	
KS098	center of stock	35.43	0.06	11.9	8	$^{40}Ar/^{39}Ar$	Single crystal fusion	sanidine	igneous	539808	4417729	
KS099	NW interior, altered	n/a	n/a	n/a	n/a	$^{40}Ar/^{39}Ar$	Bulk grain step-heating	illite	alteration	539790	4417891	poor spectra, too old >38 Ma
Twq	**Walti quartz monzonite**											
KS014	W margin of pluton	35.05	0.41	4.2	31	U-Pb	LA-ICP-MS	zircon	igneous	536914	4417273	
KS137	drill core @ 530 m, N margin	35.52	0.14	0.83	4	$^{40}Ar/^{39}Ar$	Bulk grain step-heating	biotite	igneous	537931	4419755	
KS029	N interior, altered, qz veins	36.27	0.1	183.49	2	$^{40}Ar/^{39}Ar$	Bulk grain step-heating	illite	alteration	537965	4418926	poor spectra, too old
Twd	**Walti diorite**											
KS041	NE margin of pluton	35.51	0.19	4.9	8	$^{40}Ar/^{39}Ar$	Single crystal step-heating	plagioclase	igneous	539286	4418457	
KS086	SE margin of pluton	35.38	0.06	1.6	8	$^{40}Ar/^{39}Ar$	Single crystal step-heating	plagioclase	igneous	538743	4417226	
KS093	E margin of pluton	35.24	0.22	12	14	$^{40}Ar/^{39}Ar$	Single crystal step-heating	plagioclase	igneous	538999	4417534	
KS068	S interior, enclave in Walti	34.81	0.42	0.33	8	$^{40}Ar/^{39}Ar$	Single crystal fusion	plagioclase	igneous	537785	4416879	wide error
Twp	**Walti intermediate porphyritic dikes**											
KS126	dike cutting Mud Springs, altered	34.96	0.38	2.8	20	U-Pb	LA-ICP-MS	zircon	igneous	540073	4417170	
KS095	dike cutting RMA, E of Walti	35.68	0.04	1.11	2	$^{40}Ar/^{39}Ar$	Bulk grain step-heating	hornblende	igneous	539013	4417380	
Tta	**Trachyandesite dikes**											
KS025	altered dike, W of Walti	34.69	0.39	3.9	32	U-Pb	LA-ICP-MS	zircon	igneous	536760	4418145	
Tvc	**Volcaniclastics + aphyric rhyolite**											
KS050	NE of Mud Springs, flow-banded	35.6	0.38	3.2	31	U-Pb	LA-ICP-MS	zircon	igneous	540585	4417921	
KS001	NE of Mud Springs, tuffaceous	42.06	0.07	n/a	n/a	$^{40}Ar/^{39}Ar$	Bulk grain step-heating	illite	alteration	540616	4417887	poor spectra, too old
Ta	**Andesite of McClusky Creek**											
KS144	far SE end of study area, lava	35.99	0.04	0.75	6	$^{40}Ar/^{39}Ar$	Bulk grain step-heating	hornblende	igneous	540610	4414578	
KS135	E of Mud Springs, lava	35.85	0.08	4.98	2	$^{40}Ar/^{39}Ar$	Bulk grain step-heating	hornblende	igneous	541388	4417035	
KS139	drill core @ 332 m, NE of Walti,	35.54	0.06	8.3	5	$^{40}Ar/^{39}Ar$	Bulk grain step-heating	illite	alteration	539354	4419536	acceptable
KS019	altered dike, N of rhyolite porphyry	35.71	0.12	26.56	3	$^{40}Ar/^{39}Ar$	Bulk grain step-heating	illite	alteration	540069	4418575	acceptable
Tda	**Dacite Agglomerate**											
KS051	E of Mud Springs pluton	34.68	0.54	4.1	26	U-Pb	LA-ICP-MS	zircon	igneous	540994	4417038	

Unit / Sample	Location, Type	Age (Ma)	±2σ	MSWD	n[1]	Method	Method	Mineral	Age type	UTM NAD27 East	North	Comment
Ovb	Valmy basalt											
KS143	W of Walti pluton	466.1	0.7	1.59	6	$^{40}Ar/^{39}Ar$	Bulk grain step-heating	biotite	igneous	536833	4418073	
KS063	SE of Walti pluton	n/a	n/a		6	$^{40}Ar/^{39}Ar$	Single crystal step-heating	plagioclase	igneous	538377	4416821	spread of ages 55-130 Ma
Tcg	Tertiary conglomerate											
KS048	N of Mud Springs pluton	35.62	0.32	4.1	136	U-Pb	LA-ICP-MS	zircon	detrital	540304	4418097	max depositional age

[1]Number of analyses indicates number of crystals analyzed for U-Pb zircon and $^{40}Ar/^{39}Ar$ single crystal, or number of steps in plateau
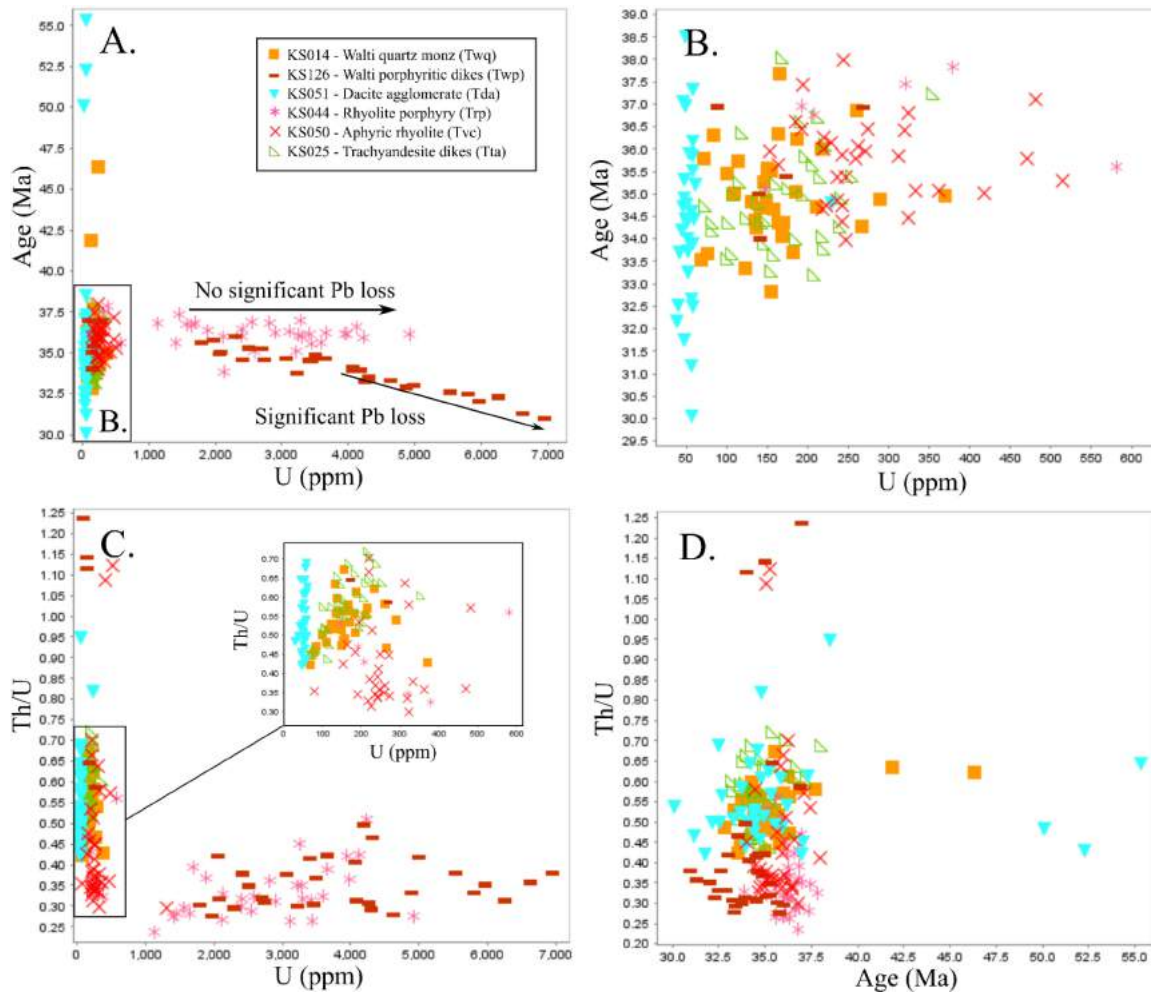
Figure 49. LA-ICP-MS results of zircon analyses. A) Age vs. uranium content. Samples KS126 and KS044 zircon U are a factor greater than other samples (thousands ppm vs. hundreds ppm). Sample KS126 has evidence of Pb loss with increasing U, causing an apparent younger age. KS044 has high U, but does not have evidence of Pb loss. B) Zoomed view of age vs. uranium. C) Th/U ratio vs. U. D) Th/U ratio vs. age.

All six igneous samples have a notably wide spread of individual zircon ages (Figure 50). Mean square weighted deviations (MSWD) range from 2.8 to 4.2. A MSWD >1 generally means the data do not represent a single value, or in this case, a single age of crystallization. Alternatively, the data spread may be a product of the analytical uncertainties related to LA-ICP-MS, mixing of more than one generation of zircon rims, or other factors including variable Pb loss. There was no correlation between the laser spot analysis location and age, and between the morphology of the crystal and age (Appendix B).
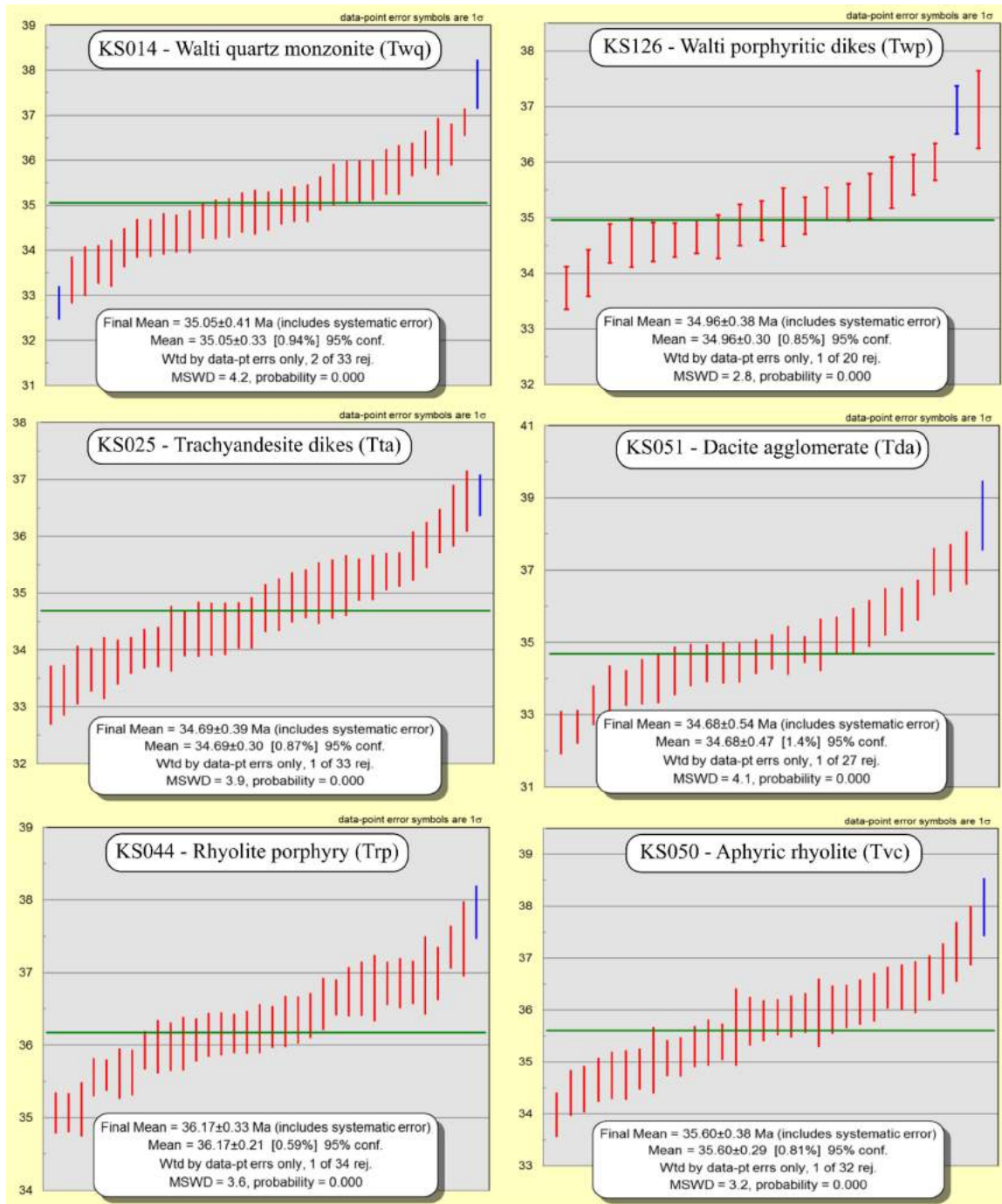
Figure 50. Weighted mean ^{206}Pb/^{238}U ages measured by LA-ICP-MS. Final mean age (green line) includes systematic error of zircon standards. Analyses in blue are those statistically rejected from weighted mean calculation.

Detrital zircons from basal conglomerate sample KS048 showed a youngest population cluster at ~36 Ma (Figure 51). Only 37 of the 195 analyses from KS048 were older than 41 Ma. Of those, six are Paleozoic and of different ages without any clustering. Of those analyses Proterozoic and older, clusters occur at ~1090, 1350, 1850, and 2670 Ma, consistent with the main ages of zircons in rocks of the Roberts Mountains allochthon and rocks therein derived (Linde et al., 2016). After omitting analyses that were discordant or showed Pb loss, 145 analyses were considered for determination of the maximum depositional age (Figure 52). Nine analyses were statistical outliers, and the weighted mean age of 134 grains was 35.62±0.32 Ma (MSWD=4.1). The significance of this age is addressed further in the discussion section.
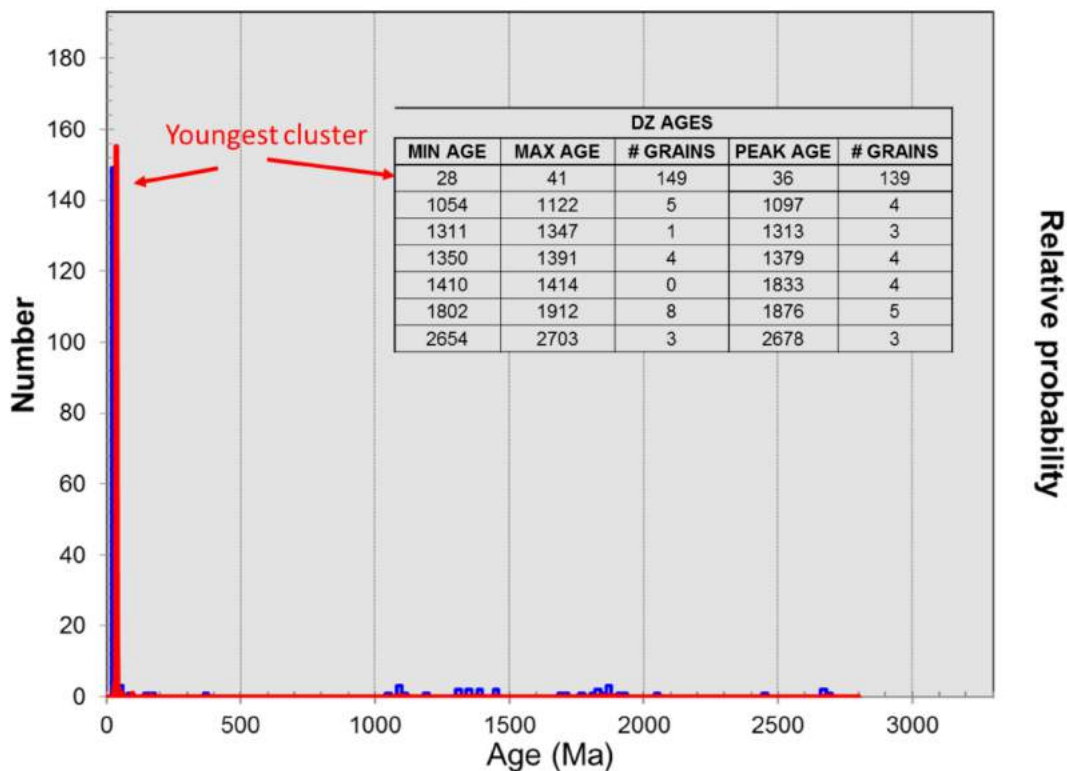
Figure 51. Distribution of detrital zircon analyses from basal conglomerate sample KS048. Most zircons are Eocene and clustered around 36 Ma. Proterozoic population clusters at ~1090, 1350, 1850, and 2670 Ma generally fit provenance of the Roberts Mountains allochthon as determined from Linde et al. (2016).
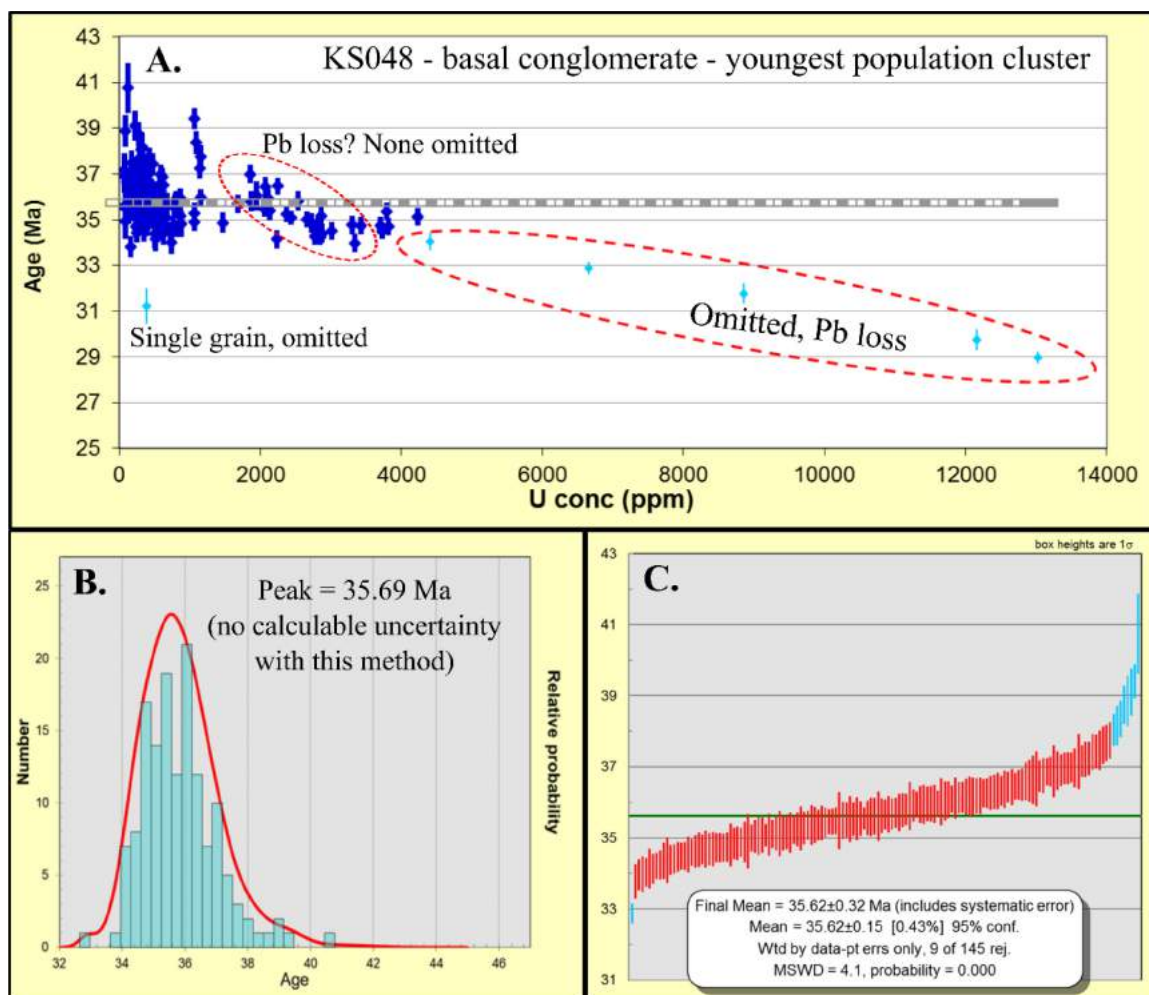
Figure 52. U-Pb detrital zircon analyses of the youngest population cluster of basal conglomerate sample KS048. A) Age of analyses vs. U (ppm), showing zircons with very high U experienced Pb loss, resulting in a younger age. B) Peak age of the youngest cluster after omissions that may represent the max depositional age of the basal conglomerate. However, no calculable uncertainty is possible with this method. C) Weighted mean age of the youngest cluster that may represent the max depositional age of the basal conglomerate.

^{40}Ar/^{39}Ar results

Mineral separates from 21 igneous samples were analyzed, including 7 plagioclase, 1 orthoclase, 1 sanidine, 2 biotite, 5 hornblende, and 5 illite (alteration) separates. The plagioclase and sanidine separates were analyzed using single crystal step-heating and single crystal total fusion methods, while the remainder were bulk grain step-heating analyses. Results are summarized in Table 4. Full ^{40}Ar/^{39}Ar results are provided in Appendix C.

Mud Springs diorite (Tmd)

Plagioclase from sample KS003 from the Mud Springs diorite (Tmd) was analyzed by single crystal step-heating and most grains produced flat spectra (Figure 53). Thirteen of the 15 analyses yielded plateaus, and although several of the plateaus were comprised of only 2 steps they had >50% of the total ^{39}Ar gas released. The distribution of the ages shows two population centers at 35.49 and 35.87 Ma, with the older forming a tighter cluster. Given the proximity of this diorite to nearby volcanics and the rhyolite porphyry that cuts the Mud Springs diorite, the cooling age of the plagioclase may have been compromised. Mafic minerals were still mostly altered to chlorite and plagioclase was unaltered but relatively weathered (Figure 54A). The weighted mean of the older cluster at 35.87±0.06 Ma is therefore the preferred age.

Mud Springs pegmatite (Tmp)

Orthoclase from sample KS110 from the Mud Springs pegmatite unit (Tmp) was analyzed by single crystal step-heating, but results had variable K/Ca and non-radiogenic Ar released in the initial heating steps. Ages were inconsistent from 34 to 37 Ma. Orthoclase in the pegmatite did not appear altered in thin section but dusted from weathering (Figure 54I). No preferred age determined.

Gund diorite (Tgd)

Plagioclase from sample KS079 from the Gund diorite (Tgd) was analyzed by single crystal step-heating. Data were inconsistent with widely different plateau ages ranging from 2 to 35 Ma. The Eocene population also did not yield a meaningful age. This sample had the least alteration of those collected from the main Gund stock, although plagioclase crystals were mildly sericitized (Figure 54E) and all mafic minerals were altered to chlorite and clay minerals. No preferred age was determined.

Hornblende from sample KS023 from a dike of the Gund diorite (Tgd) was analyzed by bulk grain step-heating (Figure 55C). Initial heating steps had variable K/Ca, low radiogenic Ar, and spurious ages. Steps G through L with >80% ^{39}Ar yield, gave a weighted mean age of 34.8±0.3 Ma (MSWD=70.51). In thin section the hornblende phenocrysts of this dike are relatively coarse and can be >1 mm, but often have inclusions of plagioclase, clinopyroxene, and groundmass (Figure 56A).
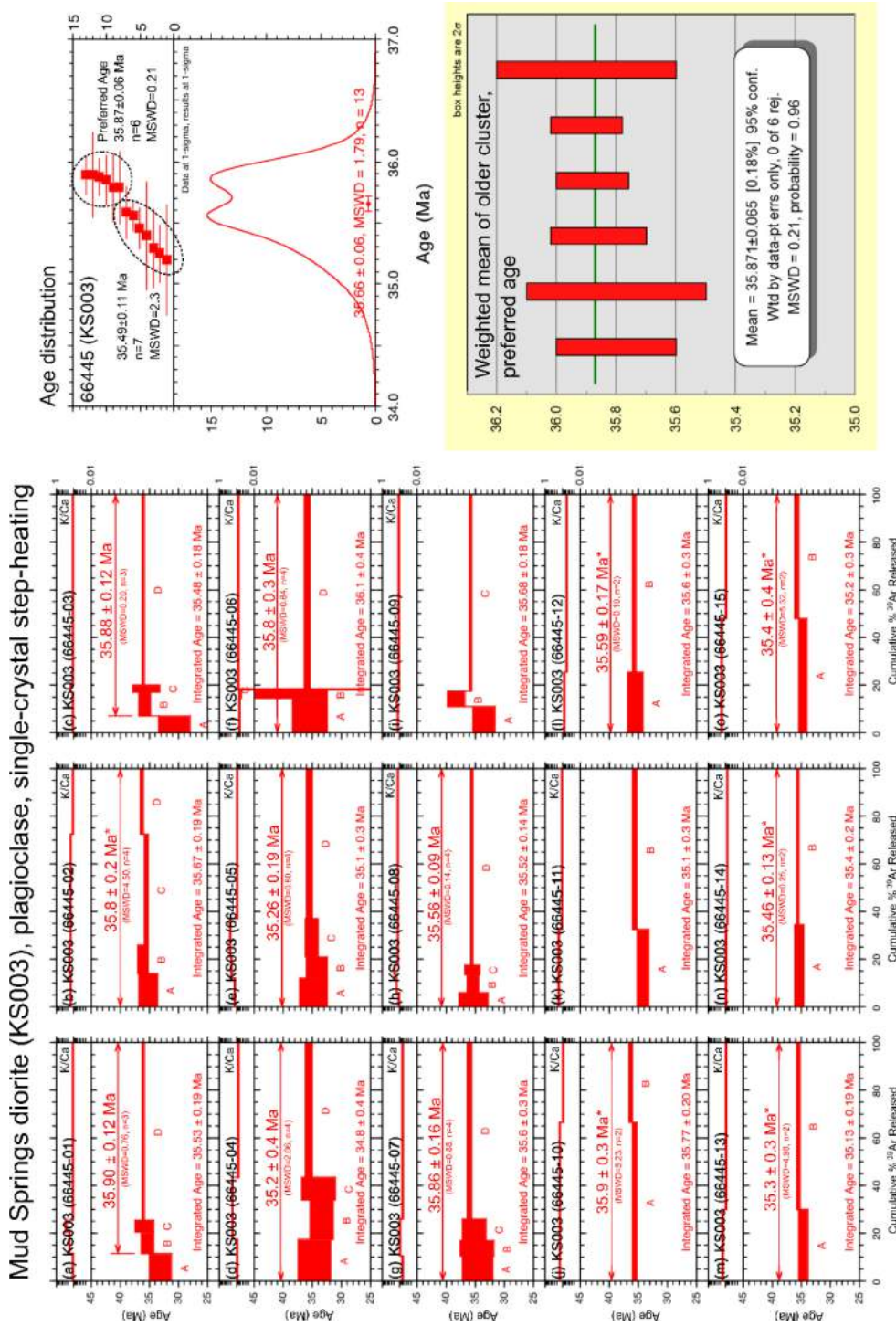
Figure 53. ^{40}Ar/^{39}Ar single crystal step-heating spectra of plagioclase from sample KS003 from the Mud Springs diorite. Forced plateaus indicated by *. Left: Spectra of 15 plagioclase crystals. Upper right: Age distribution of plateaus shows two population centers. Bottom right: Weighted mean of the older population cluster is the preferred age.
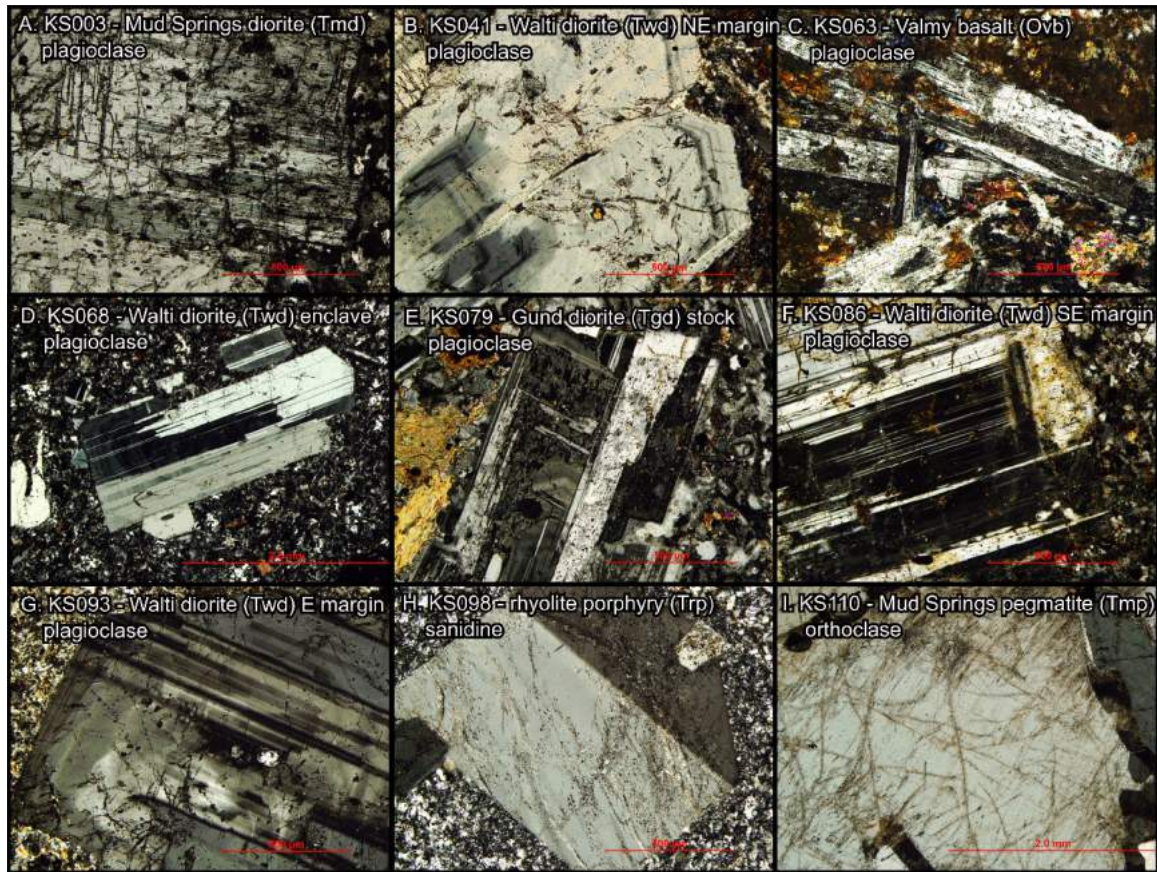
Figure 54. Micrographs of representative plagioclase, sanidine, and orthoclase of samples selected for Ar^{40}/Ar^{39} analysis. All micrographs were taken in cross-polarized light and at the same scale (10x) except for D. and I. (4x).

Hornblende from sample KS114A from the western sill of the Gund diorite was analyzed by bulk grain step-heating (Figure 55E). A plateau of six steps resulted although the K/Ca varies towards the end of the spectrum. Hornblende in thin section are smaller but unaltered with few inclusions compared to hornblende from other samples (Figure 56C). The preferred age is 35.82±0.08 Ma (MSWD=0.71).
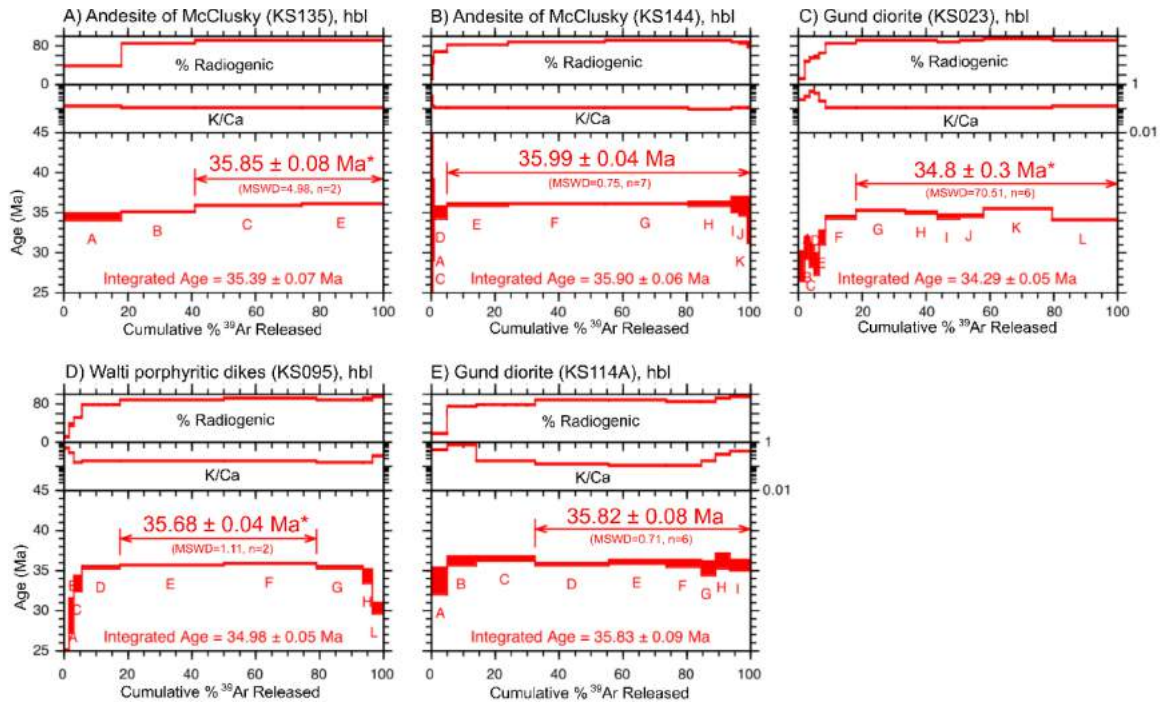
Figure 55. ^{40}Ar/^{39}Ar bulk grain step-heating spectra of hornblende samples. Forced plateaus indicated by *. A) Sample KS135 from the andesite lava of McClusky Creek has a climbing spectrum and forced plateau through the final two steps. B) Sample KS144 from the andesite lava of McClusky Creek has a flat spectrum with robust plateau. C) Sample KS023 from the Gund diorite has a climbing spectrum and very poor forced plateau. D) Sample KS095 from the Walti intermediate porphyritic dikes has forced plateau of two steps in the middle of spectrum. E) Sample KS114A from the Gund diorite has a relatively flat spectrum and good plateau age.

Walti quartz monzonite (Twq)

Biotite from sample KS137 from the Walti quartz monzonite phase (Twq) was analyzed by bulk

grain step-heating (Figure 57). No plateau resulted, and the K/Ca ratio was variable throughout the

analysis. This sample was taken from drill core that intercepted the pluton at depth. The Walti had a coarse-

grained texture and biotite phenocrysts were >1 mm and mostly unaltered (Figure 56F). It is unclear what

caused the variable K/Ca. An isochron through the final four heating steps intercepts atmospheric Ar and

yields a preferred age of 35.52±0.14 Ma (MSWD=0.83).
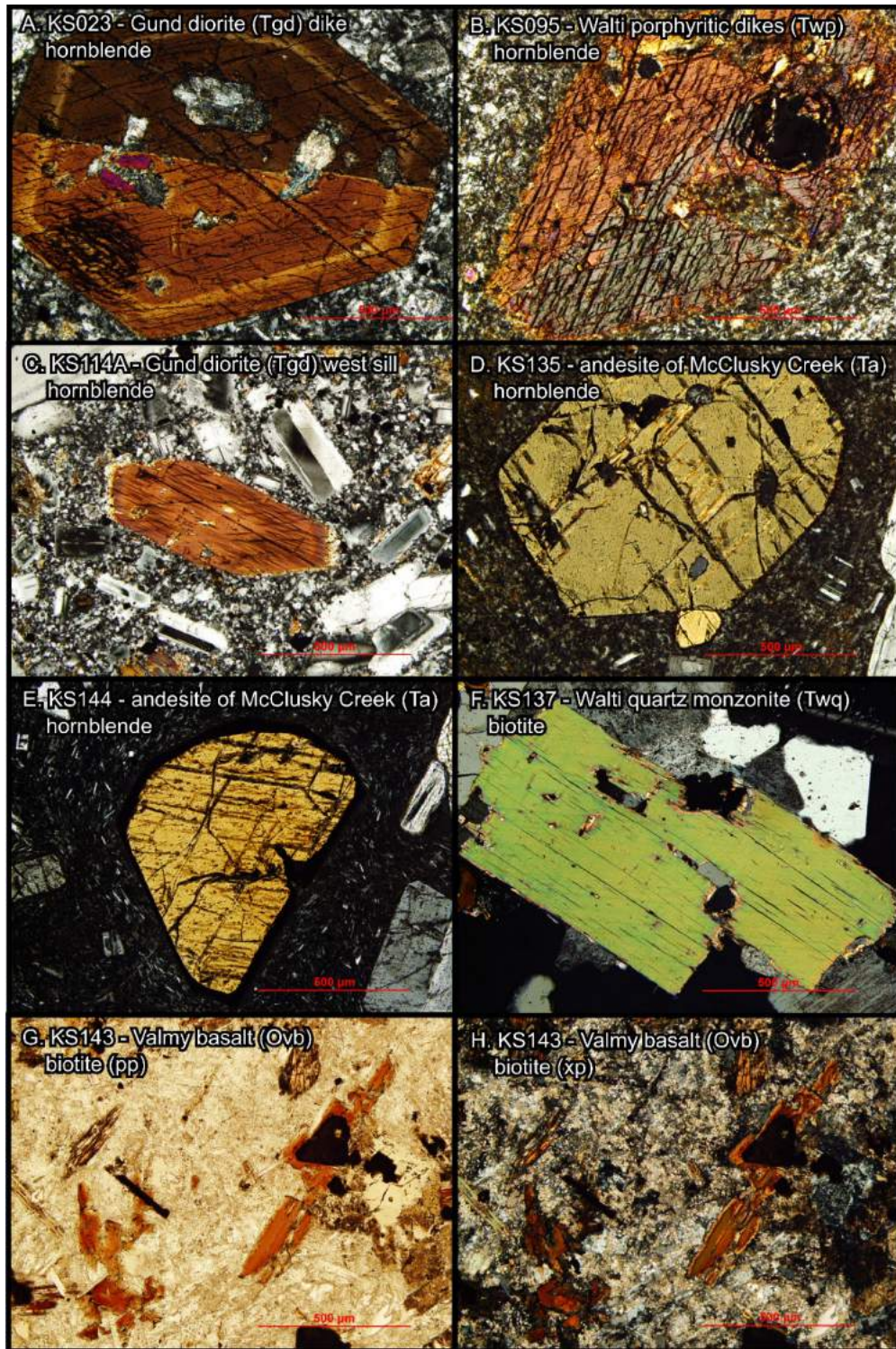
Figure 56. Micrographs of representative hornblende and biotite of samples selected for Ar^{40}/Ar^{39} analysis. Micrographs A. through F. were taken in cross-polarized light and at the same scale (10x). Micrographs G. and H. are of the same view in plane-polarized light and cross-polarized light, respectively.
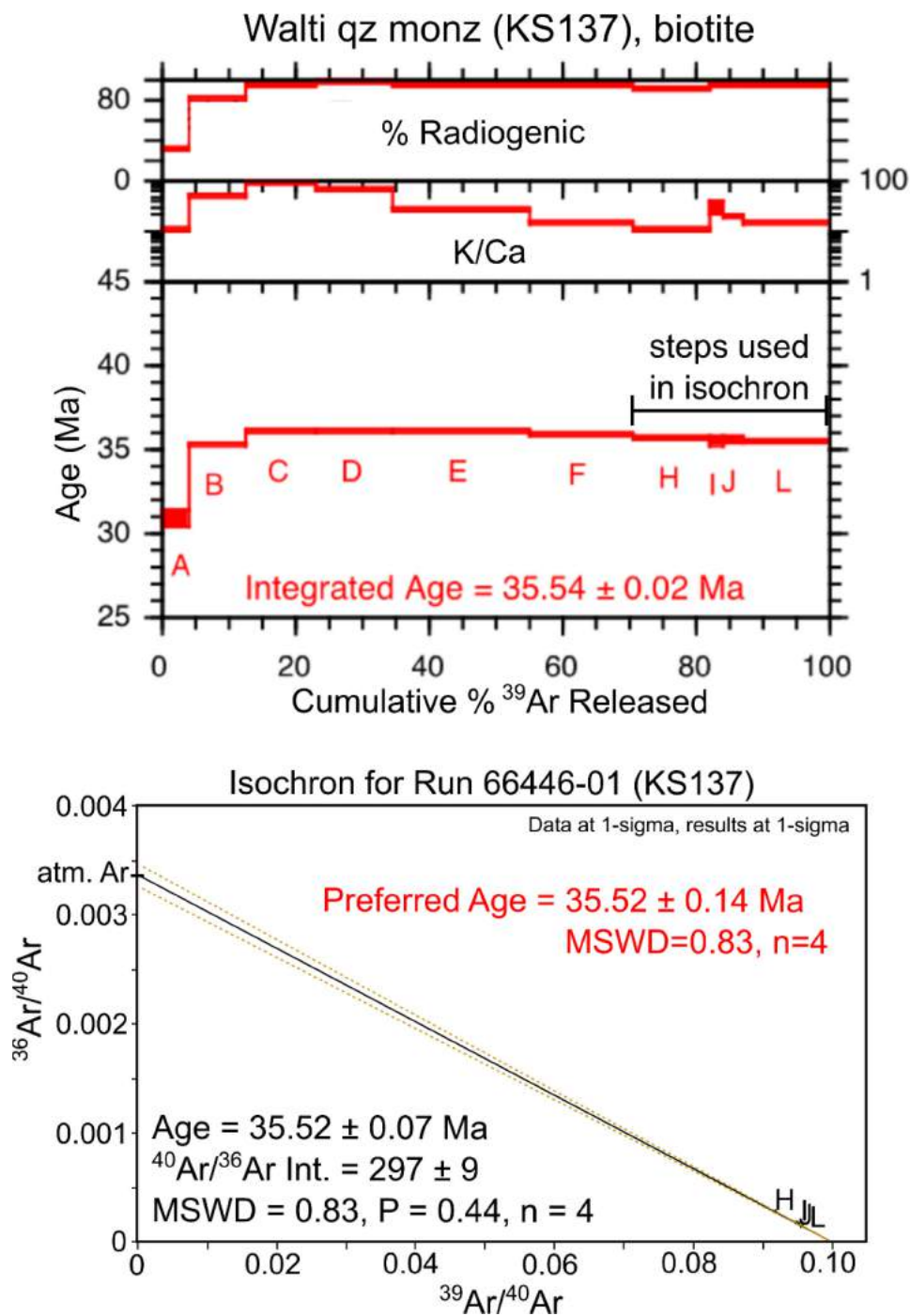
Figure 57. $^{40}Ar/^{39}Ar$ step-heating spectrum and isochron of biotite from sample KS137 from the Walti quartz monzonite. K/Ca was variable, and no plateau resulted. An isochron through the final four steps intercepts atmospheric Ar and agrees with integrated age.

Walti diorite (Twd)

Plagioclase from sample KS041 from the Walti diorite phase (Twd) at the pluton's northeast margin was analyzed by single crystal step-heating (Figure 58). Mafic minerals were partly chloritized, but plagioclase was relatively unaltered (Figure 54B). Most of the 15 analyses had climbing spectra that flattened to plateaus in the higher-temperature steps; 2 analyses did not yield plateaus, and 6 had plateaus based on only 2 steps with <50% of the total ^{39}Ar gas released. The youngest 5 analyses were considered outliers and a weighted mean age of 35.51±0.19 Ma (MSWD=4.9) is preferred.

Plagioclase from sample KS068 from a Walti diorite enclave (Twd) within the Walti quartz monzonite was analyzed by both single crystal and multi-grain step-heating (Figure 59). Spectra had relatively low precision and inconsistent ages. Plagioclase crystals in thin section show no signs of alteration (Figure 54D). However, thermal resetting of plagioclase is very likely given the geologic context of the diorite enclave that crystallized prior to the quartz monzonite phase. The weighted mean age is 34.8±0.42 Ma (MSWD=0.33).

Plagioclase from sample KS086 from the Walti diorite phase (Twd) at the pluton's southeast margin was analyzed by single crystal step-heating (Figure 60). Spectra were mostly flat with 12 of 14 analyses having plateaus, 2 of which involved only 2 steps but with >50% of the total ^{39}Ar gas released. Age distribution has 3 young outliers and 1 older outlier. Plagioclase crystals in thin section are light to moderately sericitized and weathered (Figure 54F). The weighted mean age is 35.38±0.06 Ma (MSWD=1.6).

Plagioclase from sample KS093 from the Walti diorite phase (Twd) at the pluton's eastern margin was analyzed by single crystal step-heating (Figure 61). Spectra varied from flat to climbing and while all had plateaus, several were comprised of only 2 steps with <50% of the total ^{39}Ar gas released. Plagioclase in thin section showed little to no alteration and only minor weathering (Figure 54G). The weighted mean age is 35.24±0.22 Ma (MSWD=12).

Walti intermediate porphyritic dikes (Twp)

Hornblende from sample KS095 from the Walti intermediate porphyritic dikes (Twp) was analyzed by bulk grain step-heating (Figure 55D). A plateau of only two steps (but with 61.2% of total ^{39}Ar released) occurred in the middle of the analysis with an age of 35.68±0.04 Ma (MSWD=1.11). Hornblende phenocrysts in thin section frequently show inclusions (Figure 56B) but given the precision the plateau age is accepted.
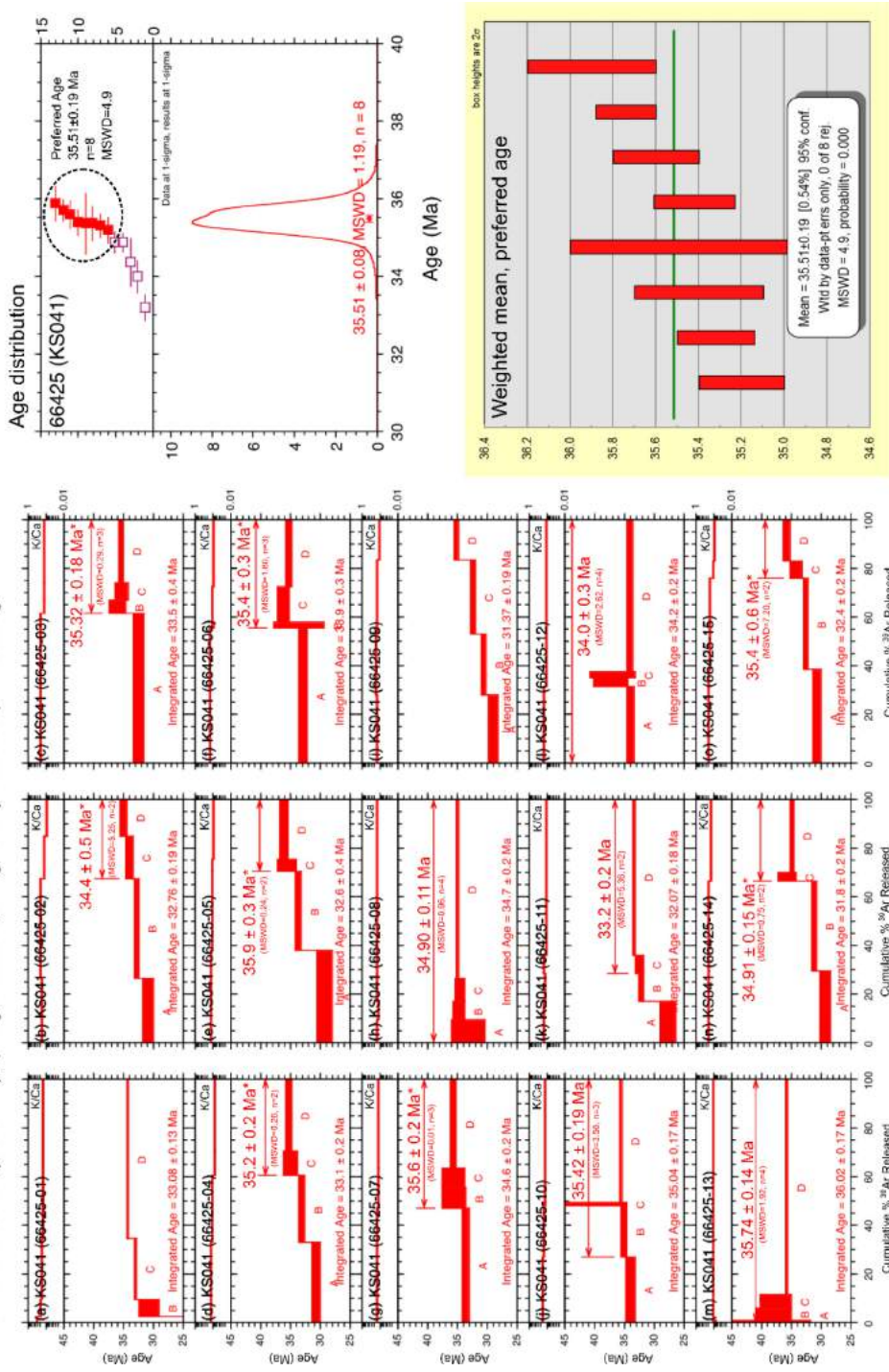
Figure 58. ^{40}Ar/^{39}Ar single crystal step-heating spectra of plagioclase from sample KS041 from the Walti diorite. Forced plateaus indicated by *. Left: Spectra of 15 plagioclase crystals. Upper right: Age distribution of plateaus, open squares are omitted outliers. Bottom right: Weighted mean of the older population cluster is the preferred age.
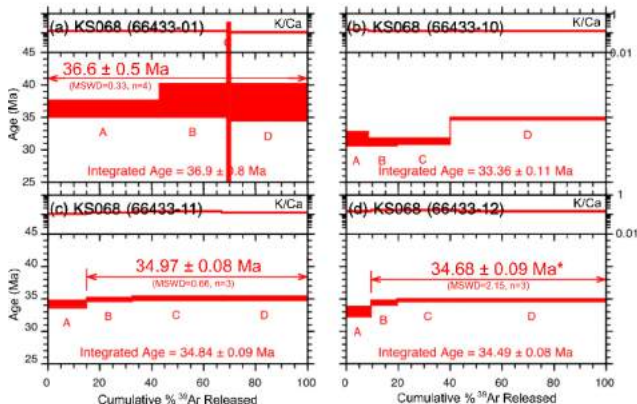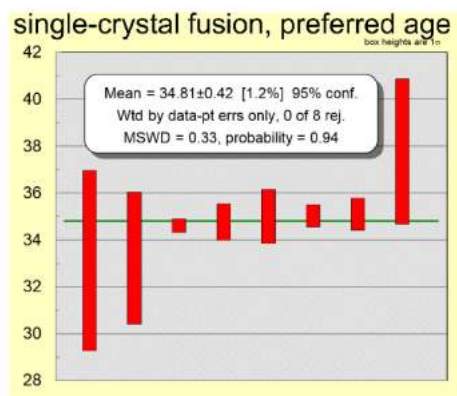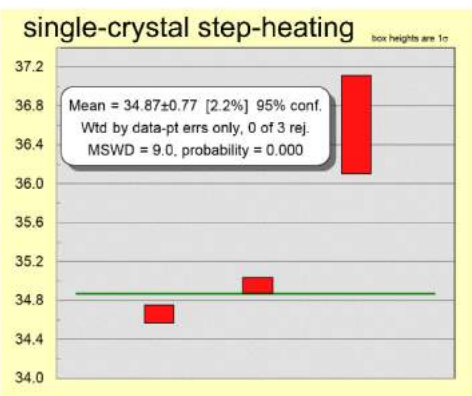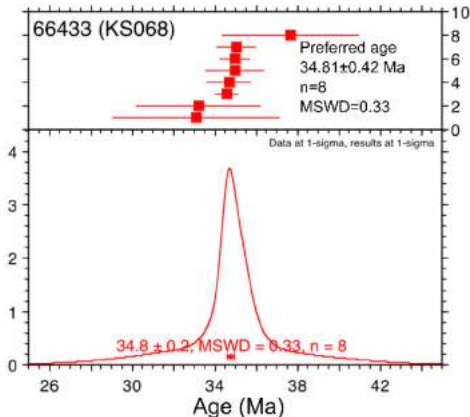
Figure 59. ^{40}Ar/^{39}Ar single crystal step-heating spectra and total fusion results of plagioclase from sample KS068 from the Walti diorite. Forced plateaus indicated by *. Left: Spectra of 4 plagioclase crystals. No meaningful age determined. Right: Age distribution of total fusion results. Weighted mean is the preferred age.
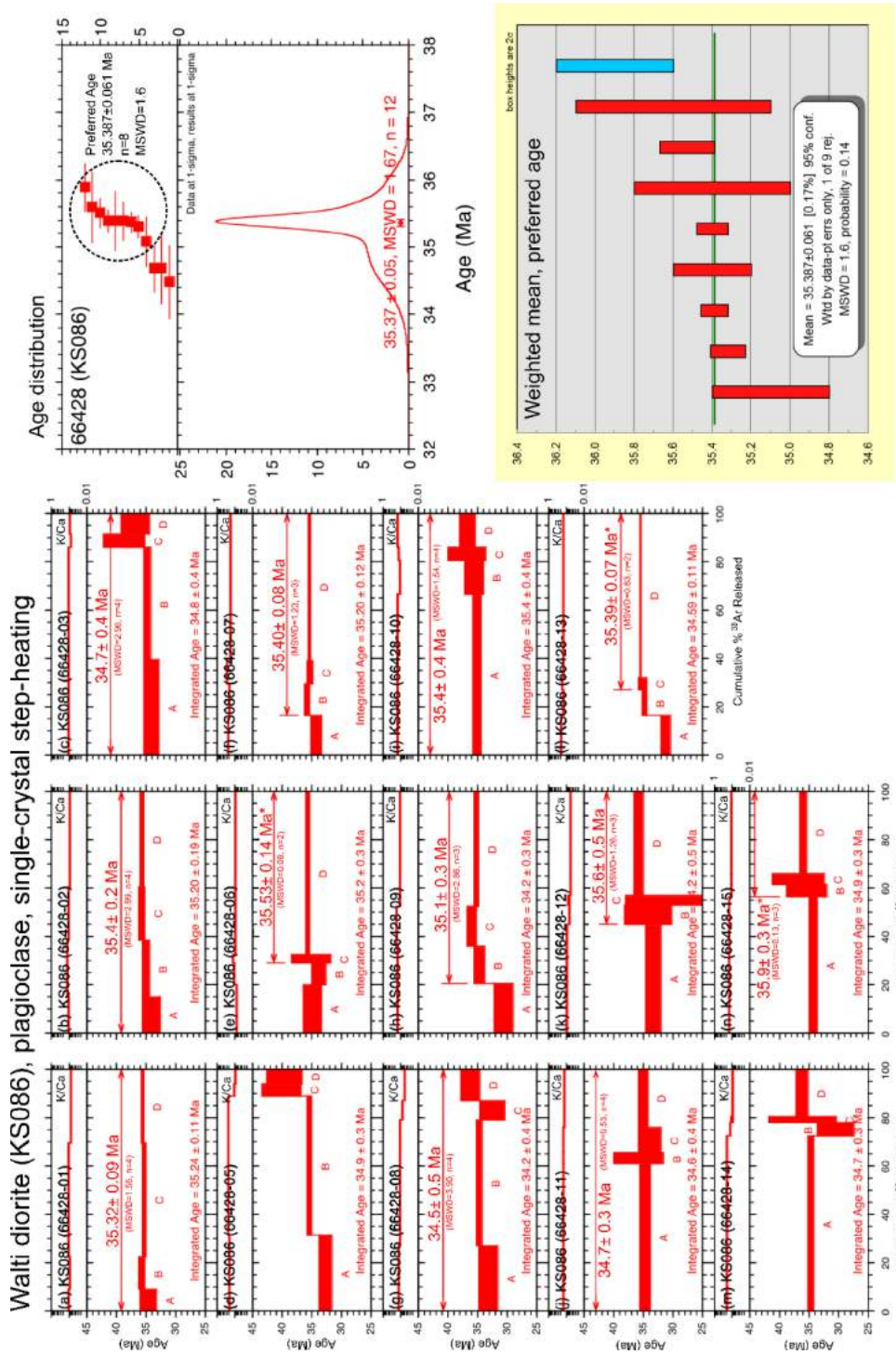
Figure 60. ^{40}Ar/^{39}Ar single crystal step-heating spectra of plagioclase from sample KS086 from the Walti diorite. Forced plateaus indicated by *. Left: Spectra of 14 plagioclase crystals. Upper right: Age distribution of plateaus. Bottom right: Weighted mean of circled population cluster is the preferred age.
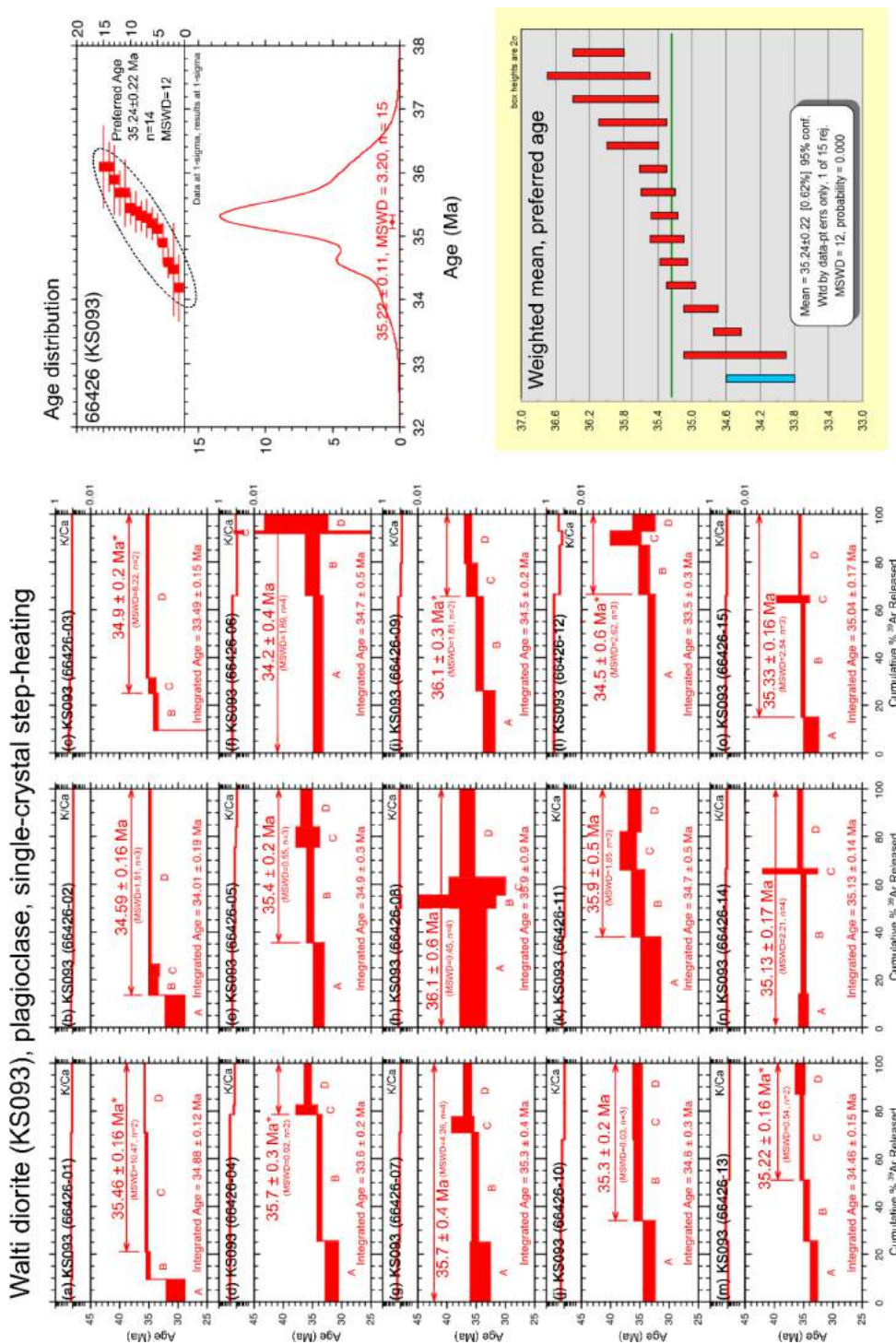
Figure 61. $^{40}Ar/^{39}Ar$ single crystal step-heating spectra of plagioclase from sample KS093 from the Walti diorite. Forced plateaus indicated by *. Left: Spectra of 15 plagioclase crystals. Upper right: Age distribution of plateaus. Bottom right: Weighted mean is the preferred age.

Rhyolite porphyry (Trp)

Sanidine from sample KS098 from the rhyolite porphyry unit (Trp) was analyzed by single crystal total fusion (Figure 62) and single crystal step-heating (Appendix C). Spectra were mostly flat but varied in age, as did the total fusion results. While the margins of the intrusion were bleached and had pervasive sericitic alteration, sample KS098 was collected from the relatively unaltered center in which sanidine was petrographically pristine (Figure 54H). In the total fusion results there is a relationship between low radiogenic argon and younger ages that would be attributed to partial argon loss, but this is not observed in the initial steps of the spectra. Eight of the 15 total fusion ages make a population at 35.43±0.06 Ma (MSWD=11.90), and this is the preferred age of emplacement.
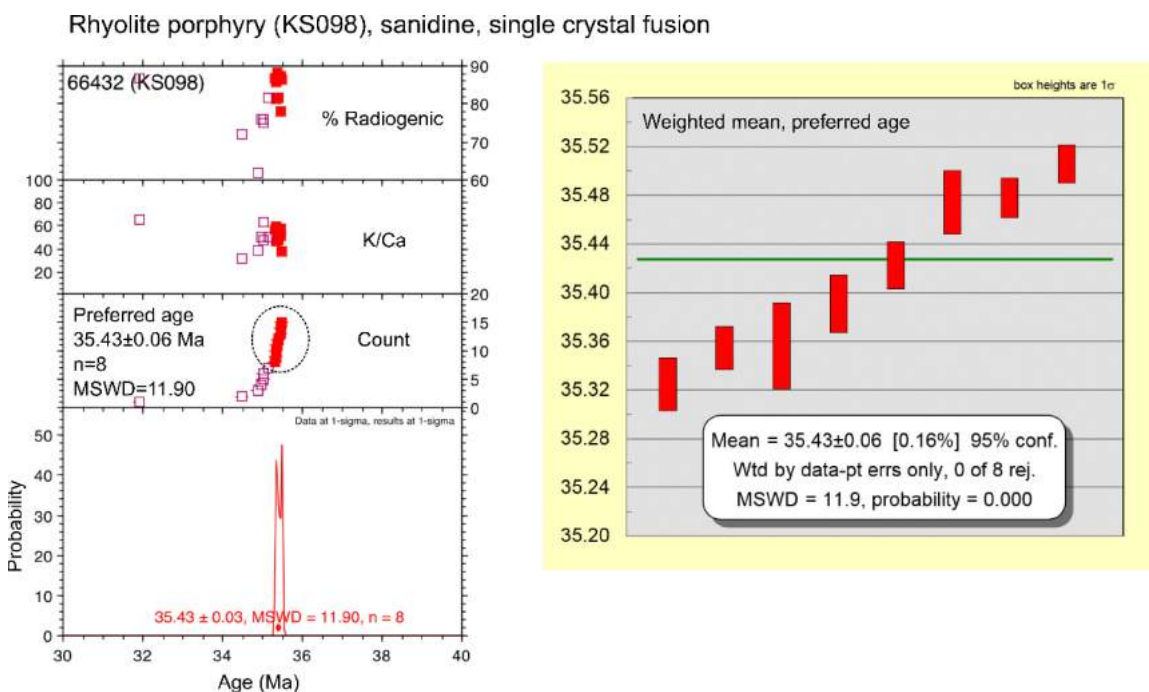
Figure 62. ^{40}Ar/^{39}Ar single crystal total fusion results of sanidine from sample KS098 from the rhyolite porphyry. Total fusion ages have less spread than single crystal step-heating results. Oldest cluster is the preferred age.

Andesite of McClusky Creek (Ta)

Hornblende from sample KS135 from the andesite lavas of McClusky Creek (Ta) was analyzed by bulk grain step-heating (Figure 55A). It yielded a climbing spectrum and a plateau of only two steps (with 58.8% of the total ^{39}Ar released) occurred at the end of the analysis with an age of 35.85±0.08 Ma

(MSWD=4.98). Hornblende in thin section appeared unaltered but with minor inclusions of groundmass and apatite (Figure 56D). The plateau age is not entirely acceptable given the imprecision.

Hornblende from sample KS144 from the andesite lavas of McClusky Creek (Ta) was analyzed by bulk grain step-heating (Figure 55B). A plateau of seven steps resulted with an age of 35.99±.04 Ma (MSWD=0.75). This sample showed no signs of alteration or weathering, and hornblende rarely had inclusions (Figure 56E). The plateau age is the preferred age of the andesite.

Valmy basalt (Ovb)

Plagioclase from sample KS063 from Valmy basalt (Ovb) yielded no useful data. Single crystal step-heating ages ranged from 55 to 128 Ma (Figure 63). The relatively low radiogenic argon released make it likely the plagioclase had very little K, possibly because of albitization (Figure 54C). No age was accepted for this sample.

Biotite from sample KS143 from the Valmy basalt (Ovb) was analyzed by bulk grain step-heating (Figure 64). A plateau of six steps resulted in the latter half of the analysis, albeit with somewhat variable K/Ca ratio. Biotite was fine grained (typically <0.1mm), and although the basalt showed calcite and serpentine alteration, the biotite appeared unaltered (Figure 56G-H). The plateau was acceptable with an age of 466.1±0.7 Ma (MSWD=1.59).
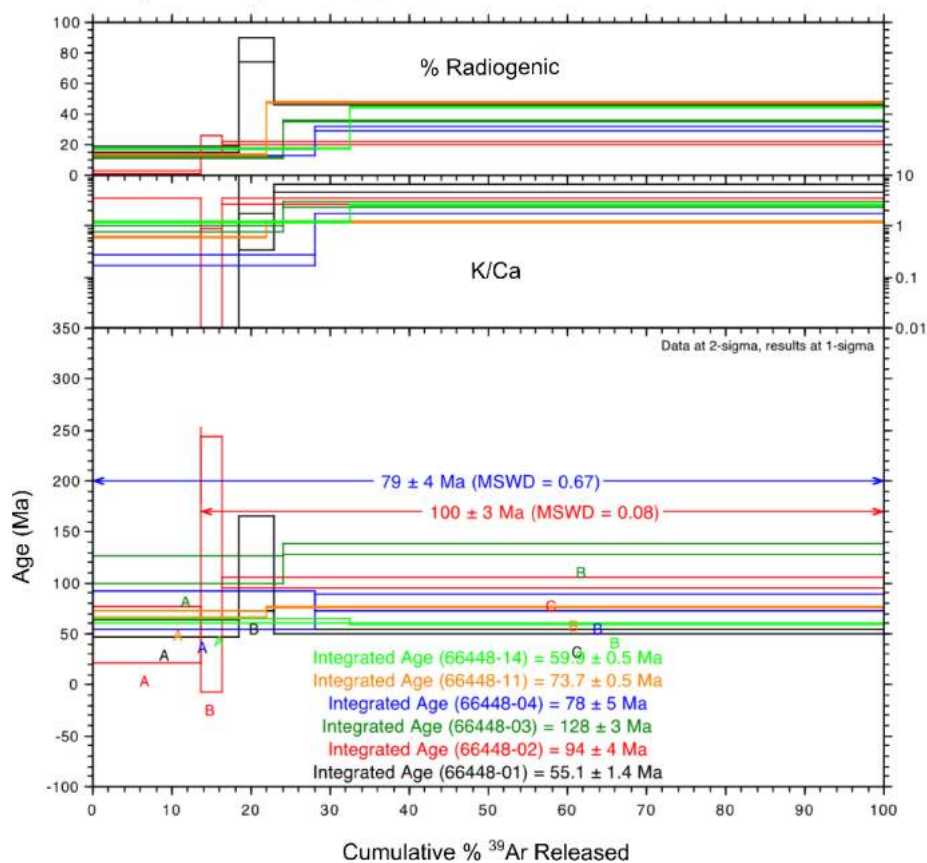
Figure 63. ^{40}Ar/^{39}Ar single crystal step-heating spectra of plagioclase from sample KS063 from basalt of the Valmy Formation. Low radiogenic Ar and no consistent age determined.
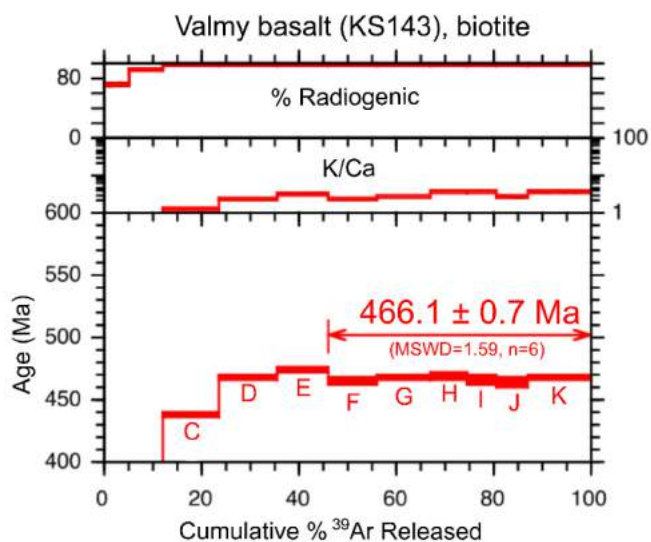
Figure 64. ^{40}Ar/^{39}Ar bulk grain step-heating spectrum of biotite from sample KS143 from basalt of the Valmy formation. Plateau age is Ordovician.

Hydrothermal illite

Dating of illite from hydrothermal alteration of feldspar phenocrysts was in general not successful in producing precise ages. Five samples were analyzed and only two yielded ages that were reasonable (Figure 65) based on geologic constraints. Illite from samples KS001 (aphyric rhyolite), KS029 (Walti quartz monzonite), and KS099 (rhyolite porphyry) had complex spectra and yielded Eocene ages that were somewhat older than their respective host rocks. Samples KS019 and KS139 of altered andesite of McClusky Creek also had complex spectra however their final steps had relatively stable K/Ca, flat patterns, and yielded ages younger than their host rocks. Typical problems encountered with ^{40}Ar/^{39}Ar dating of illite from altered feldspars include excess argon, mixed clays with the illite, and recoil loss of ^{39}Ar during irradiation (Onstott et al., 1995; Kelley, 2002; Clauer, 2013). There is evidence of mixed clays or at least two populations of illite including a very fine-grained population (Figure 66), which can explain both the variable K/Ca and recoil effect. The final heating steps for samples KS019 and KS139 are interpreted as heating of the coarser fraction of illite and offer acceptable ages of 35.71±0.12 Ma and 35.54±0.06 Ma, respectively, consistent with alteration closely following emplacement of the McClusky Creek andesite lavas. KS029 illite from altered Walti quartz monzonite produced a similar pattern to KS019 and KS139 illites with progressively younging steps with increased temperature; the final produced a relatively flat forced plateau of 36.27 ± 0.10 Ma but with a high MSWD of 183.49.

Despite imprecise results, all illite samples yielded forced plateaus or integrated (total gas) ages that are late Eocene, from ~35.5 to 42.1 Ma. Two of the ages for illite in the andesite of McClusky Creek are geologically reasonable and indicate that hydrothermal alteration of the andesite closely followed its emplacement. The other three illite samples (KS001, KS029, and KS099) produced ages that are unreasonably old based on more precise ages obtained in dating igneous minerals from unaltered versions of the same rock units. Although the illite ages for these three samples are clearly erroneous, there is good reason to suggest that they too reflect Eocene alteration and mineralization that, like samples KS019 and KS139, closely followed emplacement of their host units. The well-documented problems with dating illite: potential for excess Ar and ^{39}Ar recoil, are likely to have affected the Keystone illite analyses and produced

the older ages. However, quantifying these effects are difficult and require additional study and analyses not part of the scope of this study.
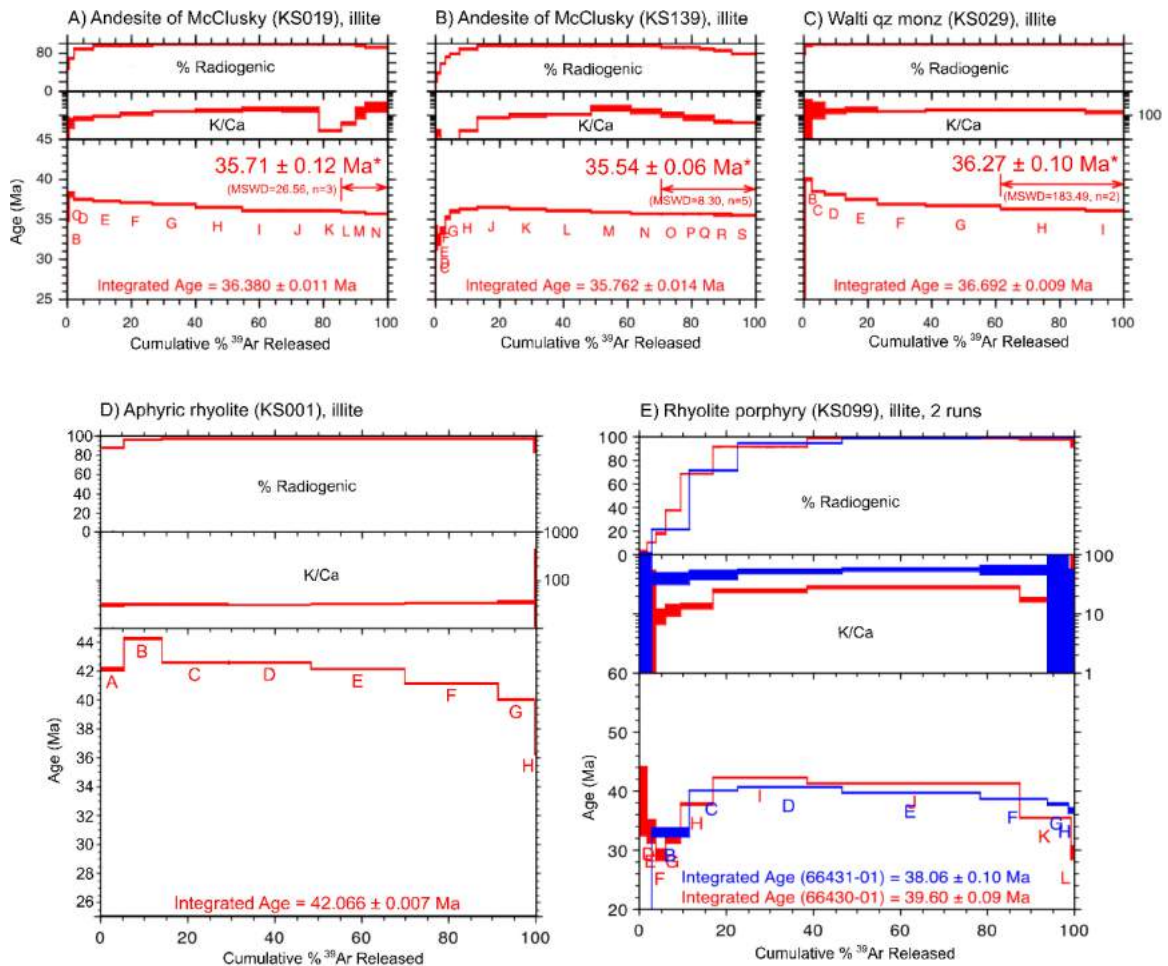
Figure 65. ^{40}Ar/^{39}Ar step-heating spectra of hydrothermal illite samples. Forced plateaus indicated by *. A) Sample KS019 from outcrop of altered andesite dike of McClusky Creek. Forced plateau through the final three steps yielded a reasonable age. B) Sample KS139 from drill core of altered andesite dike of McClusky Creek. Forced plateau through final five steps yielded a reasonable age. C) Sample KS029 from outcrop of altered Walti quartz monzonite. Forced plateau through final two steps yielded an age slightly older than the unit. Similarly, the integrated (total gas) age is too old (constrained by U-Pb zircon and biotite age). D) Sample KS001 from altered aphyric rhyolite produced a poor spectrum with no plateau, and an integrated (total gas) age that is unreasonably old (constrained by U-Pb zircon age) but also Eocene. E) Sample KS099 from altered rhyolite porphyry, analyzed twice. Poor spectra with no plateau and integrated (total gas) ages are too old but also Eocene (constrained by sanidine age). The ^{40}Ar/^{39}Ar integrated or total gas age is similar to a conventional K-Ar age determination but does not require a separate analysis for determination of total potassium.
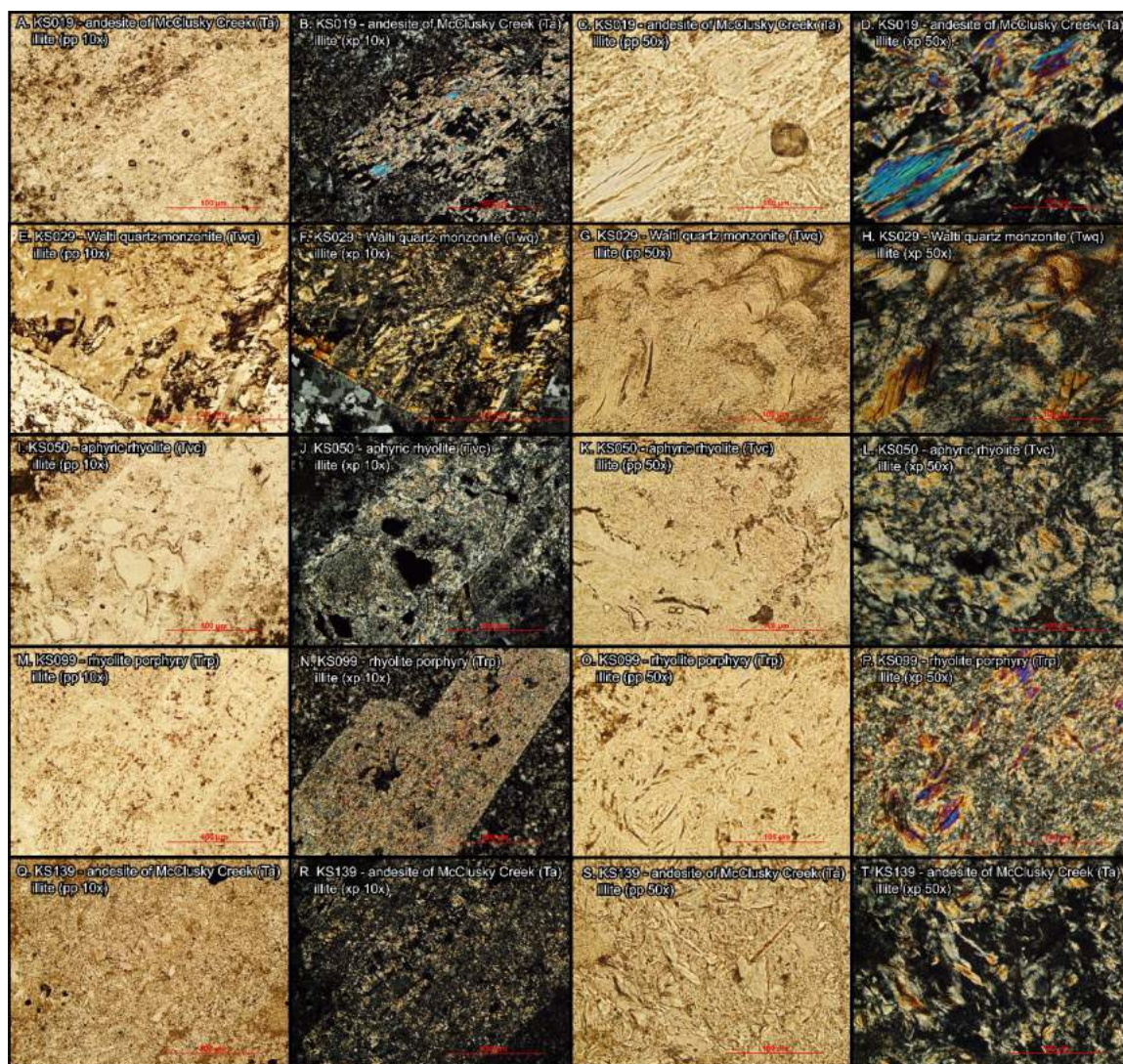
Figure 66. Micrographs of representative illite of samples selected for Ar^{40}/Ar^{39} analysis. A-D) Sample KS019 in plane and cross-polarized light and at 10x and 50x. E-H) Sample KS029 in plane and cross-polarized light and at 10x and 50x. I-L) Sample KS050 in plane and cross-polarized light and at 10x and 50x. M-P) Sample KS099 in plane and cross-polarized light and at 10x and 50x. Q-T) Sample KS139 in plane and cross-polarized light and at 10x and 50x.

Discussion

Timeline of igneous activity at Keystone

Ages determined by U-Pb zircon have larger uncertainties than $^{40}Ar/^{39}Ar$ ages. Especially when considering the individual zircon analyses, all six igneous samples essentially overlap (Figure 67). Weighted means of the U-Pb data have relatively high MSWDs (>2.8), and so these mean ages have little statistical significance. Either the analytical uncertainties associated with LA-ICP-MS are too high, or the zircon populations for each sample are not of the same age but of different zircon crystallization events, or both. If these samples were re-analyzed with a higher precision method such as TIMS, then perhaps the youngest zircons for each sample could justifiably represent the true age of emplacement.

Nonetheless, the U-Pb data confirm the Eocene age of nearly all igneous rocks at Keystone. Most zircons had ages between 34 and 37 Ma. A few zircons from the Walti quartz monzonite and dacite agglomerate were older than this range, up to 55.3±1.8 Ma. These Eocene to Paleocene zircons have magmatic morphologies (Corfu et al. 2003) that appear no different from the 34-37 Ma population. They may have been inherited from an older and deeper magmatic system that was still part of the same arc magmatism related to the subducted Farallon slab, although no Eocene magmatic ages older than ~45 Ma are known in the Great Basin.

There is no evidence for Cretaceous or Jurassic magmatism in the Keystone area. Although the Mill Canyon stock 25 km north in the Cortez Mountains is Jurassic at 158-160 Ma (Arehart et al., 2003), no Jurassic rocks were found at Keystone and no zircons derived from unequivocally local-sourced units gave Jurassic or Cretaceous ages. The volcaniclastics and aphyric rhyolite unit (Tvc) had three pre-Eocene zircons, including a date of 81.7±0.7 Ma that was likely derived from Cretaceous igneous rocks and later transported as an alluvial clast to the study area during the Eocene. Similarly, the detrital zircons from sample KS048 of the basal conglomerate had two Cretaceous zircons at 96.5±1.3 and 142.7±5.1 Ma, as well as a Jurassic zircon at 165.2±2.5 Ma, that were likely transported and deposited at the Tertiary unconformity in the Eocene.
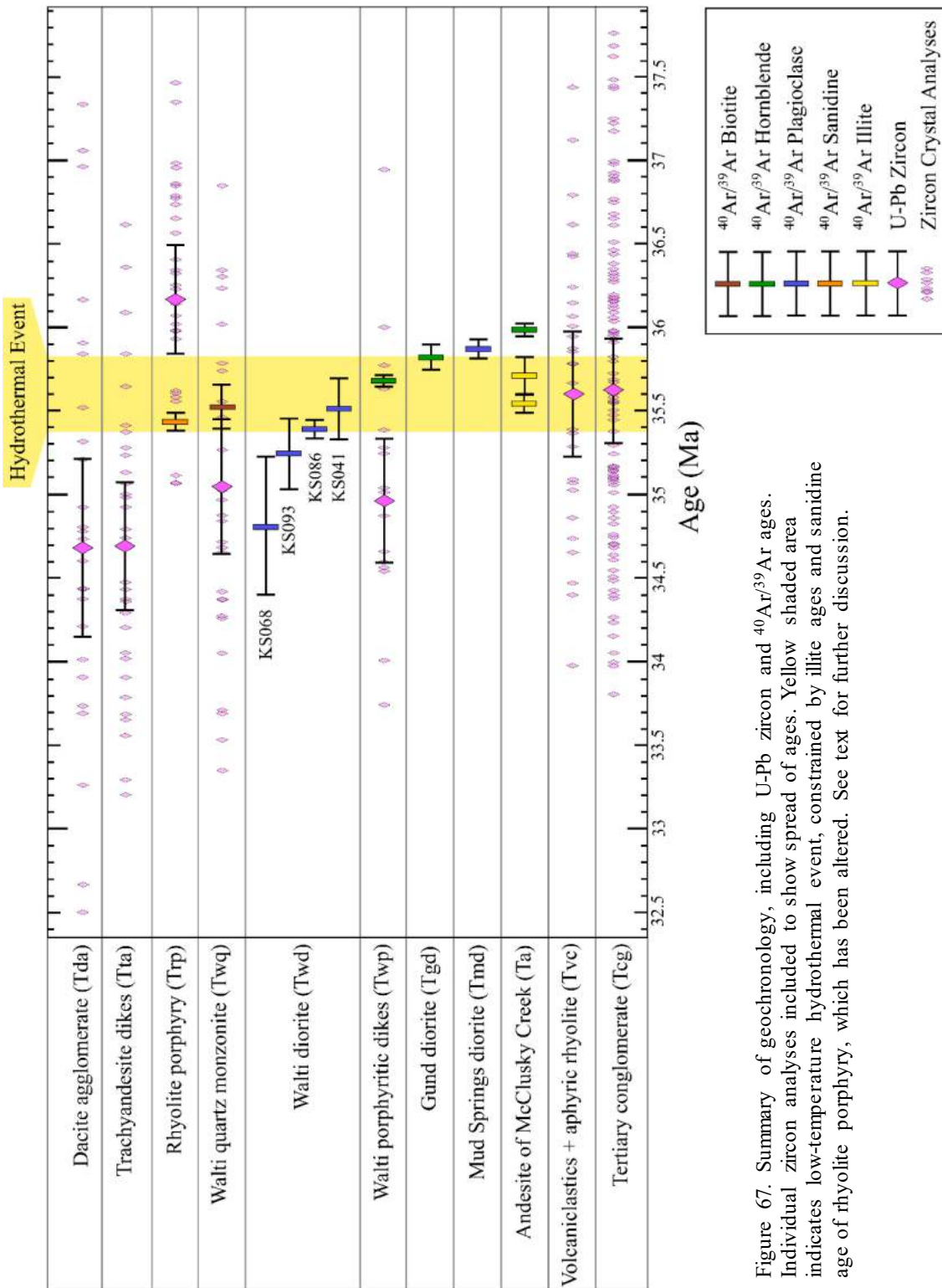
Figure 67. Summary of geochronology, including U-Pb zircon and $^{40}Ar/^{39}Ar$ ages. Individual zircon analyses included to show spread of ages. Yellow shaded area indicates low-temperature hydrothermal event, constrained by illite ages and sanidine age of rhyolite porphyry, which has been altered. See text for further discussion.

Cross-cutting relationships, U-Pb zircon, and Ar data together allow interpretation of a timeline for the emplacement of the various igneous units at Keystone (Figure 67). The following section summarizes the timeline and then addresses the geologic context of each unit from oldest to youngest.

Summary

Mafic rocks at Keystone are ocean island basalts (OIBs) that cropped out solely within the Ordovician Valmy Formation or Cambrian-Ordovician Comus Formation and most likely reflect intraplate magmatism during deposition of the Valmy and Comus. They are the oldest igneous rocks at Keystone and are unrelated to Eocene arc magmatism. Felsic tuffaceous volcaniclastics and aphyric rhyolite flows were the first Eocene igneous rocks, determined by field relations as they rest directly on the Tertiary basal conglomerate that has a maximum depositional age of 35.62 ± 0.32 Ma. Andesite lavas of McClusky Creek are ~35.99 ± 0.04 Ma, which overlaps within uncertainty with, but in places may be slightly older than, the Eocene basal conglomerate. The Mud Springs and Gund diorites are chemically similar to the andesite and were emplaced at 35.87 ± 0.06 Ma and 35.82 ± 0.08 Ma, respectively. Igneous rocks of the Walti magmatic system followed next, beginning with the Walti intermediate porphyritic dikes at 35.68 ± 0.04 Ma. The Walti is a composite pluton that likely emplaced and cooled in stages. The oldest ages for the diorite and quartz monzonite phases are 35.51 ± 0.19 Ma and 35.52 ± 0.14 Ma, respectively. The rhyolite porphyry emplaced next, cutting the Mud Springs, at 35.43 ± 0.06 Ma. Interestingly, the rhyolite porphyry had the oldest U-Pb zircon ages, suggesting the melt evolved from or incorporated inherited zircons from an older and deeper chamber, unrelated to the Walti. The trachyandesite and dacite agglomerate mark the end of magmatic activity at Keystone, however their Eocene ages are poorly constrained.

Basalts of the Valmy Formation (Ovb)

$^{40}Ar/^{39}Ar$ dating of biotite from sample KS143 yielded an age of 466 ± 0.7 Ma, which is Middle Ordovician and consistent with biostratigraphic ages from limestone at Keystone (Table 1). All basalts, mafic sills, and greenstones at Keystone crop out solely within the Ordovician Valmy or Cambrian-Ordovician Comus Formations. All samples of basalts have distinctive and notably high concentrations of

compatible and incompatible trace elements consistent with ocean island basalts (OIB) and unlike depleted mid-ocean ridge basalts (MORB) or arc-related basalts. The basalts and ultramafic rocks most likely reflect intraplate magmatism during deposition of the Valmy and Comus in a deep basin setting away from the passive margin slope. However, the presence of abundant limestone is indicative of relatively shallow water depths that may have accompanied constructional volcanic centers (e.g., Bloomstein et al., 1991; Breit et al., 2005; Cook, 2015). Modern OIBs are associated with intraplate hot spots or mantle plumes and rarely with oceanic ridges. The Valmy and Comus formations at Keystone are part of the Roberts Mountains allochthon, and therefore, the magmatism that produced the basalts did not occur at Keystone but possibly was transported 10s of kms or more from the west.

Volcaniclastics and aphyric rhyolite (Tvc)

U-Pb zircon results had wide uncertainties that do not resolve the time of emplacement. However, the distribution of zircon ages was similar to the underlying Tertiary basal conglomerate's (Tcg) detrital zircons, supporting the interpretation that the two were sequentially deposited. The occurrence of the volcaniclastics unit on either side of the Keystone window and resting directly on Paleozoic rocks strongly support it being the first Eocene volcanic unit at Keystone. The aphyric rhyolite lava differs petrographically and chemically from the younger Trp porphyritic rhyolite, excluding it as a possible source. Therefore, no source pluton is currently identified for the aphyric rhyolite.

Andesite of McClusky Creek (Ta)

^{40}Ar/^{39}Ar dating of hornblende from samples KS135 and KS144 of the andesite lavas of McClusky Creek yielded the oldest ages. Hornblende is shown to be the most retentive of radiogenic ^{39}Ar, with diffusion studies demonstrating a closure temperature ~500 °C, which varies slightly based on cooling rate and grain size (McDougall and Harrison, 1999, p.158-159). Given the sampling of a lava that rapidly cooled as evident from glassy matrices of some samples, the lack of visible alteration of hornblende, and the quality of flat spectra, the cooling age is representative of the emplacement age of the andesite unit.

Sample KS144's spectrum has a robust plateau compared to KS135's, which has a slight climbing spectrum. Sample KS135 was collected from an outcrop only 500 m west of the Mud Springs pluton, which

has a plagioclase $^{40}Ar/^{39}Ar$ age of 35.87±0.065 Ma from sample KS003. The initial steps in KS135's

spectrum had low radiogenic Ar, and a low precision plateau of only two steps (with 58.8% of the total ^{39}Ar

released) occurs at the end of the analysis at 35.85±0.08 Ma (MSWD=4.98). In contrast, sample KS144

was collected from 2 km south of the Mud Springs pluton and was most likely unaffected by any reheating

that may have accompanied intrusion of the Mud Springs diorite. KS144's plateau at 35.99±.04 Ma

(MSWD=0.75) is therefore the preferred age.

Mapping shows the only unit resting on the andesite are Tertiary to Quaternary gravels and

alluvium. Units underlying the andesite include the Tda dacite agglomerate and siliceous rocks of the

Valmy Formation. Field relations between the McClusky andesite and the volcaniclastics and aphyric

rhyolite unit (Tvc) are unknown, although mapping suggests the volcaniclastics unit underlies the dacite

agglomerate's western margin. The volcaniclastics unit and dacite agglomerate are therefore likely older

than the andesite lavas of McClusky Creek. However, the textures observed in the dacite agglomerate allow

for subvolcanic emplacement of the unit, making it potentially younger than the andesite. This possibility is

supported by the presence of zircons in the dacite that are younger than any other zircons analyzed from

other units at Keystone (Figure 49B).

Mud Springs diorite (Tmd)

The proximity to approximately coeval volcanics and presence of miarolitic cavities suggest the

Mud Springs pluton was shallowly emplaced. Most of the pluton has alteration of mafic minerals to chlorite

and sample KS003 (selected for $^{40}Ar/^{39}Ar$ of plagioclase) from the eastern margin of the pluton exhibited

the least amount of alteration. Single-crystal step-heating spectra yielded two age population clusters, with

the older having a tighter distribution. The older population at 35.87±0.06 Ma (MSWD=0.21) is the best

approximation for the emplacement of the pluton, overlapping with the Gund diorite. Differences in trace-

element concentrations and Nb/Zr suggest the two are not directly related. However, it is possible that the

Mud Springs diorite, being slightly more silicic and alkaline than the Gund diorite, could represent a more

evolved and hydrous melt from the Gund system that was emplaced higher in the crust.

Interestingly, the younger population cluster has a weighted mean age of 35.49±0.11

(MSWD=2.3), which overlaps with the $^{40}Ar/^{39}Ar$ age of sanidine (35.43±0.06 Ma) from the rhyolite

porphyry. This intrusion cuts the northwest margin of the Mud Springs and is only 800 m from sample KS003. The bimodal cooling ages of plagioclase from sample KS003 may therefore be attributed to reheating and some argon loss during the emplacement of the Trp rhyolite porphyry.

Gund diorite (Tgd)

Plagioclase from sample KS079 and hornblende from sample KS114A were dated by $^{40}Ar/^{39}Ar$ to determine the age of the Gund diorite. The samples were taken from different locations: sample KS079 from the larger lopolith-shaped stock 400 m south of the Walti pluton, and sample KS114A from the smaller sill 850 m southwest of the Walti pluton. All outcrops of the larger Gund stock had mafic minerals altered to chlorite and sample KS079 had the least disturbed plagioclase (Figure 54E). However, plagioclase spectra were poor, and no meaningful age was derived. The Gund stock was emplaced along the thrust fault that juxtaposes allochthonous Ordovician rocks of the Valmy Formation above autochthonous Devonian carbonates. The wall rocks proximal to the Gund stock are contact metamorphosed to marble and calc-silicate hornfels, but silicification and jasperoid alteration follows the thrust fault on either side of the stock. Since plagioclase has a relatively low closure temperature ~225-300 °C (Cassata et al., 2009), it is possible that hydrothermal activity responsible for the alteration disturbed the retention of radiogenic Ar in plagioclase. Alternatively, another heat source such as the nearby Walti pluton, only 400 m to the north, could have contributed to argon loss.

In contrast, hornblende from sample KS114A of the Gund sill yielded a flat spectrum with a plateau at 35.82±0.08 Ma (MSWD=0.71). Unlike the stock, the Gund sill was emplaced into a low-angle fault bounded on either side by lower plate carbonates. Wall rocks proximal to the sill are contact metamorphosed to marble or calc-silicate hornfels depending on the protolith, but are not hydrothermally altered. The lack of visible alteration of mafic minerals, the greater distance of the sample from the Walti pluton, and a flat spectrum support this hornblende cooling age as reflecting the emplacement age of the Gund diorite. This age is slightly younger than but overlaps within uncertainty, the andesite of McClusky Creek. The similarities in age as well as the major and trace element geochemistry and plagioclase compositions are permissive for a genetic relationship between the two units. The Gund diorite may therefore represent an intrusive equivalent of the andesite lavas of McClusky Creek.

Walti intermediate porphyritic dikes (Twp)

Hornblende from sample KS095 yielded a plateau of only two steps (with 61.2% of the total ^{39}Ar released) of 35.68±0.04 (MSWD=1.11). This is older than sample KS126's U-Pb zircon weighted mean age of 34.96±0.38 (MSWD=2.8), however the hornblende age is captured within the range of zircon ages (Figure 67). Sample KS126 is from a dike cutting the interior of the Mud Springs pluton. Sample KS095 is from a dike cutting the Paleozoic rocks, 500 m west of the Mud Springs, and <100 m east of outcrops of the Walti diorite. The Walti porphyritic dikes that cut the Mud Springs are pervasively altered to chlorite, sericite, epidote, and calcite, and were not viable for ^{40}Ar/^{39}Ar dating. Sample KS095 contained biotite that was altered to chlorite and epidote, oxidized and chloritized mafic glomerocrysts, and resorbed K-feldspar and quartz phenocrysts suggesting disequilibrium. Hornblende phenocrysts had minor alteration to clay, and had inclusions of groundmass (Figure 56B), which may explain the climbing and then descending ^{40}Ar/^{39}Ar spectrum (Figure 55D). Steps with younger age and higher K/Ca could reflect the analysis of the altered rims and groundmass inclusions.

As discussed previously, the Walti intermediate porphyritic dikes are interpreted as related to the magmatic system of the Walti pluton. Phenocryst assemblages in the dikes are variable but similar to the Walti pluton, with consistent features such as a porphyritic texture with widely spaced coarse (>5mm) plagioclase of similar anorthite content (Figure 14). Their major and trace element concentrations in Walti dikes were also variable but typically plotted along a line joining the Walti diorite and Walti quartz monzonite, possibly representing a general differentiation trend or mixing line (Figure 42; Figure 44). Field evidence of their connection includes the presence of >1 cm K-feldspar megacrysts in outcrops of the Walti diorite only 80 m west of the sample KS095 of the Walti dikes. K-feldspar megacrysts were not observed in any other part of the Walti pluton, and were unusual as they occurred in a dark gray, relatively more mafic matrix. Sample KS095 in a Walti intermediate porphyritic dike also had >1 cm K-feldspar megacrysts that were resorbed and partly rimmed to K-bearing mafic minerals like biotite (Figure 30). This strongly suggests the dike was a direct injection of melt from the diorite and carried the same phenocryst assemblage but was subject to disequilibrium during cooling.

Sample KS126 in a Walti intermediate porphyritic dike was one of two samples dated by U-Pb that had high-U zircons (1000s ppm vs. 100s ppm) (Figure 49A). Uranium was high enough in KS126 zircon to cause Pb loss which made a younger integrated age before the high-U zircon analyses were omitted from the age calculation. High-U zircons are typically observed in igneous rocks derived from evolved or highly differentiated melts. However, causes for high U and other trace elements in zircon may include local disequilibrium and poor diffusion rates. High-U zircons are unlikely to crystallize in equilibrium with its melt, as studied zircon-melt partition coefficients require felsic melts to have unreasonably high (>100 ppm) U (Xiang et al., 2011). Whole-rock geochemistry of igneous rocks at Keystone have <5 ppm U, with few samples as high as 9.5 ppm. Instead, high-U zircons likely crystallized with local disequilibrium caused by rapid growth relative to diffusion. Samples from the Walti intermediate porphyritic dikes often show evidence of magma disequilibrium, with resorbed quartz and feldspar phenocrysts mantled by biotite probably caused by reaction with a relatively mafic melt (Figure 30).

The Walti intermediate porphyritic dikes most likely represent roof dikes of the Walti pluton. The pluton was mostly emplaced into lower plate carbonate rocks with the diorite phases partly intruding the upper plate siliciclastics. Outcrops of the dikes are found in stratigraphic horizons above the pluton, and in the shallowly emplaced Mud Springs pluton. Individual dikes likely formed at different times during the development of the composite pluton, producing the variable compositions and phenocryst assemblages. The hornblende cooling age from sample KS095 suggests it may have been one of the first dikes to intrude, and its age overlaps with the rhyolite porphyry. Outcrops of the dikes are found close to the southern and western margins of the rhyolite porphyry, but none cut the rhyolite itself.

Walti diorite (Twd)

Four samples of the Walti diorite were dated by $^{40}Ar/^{39}Ar$ on plagioclase. Three samples were from different bodies along the composite pluton's eastern margin, which reflect the top of the east-tilted pluton where the diorites intrude upper plate rocks. The fourth sample was from an enclave of diorite within the quartz monzonite body. The Walti diorite typically exhibits chloritization of mafic minerals, resulting in no viable hornblende or biotite for $^{40}Ar/^{39}Ar$ dating. Plagioclase from all samples were relatively unaltered, with sample KS068 having near pristine plagioclase phenocrysts (Figure 54D).

Given the low closure temperature of plagioclase and geologic context of a composite pluton, the wide spread of ages is not surprising. Interestingly, the three separate samples from the Walti diorite marginal phases overlap in age, having a cumulative weighted mean age of 35.39±0.11 Ma, whereas the sample from the enclave is younger at 34.81±0.42 Ma. Mafic enclaves are recognized in other composite plutons, with models proposing they are early crystal accumulations cogenetic with a progressively evolving host granitoid (Zhang et al., 2014; Zhang and Zhao, 2017). A similar model is called upon for the relationship between the Walti diorite and Walti quartz monzonite (Figure 68). The cooling age of sample KS068 from the enclave may reflect the cooling of the surrounding Walti quartz monzonite phase, which crystallized after the more mafic diorite phase.
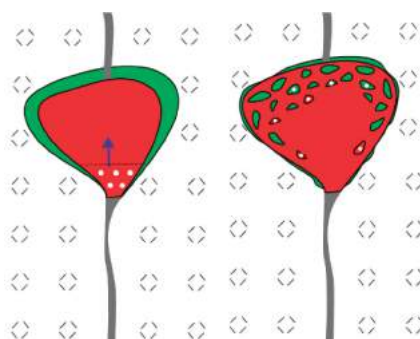
Figure 68. Schematic cartoon illustrating the formation of a granitoid pluton (red) and its cogenetic dioritic enclaves (green). Modified from Zhang and Zhao (2017).

Walti quartz monzonite (Twq)

Sample KS137 was collected from drill core at 530 m. Biotite was coarse and unaltered, yet the $^{40}Ar/^{39}Ar$ spectrum did not yield a plateau and had variable K/Ca for every step (Figure 57). An isochron through the final four steps yielded an age of 35.52±0.07 Ma, which is older than but overlaps within uncertainty with the U-Pb zircon age of 35.05±0.41 Ma; the biotite age is also within the range of individual zircon ages (Figure 67). The isochron age, however, does not overlap with a published K-Ar age of biotite from the Walti pluton at 34.2±0.7 Ma (Silberman and McKee, 1971; recalculated using decay constants and isotopic abundances of Steiger and Jäger (1977)).

The biotite age is as old as some of the plagioclase ages from the Walti diorite, and may reflect simultaneous cooling of different parts of the composite pluton. An aeromagnetic survey provided by U.S. Gold Corp. shows a ~25 km² high magnetic anomaly centered on the Walti, which extends past its surface exposure (Figure 69). Sample KS137 is located near the northernmost extent of this magnetic anomaly, and likely represents the lateral limit of the pluton at depth. This distal area of the pluton therefore likely crystallized and cooled first whereas the interior of the pluton remained relatively hotter.
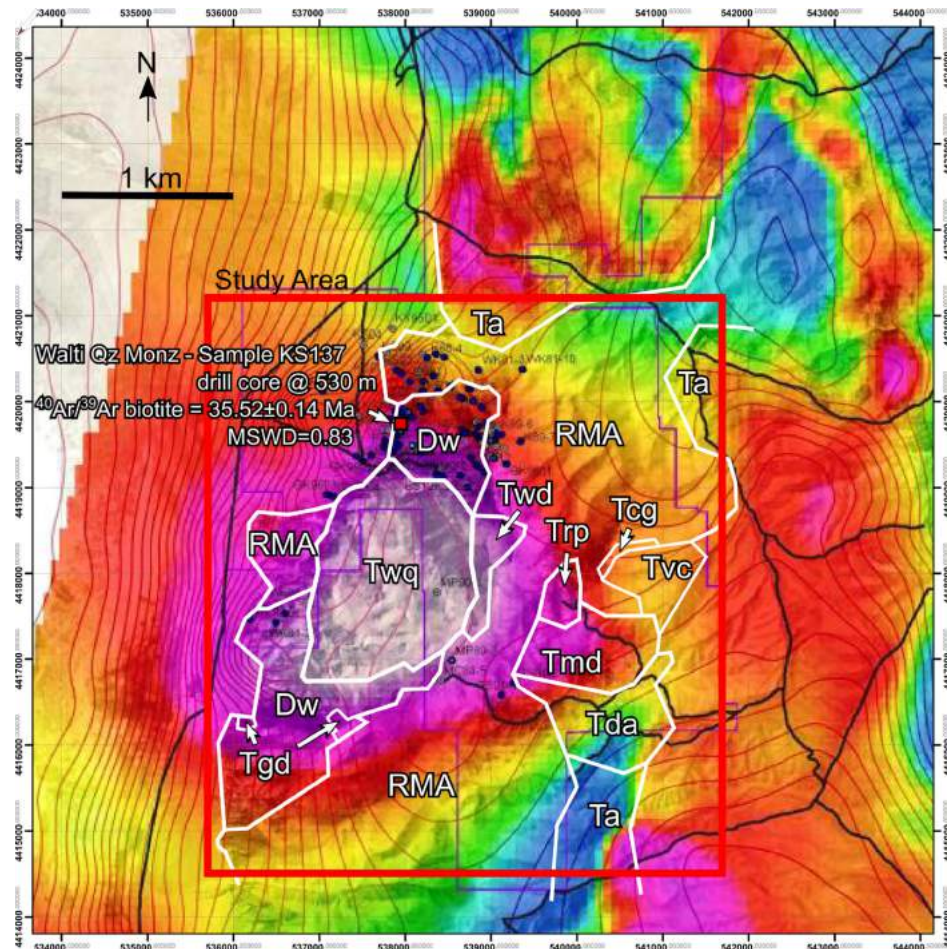
Figure 69. Reduced-to-pole aeromagnetic map of the Keystone project. Thesis study area outlined in red. Simplified geologic map units outlined in white. The magnetic high is centered on the Walti pluton (Twq), and the anomaly continues beyond the pluton's surface exposure, indicating a much larger intrusion at depth. Location of sample KS137 indicated by red square. Walti pluton was intercepted 530 m below surface and was dated by $^{40}Ar^{39}Ar$ on biotite. Adjacent magnetic high-low chatters are products of the andesite of McClusky Creek (Ta), and extend past the study area.

Rhyolite porphyry (Trp)

Sample KS098 was collected from the unaltered interior of the rhyolite porphyry intrusion. Although the margins of the intrusion exhibit pervasive sericitic alteration and bleaching, sample KS098's feldspars were intact and sanidine was acceptable for $^{40}Ar/^{39}Ar$ dating. The single-crystal total fusion age of 35.43±0.06 Ma (MSWD=11.90) is the best approximation for the emplacement age. Interestingly, the U-Pb zircon weighted mean age is significantly older at 36.17±0.33 Ma (MSWD=3.6). However, when considering the individual zircon analyses, the sanidine age falls within the range of zircon ages.

The sample KS044 of the rhyolite porphyry unit (Trp) was one of two samples dated by U-Pb that had high-U zircons (1000s ppm vs. 100s ppm) (Figure 49A). As mentioned before, causes for high U and other trace elements in zircon include local disequilibrium and poor diffusion rates. The slightly older U-Pb zircon age may record crystallization during magma ascent, and the emplacement age is best approximated by the $^{40}Ar/^{39}Ar$ sanidine age. The older zircon ages of the rhyolite porphyry suggest the melt evolved or inherited zircons from an older magmatic body, possibly unrelated to the Walti. Since the rhyolite porphyry was preferentially altered over the adjacent Mud Springs diorite and nearby Walti intermediate porphyritic dikes, both of which are older, the rhyolite likely intruded into a major structure that also controlled hydrothermal fluids.

Trachyandesite dikes (Tta)

Zircons from sample KS025 of the trachyandesite had a wide range of ages that overlap with the Walti quartz monzonite (Figure 67). Dikes of the trachyandesite were found only cutting rocks of the Roberts Mountain allochthon, so their relationship with the Walti pluton is unclear. The dikes also only crop out in the northwest side of the study area. These rocks have a unique texture, geochemistry, and alteration with enriched K_2O and depleted CaO and Na_2O. Little beyond their Eocene age can be confirmed.

Dacite agglomerate (Tda)

The dacite is different from all other Eocene rocks with unique geochemistry suggesting its melt may have incorporated more crust than other rocks. Evidence suggesting a greater crustal involvement in

its magma genesis include its high alumina saturation index (ASI), which plots in the peraluminous field, well beyond other fresh igneous rocks at Keystone. The dacite also has higher Nb/Y and has a subdued Eu anomaly, both of which are unusual compared to other more evolved Eocene igneous rocks at Keystone. The presence of zircons possibly younger than those from any other unit (~34.68 ± 0.54 Ma) support it being the last Eocene magmatic event at Keystone (Figure 67). This contradicts field constraints for the agglomerate since it it underlies the widespread andesite of McClusky Creek. However, the textures of the dacite, including its breccia texture, reflect a volcanic and/or subvolcanic origin, thus allowing for a part-intrusion, part-volcanic dome emplacement style. Dikes related to the dacite have similar alteration to dikes of the andesite of McClusky Creek, suggesting both had intruded prior to hydrothermal activity. Mapping at greater detail may resolve different lavas and pyroclastic units within the agglomerate and provide context for sample KS051's U-Pb zircon results.

Relationship of Eocene magmatism at Keystone to regional magmatism

The Keystone igneous center is similar in age, duration of magmatism, and composition to other Eocene centers that are widespread in north-central Nevada and is consistent with the regional southwestward sweep of calc-alkaline arc magmatism in Nevada from ~44 to 34 Ma (e.g., Henry, 2008; Christiansen and Yeats, 1992). Magmatism at Keystone spanned ~36.0-34.7 Ma (Table 4), a ~1.3 Ma span during which numerous intrusions and volcanic rocks ranging in composition from intermediate to silicic were emplaced. The span of magmatism at Keystone is comparable to other moderate to large Eocene centers in north-central Nevada. For example, magmatism in the southern Carlin trend in the Piñon Range lasted about 1.0 Ma (Hollingsworth et al., 2017), and magmatism at nearby Cortez and Fye Canyon spanned from ~35.7-35.3 Ma for early rhyolite dikes and lavas with brief Caetano caldera-related magmatism lasting only from ~33.9-33.7 Ma (Colgan et al., 2011). No mafic rocks beyond the alkaline basalts of the Valmy and Comus were found at Keystone, which is consistent with the dominantly andesitic to dacitic volcanic fields that characterize northeast Nevada during the Eocene. This regional style of magmatism transitioned at ~34 Ma to felsic caldera-forming magmatism that continued southwestward,

culminating in the Oligocene ignimbrite flareup. Keystone lies at the southwestern end of a "caldera gap"

in northeastern Nevada (Figure 70). Indeed, the ~34 Ma Caetano and Hall Creek calderas are among the

first to mark this transition and both are only 25 km from Keystone (Figure 71).
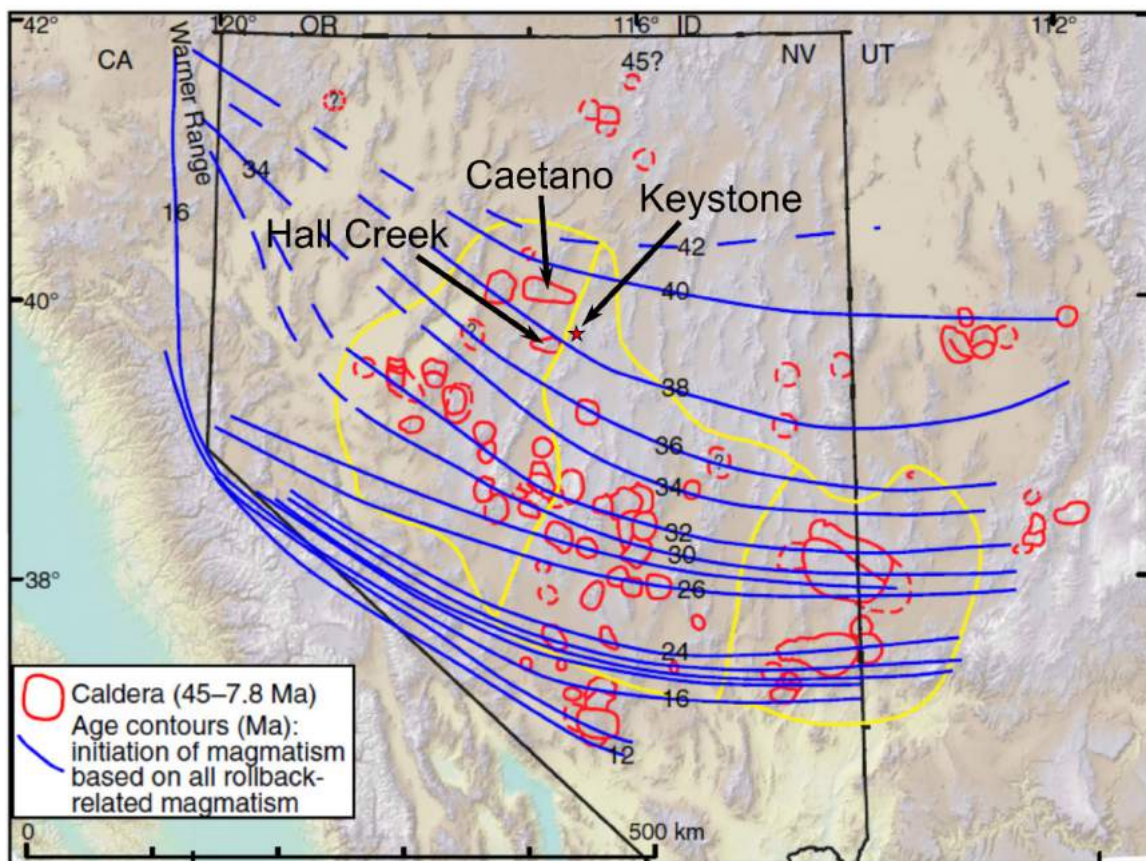
Figure 70. Regional map of Eocene through Miocene magmatism and calderas of Nevada and Utah. Location of Keystone marked by red star. Nearby Caetano and Hall Creek calderas indicated, both of which are ~34 Ma. Keystone lies at the southwest end of the "caldera gap" in northeast Nevada, at the transition from intrusive/effusive to pyroclastic magmatism. Modified from Henry and John (2013).

Thirty km southeast of Keystone is the ~35.92-36.15 Ma (Long et al., 2014) Mt. Hope igneous

complex and associated porphyry molybdenum deposit (Figure 71; Westra and Riedell, 1995). At Mt.

Hope, numerous intrusions and volcanics are relatively silicic (high-Si rhyolite to dacite) compared to rocks

at Keystone. Small-volume rhyolitic tuffs surround rhyolite porphyry intrusions composed of subhedral to

euhedral quartz, K-feldspar, and plagioclase phenocrysts. The widely contrasting styles of hydrothermal

activity between Mt. Hope and Keystone is interesting, especially considering that their ages are quite

similar. Neither porphyry mineralization nor molybdenite were observed at Keystone, suggesting that strongly contrasting magmatic composition and possibly emplacement style and efficiency of fluid extraction and focusing (e.g. high fluorine and highly evolved rhyolitic apophyses; Audétat and Li, 2017) contributed to the differences.

Closer to magmatic activity at Keystone are quartz porphyry dikes and sills in and near the Cortez Hills Carlin-type gold deposit, 25 km north of Keystone (Figure 71). Several $^{40}Ar/^{39}Ar$ dates of sanidine from these dikes repeatedly overlap in time with igneous rocks at Keystone and range from 35.29±0.08 to 35.69±0.06 Ma (Artz, 2004; Colgan et al., 2011). Interestingly, these ages overlap in time with the rhyolite porphyry Trp at Keystone (35.43±0.06 Ma) as well as rhyolite lava from the large silicic center at Fye Canyon, half way between Cortez and Keystone. The abundant quartz porphyry dikes at Cortez are rhyolitic and commonly have quartz, sanidine, plagioclase, and biotite phenocrysts, like the Trp rhyolite at Keystone. Importantly, although most quartz porphyry dikes crosscut the Carlin-type mineralization at Cortez Hills, a few dikes are altered and contain realgar, pyrite, and low Au concentrations. One such dike with pyrite veinlets and disseminated realgar and orpiment gave a $^{40}Ar/^{39}Ar$ age of 35.37±0.07 Ma on igneous biotite, leading to the interpretation that the dikes were emplaced during the late stages of Carlin-type mineralization (Henry, 2009; Arbonies et al., 2011). It is possible the rhyolite porphyry Trp was the last intrusion at Keystone, given the larger uncertainties for the U-Pb zircon ages of the trachyandesite and dacite agglomerate (Figure 67). The quartz porphyry dikes at Cortez predated major explosive silicic volcanism associated with the Caetano caldera by about 1.3 Ma, suggesting that the two are unrelated, or if related, there was a substantial lull between activity. Compositionally the Cortez center is much more silicic overall than the Keystone center. The quartz-phyric rhyolite dikes at Cortez are not obviously associated with less evolved intermediate rocks, which are abundant at Keystone. This compositional difference in concert with the depth that major intrusions were emplaced in the upper crust may have influenced the Eocene metallogeny of the Battle Mountain-Eureka mineral belt.
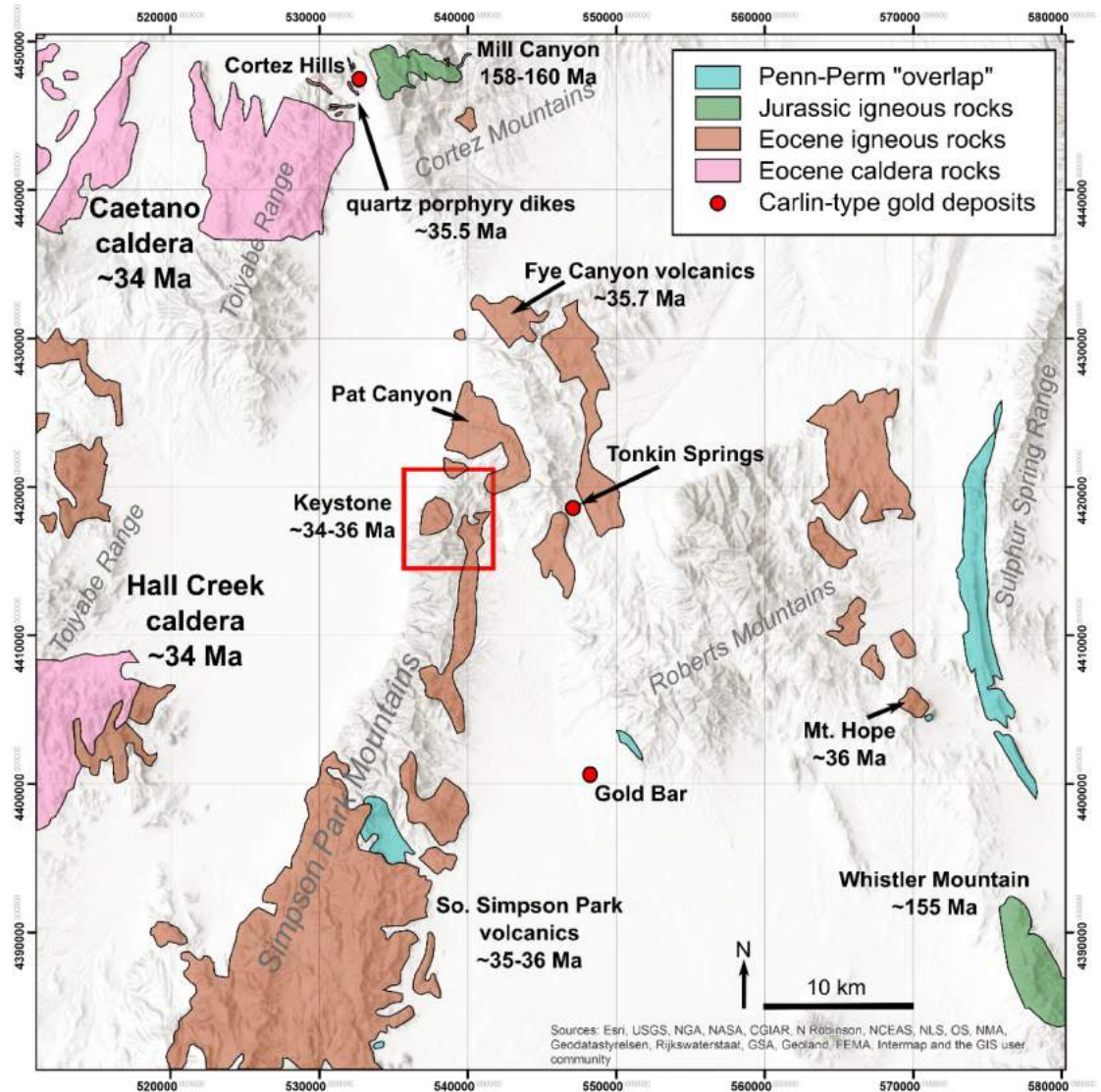
Figure 71. Simplified geologic map of Jurassic and Eocene igneous rocks in the region surrounding Keystone. Miocene volcanics omitted for clarity. Study area outlined in red box. Locations discussed in text. Pennsylvanian-Permian "overlap" rocks shown for discussion on Cenozoic conglomerates. Radiometric ages are from McKee et al. (1971), Silberman and McKee (1971), Westra and Riedell (1996), Artz (2004), Arbonies et al. (2011), Colgan et al. (2011), and Henry and John (2013). K-Ar ages have been recalculated to decay constants and isotopic abundances after Steiger and Jäger (1977).

Unfortunately, there are few publications on the volcanic fields of the northern and southern Simpson Park Mountains. In the northern Simpson Park Mountains are volcanic rocks of Fye Canyon, 12 km north of Keystone (Figure 71). Rocks here include andesitic, dacitic, and rhyolitic lava flows and domes. $^{40}Ar/^{39}Ar$ ages of plagioclase from rhyolite are 35.73 ± 0.06 Ma and 35.82 ± 0.12 Ma, and from

andesite are 34.92 ± 0.37 Ma (Colgan et al., 2011). Undivided volcanics have been mapped in the area surrounding Pat Canyon, immediately north of the Keystone study area. It is likely this area includes an extension of the andesite of McClusky Creek (Ta) mapped at Keystone. Undivided Tertiary volcanics have been mapped south and east of Tonkin Springs, and include rhyolitic to dacitic tephra, ignimbrites, and local lava flows (Noble, 2008, Technical Report on the Tonkin Project, prepared for US Gold Corporation, now McEwen Mining). This area appears to have continuity with the andesite of McClusky Creek, to the west and across McClusky Pass. A >600 km^2 Eocene volcanic field covers the southern Simpson Park Mountains (Figure 71; McKee, 1968). Most of the rocks are andesite to dacite flows and rhyolitic to dacitic intrusions. K-Ar ages of biotite from a dacite flow and hornblende from an andesite flow are 35.4 and 36.3 Ma, respectively (McKee et al., 1971; recalculated to decay constants and isotopic abundances after Steiger and Jäger (1977), no age uncertainties provided). The overlapping ages suggest volcanics across the Simpson Park Mountains are coeval with magmatic activity at Keystone. Three sizeable intrusions (1 to 3 km^2) of dacite and rhyolite composition occur in the central and southern Simpson Park Mountains (McKee, 1968), but intrusions are rare owing to an abundance of intermediate lavas. Certainly, the large volume of intermediate lavas requires large intrusions at depth however, the great thickness of lavas and/or insufficient extension and/or erosion have yet to expose Eocene intrusions in underlying, covered Paleozoic strata.

Hydrothermal activity and distribution at Keystone

Hydrothermal alteration of Eocene age at Keystone is broadly divided into three categories according to styles (Table 5): 1) high-temperature alteration associated primarily with the Walti pluton, resulting in skarn, endoskarn, and sodic-calcic alteration, 2) relatively low-temperature acidic alteration present in Paleozoic rocks along major structures and a few igneous units including andesite dikes of McClusky Creek (Ta), dacite dikes (Twp), volcaniclastic rocks (Tvc), and the rhyolite porphyry (Trp), and 3) chlorite-epidote-calcite alteration present throughout many of the intrusions, which is classified as propylitic alteration.

Table 5. Summary of hydrothermal alteration

Alteration	Distribution	Minerals and Textures	Geochemistry
High-temperature			
Skarn	Historic Keystone mine at northern margin of Walti in Wenban limestone (Dw). Minor occurrences at limestone roof pendants of the Walti.	Garnet, quartz, calcite, and base metal sulfide mineralization including pyrite, chalcopyrite, and galena	+Cu, Pb, Zn, Fe, S
Skarnoid/ Hornfels	Thermal halo around major intrusions. Affects both upper and lower plate rocks.	Fine-grained garnet and pyroxene in calcareous rocks, resulting in tan to green color. Hardening of siliciclastics.	No significant change in whole-rock chemistry
Endoskarn	Local to intrusion-marble contacts in the Walti (Twq+Twd), Mud Springs (Tmd), and Gund (Tgd)	Oligoclase, diopside, titanite	+ Ca, Na -Si, Fe
Sodic-calcic	Common throughout Walti pluton (Twq+Twd)	Oligoclase to albite, diopside, actinolite, tremolite, epidote, calcite	+ Ca, Na -Si, Fe
Low-temperature			
Epithermal	Pervasive in upper plate rocks and dikes cutting the upper plate, Tertiary conglomerate (Tcg), volcaniclastics and aphyric rhyolite (Tvc), and rhyolite porphyry (Trp).	Quartz veins, oxidized and silicified breccias, pyrite, kaolinite, illite	+As, Hg, Bi, W, S, Se, Tl, Sb, S, Ba -Ca, Na, Sr
Carlin-style	Along upper-lower plate transitions, lower plate carbonates, andesite dikes (Tad) cutting lower plate.	Silicified breccias, jasperoid, decarbonatized limestone, pyrite, illite	+Au, As, Hg, Sb, Tl, S, Se, Ba, W, K, Rb -Na, Ca, Sr
Propylitic	Typical of all intrusions, most pervasive in Mud Springs (Tmd), Gund (Tgd), and Walti dikes (Twp). Common in the Walti pluton.	Chloritized mafics minerals, epidote, calcite	No significant change in whole-rock chemistry

Base metal skarn mineralization is restricted to the limestone contacting the Walti pluton and is undoubtedly a product of magmatic-hydrothermal fluids from the Walti system. Both the diorite and quartz monzonite phases show endoskarn alteration proximal to marble contacts, and it is not clear which phase generated the fluids responsible for skarn mineralization. The diorite phase occurs sporadically throughout the pluton as enclaves, yet is ubiquitous in its proximity to skarn occurrences.

Throughout the interior of the Walti pluton are broad zones of sodic-calcic alteration of varying intensity, expressed as an increase in Na_2O and CaO, and decrease in FeO and SiO_2. Outcrops are white to light gray and resistant to weathering, in contrast with clay-altered rocks that are also bleached but weather more easily. This type of alteration may represent downwelling and warming of meteoric saline fluids, examples of which are widespread in Nevada including the Jurassic Yerington porphyry (Carten, 1986) and several Eocene intrusions in the Battle Mountain district (King, 2017). Like associated skarn alteration, this hydrothermal alteration is tied to the emplacement and cooling of the Walti pluton.

Low-temperature clay and quartz alteration affected the rhyolite porphyry (Trp), volcaniclastic and aphyric rhyolite unit (Tvc), upper plate rocks following the trace of Tad andesite dike outcrops, and faulted lower and upper plate rocks near and within the Keystone window (Plate 1). Drilling by U.S. Gold Corp. frequently intercepted mineralized breccias and jasperoid at the upper to lower plate transition, and argillized dikes adjacent to decarbonatized lower plate carbonate, both of which contain anomalous gold and high concentrations of As, Sb, Hg, and/or Tl; this alteration and mineralization resembles Carlin-type mineralization where it occurs in Paleozoic sedimentary rocks and altered Eocene dikes. The clays associated with altered dikes are illite and kaolinite, determined by SWIR spectroscopy.

Illite from two samples of altered andesite dikes of McClusky Creek yielded forced plateau $^{40}Ar/^{39}Ar$ ages of 35.71±0.12 Ma and 35.54±0.06 Ma (Figure 65), similar to but slightly older than the host lavas. Three other illite samples yielded ages that were older than their host rocks' igneous ages, but were also Eocene (Figure 65). Problems associated with dating fine-grained, low-temperature illite include excess argon, induced ^{39}Ar recoil or loss from neutron bombardment in a reactor, and complications of dating mixed-layer illite-smectite. All of these can lead to erroneous ages and the first two are commonly implicated in older-than-reasonable apparent ages. Based on dating of igneous minerals in the same units, it is certain that the true age of illites at Keystone is younger than their apparent ages, and likely, illite ages are similar to the age of Eocene magmatic activity. The sanidine age of the rhyolite porphyry provides a maximum age constraint for hydrothermal activity affecting it. Since the Walti intermediate porphyritic dikes do not have this alteration, this activity is likely unrelated to emplacement of the Walti pluton.

Propylitic alteration is widespread across all igneous units. The Walti intermediate porphyritic dikes were typically altered to chlorite and calcite, with minor sericitization. The Mud Springs pluton is similarly chloritized because of widespread propylitic alteration, and locally intense calcite and epidote alteration proximal to outcrops of marble xenoliths. Where not affected by sodic-calcic alteration, the Walti pluton typically has mafic minerals altered to chlorite and/or epidote.

To summarize, skarn mineralization associated with emplacement of the Walti may overlap in time with low-temperature alteration, but there is no evidence for a spatial relationship. The rhyolite porphyry was preferentially altered over the adjacent Mud Springs and Walti intermediate porphyritic

dikes, both of which are older. This suggests the rhyolite porphyry intruded a major structure that also controlled hydrothermal fluids responsible for epithermal alteration and potentially Carlin-type alteration of the dikes to the north and at depth. Characterization of the continuum between epithermal and Carlin-type alteration requires further study.

Structures and depth of emplacement

Geologic mapping combined with geochronology provide important constraints on the depth of intrusion and mineralization at Keystone (Figure 72). The major paleosurface between Paleozoic strata and overlying late Eocene conglomerate and volcaniclastic rocks is no older than 35.72±0.32 Ma. A disconformity or very slight angular unconformity is present between Paleozoic and Cenozoic units suggesting all bedded rocks were close to horizontal at Keystone prior to doming by intrusion and later (post-late Eocene) tilting. The andesite lavas of McClusky Creek are the oldest unit dated by ^{40}Ar/^{39}Ar, and offer a higher resolution constraint for the paleosurface at 35.99±0.04 Ma before emplacement of any intrusions at Keystone.

Two problems arise with determining the depth of emplacement of various intrusions. First, it is unclear how thick the andesite of McClusky Creek is. Much of it is buried by Tertiary to Quaternary gravels that fill the valley east of Keystone (unit QToa). A foliation measurement in the andesite suggests the lavas are approximately concordant with underlying upper-plate rocks; if so, then the thickness of the andesite is no less than ~300 m. Similarly, the Tertiary conglomerate (Tcg) and volcaniclastics units (Tvc) have a combined thickness that is no less than ~250 m thick where exposed just west of upper McClusky Creek, although the localized nature of the Tcg and Tvc units suggest they were likely deposited in a paleochannel, unlike the McClusky andesites, which are laterally extensive. The observation that tilts in Eocene sedimentary and volcanic rocks and underlying Paleozoic sedimentary rocks are similar suggests that all rocks were initially domed by intrusion and subsequently tilted east by major late Cenozoic normal faulting.

Second, there is evidence of internal thrusts or duplexing in the Roberts Mountains allochthon, changing the thickness of the Valmy over moderate lateral distances at Keystone. The occurrence of Comus

also confounds how thick the upper plate may be in that area, and the nature of the contact with the lower plate is unknown. It is possible the Comus occurs as an internal wedge within the allochthon, as shown schematically (Figure 72), or it could lie directly above the lower plate. Approximate true thicknesses of the Comus and Valmy as determined by detailed mapping and stratigraphy (Chapin, 2017, unpublished report for U.S. Gold Corp.) are 300 and 330 m, respectively.

Taking into account sources of uncertainty in determining average unit thicknesses, the combined estimated thickness of the Paleozoic upper-plate sedimentary rocks and overlying Eocene conglomerate, volcaniclastic, and volcanic rocks above the Walti pluton is ~1180 m (Figure 72); this value is likely a minimum considering some degree of Eocene erosion that predates units Tcg, Tvc, and Ta. It is possible the thicknesses of some units are overestimated, in which case the total stratal thickness, and therefore, the pre-tilt depth to the top of the Walti pluton, would be less.

Mineralized skarn at the historic Keystone mine occurs adjacent to the Walti in the upper Wenban approximately 240 m beneath the base of the upper plate, thus at a minimum Eocene paleodepth of ~1420 m. The Gund diorite stock occupies a similar horizon in the Wenban to the Keystone skarn. However, the presence of Elder sandstone (Figure 72, unit "Se"), which is absent to the north, above the Gund, suggests a thicker allochthon to the south. The Gund stock may therefore, have been emplaced at ~200 m greater depth than the Walti. The Gund sill, farther to the west and therefore lower in the east-tilted section, intrudes a thrust fault within the lower plate and therefore, has an extra ~830 m thickness of repeated section of overlying Wenban and Horse Canyon units, resulting in a minimum emplacement depth of ~2010 m. The tops of other intrusions including the Mud Springs diorite, the rhyolite porphyry, and the dacite agglomerate (units Tmd, Trp, and Tda), cut only the Valmy Formation and lie very near the Eocene unconformity; therefore, the tops of these intrusions were likely emplaced within 1000 m of the Eocene surface.

Carlin-type gold mineralization occurs in several locations at Keystone. Generally, mineralization occurs in the Horse Canyon unit as well as near the top of the Wenban Limestone distal to the hornfels aureole. Based on these observations and taking into account the limitations of depth estimates because of uncertainties in absolute unit thicknesses, Carlin-type gold mineralization at Keystone likely occurred at

Eocene paleodepths of between 1 and 2 km, a range consistent with estimates from major districts such as the Carlin trend (e.g., Hollingsworth et al., 2017; Ressel and Henry, 2006; Cline et al., 2005; Ressel et al., 2000).

Figure 72. Top: schematic cross section of rocks at Keystone in the Eocene. Bottom: approximate locations of skarn, Carlin-type, and epithermal mineralization. Depth of emplacement and mineralization are discussed in text. Abbreviations are same as map units in geologic map (Plate 1).

Doming of sedimentary rocks at Keystone is supported by beds dipping in all directions away from the Walti pluton. Indeed, it is likely the Walti was responsible for doming and aided exposure of lower plate rocks after tilting caused by extension. Further study of sedimentary structures is required to rule out involvement of any folding or shortening during the Antler or later Mesozoic orogenies for the window. A major range front fault runs along the west side of Keystone, but the presence of older gravels along McClusky Creek (QToa) suggests earlier faulting and extension on the range's eastern side. The abundance of igneous clasts in these gravels supports major extension postdating igneous activity at Keystone.

Eocene conglomerate – its recognition and significance

Chert-quartzite pebble to cobble conglomerates are commonly interpreted as Paleozoic Antler "overlap" sequence in northeastern Nevada. After Late Devonian-Early Mississippian Antler thrusting, siliceous rocks of the Antler highlands eroded and deposited coarse clastic material into submarine fans, proximal delta complexes, and remnants of the Antler foreland basin to the east. Permian limestone, conglomerate, and shale of the Garden Valley Formation is one example of the "overlap" and has been mapped in the Roberts Mountains and Sulphur Spring Range east of Keystone. In the Simpson Park Mountains, Pennsylvanian-Permian conglomerates and limestone crop out 20 km south of Keystone (Figure 71). At Keystone, chert-quartzite conglomerates (unit Tcg) that in places resemble Paleozoic overlap, rest above upper-plate rocks of the Valmy Formation. Tcg's discontinuous spatial distribution suggests it likely filled paleochannels. On further mapping, it was recognized that clast compositions in the conglomerate changed drastically from ridge to ridge. Some conglomerate contained obvious porphyritic felsic igneous clasts, whereas other conglomerate and coarse sandstone contained a preponderance of clay-altered clasts considered to be derived from alteration of feldspar in igneous-derived material. The Tcg unit, therefore, was clearly not Paleozoic overlap, although initial mapping of its chert-quartzite-dominant facies suggested it was.

U-Pb detrital zircon dating of the Tcg conglomerate that rests on Ordovician Valmy in an area that contains abundant igneous clasts, produced mostly Eocene zircons and resulted in a maximum depositional age of 35.62±0.32 Ma. This conglomerate is unequivocally not Paleozoic "overlap", but an Eocene basal conglomerate. The Tertiary conglomerate not only marks the paleosurface in the Eocene but also indicates a rapidly eroding Eocene highland comprised of upper-plate strata and abundant Eocene volcanic rocks. The localized occurrence of unit Tcg north of Mud Springs also suggests its deposits represent a paleochannel through which siliceous rocks of the RMA and abundant igneous material was transported from proximal sources. The Tertiary conglomerate is hydrothermally altered, with red limonite and local silicification; it therefore predates hydrothermal activity at Keystone. Silurian Elder and Devonian Slaven have been mapped to the south of Keystone. The fact that Tertiary conglomerate rests on siltstone of the Valmy and not the younger Elder or Slaven suggests there was significant pre-Eocene erosion of the RMA, or more likely, Paleozoic or Mesozoic deformation that disrupted the upper-plate strata.

OIB volcanism and correlation with the Comus Formation

Biostratigraphy and mapping support the presence of Ordovician Valmy and Cambrian-Ordovician Comus formations in the RMA at Keystone (Table 1; T. Chapin, 2017, unpublished report for U.S. Gold Corp.). Basalts within these two formations were studied for their map distribution, petrography, geochemistry, and isotopic dating. All basalts are alkaline and contain fairly abundant hydrous mafic minerals, biotite or rarely, amphibole, in addition to olivine and orthopyroxene, where they have not been severely altered. Geochemically, the alkali basalts at Keystone have very high concentrations of compatible and incompatible trace elements. The chemistry of Keystone basalts is uncharacteristic of most seafloor basalt or arc-related basalt, both of which generally derive from depleted mantle sources, but it is consistent with ocean island basalts (OIBs). The presence of biotite and rare hornblende are consistent with the hydrous, alkalic composition of some OIBs. $^{40}Ar/^{39}Ar$ dating of biotite from a basalt intercalated with limestone of the Valmy Formation yielded a plateau age of 466.1±0.7 Ma, which is Middle Ordovician. The age is consistent with fossil ages (Table 1) from intercalated sedimentary rocks.

The geologic setting of the Keystone OIBs is uncertain. However, similar basalt-limestone units of Cambrian and Ordovician age exist elsewhere in north-central Nevada. Bloomstein et al. (1991) provided a depositional model for the Comus at the Twin Creeks mine area of the Osgood Mountains involving a Late Cambrian to Early Ordovician carbonate-mantled basaltic seamount, in which intraplate submarine volcanic rocks may have accumulated to shallow enough depths for a carbonate depositional system to develop. At Twin Creeks, the Comus lies in the footwall of a major thrust and has therefore been interpreted as autochthonous or parautochthonous. At Keystone, in contrast, Comus-like alkali basalt-limestone exists entirely within the deformed sequence comprising the RMA and was therefore transported from the west, very likely along Antler-affinity thrusts.

Similar ages, lithologies, and geochemistry between Keystone alkali basalts and the alkali basalts of the Comus Formation in the Osgood Mountains, 150 km to the north-northwest, are permissive for their tentative correlation. Such a correlation is particularly important, because the Comus is the principal host unit for Carlin-type deposits in the Getchell trend. This also implies intraplate volcanism and carbonate-capped seamounts may have been much more extensive in Lower Paleozoic basinal rocks. The Cambrian-Ordovician Hales Formation at Tonkin Springs, a cluster of Carlin-type gold deposits located only 8 km east of Keystone, may also be correlative with the Comus (Noble, 2008, Technical Report on the Tonkin Project, prepared for U.S. Gold Corporation (McEwen Mining)). The Hales is described as sandy limestone and calcareous siltstone with mafic tuffs and sills. These rocks are important hosts for Carlin-type deposits and future studies on intraplate volcanism in the Paleozoic should include Keystone.

Conclusions

Keystone is an early-stage exploration project for Carlin-type gold deposits in the Battle Mountain-Eureka mineral belt. The property includes a very well exposed Eocene igneous center centered on the Keystone lower-plate carbonate window. This study details the igneous geology of the Keystone property and provides 25 new isotopic ages from 11 Eocene volcanic and intrusive units, one Eocene conglomerate, and one Ordovician volcanic unit. In addition, the study assesses the relationship of Eocene magmatism to the formation of Carlin-type and other hydrothermal ore deposits.

Detailed mapping and petrography of igneous rocks at Keystone has not been documented before this thesis. The only mafic rocks found at Keystone are Cambrian to Ordovician alkaline basalts that formed during deposition of the Comus and Valmy formations, and were later tectonically transported to the Keystone area during Late Devonian/Early Mississippian Antler thrusting. Ordovician basalt is dated at 466.1 ± 0.7 Ma, corroborating fossil data from intercalated limestone. The ages, lithologic, and geochemical similarities of these Keystone rocks to the Comus Formation in the Osgood Mountains is permissive for their correlation and therefore implies that the Comus seamounts may have been much more extensive. This is particularly important, because the Comus Formation is the principal host in the Getchell trend Carlin-type deposits.

Results of this study also identified conglomeratic rocks commonly correlated elsewhere with the Paleozoic Antler overlap sequence based on the abundance of RMA-derived chert and quartzite clasts as Eocene. The recognition of Eocene coarse clastics at Keystone and in the Carlin Trend (Hollingsworth et al., 2017) is important not only for regional mapping, but also for improving our understanding of the development of Eocene basins, some of which are hydrocarbon-bearing, and for characterizing the switch from late Cretaceous Sevier contraction to an early Cenozoic extensional regime. Basal Eocene conglomerate at Keystone is the oldest exposed Cenozoic unit, and therefore it is used to constrain the Eocene paleosurface, which is useful in estimating the depth that Eocene intrusion and mineralization occurred.

Other than the Ordovician and Cambrian alkali basalts, igneous rocks at Keystone are entirely Eocene, shoshonitic to high-K calc-alkaline, intermediate to felsic, and occur as both volcanics and shallow intrusions emplaced from ~36.0 to 34.7 Ma. Eocene igneous rocks at Keystone are temporally, spatially, and compositionally consistent with other Eocene igneous rocks formed over a broad area of the northern Great Basin. For example, the Keystone rocks fit with the rapid migration of magmatism southwestward during this time in the northern and central Great Basin. Compositionally, the age for Keystone magmatism reflects the last stages of regional intermediate magmatism dominated by shallow intrusion and effusive volcanism, after which magmatism was dominantly silicic and pyroclastic. The pyroclastic character of subsequent magmatism is evident in the nearby ~34 Ma Caetano and Hall Creek calderas. Despite the spatial and temporal proximity of Eocene igneous rocks at Keystone, diverse mineralogic compositions and trace geochemistry support a complex magmatic evolution and possibly varied sources. The early andesite of McClusky Creek, Mud Springs diorite, and Gund diorite are possibly a separate ~36 Ma magmatic system from the ~35.5 Ma Walti intrusion and related rocks. The dacite agglomerate is unique for its high ASI, Nb/Y, and other characteristic, which may reflect a higher degree of crustal involvement.

Geochronology of igneous rocks at Keystone documented by U-Pb zircon and ^{40}Ar/^{39}Ar analyses indicates a complex and intense ~1.3 m.y. pulse of Eocene magmatism. The lower resolution of U-Pb zircon dating by LA-ICP-MS does not allow for detailed age discrimination of specific Eocene magmatic events indicated by cross-cutting relationships, which commonly resulted in overlapping ages. U-Pb dating was still important for dating of hydrothermally altered igneous rocks for their crystallization age, and for establishing that the Keystone area lacks evidence of any Jurassic or Cretaceous magmatic activity, unlike nearby Cortez. High-U zircons also shed light on the evolved nature of the rhyolite porphyry and some Walti intermediate porphyritic dikes. ^{40}Ar/^{39}Ar dating does have a high enough resolution to construct a timeline of events.

Felsic tuffaceous volcaniclastics and aphyric rhyolite flows were the first Eocene igneous rocks, determined by field relations as they rest directly on the Tertiary basal conglomerate. Andesite lavas of McClusky Creek followed at 35.99±0.04 Ma. The Mud Springs and Gund diorites were the first intrusions, emplaced at 35.87±0.06 Ma and 35.82±0.08 Ma, respectively. Igneous rocks of the Walti magmatic system

followed next, beginning with the Walti intermediate porphyritic dikes at 35.68±0.04 Ma. The Walti is a composite pluton and the ages for the diorite and quartz monzonite phases are 35.51±0.19 Ma and 35.52±0.14 Ma, respectively. The rhyolite porphyry emplaced next, cutting the Mud Springs, at 35.43±0.06 Ma. Interestingly, the rhyolite porphyry had the oldest U-Pb zircon ages, suggesting the melt evolved from an older and deeper magma body, possible unrelated to the Walti. The trachyandesite and dacite agglomerate mark the end of magmatic activity at Keystone, however their ages are poorly constrained because of wide U-Pb zircon uncertainties.

^{40}Ar/^{39}Ar dating of hydrothermal illite from low-temperature Carlin-style sedimentary rock-hosted and igneous-hosted epithermal styles of mineralization provided constraints on the hydrothermal activity at Keystone. The illite data, although not highly precise because of inherent difficulties in dating illite, indicate that hydrothermal activity at Keystone was broadly coeval with Eocene magmatism. Based on various geologic and isotopic age data, lower temperature sericitic alteration is possibly associated with the Trp rhyolite porphyry intrusion. The preferred alteration of the rhyolite porphyry over surrounding rocks suggests it intruded a structure that also controlled hydrothermal fluids, which is important for gold exploration. Quartz porphyry dikes at the nearby Cortez Hills Carlin-type gold deposit have been demonstrated as syn-late stage mineralization and are similar to the rhyolite porphyry at Keystone in mineralogy, texture, and age. Although rhyolite at Keystone is similar in composition to abundant dikes at Cortez, differences include the dominance of silicic magmatism at Cortez versus a greater component of rocks with intermediate compositions at Keystone. Pb-Zn-Cu skarn, endoskarn, and other high-temperature alteration are almost certainly related to the emplacement of the Walti pluton, which possibly was the last major magmatic event at Keystone.

Evaluation of the depth that Eocene mineralization occurred using the Eocene unconformity as occurred a guide suggests that Carlin-type gold mineralization formed at paleodepths of approximately 1.2 km, and possibly somewhat more given some degree of pre-mineral Eocene erosion. These depth estimates for Carlin-type deposits are similar to those made from other areas and further support a shallow origin for Carlin-type deposits. The Pb-Zn-Cu skarns at Keystone formed deeper, but probably not much deeper than about 1.5 km paleodepth. The Keystone lower-plate window is cored by the Walti stock, and surrounding

Paleozoic to Eocene rocks dip consistently away from the stock. Thus, the Walti stock likely domed the surrounding rocks because of its shallow emplacement, and is the principal reason for the existence of the Keystone 'window'. The relationship between doming and structures that controlled hydrothermal fluids at Keystone requires further study. Subsequently, the rocks at Keystone have been tilted eastward by probable Neogene normal faulting along the western escarpment of the northwest Simpson Park Mountains.

References

Arehart, G.B., Chakurian, A.M., Tretbar, D.R., Christiansen, J.N., McInnes, B.A., and Donelick, R.A., 2003, Evaluation of Radioisotope Dating of Carlin-Type Deposits in the Great Basin, Western North America, and Implications for Deposit Genesis: Economic Geology v. 98, p. 235–248.

Arbonies, D. G., Creel, K. D., Jackson, M. L., Steininger, R., and Pennell, B., 2011, Cortez Hills Lower Zone discovery and geologic update, in Steininger, R.C., and Pennell, W.H., Great Basin Evolution and Metallogeny Symposium: Geological Society of Nevada proceedings, Reno p. 447-462.

Arney, E., 2013, Structure of the Paleozoic rocks in the Tonkin Summit Quadrangle, Eureka County, Nevada: Unpublished M.S. thesis, California State University, Long Beach, 64 p.

Artz, Z. J., 2004, Igneous geochronology and petrography of the Cortez-Hills Carlin-type gold deposit, Cortez, Nevada: Unpublished M.Sc. thesis, Las Vegas, NV, University of Nevada Las Vegas, 40 p.

Audétat, A., and Li, W., 2017, The genesis of Climax-type porphyry Mo deposits: Insights from fluid inclusions and melt inclusions: Ore Geology Reviews, v. 88, p. 436–460.

Bakken B.M., 1990, Gold mineralization, wall-rock alteration and the geochemical evolution of the hydrothermal system in the main ore body, Carlin Mine, Nevada: Unpublished Ph.D. thesis, Stanford, CA, Stanford University, 236 p.

Bloomstein, E.I., Massingill, G.L., Parratt, R.L., Peltonen, D.R., 1991, Discovery, geology, and mineralization of the Rabbit Creek gold deposit, Humboldt County, Nevada, in Raines, G.L., Schafer, R.G., and Wilkinson, W.H., eds., Geology and Ore Deposits of the Great Basin Symposium: Geological Society of Nevada, proceedings, v. 2, p. 821-843.

Breit, F., Ressel, M., Anderson, S., and Muirhead, E., 2005, Geology and gold deposits of the Twin Creeks Mine, Humboldt County, Nevada in Rhoden, R.N., Steininger, R.C., and Vikre, P.G., Window to the World Symposium: Geological Society of Nevada, proceedings, v. 1 p. 431-452.

Cann, J.R., 1970, Rb, Sr, Y, Zr and Nb in some ocean floor basaltic rocks: Earth and Planetary Science Letters, v. 10, p. 7–11.

Cassata, W.S., Renne, P.R., and Shuster, D.L., 2009, Argon diffusion in plagioclase and implications for thermochronometry: A case study from the Bushveld Complex, South Africa: Geochimica et Cosmochimica Acta, v. 73, p. 6600–6612.

Carten, R.B., 1986, Sodium-calcium metasomatism; chemical, temporal, and spatial relationships at the Yerington, Nevada, porphyry copper deposit: Economic Geology, v. 81, p. 1495–1519.

Cassel, E.J., Breecker, D.O., Henry, C.D., Larson, T.E., and Stockli, D.F., 2014, Profile of a paleo-orogen: High topography across the present-day Basin and Range from 40 to 23 Ma: Geology, v. 42, p. 1007–1010.

Christiansen, R.L., and Yeats, R.L., 1992, Post-Laramide geology of the U.S. Cordillerian region: in Burchfiel, B.C., Lipman, P.W., and Zoback, M.L., eds., The Cordillerian Orogen: Conterminous U.S.: Boulder, CO, Geological Society of America, Geology of North America: v. G-3, p. 261–406.

Clauer, N., 2013, The K-Ar and ^{40}Ar/^{39}Ar methods revisited for dating fine-grained K-bearing clay minerals: Chemical Geology, v. 354, p. 163–185.

Cline, J.S. and Hofstra, A.H., 2000, Ore fluid evolution at the Getchell Carlin-type gold deposit, Nevada, USA: European Journal of Mineralogy, v. 12, p. 195–212.

Cline, J.S., Hofstra, A.H., Muntean, J.L., Tosdal, R.M., and Hickey, K.A., 2005, Carlin-type gold deposits in Nevada: Critical geologic characteristics and viable models: Economic Geology 100th anniversary volume, v. 451, p. 484.

Colgan, J. P. and Henry, C. D. 2009. Rapid middle Miocene collapse of the Mesozoic orogenic plateau in north-central Nevada: International Geology Review, v. 51, p. 920–961.

Colgan, J. P., Henry, C.D., John, D.A., 2011, Geologic map of the Caetano caldera, Lander and Eureka Counties, Nevada: Nevada Bureau of Mines and Geology Map 174, 1:75,000, 10 p.

Cook, H.E., 2015, The evolution and relationship of the western North American Paleozoic carbonate platform and basin depositional environments to Carlin-type gold deposits in the context of carbonate sequence stratigraphy, *in* Pennell, W.M., and Garside, L.J., eds., New concepts and

discoveries, Geological Society of Nevada 2015 Symposium Proceedings: Reno, Nevada, Geological Society of Nevada, p. 1–80.

Cook, H.E., and Corboy, J.J., 2004, Great Basin Paleozoic Carbonate Platform: Facies, Facies Transitions, Depositional Models, Platform Architecture, Sequence Stratigraphy, and Predictive Mineral Host Models, U.S. Geological Survey Open-File Report 2004-1078, 129 p.

Crafford, A.E.J., 2008, Paleozoic tectonic domains of Nevada: An interpretive discussion to accompany the geologic map of Nevada: Geosphere, v. 4, p. 260–291.

Dickinson, W.R., 2006, Geotectonic evolution of the Great Basin: Geosphere, v. 2, p. 353.

Espell, R.A., and Rich, T.B., 1991, Geology and mineralization of the Tonkin Springs mining district, in Buffa, R.H., and Coyner, A.R., eds., Geology and Ore Deposits of the Great Basin Symposium: Field Trip Guidebook Compendium, v. 2, p. 949–958.

Fair, C.L., 2012, Structure of the Roberts Mountains allochthon in the Three Bar Ranch quadrangle, Roberts Mountains, Eureka County, Nevada: Unpublished M.S. thesis, California State University, Long Beach, 104 p.

Ferguson, H.G., Roberts, R.J., and Muller, S.W., 1952, Geology of the Golconda quadrangle, Nevada: U.S. Geological Survey Geologic Quadrangle Map GQ15, scale 1:125,000.

Finney, S.C., Noble, P., and Cluer, J.K., 2000, Lower Paleozoic stratigraphy and structure of central Nevada: Comparisons and contrasts between the lower and upper plates of the Roberts Mountains thrust, in GSA Field Guide 2: Great Basin and Sierra Nevada, Geological Society of America, v. 2, p. 279–300.

Finney, S.C., Kelty, T., Fair, C., and Arney, E., 2015, Tectonic Erratics - Remarkable exotic blocks emplaced by the Henderson thrust during the Sonoma Orogeny, Eureka County Nevada, in Pennell, W. M. and Garside, L. J. eds., New Concepts and Discoveries, Geological Society of Nevada 2015 Symposium: v. 1, p. 921–928.

Frost, B.R., and Frost, C.D., 2008, A Geochemical Classification for Feldspathic Igneous Rocks: Journal of Petrology, v. 49, p. 1955–1969.

Gilluly, J., and Masursky, H., 1965, Geology of the Cortez quadrangle, Nevada, with a section on gravity and aeromagnetic surveys by D. R. Mabey: U.S. Geological Survey Bulletin 1175, 117 p.

Groff, J.A., Heizler, M.T., McIntosh, W.C., and Norman, D.I., 1997, 40Ar/39Ar dating and mineral paragenesis for Carlin-type gold deposits along the Getchell trend, Nevada: Evidence for Cretaceous and Tertiary gold mineralization: Economic Geology, v. 92, p. 601–622.

Hall, C.M., Kesler, S.E., Simon, G., and Fortuna, J., 2000, Overlapping Cretaceous and Eocene Alteration, Twin Creeks Carlin-Type Deposit, Nevada: Economic Geology, v. 95, p. 1739–1752.

Henry, C.D., and Boden, D.R., 1998, Eocene magmatism: The heat source for Carlin-type gold deposits of northern Nevada: Geology, v. 26, p. 1067–1070.

Henry, C.D., and Ressel, M.W., 2000, Eocene magmatism of northeastern Nevada: the smoking gun for Carlin-type gold deposits, *in* Cluer, J.K., Price, J.G., Struhsacker, E.M., Hardyman, R.F., and Morris, C.L., eds., Geology and Ore Deposits 2000: The Great Basin and Beyond Symposium: Geological Society of Nevada, proceedings, p. 365–388.

Henry, C.D., Faulds, J.E., Boden, D.R., and Ressel, M.W., 2001, Timing and styles of Cenozoic extension near the Carlin trend, northeastern Nevada: Implications for the formation of Carlin-type gold deposits: Regional Tectonics and Structural Control of Ore: The Major Gold Trends of Northern Nevada: Geological Society of Nevada Special Publication, v. 33, p. 115–128.

Henry, C.D., 2008, Ash-flow tuffs and paleovalleys in northeastern Nevada: Implications for Eocene paleogeography and extension in the Sevier hinterland, northern Great Basin: Geosphere, v. 4, p. 1–35.

Henry, C.D., 2009, Unpublished ^{40}Ar/^{39}Ar age dates as part of studies related to timing and distribution of caldera magmatism in Nevada, prepared for Barrick Goldstrike Mines, Inc..

Henry, C.D., and John, D.A., 2013, Magmatism, ash-flow tuffs, and calderas of the ignimbrite flareup in the western Nevada volcanic field, Great Basin, USA: Geosphere, v. 9, p. 951–1008.

Hofstra, A.H., Snee, L.W., Rye, R.O., Folger, H.W., Phinisey, J.D., Loranger, R.J., Dahl, A.R., Naeser, C.W., Stein, H.J., and Lewchuk, M., 1999, Age constraints on Jerritt Canyon and other Carlin-type

gold deposits in the western United States—relationship to Mid-Tertiary extension and magmatism: Economic Geology, v. 94, p. 769–802.

Holm-Denoma, C., Hofstra, A., Noble, P., and Leslie, S., 2011, Paleozoic stratigraphy and kinematics of the Roberts Mountains allochthon in the Independence Mountains, northern Nevada: Geological Society of Nevada Proceedings, p. 1039–1954.

Holm-Denoma, C.S., Hofstra, A.H., Rockwell, B.W., and Noble, P.J., 2017, The Valmy thrust sheet: A regional structure formed during the protracted assembly of the Roberts Mountains allochthon, Nevada, USA: GSA Bulletin, v. 129, p. 1521–1536.

Hollingsworth, E.R., Ressel, M.W., Henry, C.D., 2017, Age and depth of Carlin-type gold deposits in the southern Carlin Trend: Eocene mountain lakes, big volcanoes, and widespread, shallow hydrothermal circulation in Shallow Expressions of Carlin-type Gold Deposits: Alligator Ridge and Emigrant Mines, Nevada: Geological Society of Nevada, Special Publication 64, p. 149-173.

Hotz, P.E., and Willden, R., 1964, Geology and mineral deposits of the Osgood Mountains quadrangle, Humboldt County, Nevada: U.S. Geological Survey Professional Paper 431, 129 p.

Humphreys, E.D., 1995, Post-Laramide removal of the Farallon slab, western United States: Geology, v. 23, p. 987–990.

Jackson, M., Arbonies, D., and Creel, K., 2010, Architecture of the Cortez Hills breccia body: Geological Society of Nevada, Symposium, Reno, Nevada, 14-22 May 2010, Proceedings, p. 97-123.

John, D.A., Henry, C.D., and Colgan, J.P., 2008, Magmatic and tectonic evolution of the Caetano caldera, north-central Nevada: A tilted, mid-Tertiary eruptive center and source of the Caetano Tuff: Geosphere, v. 4, p. 75–106.

Johnson, J.G., 1959, Geology of the Northern Simpson Park Range, Eureka County, Nevada: Unpublished Ph.D. thesis, University of California, Los Angeles, 101 p.

Kelley, S., 2002, K-Ar and Ar-Ar dating: Reviews in Mineralogy and Geochemistry, v. 47, p. 785–818.

Ketner, K.B., and Alpha, A.G., 1992, Mesozoic and Tertiary rocks near Elko Nevada—Evidence for Jurassic to Eocene folding and low-angle faulting: U.S. Geological Survey Bulletin 1988-C. 13 p.

Ketner, K.B., 2013, Stratigraphy of lower to middle Paleozoic rocks of northern Nevada and the Antler
orogeny: US Geological Survey, Professional Paper 1799, 18 p.

King, C.A., 2017, Igneous Petrology, Geochronology, Alteration, and Mineralization Associated with
Hydrothermal Systems in the Battle Mountain District, Nevada: Unpublished Ph.D. dissertation,
Tucson, AZ, University of Arizona, 707 p.

Kuehn, C.A., and Rose, A.R., 1992, Geology and geochemistry of wall-rock alteration at the Carlin gold
deposit, Nevada: Economic Geology, v. 87, p. 1697–1721.

LeBas et al., 1986

LeMaitre et al., 1989

Linde, G.M., Trexler, J.H., Jr, Cashman, P.H., Gehrels, G., and Dickinson, W.R., 2016, Detrital zircon U-
Pb geochronology and Hf isotope geochemistry of the Roberts Mountains allochthon: New
insights into the early Paleozoic tectonics of western North America: Geosphere, v. 12, p. 1016–
1031.

Linde, G.M., Trexler, J.H., Jr, Cashman, P.H., Gehrels, G., and Dickinson, W.R., 2017, Three-Dimensional
Evolution of the Early Paleozoic Western Laurentian Margin: New Insights from Detrital Zircon
U-Pb Geochronology and Hf Isotope Geochemistry of the Harmony Formation of Nevada: Early
Paleozoic Western Laurentia: Tectonics, v. 36, p. 2347–2369.

Long, S.P., Henry, C.D., Muntean, J.L., Edmondo, G.P., and Thomas, R.D., 2014, Geologic map of the
southern part of the Eureka mining district and surrounding areas of the Fish Creek Range,
Mountain Boy Range, and Diamond Mountains, Eureka and White Pine counties, Nevada: Nevada
Bureau of Mines and Geology Map 183, 2 plates, scale 1:24,000, 36 p.

Longo, A.A., Cline, J.S., and Muntean J.L., 2009b, Using pyrite to track evolving fluid pathways and
chemistry in Carlin-type deposits: Geological Society of Nevada, Special Publication 49, p. 63-65.

Madrid, R. J., 1987, Stratigraphy of the Roberts Mountains allochthon in north central Nevada:
Unpublished Ph.D. Dissertation, Stanford University, Stanford, 341 p.

Mathewson, D., 2001, Tectono-stratigraphic setting for the Rain district gold deposits, Carlin trend,
Nevada: Geological Society of Nevada Special Publication 33, p. 91–109.

McKee, E.H., 1968, Geologic map of the Ackerman Canyon quadrangle, Lander and Eureka Counties, Nevada: Geologic Quadrangle USGS Numbered Series 761, scale 1:62,500.

McKee, E.H., 1986, Geologic map of the Roberts Wilderness study area, Eureka County, Nevada: U.S. Geological Survey miscellaneous field studies map MF-1844, scale: 1:48,000.

McKee, E.H., Barton, H.N., Ponce, D.A., Benjamin, D.A., and Johnson, F.L., 1986, Mineral resources of the Roberts Wilderness study area, Eureka County, Nevada, U.S. Geological Survey open-file report 1731-k.

McKee, E.H., and Conrad, J.E., 1994, Geologic map of the northern part of the Simpson Park Mountains, Eureka County, Nevada: U.S. Geological Survey Miscellaneous Field Studies Map MF-2257, scale 1:24,000.

Mehrtens, M.B., 1987, Case history and problem 1: The Tonkin Springs Gold Mining District, Nevada, U.S.A., in Fletcher, W.K., et al., eds., Exploration geochemistry: design and interpretation of soil surveys, Reviews in Economic Geology, vol. 3, p. 129-134.

Merriam, C. W., 1940, Devonian stratigraphy and paleontology of the Roberts Mountains region, Nevada: Geol. Soc. America Spec. Paper 25, 114 p., 16 pls.

Merriam, C. W., and McKee, E. H., 1976. The Roberts Mountains Formation, a regional stratigraphic study with emphasis on rugose coral distribution, with a section on conodonts by John W. Huddle: U.S. Geological Survey, Professional Paper 973, 51 p.

Muntean, J.L., Cline, J.S., Simon, A.C., and Longo, A.A., 2011, Magmatic–hydrothermal origin of Nevada's Carlin-type gold deposits: Nature Geoscience, v. 4, p. 122.

Muntean, J.L., Davis, D.A., Ayling, B., 2017, The Nevada Minerals Industry: Nevada Bureau of Mines and Geology, Special Publication MI-2016, 187 p. http://pubs.nbmg.unr.edu/The-NV-mineral-industry-2016-p/mi2016.htm

Nakamura, N., 1974, Determination of REE, Ba, Fe, Mg, Na and K in carbonaceous and ordinary chondrites: Geochim. Cosmochim. Acta, v. 38, p. 757-775.

Noble, A.C., Brown, S., Gowans, R., 2008, Technical Report on the Tonkin Project, Eureka County,
    Nevada, USA, prepared for US Gold Corporation (McEwen Mining), dated May 16, 2008, 208 p.
    http://s21.q4cdn.com/390685383/files/doc_downloads/governance/reserves-and-
    resources/technical-report.pdf

Onstott, T.C., Miller, M.L., Ewing, R.C., Arnold, G.W., and Walsh, D.S., 1995, Recoil refinements:
    Implications for the 40Ar/39Ar dating technique: Geochimica et Cosmochimica Acta, v. 59, p.
    1821–1834.

Pearce, J.A., 1996, A User's Guide to Basalt Discrimination Diagrams, In: Wyman, D.A., Ed., Trace
    Element Geochemistry of Volcanic Rocks: Applications for Massive Sulphide Exploration,
    Geological Association of Canada, Short Course Notes, Vol. 12, 79-113.

Pearce, J.A., 2014, Immobile Element Fingerprinting of Ophiolites: Elements, v. 10, p. 101–108.

Pullen, A., Ibáñez-Mejia, M., Gehrels, G.E., Giesler, D., and Pecha, M., 2018, Optimization of a Laser
    Ablation-Single Collector-Inductively Coupled Plasma-Mass Spectrometer (Thermo Element 2)
    for Accurate, Precise, and Efficient Zircon U-Th-Pb Geochronology: Geochemistry, Geophysics,
    Geosystems, 17 p.

Ressel, M.W., Noble, D.C., Henry, C.D., and Trudel, W.S., 2000a, Dike-hosted ores of the Beast deposit
    and the importance of Eocene magmatism in gold mineralization of the Carlin trend, Nevada:
    Economic Geology, v. 95, p. 1417–1444.

Ressel, M.W., Noble, D.C., Volk, J.A., Lamb, J.B., Park, D.E., Conrad, J.E., Heizler, M.T., and Mortensen,
    J.K., 2000b, Precious-metal mineralization in Eocene dikes at Griffin and Meikle: Bearing on the
    age and origin of gold deposits of the Carlin trend, Nevada, *in* Cluer, J.K., Price, J.G., Struhsacker,
    E.M., Hardyman, R.F., and Morris, C.I., eds., Geology and Ore Deposits 2000: The Great Basin
    and Beyond, Geological Society of Nevada, Symposium Proceedings, p. 79–101.

Ressel, M.W., and Henry, C.D., 2006, Igneous geology of the Carlin trend, Nevada: Development of the
    Eocene plutonic complex and significance for Carlin-type gold deposits: Economic Geology, v.
    101, p. 347–383.

Rhys, D., Valli, F., Burgess, R., Heitt, D., Greisel, G., Hart, K., Pennell, W.M., and Garside, L.J., 2015, Controls of fault and fold geometry on the distribution of gold mineralization on the Carlin trend, in Pennell, W. M. and Garside, L. J. eds., New Concepts and Discoveries Symposium: Geological Society of Nevada, proceedings, v. 1, p. 333–389.

Roberts, R.J., 1951, Geologic map of the Antler Peak quadrangle, Nevada: Geologic Quadrangle Report 10.

Roberts, R.J., Hotz, P.E., Gilluly, J., and Ferguson, H.G., 1958, Paleozoic rocks of north-central Nevada: American Association of Petroleum Geologists Bulletin, v. 42, no. 12, p. 2813–2857.

Roberts, R.J., 1964, Stratigraphy and structure of the Antler Peak quadrangle, Humboldt and Lander counties, Nevada: U.S. Geological Survey Professional Paper 459-A, 93 p.

Roberts, R.J., Montgomery, K.M., and Lehner, R.E., 1967, Geology and Mineral Resources of Eureka County, Nevada: Nevada Bureau of Mines and Geology Bulletin 64, 152 p., 12 pl.

Silberman, M. L., & McKee, E. H., 1971, K-Ar ages of granitic plutons in north-central Nevada: Isochron/West, v. 1, p. 15-32.

Sillitoe, R.H., 2010, Porphyry copper systems: Economic geology, v. 105, p. 3–41.

Smith, M.E., Cassel, E.J., Jicha, B.R., Singer, B.S., and Canada, A.S., 2017, Hinterland drainage closure and lake formation in response to middle Eocene Farallon slab removal, Nevada, U.S.A.: Earth and Planetary Science Letters, v. 479, p. 156–169.

Steiger, R.H., and Jäger, E., 1977, Subcommission on geochronology: convention on the use of decay constants in geo- and cosmochronology: Earth and Planetary Science Letters, v. 36, p. 359-362.

Stewart, J.H., and Carlson, J.E., 1976, Geologic map of north-central Nevada: Nevada Bureau of Mines and Geology Map 50, scale 1:250,000.

Teal, L., Jackson, M., 1997, Geologic overview of the Carlin trend gold deposits and description of recent deep discoveries: SEG Newsletter, v. 31, p. 1, 13–25.

Trexler, J.H., Jr, Cashman, P.H., Snyder, W.S., and Davydov, V.I., 2004, Late Paleozoic tectonism in Nevada: Timing, kinematics, and tectonic significance: Geological Society of America Bulletin, v. 116, p. 525–538.

Tretbar, D.R., Arehart, G.B., and Christensen, J.N., 2000, Dating gold deposition in a Carlin-type gold deposit using Rb/Sr methods on the mineral galkhaite: Geology, v. 28, p. 947–950.

Winchester, J.A., and Floyd, P.A., 1977, Geochemical discrimination of different magma series and their differentiation products using immobile elements: Chemical Geology, v. 20, p. 325-343.

Xiang, W., Griffin, W.L., Jie, C., Pinyun, H., Xiang, L., 2011, U and Th contents and Th/U ratios of zircon in felsic and mafic magmatic rocks: improved zircon-melt distribution coefficients: Acta Geol. Sin., v. 85 (1), p. 164–174.

Yigit, O., Hofstra, A.H., Hitzman, M.W., and Nelson, E.P., 2006, Geology and geochemistry of jasperoids from the Gold Bar district, Nevada: Mineralium Deposita, v. 41, p. 527–547.

Zhang, J.-Y., Ma, C.-Q., Zhang, C., and Li, J.-W., 2014, Fractional crystallization and magma mixing: evidence from porphyritic diorite-granodiorite dykes and mafic microgranular enclaves within the Zhoukoudian pluton, Beijing: Mineralogy and Petrology, v. 108, p. 777–800.

Zhang, S.-H., and Zhao, Y., 2017, Cogenetic origin of mafic microgranular enclaves in calc-alkaline granitoids: The Permian plutons in the northern North China Block: Geosphere, v. 13, p. 482–517.

Appendix A – Geochemistry
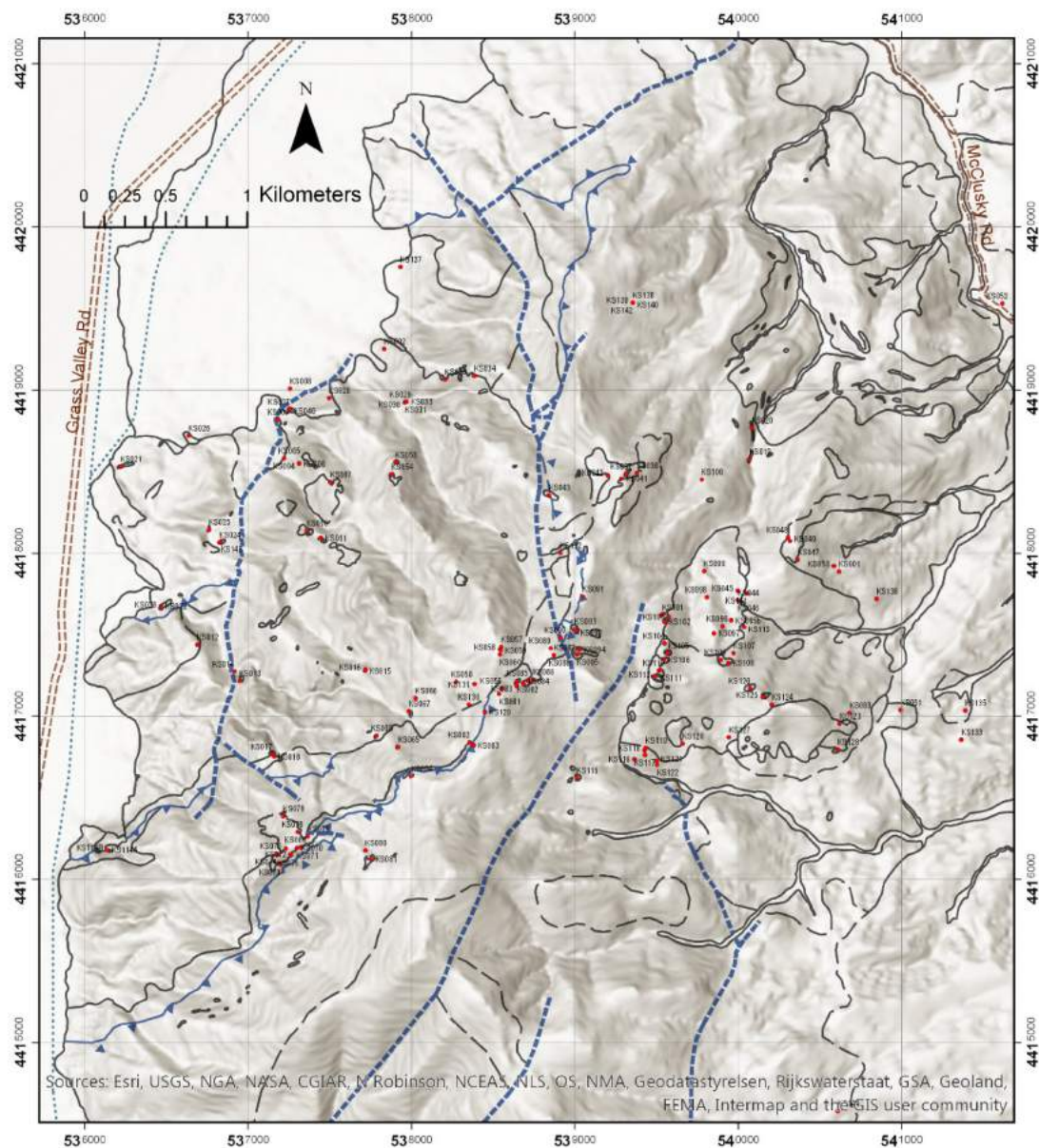
Figure A1. Location map of samples collected by Gabriel Aliaga. Geologic contacts and fault lines are same as Plate 1.
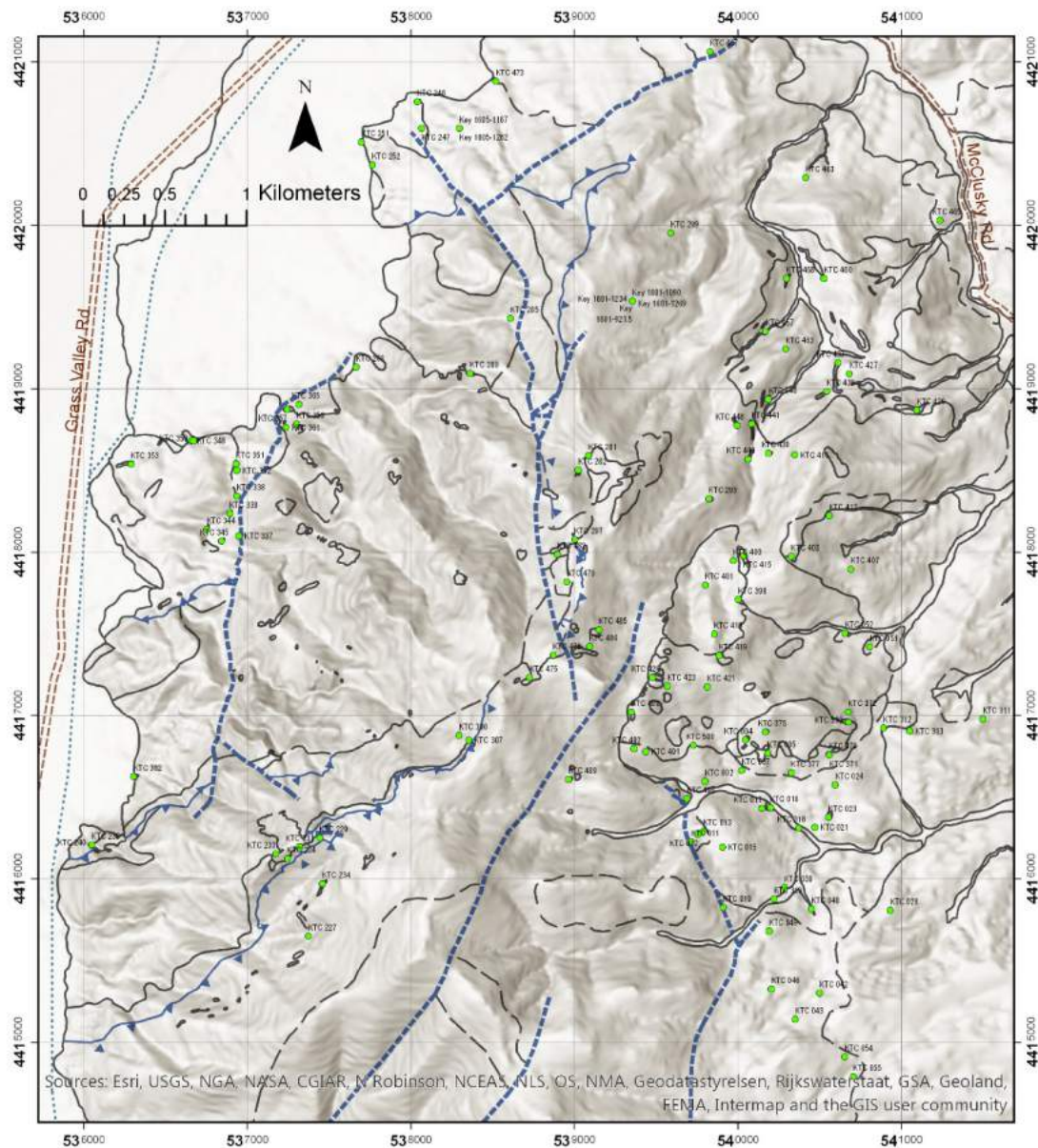
Figure A2. Location map of samples collected by Tom Chapin for U.S. Gold Corp. Geologic contacts and fault lines are same as Plate 1.

Table A1. Multi-element geochemistry of unaltered and altered rocks.

Sample ID		KS001	KS002	KS003	KS004	KS005	KS006	KS007	KS008	KS009	KS010	KS011	KS012	KS013
UTM NAD27	East	540616	537834	540682	537219	537220	537313	537503	537257	537184	537357	537445	536688	536947
	North	4417887	4419254	4417021	4418582	4418582	4418549	4418434	4419009	4418818	4418137	4418093	4417440	4417215
Unit		Tvc	Twq	Tmd	Dw	Twq	Dw	Twq	Ov	Tta	Twq	Twd	Dhc	Twd
Comment/Alteration		clay	unaltered	unaltered	jasperoid	sodic-calcic	skarn	unaltered	limonite, bx	chlorite, bx	endo-skarn	unaltered	limonite, bx	Mingled
Whole-rock[1]			Y	KTC372		Y		Y		Y	Y	Y		Y
Ore chemistry									Y				Y	
Thin Section			Y	Y		Y	Y	Y		Y	Y	Y		2
SiO2	%		69.78			67.82		69.52		65.30	59.74	63.58		66.65
Al2O3	%		15.58			15.20		14.46		17.39	17.89	16.46		15.81
FeO*	%		1.75			1.29		3.05		4.62	5.47	5.57		3.77
CaO	%		2.47			5.81		2.50		3.22	4.81	3.68		3.49
MgO	%		1.16			1.64		1.21		1.71	2.41	2.13		1.55
Na2O	%		3.29			3.20		3.21		2.78	4.13	3.21		3.21
K2O	%		5.02			4.07		5.18		3.61	3.84	4.03		4.36
Cr2O3	%		0.01			0.01		0.01		0.01	0.01	0.01		0.01
TiO2	%		0.53			0.56		0.51		0.66	0.90	0.77		0.62
MnO	%		0.01			0.03		0.03		0.12	0.06	0.11		0.08
P2O5	%		0.18			0.18		0.13		0.23	0.48	0.25		0.24
SrO	%		0.06			0.08		0.06		0.06	0.10	0.06		0.06
BaO	%		0.16			0.12		0.13		0.29	0.15	0.13		0.14
LOI			1.15			1.25		0.6		5.9	1.92	1.68		2.04
Ag	ppm		<0.5			<0.5		<0.5	0.08	<0.5	<0.5	<0.5	0.02	<0.5
Al	%								0.92				0.26	
As	ppm		4.5			2.5		2.5	383	14.9	2.7	2.5	61.1	5.4
Au	ppm								0.01				<0.005	
B	ppm								10				<10	
Ba	ppm		1420			1050		1195	110	2390	1380	1185	740	1305
Be	ppm								1.18				2.52	
Bi	ppm		3.88			0.27		0.04	0.65	0.06	0.08	0.34	0.08	0.17
C	%		0.05			0.18		0.04	0.49	0.05	0.03			0.02
Ca	%								0.4				11.05	
Cd	ppm		<0.5			<0.5		<0.5	0.61	<0.5	<0.5	<0.5	0.47	<0.5
Ce	ppm		109			85.6		104.5	2.45	61.2	104.5	85.9	12.1	100.5
Co	ppm		4			3		6	7.7	7	6	13	3.9	8
Cr	ppm		20			30		20	10	10	10	10	6	30
Cs	ppm		3.96			1.94		3.73	2.47	2.68	2.54	9.25	2.18	3.31
Cu	ppm		12			9		7	66.4	8	9	13	7.7	7
Dy	ppm		3.13			3.3		3.25		2.81	3.29	3.9		3.46
Er	ppm		1.68			1.85		1.87		1.44	1.24	2.14		1.77
Eu	ppm		1.23			1.3		1.06		1.27	1.64	1.42		1.33
Fe	%								5.86				1.4	
Ga	ppm		21.8			20.8		20.1	2.28	22.6	24.2	22	1.92	23.4
Gd	ppm		4.56			4.77		4.44		4.16	5.67	4.92		4.87
Ge	ppm		<5			<5		<5	0.16	<5	<5	<5	<0.05	<5
Hf	ppm		6.8			6		5.5	0.05	5.2	6	5	0.03	6.1
Hg	ppm		0.014			0.014		0.007	0.54	0.326	0.012	0.006	0.78	0.007
Ho	ppm		0.57			0.6		0.61		0.55	0.52	0.82		0.69
In	ppm		0.009			0.007		0.007	0.012	0.021	0.006	0.027	0.009	0.013
K	%								0.05				0.06	
La	ppm		60.3			48.3		60	1.1	31.3	55.3	46	5.7	54.8
Li	ppm		20			20		20	9.5	30	10	40	1.8	20
Lu	ppm		0.24			0.26		0.27		0.24	0.16	0.34		0.26
Mg	%								0.05				0.12	
Mn	ppm								36				122	
Mo	ppm		1			1		1	2.01	<1	<1	1	2.85	1
Na	%								0.01				0.01	
Nb	ppm		18.4			17.2		19		13.5	14.5	13.3		18.3
Nd	ppm		40.9			34.2		38		28.1	46.2	36.5		39.3
Ni	ppm		4			9		6	75.1	3	3	4	16.1	6
P	ppm								2100				90	
Pb	ppm		12			10		17	2.7	6	11	30	8.2	12
Pr	ppm		11.6			9.35		11.05		7.32	12.05	9.99		11.1
Rb	ppm		154.5			95.4		182	3	98.5	118.5	124	3.7	149.5
Re	ppm		<0.001			<0.001		<0.001	0.001	<0.001	<0.001	<0.001	<0.001	<0.001
S	%		<0.01			<0.01		<0.01	0.02	<0.01	<0.01	<0.01	0.01	0.01
Sb	ppm		0.56			0.63		0.43	233	0.45	0.44	0.38	43.4	0.29
Sc	ppm		5			6		4	1.4	6	5	11	3.1	7
Se	ppm		0.4			0.2		<0.2	0.5	0.2	<0.2	<0.2	0.7	0.3
Sm	ppm		6.8			6.11		6.3		5.22	7.89	6.76		7.01
Sn	ppm		6			6		2	0.3	3	3	3	0.5	3
Sr	ppm		510			663		510	99.3	464	837	554	50	513
Ta	ppm		1.4			1.4		1.7		0.8	0.8	0.9		1.5
Tb	ppm		0.64			0.66		0.63		0.55	0.71	0.7		0.7
Te	ppm		2.14			0.03		<0.01	0.25	0.02	<0.01	0.01	0.03	0.03
Th	ppm		27.9			26.5		29.4	1.2	10.55	12.8	15.3	1.2	24
Ti	%								<0.005				<0.005	
Tl	ppm		0.09			0.03		0.19	0.44	0.13	0.06	0.1	0.19	0.03
Tm	ppm		0.24			0.26		0.26		0.26	0.19	0.32		0.28
U	ppm		4.18			5.21		4.93	5.89	2.27	2.67	3.06	0.6	3.29
V	ppm		58			67		54	75	70	120	132	10	74
W	ppm		1			1		2	49.7	1	2	4	31.9	1
Y	ppm		16.8			17.7		17.8	7.75	15.9	15.2	20.7	5.14	18.2
Yb	ppm		1.68			1.78		1.81		1.67	1.22	2.16		1.62
Zn	ppm		20			14		25	98	89	37	91	25	47
Zr	ppm		258			228		190	1.5	211	254	192	1	231

Major oxides are reported in weight percent normalized to 100% anhydrous. Abbreviations are same as map units in geologic map (Plate 1).
Samples "KS###" collected by Gabriel Aliaga. Samples "KTC###" and "Key XXXX" collected by Tom Chapin for U.S. Gold Corp.
[1] Whole-rock geochemistry not submitted for outcrops previously sampled to avoid repeat analyses. Equivalent sample indicated.

Table A1. Multi-element geochemistry of unaltered and altered rocks.

Sample ID		KS016	KS017	KS018	KS019	KS020	KS021	KS022	KS023	KS024	KS025	KS026	KS027	KS028
UTM	East	537717	537148	537159	540069	540082	536219	536466	536466	536823	536760	536635	537254	537494
NAD27	North	4417287	4416766	4416752	4418575	4418768	4418531	4417674	4417671	4418066	4418145	4418721	4418882	4418951
Unit		Twq	Twd	Dw	Tad	Tad	Tta	Ovb	Tgd	Ovb	Tta	Tvc	Twq	Twq
Comment/Alteration		sodic-calcic	mingled	limonite; sanded	clay	clay	chlorite	green stone		green stone	chlorite	oxidized	clay	endo-skarn
Whole-rock[1]		Y	Y		KTC440	Y	KTC353	Y	Y	KTC345	KTC344	Y	Y	Y
Ore chemistry				Y										
Thin Section		Y			Y	Y	Y	Y	Y	Y	Y	Y	Y	Y
SiO₂	%	64.23	71.40			71.42		48.90	60.80			83.09	80.48	56.74
Al₂O₃	%	16.08	18.79			18.76		16.44	17.16			9.31	17.06	16.59
FeO*	%	4.50	2.51			2.53		9.99	5.67			3.20	0.58	5.13
CaO	%	4.61	0.18			0.18		8.14	4.42			0.34	0.50	6.64
MgO	%	2.01	0.96			0.96		6.47	3.10			0.49	0.17	3.00
Na₂O	%	3.32	0.08			0.07		4.48	3.18			0.11	0.09	2.09
K₂O	%	3.93	4.91			4.91		1.26	4.11			2.82	0.11	7.96
Cr₂O₃	%	0.01	0.01			0.01		0.02	0.01			0.01	0.01	0.01
TiO₂	%	0.77	0.82			0.82		2.96	0.79			0.24	0.72	1.12
MnO	%	0.07	0.01			0.01		0.14	0.10			0.03	0.04	0.10
P₂O₅	%	0.24	0.17			0.18		0.81	0.32			0.16	0.22	0.29
SrO	%	0.07	0.01			0.01		0.14	0.08			0.09	0.01	0.13
BaO	%	0.16	0.16			0.16		0.26	0.26			0.11	0.02	0.19
LOI		0.91	4.94			5.02		3	2.82			3.7	6.98	1.25
Ag	ppm	<0.5	<0.5	0.02		<0.5		<0.5	<0.5			0.8	2.6	<0.5
Al	%			0.61										
As	ppm	2.7	39.1	8.3		38.3		8.1	2.2			70.2	14.1	3.9
Au	ppm			<0.005										
B	ppm			40										
Ba	ppm	1515	1420	340		1370		2260	2180			986	214	1675
Be	ppm			0.14										
Bi	ppm	0.06	0.03	0.07		0.03		0.01	0.01			0.19	0.12	0.02
C	%	0.02	0.06			0.06		0.02	0.12			0.12	0.05	0.06
Ca	%			>25.0										
Cd	ppm	0.5	<0.5	0.1		<0.5		0.7	<0.5			<0.5	<0.5	<0.5
Ce	ppm	96.6	94.4	25		91.7		113.5	83.3			79.7	158.5	85.8
Co	ppm	13	2	4.6				34	13			1	1	15
Cr	ppm	20	20	5		20		130	30			40	30	40
Cs	ppm	3.56	13.4	0.87		12.85		2.04	5.53			4.06	2.58	2.57
Cu	ppm	16	22	8.8		22		35	15			25	13	11
Dy	ppm	3.97	3.57			3.28		5.82	3.65			3.24	4.16	3.42
Er	ppm	2.1	1.74			1.8		2.55	1.97			1.9	2.05	1.69
Eu	ppm	1.39	1.28			1.16		3.03	1.38			0.85	1.72	1.6
Fe	%			1.09										
Ga	ppm	22	23.5	1.22		23.2		23.5	21.5			14.7	24	24.1
Gd	ppm	5.41	4.31			4.16		8.52	4.79			3.88	6.84	5.02
Ge	ppm	<5	<5	<0.05		<5		<5	<5			<5	<5	<5
Hf	ppm	6.1	6.8	0.14		6.6		7.4	4.9			3.7	7.1	5.6
Hg	ppm	0.009	0.019	0.03		0.022		0.02	0.099			0.949	0.054	0.012
Ho	ppm	0.72	0.65			0.59		1.04	0.66			0.66	0.77	0.63
In	ppm	0.011	0.02	0.014		0.02		0.043	0.026			0.023	0.03	0.008
K	%			0.18										
La	ppm	53.2	51.9	14.3		49.7		57.1	45.5			50.6	96.7	47.2
Li	ppm	30	10	3.3		10		40	30			20	50	20
Lu	ppm	0.3	0.24			0.26		0.32	0.28			0.29	0.24	0.26
Mg	%			0.28										
Mn	ppm			140										
Mo	ppm	1	2	0.63		2		2	2			2	1	1
Na	%			0.03										
Nb	ppm	17.4	13.6	0.6		13.3		54	10.5			11.7	17.3	14
Nd	ppm	38.9	37.1			36		53.4	35.6			29.9	57.6	37.6
Ni	ppm	8	7	17.5		5		67	3			4	4	12
P	ppm			270										
Pb	ppm	20	28	5.7		28		4	13			40	70	21
Pr	ppm	10.95	10.5			10.35		13.5	9.49			8.74	16.65	9.84
Rb	ppm	135	179	14.5		174		23.1	95.4			102	4.8	145
Re	ppm	0.001	0.001	<0.001		0.001		<0.001	<0.001			0.001	<0.001	<0.001
S	%	0.01	0.07	<0.01		0.07		0.01	0.42			0.02	0.02	0.02
Sb	ppm	0.39	1.86	0.38		1.83		0.62	0.69			18.9	7.02	0.57
Sc	ppm	10	10	0.9		10		17	13			5	6	11
Se	ppm	<0.2	0.2	0.2		0.2		0.8	0.4			0.9	0.4	<0.2
Sm	ppm	6.96	5.65			5.81		10.55	6.38			5.08	9.14	6.55
Sn	ppm	2	1	0.3		2		4	1			2	3	1
Sr	ppm	595	100.5	492		96.1		1095	699			749	37.4	1080
Ta	ppm	1.3	1.4	0.01		0.8		3.4	0.6			0.7	1.2	0.7
Tb	ppm	0.74	0.63			0.59		1.12	0.68			0.6	0.82	0.65
Te	ppm	0.02	<0.01	0.02		<0.01		0.04	0.01			0.07	0.03	0.01
Th	ppm	19.9	14	2.6		13.3		6.96	13.35			9.4	25.5	12.8
Ti	%			0.017										
Tl	ppm	0.17	0.38	0.18		0.36		0.08	1.81			0.12	0.17	0.14
Tm	ppm	0.32	0.24			0.24		0.37	0.27			0.27	0.27	0.28
U	ppm	3.69	3.19	0.46		3.06		1.9	3.03			3.17	3.68	2.53
V	ppm	109	109	6		103		219	143			101	71	128
W	ppm	1	4	0.53		3		1	1			47	53	1
Y	ppm	21	16.2	6.65		15.5		26.5	18.7			21.5	25.2	18.3
Yb	ppm	2.07	1.69			1.69		2.1	2.04			1.93	1.58	1.65
Zn	ppm	43	33	30		33		112	91			57	64	73
Zr	ppm	227	273	5.4		264		321	204			136	280	228

Major oxides are reported in weight percent normalized to 100% anhydrous. Abbreviations are same as map units in geologic map (Plate 1).

Samples "KS###" collected by Gabriel Aliaga. Samples "KTC###" and "Key XXXX" collected by Tom Chapin for U.S. Gold Corp.

[1]Whole-rock geochemistry not submitted for outcrops previously sampled to avoid repeat analyses. Equivalent sample indicated.

Table A1. Multi-element geochemistry of unaltered and altered rocks.

Sample ID		KS029	KS030	KS031	KS032	KS033	KS034	KS035	KS036	KS037	KS038	KS039	KS040	KS041
UTM East		537965	537958	537961	537965	537970	538384	538205	539379	539316	537970	537253	537253	539286
NAD27 North		4418926	4418925	4418926	4418927	4418929	4419088	4419065	4418489	4418485	4418929	4418886	4418886	4418457
Unit		Twq	Twq	Twq	Twq	Twq	Twd	Dw	Dw	Twd	Twq	Dw	gossan	Twd
Comment/Alteration		clay	qz veins				endo-skarn	skarn ore	marble	endo-skarn	qz veins	jasp bx	gossan	
Whole-rock[1]		Y		Y		Y	Y			Y	Y			Y
Ore chemistry			Y					Y		Y	Y	Y	Y	
Thin Section		Y						Y	Y	Y				Y
SiO₂	%	76.69		69.40		69.22	57.04			57.26	87.36			61.75
Al₂O₃	%	16.18		15.46		15.49	14.71			16.98	8.24			17.20
FeO*	%	0.94		2.89		2.04	4.46			5.84	0.84			5.74
CaO	%	0.33		2.83		3.57	10.28			6.29	0.35			4.90
MgO	%	0.37		1.02		1.24	3.04			2.15	0.22			2.23
Na₂O	%	0.13		2.97		3.25	3.59			4.79	0.08			3.37
K₂O	%	4.52		4.52		4.20	4.91			5.00	2.45			3.18
Cr₂O₃	%	0.01		0.01		0.01	0.01			0.01	0.01			0.01
TiO₂	%	0.53		0.52		0.52	1.07			0.90	0.26			0.91
MnO	%	0.02		0.02		0.03	0.10			0.12	0.05			0.11
P₂O₅	%	0.19		0.15		0.20	0.46			0.32	0.09			0.36
SrO	%	0.01		0.06		0.07	0.13			0.15	0.01			0.08
BaO	%	0.09		0.15		0.15	0.19			0.18	0.04			0.15
LOI		2.65		1.24		1.05	0.95			1.11	1.64			1.24
Ag	ppm	0.5		<0.5		<0.5	<0.5	156		<0.5	6	1.4	111	<0.5
Al	%											0.15	0.77	
As	ppm	1.6		9		7	10.9	268		2.4	16.3	582	848	2
Au	ppm							0.021			<0.005	0.087	0.134	
B	ppm							<10				<10	10	
Ba	ppm	774		1295		1310	1675	10		1590	342	400	220	1360
Be	ppm							0.08				0.29	5.09	
Bi	ppm	0.64		0.31		0.38	0.04	10.8		0.03	2.14	0.36	56.2	0.03
C	%	0.04		0.02		0.04	0.12			0.04	0.02			0.04
Ca	%							3.82				1.37	0.43	
Cd	ppm	<0.5		<0.5		<0.5	0.6	371		<0.5	<0.5	1.68	29	<0.5
Ce	ppm	46.1		91.1		104.5	112	8.36		81.6	53	56.4	44.5	96.7
Co	ppm	1		5		5	15	25.5		11	2	2.4	33.1	10
Cr	ppm	20		30		30	50	8		10	30	20	7	10
Cs	ppm	1.91		3.98		1.98	2.85	0.14		5.99	5.14	0.42	10.2	5.85
Cu	ppm	25		6		5	36	2460000		6	97	72.3	1665000	6
Dy	ppm	2.28		2.84		3	3.83			3.96	1.37			4.56
Er	ppm	1.22		1.36		1.5	1.84			2.23	0.62			2.52
Eu	ppm	0.72		1.11		1.23	1.73			1.68	0.57			1.65
Fe	%							12.1				0.55	9.5	
Ga	ppm	18.5		21.4		21.7	21.5	0.7		24	9.8	0.97	9.27	25.2
Gd	ppm	3.14		4.02		4.17	5.94			5.3	2.09			6.16
Ge	ppm	<5		<5		<5	<5	0.21		<5	<5	0.1	0.37	<5
Hf	ppm	5.7		6.2		5.7	5.8	0.07		5.4	3.2	0.05	0.1	6.6
Hg	ppm	0.017		0.015		0.022	0.008	0.6		0.01	0.051	0.65	1.72	0.009
Ho	ppm	0.42		0.5		0.58	0.69			0.8	0.28			0.88
In	ppm	0.016		0.021		0.021	0.009	1.015		0.009	0.066	0.028	1.805	0.021
K	%							0.01				0.01	0.04	
La	ppm	25.6		51		57.8	59.4	4.1		44.7	29.7	52.1	21.9	50.9
Li	ppm	10		20		20	10	1		30	30	1.2	1.6	10
Lu	ppm	0.21		0.2		0.25	0.26			0.31	0.13			0.32
Mg	%							0.16				0.03	0.29	
Mn	ppm							1200				194	326	
Mo	ppm	<1		1		1	3	19.05		4	3	1.62	66.9	1
Na	%							0.01				0.01	0.01	
Nb	ppm	16.5		16.7		16.8	21.8	0.09		12	8.2	0.1	0.18	16.1
Nd	ppm	20		34.1		37	48.9			35.8	20.6			42.7
Ni	ppm	4		6		6	13	14.4		2	3	14.8	9.9	1
P	ppm							150				380	210	
Pb	ppm	35		15		16	12	2950000		21	1840	156	4200000	16
Pr	ppm	5.48		9.77		11	12.8			9.44	6.19			11.4
Rb	ppm	130		122.5		102	122.5	0.3		156	195	0.9	9	99.4
Re	ppm	0.001		<0.001		<0.001	<0.001	0.002		0.001	<0.001	0.004	0.002	<0.001
S	%	<0.01		<0.01		<0.01	<0.01	>10.0		0.02	0.03	0.11	0.03	<0.01
Sb	ppm	0.31		0.39		0.45	0.98	23.1		0.32	2.27	42.1	360	0.17
Sc	ppm	6		5		5	12	1.5		11	2	1.6	1.7	10
Se	ppm	<0.2		0.2		<0.2	<0.2	68.9		0.3	1.6	0.8	22.9	<0.2
Sm	ppm	4.29		5.59		5.92	8.2			6.94	3.37			7.8
Sn	ppm	4		2		2	2	1.6		2	3	0.4	2	2
Sr	ppm	23.6		465		561	1075	44.5		1250	17.7	42.1	94	719
Ta	ppm	1.3		1.3		1.3	1.3			0.7	0.7			1
Tb	ppm	0.44		0.52		0.6	0.77			0.73	0.26			0.86
Te	ppm	0.02		0.03		0.06	0.02	3.26		0.01	0.61	0.08	7.24	<0.01
Th	ppm	22.8		22.7		23.8	15.8	1.8		13.6	12.05	4.1	10.6	16.85
Ti	%							<0.005				<0.005	<0.005	
Tl	ppm	0.23		0.17		0.05	0.05	0.04		0.36	0.33	0.71	0.36	0.34
Tm	ppm	0.2		0.21		0.23	0.25			0.33	0.12			0.37
U	ppm	2.65		3.73		3.57	3.87	2.69		2.94	1.85	2.18	96.8	3.18
V	ppm	60		56		50	138	11		122	52	15	97	113
W	ppm	4		1		1	2	1.59		1	6	7.28	219	1
Y	ppm	12.4		14.1		16.4	18.6	2.72		21.3	7.3	21.3	5.32	24.6
Yb	ppm	1.21		1.32		1.55	1.68			2.35	0.76			2.4
Zn	ppm	16		22		22	72	4550000		105	147	208	3410000	99
Zr	ppm	205		235		214	222	2.8		218	125	1.4	1.9	261

Major oxides are reported in weight percent normalized to 100% anhydrous. Abbreviations are same as map units in geologic map (Plate 1).

Samples "KS###" collected by Gabriel Aliaga. Samples "KTC###" and "Key XXXX" collected by Tom Chapin for U.S. Gold Corp.

[1]Whole-rock geochemistry not submitted for outcrops previously sampled to avoid repeat analyses. Equivalent sample indicated.

Table A1. Multi-element geochemistry of unaltered and altered rocks.

Sample ID		KS042	KS043	KS044	KS045	KS046	KS047	KS048	KS049	KS050	KS051	KS052	KS053	KS054
UTM	East	539202	538842	539997	539997	539997	540365	540304	540317	540585	540994	541618	537902	537878
NAD27	North	4418479	4418355	4417710	4417771	4417710	4417960	4418097	4418074	4417921	4417038	4419530	4418556	4418483
Unit		Twq	Twd	Trp	Trp	Trp	Tvc	Tcg	Tcg	Tvc	Tda	Ta	Twd	Twd
Comment/Alteration		mingled	mingled	clay	qz veins	qz veins	clay	limonite	silicified	clay			sodic-calcic	
Whole-rock[1]		Y	Y	KTC398			Y			Y	Y	Y	Y	
Ore chemistry					Y	Y			Y					
Thin Section		Y	Y			Y	Y			Y	Y	Y	2	Y
SiO$_2$	%	68.57	62.68				82.86			81.35	67.54	64.44	62.28	
Al$_2$O$_3$	%	16.20	16.76				11.75			12.62	16.68	16.44	16.91	
FeO*	%	1.90	5.14				2.04			1.01	3.04	4.65	2.31	
CaO	%	3.79	4.44				0.24			0.10	3.34	4.70	8.37	
MgO	%	1.18	1.91				0.38			0.54	0.82	1.98	2.82	
Na$_2$O	%	3.31	3.55				0.07			0.05	3.46	3.49	3.84	
K$_2$O	%	4.04	3.90				2.38			4.07	4.23	3.03	1.95	
Cr$_2$O$_3$	%	0.01	0.01				0.01			0.01	0.01	0.01	0.01	
TiO$_2$	%	0.52	1.03				0.12			0.12	0.41	0.70	1.01	
MnO	%	0.05	0.03				0.01			0.03	0.07	0.08	0.03	
P$_2$O$_5$	%	0.20	0.31				0.07			0.02	0.15	0.26	0.30	
SrO	%	0.07	0.08				0.01			0.01	0.06	0.07	0.10	
BaO	%	0.15	0.16				0.05			0.07	0.19	0.14	0.07	
LOI		2.95	1.31				3.62			2.92	2.07	2.86	3.47	
Ag	ppm	<0.5	<0.5		2.14	0.21	<0.5		2.06	<0.5	<0.5	<0.5	<0.5	
Al	%				0.11	0.33			2.46					
As	ppm	6.7	5.9		23.8	7.7	53.5		266	15.5	0.9	0.4	2.7	
Au	ppm				0.005	<0.005			0.006					
B	ppm				<10	<10			10					
Ba	ppm	1385	1420		1090	140	401		640	561	1560	1135	591	
Be	ppm				0.07	0.17			1.6					
Bi	ppm	0.06	0.17		0.49	0.42	0.09		1.15	0.26	0.02	0.01	0.01	
C	%	0.26	0.02				0.08			0.03	0.11	0.27	0.03	
Ca	%				0.07	0.14			2.01					
Cd	ppm	<0.5	<0.5		2.89	0.19	<0.5		2.62	<0.5	<0.5	<0.5	<0.5	
Ce	ppm	73	96.1		13.75	29.3	75.3		28.3	27.5	108.5	79.2	95.8	
Co	ppm	2	7		0.4	0.2	2		27	4	9	5		
Cr	ppm	20	10		7	6	10		34	10	20	10	10	
Cs	ppm	1.74	2.7		0.26	0.41	4.71		1.17	2.13	1.68	1.64	8.14	
Cu	ppm	2	5		211	10.8	5		337	9	5	8	1	
Dy	ppm	3.99	3.98				2.52			1.66	4.12	3.05	4.59	
Er	ppm	2.12	2.17				1.43			1.29	2.2	1.76	2.54	
Eu	ppm	1.17	1.52				0.96			0.23	1.66	1.36	1.56	
Fe	%				0.43	0.28			4.61					
Ga	ppm	22.7	23.2		0.52	1.15	14.8		6.09	19.3	21.4	19.7	21.7	
Gd	ppm	5.22	5.62				3.25			1.29	5.22	4.16	5.46	
Ge	ppm	<5	<5		<0.05	<0.05	<5		0.06	<5	<5	<5	<5	
Hf	ppm	6.1	6.7		0.06	0.16	3.6		0.21	3.8	8.3	5.5	5.4	
Hg	ppm	0.019	0.011		0.22	0.04	0.024		0.1	0.022	0.006	0.04	0.005	
Ho	ppm	0.73	0.75				0.5			0.38	0.79	0.6	0.84	
In	ppm	0.032	0.017		0.017	0.006	0.008		0.162	0.021	0.028	0.033	0.005	
K	%				0.11	0.13			0.15					
La	ppm	34.1	52.7		6.3	16	38.9		14.1	16.9	58	42.4	51.2	
Li	ppm	20	20		0.4	0.7	20		10.1	10	10	10	20	
Lu	ppm	0.31	0.28				0.25			0.25	0.3	0.27	0.34	
Mg	%				0.01	0.05			0.07					
Mn	ppm				38	20			6420					
Mo	ppm	1	2		3.21	2.06	2		6.74	1	2	2	1	
Na	%				0.01	0.01			0.01					
Nb	ppm	15.3	18.6		0.14	0.12	13		0.16	14.5	13.7	10.6	17.8	
Nd	ppm	36.1	40.7				28.4			9.3	41.3	29.8	38.2	
Ni	ppm	1	6		1.1	0.7	5		23.3	1	2	1	6	
P	ppm				120	120			1350					
Pb	ppm	12	3		416	55.4	9		883	19	21	22	5	
Pr	ppm	9.32	11.1				8.56			2.87	12.25	8.87	10.95	
Rb	ppm	114.5	107.5		4.2	5.2	82.9		7.2	142	124	80.6	56	
Re	ppm	0.001	<0.001		<0.001	<0.001	<0.001		0.001	<0.001	<0.001	<0.001	<0.001	
S	%	0.01	<0.01		0.1	<0.01	0.01		0.16	0.11	<0.01	<0.01	<0.01	
Sb	ppm	0.23	1.77		1.75	0.66	1.06		9.5	0.71	0.07	0.05	1.08	
Sc	ppm	5	9		0.2	0.5	3		3.4	3	4	8	11	
Se	ppm	0.3	<0.2		0.9	<0.2	0.8		0.6	0.5	0.2	<0.2	0.3	
Sm	ppm	6.69	7.18				5.3			1.68	7.38	5.43	7.57	
Sn	ppm	3	1		0.3	0.2	1		1	5	2	1	1	
Sr	ppm	664	628		23.8	15.8	50.4		54	34.2	543	593	847	
Ta	ppm	1.2	1.1				0.8			1	0.9	0.6	1.1	
Tb	ppm	0.72	0.76				0.45			0.24	0.74	0.57	0.81	
Te	ppm	<0.01	<0.01		0.27	0.03	0.03		0.52	0.03	<0.01	<0.01	<0.01	
Th	ppm	21.5	18.65		2.9	10.1	11.8		3.2	11.5	18.2	11.25	14.55	
Ti	%				<0.005	<0.005			<0.005					
Tl	ppm	0.05	0.12		0.12	0.1	0.39		0.21	0.54	0.04	<0.02	0.02	
Tm	ppm	0.32	0.3				0.23			0.21	0.32	0.27	0.35	
U	ppm	4.16	3.56		0.98	1.83	3.27		2.73	3.03	3.31	2.32	4.11	
V	ppm	55	95		2	3	6		95	32	99	137		
W	ppm	1	3		1.3	0.45	1		5.2	1	1	1	1	
Y	ppm	20.7	20.3		1.71	5.26	14.7		20.3	12	22.6	17.8	24.7	
Yb	ppm	2.05	1.89				1.53			1.53	2.05	1.76	2.21	
Zn	ppm	89	19		471	42	58		1060	15	71	85	10	
Zr	ppm	223	270		1.8	3.9	117		6.4	129	345	225	216	

Major oxides are reported in weight percent normalized to 100% anhydrous. Abbreviations are same as map units in geologic map (Plate 1).
Samples "KS###" collected by Gabriel Aliaga. Samples "KTC###" and "Key XXXX" collected by Tom Chapin for U.S. Gold Corp.
[1]Whole-rock geochemistry not submitted for outcrops previously sampled to avoid repeat analyses. Equivalent sample indicated.

Table A1. Multi-element geochemistry of unaltered and altered rocks.

Sample ID		KS055	KS056	KS057	KS058	KS059	KS060	KS061	KS062	KS063	KS064	KS065	KS066	KS067
UTM	East	538552	538275	538549	538542	538545	538540	538537	538357	538377	537997	537918	538025	537984
NAD27	North	4417171	4417212	4417424	4417405	4417379		4417136	4416839	4416821	4416632	4416810	4417111	4417030
Unit		Ov	Twq	Twq	Twq	Twq	Twq	Ov	Ovb	Ovb	Ovb	Twd	Twq	Twd
Comment/Alteration		hornfels	mingled	garnet veins	near garnet veins	garnet veins	near garnet veins	gossan	float	green stone	green stone	endo-skarn	oxidized	mingled
Whole-rock¹			Y		Y	Y	Y			KTC307	Y	Y	Y	Y
Ore chemistry			Y					Y						
Thin Section		Y	Y	Y	Y	Y	Y			Y	Y	Y	Y	Y
SiO$_2$	%		67.35		64.38	45.94	64.91				50.12	54.85	67.13	58.01
Al$_2$O$_3$	%		16.35		15.65	11.49	15.65				11.26	15.61	15.91	16.78
FeO*	%		2.65		3.01	6.23	4.11				9.57	4.63	2.93	7.46
CaO	%		3.30		5.97	32.90	4.24				12.71	11.86	3.51	5.55
MgO	%		1.11		1.69	1.84	1.70				7.40	2.58	1.35	3.07
Na$_2$O	%		3.23		3.31	0.48	3.55				0.50	1.65	3.53	3.97
K$_2$O	%		4.80		4.80	0.23	4.64				4.21	7.08	4.54	3.32
Cr$_2$O$_3$	%		0.01		0.01	0.01	0.01				0.05	0.01	0.01	0.01
TiO$_2$	%		0.75		0.66	0.51	0.69				3.03	0.93	0.59	1.01
MnO	%		0.02		0.05	0.23	0.07				0.13	0.07	0.03	0.18
P$_2$O$_5$	%		0.20		0.22	0.09	0.21				0.51	0.31	0.24	0.40
SrO	%		0.07		0.09	0.05	0.07				0.07	0.15	0.07	0.09
BaO	%		0.15		0.15	0.01	0.14				0.43	0.27	0.16	0.15
LOI			2.03		0.55	1.62	0.57				2.99	1.44	1.09	1
Ag	ppm		<0.5		<0.5	<0.5	<0.5	0.2			<0.5	<0.5	<0.5	<0.5
Al	%							1.02						
As	ppm		5		1.9	2.7	1.1	175.5			101	3	3.4	0.7
Au	ppm		<0.005					0.076						
B	ppm							20						
Ba	ppm		1415		1200	86.3	1150	780			3490	2210	1275	1230
Be	ppm							8.44						
Bi	ppm		0.14		0.06	0.02	0.04	2.01			0.01	0.17	0.07	0.1
C	%		0.05		0.02	0.3	0.02				0.21	0.14	0.06	0.04
Ca	%							0.57						
Cd	ppm		<0.5		<0.5	0.8	<0.5	1.87			0.6	<0.5	<0.5	0.7
Ce	ppm		108		102	51.8	102	82.9			91.5	84.8	87	91.9
Co	ppm		4		8	8	10	187			45	13	5	21
Cr	ppm		30		30	20	40	13			340	20	30	30
Cs	ppm		4.2		1.79	5.44	3.43	0.58			10.25	3.36	2.1	6.52
Cu	ppm		4		10	3	8	20.2			35	32	8	28
Dy	ppm		4.27		3.68	2.37	3.53				4.66	3.62	2.73	3.68
Er	ppm		2.2		1.96	1.34	1.96				1.95	1.86	1.47	1.93
Eu	ppm		1.48		1.53	0.93	1.48				2.58	1.56	1.13	1.83
Fe	%							28.2						
Ga	ppm		21.3		21.1	15.3	21.1	2.47			16.6	20.1	19.8	20.6
Gd	ppm		5.32		4.75	3.33	4.34				6.36	5.04	3.53	4.88
Ge	ppm		<5		<5	<5	<5	0.43			<5	<5	<5	<5
Hf	ppm		6.2		6.6	4.2	7.2	0.1			5.4	5.4	5.3	5.5
Hg	ppm		0.01		0.009	0.008	0.007	0.11			0.01	0.019	0.01	0.006
Ho	ppm		0.84		0.71	0.48	0.67				0.81	0.7	0.52	0.71
In	ppm		0.013		0.01	0.073	0.013	0.22			0.026	0.016	0.006	0.017
K	%							0.1						
La	ppm		59		53.9	22.7	55.3	38.8			45.7	41.9	47.3	48.1
Li	ppm		30		20	10	20	5.1			30	10	20	30
Lu	ppm		0.34		0.3	0.21	0.32				0.23	0.21	0.22	0.28
Mg	%							0.04						
Mn	ppm							16000						
Mo	ppm		14		2	2	1	15.6			<1	2	1	2
Na	%							0.03						
Nb	ppm		17.9		15.7	20.8	16	0.11			40.3	13.5	14.1	13.1
Nd	ppm		42.7		37.1	25	36.9				41.3	35.8	30.6	37.6
Ni	ppm		4		10	6	9	551			161	9	5	10
P	ppm							3110						
Pb	ppm		15		11	3	21	36.7			5	13	11	50
Pr	ppm		12.55		11.1	6.89	11.2				10.95	10.2	9.41	10.55
Rb	ppm		183.5		139.5	8.4	165	2.1			161	187.5	144.5	135.5
Re	ppm		0.002		<0.001	0.001	0.001	0.001			0.001	0.001	<0.001	<0.001
S	%		0.13		<0.01	0.01	<0.01	0.11			0.01	<0.01	0.01	0.01
Sb	ppm		0.59		0.19	0.15	0.11	2.18			9.08	1.61	0.23	0.06
Sc	ppm		7		7	6	7	6.7			22	8	6	11
Se	ppm		0.8		<0.2	0.4	0.2	3.9			0.7	0.4	<0.2	<0.2
Sm	ppm		7.21		6.52	4.64	6.81				8.38	6.95	5.24	7.02
Sn	ppm		2		3	7	1	0.5			2	2	2	2
Sr	ppm		637		769	419	609	69.7			584	1225	558	778
Ta	ppm		1.4		1.2	1	1.2				2.5	0.9	21.2	0.8
Tb	ppm		0.81		0.61	0.43	0.64				0.92	0.66	0.52	0.69
Te	ppm		0.03		<0.01	0.01	<0.01	0.25			0.02	0.03	0.01	<0.01
Th	ppm		26.2		24.3	8.52	23.7	2.8			4.09	15.9	20.6	11.05
Ti	%							<0.005						
Tl	ppm		0.14		0.03	<0.02	0.1	0.15			0.73	0.06	0.11	0.06
Tm	ppm		0.33		0.32	0.17	0.27				0.28	0.23	0.22	0.27
U	ppm		5.15		4.28	2.89	4.57	4.38			1.18	2.99	3.7	2.96
V	ppm		83		85	163	87	77			258	122	65	158
W	ppm		2		1	2	2	0.55			5	2	1	4
Y	ppm		22		20.1	14	19.7	86.7			21.5	18.8	14.8	20.5
Yb	ppm		2.12		1.95	1.26	1.9				1.58	1.62	1.46	1.95
Zn	ppm		35		30	48	50	1880			87	50	16	286
Zr	ppm		234		254	164	287	2.8			230	219	208	227

Major oxides are reported in weight percent normalized to 100% anhydrous. Abbreviations are same as map units in geologic map (Plate 1).

Samples "KS###" collected by Gabriel Aliaga. Samples "KTC###" and "Key XXXX" collected by Tom Chapin for U.S. Gold Corp.

¹Whole-rock geochemistry not submitted for outcrops previously sampled to avoid repeat analyses. Equivalent sample indicated.

Table A1. Multi-element geochemistry of unaltered and altered rocks.

Sample ID		KS068	KS069	KS070	KS071	KS072	KS073	KS074	KS075	KS076	KS077	KS078	KS079	KS080
UTM	East	537785	537322	537298	537298	537261	537197	537175	537179	537231	537366	537304	537214	537717
NAD27	North	4416879	4416196	4416192	4416191	4416154	4416090	4416156	4416149	4416189	4416264	4416289	4416387	4416178
Unit		Twd	Dhc	Tgd	Dhc	Tgd	Dhc	Dew	Tgd	Tgd	Tgd	Tgd	Tgd	Ovb
Comment/Alteration			skarnoid	chlorite	skarnoid	endo-skarn	jasperoid	marble	sodic-calcic	chlorite	clay			
Whole-rock[1]		Y	KTC231						Y	Y	Y	Y	Y	Y
Ore chemistry							Y				Y	Y		
Thin Section		Y	2		Y				Y	Y	Y	Y	Y	
SiO₂	%	64.12							59.98	62.44	67.53	61.90	60.81	45.15
Al₂O₃	%	16.13							16.24	16.63	16.40	17.04	17.07	17.30
FeO*	%	5.23							4.90	5.45	2.10	5.57	4.78	10.58
CaO	%	4.55							5.41	4.76	2.52	4.49	6.25	8.71
MgO	%	1.87							2.94	2.50	1.42	2.79	2.57	4.70
Na₂O	%	3.14							5.20	3.74	3.54	2.90	3.93	3.49
K₂O	%	3.43							3.79	3.04	5.23	3.66	3.08	3.68
Cr₂O₃	%	0.01							0.01	0.01	0.01	0.01	0.01	0.01
TiO₂	%	0.85							0.91	0.86	0.61	0.88	0.93	4.05
MnO	%	0.11							0.05	0.05	0.03	0.10	0.06	0.18
P₂O₅	%	0.34							0.29	0.29	0.24	0.34	0.31	1.36
SrO	%	0.07							0.08	0.08	0.08	0.09	0.07	0.16
BaO	%	0.15							0.20	0.13	0.30	0.23	0.13	0.63
LOI		0.77							1.57	1.9	2.62	2.08	1.25	9.12
Ag	ppm	<0.5					0.22		<0.5	<0.5	<0.5	<0.5	<0.5	<0.5
Al	%						0.58							
As	ppm	0.7					233		1	3.7	5.4	6.3	7.8	9.6
Au	ppm						0.008				<0.005	<0.005		
B	ppm						<10							
Ba	ppm	1195					140		1665	1125	2740	2060	1090	4880
Be	ppm						0.29							
Bi	ppm	0.01					0.09		0.01	0.02	0.03	0.02	0.01	0.02
C	%	0.03							0.06	0.05	0.12	0.01	0.09	1.49
Ca	%						0.22							
Cd	ppm	<0.5					0.71		<0.5	<0.5	1.3	<0.5	<0.5	<0.5
Ce	ppm	104.5					18.55		81.4	82.5	83.4	83.9	80.2	169
Co	ppm	11					3.9		11	10	3	10	9	26
Cr	ppm	30					33		30	30	20	20	20	30
Cs	ppm	2.26					0.18		3.43	3.82	10.4	22.5	12.4	1.7
Cu	ppm	9					15.6		5	9	6	8	6	34
Dy	ppm	4.92							3.98	3.81	2.88	3.74	4.1	6.48
Er	ppm	2.62							1.98	1.97	1.37	1.88	2.2	3.03
Eu	ppm	1.68							1.68	1.63	1.19	1.65	1.54	3.82
Fe	%						1.77							
Ga	ppm	20.4					2.04		20.3	20.9	20.9	21.7	20.7	21
Gd	ppm	5.8							4.84	4.91	4.62	5.54	5	8.88
Ge	ppm	<5					<0.05		<5	<5	<5	<5	<5	<5
Hf	ppm	6.3					0.16		4.9	5.4	5.9	5.8	5.7	8.1
Hg	ppm	<0.005					0.44		<0.005	0.009	0.012	0.01	0.01	0.007
Ho	ppm	0.97							0.75	0.71	0.52	0.77	0.83	1.2
In	ppm	0.024					0.049		0.012	0.014	0.019	0.014	0.013	0.067
K	%						0.06							
La	ppm	54.7					11.2		42.4	43.2	49.9	45.4	41.5	85.2
Li	ppm	20					2.2		<10	20	20	20	10	60
Lu	ppm	0.39							0.27	0.3	0.21	0.25	0.29	0.35
Mg	%						0.05							
Mn	ppm						137							
Mo	ppm	2					3.61		1	3	1	2	2	1
Na	%						<0.01							
Nb	ppm	18					0.28		10.9	11.9	12.6	12.4	11.9	96.2
Nd	ppm	42.1							33.7	34.5	37.1	38.9	34.3	71.9
Ni	ppm	8					29.3		5	4	2	2	4	14
P	ppm						520							
Pb	ppm	22					10.2		9	10	17	18	18	9
Pr	ppm	11.95							9.42	9.63	10.8	10.5	9.28	20
Rb	ppm	112					1.2		98.7	97.7	170.5	120	104	66.4
Re	ppm	0.001					0.002		<0.001	<0.001	<0.001	<0.001	0.003	0.001
S	%	0.01					0.08		0.01	0.05	0.01	0.07	0.05	0.05
Sb	ppm	0.11					34.6		0.36	0.53	1.71	0.73	3.48	0.24
Sc	ppm	11					1.9		10	10	6	11	9	9
Se	ppm	<0.2					<0.2		<0.2	0.4	0.2	<0.2	0.4	0.3
Sm	ppm	8.03							6.28	7.03	5.94	6.8	6.51	12.25
Sn	ppm	2					0.9		2	2	1	2	1	2
Sr	ppm	606					113.5		719	708	684	755	639	1260
Ta	ppm	1.2							0.7	0.8	0.9	0.8	0.7	6.1
Tb	ppm	0.8							0.7	0.68	0.58	0.72	0.74	1.21
Te	ppm	<0.01					0.11		<0.01	<0.01	0.01	0.01	0.01	<0.01
Th	ppm	16.75					4.8		10.65	13.1	15.25	12.65	12.65	8.86
Ti	%						0.006							
Tl	ppm	0.13					0.21		0.07	0.13	0.16	0.15	1.33	0.06
Tm	ppm	0.4							0.29	0.3	0.2	0.28	0.29	0.43
U	ppm	3.31					1.56		2.4	3	3.09	3.02	2.52	2.27
V	ppm	87					38		139	121	57	122	119	213
W	ppm	1					2.95		2	1	2	1	2	2
Y	ppm	27.4					2.95		20.7	20.9	14.8	20.2	22.2	31.2
Yb	ppm	2.71							1.84	1.78	1.31	1.83	2.01	2.47
Zn	ppm	87					100		25	36	130	58	47	104
Zr	ppm	259					3.6		186	212	231	227	219	388

Major oxides are reported in weight percent normalized to 100% anhydrous. Abbreviations are same as map units in geologic map (Plate 1).

Samples "KS###" collected by Gabriel Aliaga. Samples "KTC###" and "Key XXXX" collected by Tom Chapin for U.S. Gold Corp.

[1]Whole-rock geochemistry not submitted for outcrops previously sampled to avoid repeat analyses. Equivalent sample indicated.

Table A1. Multi-element geochemistry of unaltered and altered rocks.

Sample ID	Unit	KS081	KS082	KS083	KS084	KS085	KS086	KS087	KS088	KS089	KS090	KS091	KS092
UTM East		537752	538645	538645	538684	538713	538743	538873	538873	538852	538911	539047	539007
NAD27 North		4416125	4417211	4417184	4417199	4417217	4417226	4417373	4417373	4417418	4417483	4417735	4417526
Unit		Ovb	Ovb	Ov	Twd	Twd	Twd	Twd	Twd	Twd	Twd	Dhc	Ovb
Comment/Alteration				lim	mingled			Ksp-phyric	qz veins		chlorite	skarnoid	
Whole-rock[1]		KTC234	Y		Y		Y	Y		Y	Y		KTC485
Ore chemistry			Y	Y			Y		Y				
Thin Section		Y	Y	Y	Y		Y	Y		Y	Y		Y
SiO_2	%		47.69		66.45		64.12	70.74		65.12	61.45		
Al_2O_3	%		17.21		14.71		16.44	14.58		15.07	16.06		
FeO*	%		3.63		2.81		4.50	2.11		5.87	4.49		
CaO	%		20.11		4.65		3.92	2.31		2.48	3.44		
MgO	%		5.47		2.95		1.99	1.15		1.73	2.12		
Na_2O	%		1.37		3.17		3.08	3.01		3.71	6.19		
K_2O	%		0.68		3.93		4.65	5.22		4.87	4.94		
Cr_2O_3	%		0.01		0.01		0.01	0.01		0.01	0.01		
TiO_2	%		2.88		0.75		0.75	0.46		0.63	0.82		
MnO	%		0.09		0.05		0.05	0.02		0.04	0.08		
P_2O_5	%		0.72		0.32		0.25	0.14		0.23	0.24		
SrO	%		0.09		0.06		0.07	0.05		0.06	0.06		
BaO	%		0.05		0.14		0.18	0.21		0.19	0.11		
LOI			1.85		1.76		2.11	1.53		1.35	1.32		
Ag	ppm		0.5	3.46	<0.5		0.5	<0.5	0.15	<0.5	<0.5		
Al	%			0.54					0.43				
As	ppm		101.5	193.5	48.3		87.9	2.7	9.4	8.3	6.3		
Au	ppm		0.013	0.012			<0.005		<0.005				
B	ppm		<10						<10				
Ba	ppm		472	830	1230		1655	1660	50	1555	880		
Be	ppm		0.28						0.36				
Bi	ppm		0.71	8.42	0.06		0.06	0.43	1.21	1.5	0.3		
C	%		0.01		0.04		0.03	0.04		0.03	0.08		
Ca	%			0.3					0.85				
Cd	ppm		<0.5	0.31	<0.5		<0.5	<0.5	0.18	<0.5	<0.5		
Ce	ppm		159.5	68.5	84.2		99.7	106.5	13.05	136.5	102		
Co	ppm		9	5.6	5		8	4	1.5	17	11		
Cr	ppm		10	16	30		20	20	8	20	30		
Cs	ppm		8.8	0.47	8.68		3.55	7.73	1.4	9.81	3.45		
Cu	ppm		24	51.9	18		24	19	11.5	63	9		
Dy	ppm		5.43		4.05		3.97	3.29		3.64	3.7		
Er	ppm		2.6		2.28		2.19	1.65		1.91	1.87		
Eu	ppm		3.27		1.48		1.66	1.22		1.47	1.48		
Fe	%			1.59					0.68				
Ga	ppm		22.3	2.07	19.5		21.7	18.5	2.26	19.5	19.8		
Gd	ppm		7.87		5.05		5.3	4.3		5.01	4.75		
Ge	ppm		6	0.08	<5		<5	<5	0.25	<5	<5		
Hf	ppm		6.4	0.13	5.8		6.6	6.2	0.3	5.8	6.3		
Hg	ppm		0.014	4.75	0.008		0.012	<0.005	0.03	<0.005	<0.005		
Ho	ppm		1.01		0.81		0.78	0.61		0.71	0.68		
In	ppm		0.017	0.146	0.02		0.033	0.009	0.007	0.056	0.012		
K	%			0.19					0.07				
La	ppm		84.3	26.2	43.2		50.8	59.5	6.4	76.9	55.2		
Li	ppm		20	4.7	20		20	20	4.5	30	30		
Lu	ppm		0.35		0.32		0.33	0.27		0.29	0.28		
Mg	%			0.05					0.12				
Mn	ppm			213					254				
Mo	ppm		11	11.9	2		3	1	1.16	2	1		
Na	%			0.01					0.03				
Nb	ppm		101.5	0.16	14.1		16.6	16.4	3.15	17.7	16.6		
Nd	ppm		66.6		36.5		41.7	38.5		47.9	38.8		
Ni	ppm		21	9.8	18		2	4	2.1	7	10		
P	ppm			1000					290				
Pb	ppm		13	113	7		10	21	23.6	11	15		
Pr	ppm		19.25		10.3		12	11.8		14.3	11.75		
Rb	ppm		27.4	4.9	144.5		124.5	159	4.1	135.5	139.5		
Re	ppm		0.008	0.001	<0.001		0.001	<0.001	<0.001	0.001	<0.001		
S	%		0.21	0.21	0.02		0.17	0.01	<0.01	0.01	0.05		
Sb	ppm		3.46	11.6	1.8		1.51	1.07	2.81	3.4	2.13		
Sc	ppm		11	3.6	9		10	4	1.4	8	8		
Se	ppm		0.5	1.4	0.3		1.6	<0.2	0.2	0.2	<0.2		
Sm	ppm		10.6		6.75		7.33	6.79		8.1	6.94		
Sn	ppm		17	2	3		3	2	1	2	2		
Sr	ppm		738	72.6	530		623	440	25.9	478	493		
Ta	ppm		5.7		0.9		1.2	1.2		1.2	1.2		
Tb	ppm		1.09		0.69		0.71	0.62		0.67	0.66		
Te	ppm		3.13	10.15	0.26		0.21	0.09	0.5	0.28	0.07		
Th	ppm		8.73	8	16.15		22.1	27.2	9.5	22.2	22.8		
Ti	%			<0.005					0.068				
Tl	ppm		0.11	0.4	0.58		0.14	0.39	0.1	0.79	0.14		
Tm	ppm		0.37		0.34		0.31	0.26		0.27	0.27		
U	ppm		3.29	1.22	3.76		4.4	4.53	1.26	4.24	3.96		
V	ppm		307	34	167		114	47	23	72	89		
W	ppm		23	0.94	4		3	2	0.84	2	1		
Y	ppm		27.9	7.56	24.4		22.2	19	6.08	20.1	20.6		
Yb	ppm		2.32		2.24		2.01	1.64		1.95	1.91		
Zn	ppm		90	132	31		45	24	24	27	70		
Zr	ppm		321	2.7	228		256	241	7	220	249		

Major oxides are reported in weight percent normalized to 100% anhydrous. Abbreviations are same as map units in geologic map (Plate 1).

Samples "KS###" collected by Gabriel Aliaga. Samples "KTC###" and "Key XXXX" collected by Tom Chapin for U.S. Gold Corp.

[1]Whole-rock geochemistry not submitted for outcrops previously sampled to avoid repeat analyses. Equivalent sample indicated.

Table A1. Multi-element geochemistry of unaltered and altered rocks.

Sample ID		KS093	KS094	KS095	KS095b	KS096	KS097	KS098	KS099	KS100	KS101	KS102	KS103	KS104
UTM	East	538999	539028	539013	539956	539903	539851	539808	539790	539776	539535	539549	539576	539550
NAD27	North	4417534	4417408	4417380	4417587	4417551	4417509	4417729	4417891	4418452	4417622	4417579	4417609	4417447
Unit		Twd	Twp	Twp	Trp	Trp	Trp	Trp	Trp	Ov	Twp	Tmd	Trp	Tmd
Comment/Alteration					clay	clay			clay	lim			clay/chlorite	sodic-calcic
Whole-rock[1]		Y	Y	Y		Y		Y	Y		Y	Y	Y	Y
Ore chemistry										Y				
Thin Section		Y	Y	Y		Y	Y	Y	Y		Y	Y	Y	Y
SiO_2	%	62.98	64.88	67.27		73.63		71.93	80.75		69.69	63.34	73.21	62.04
Al_2O_3	%	15.80	15.73	15.45		13.60		13.99	12.42		14.44	15.53	13.82	18.37
FeO*	%	5.82	4.47	3.28		1.84		2.62	0.80		3.18	5.15	2.35	4.26
CaO	%	4.13	4.17	3.74		1.88		2.01	0.11		2.32	4.57	0.88	4.67
MgO	%	2.62	1.96	1.83		0.95		0.75	0.37		1.22	2.39	0.82	2.47
Na_2O	%	3.63	3.17	3.03		2.53		3.34	0.12		2.97	3.11	3.04	3.04
K_2O	%	3.67	4.36	4.34		4.96		4.78	5.04		5.27	4.41	5.23	3.71
Cr_2O_3	%	0.01	0.01	0.01		0.01		0.01	0.01		0.01	0.01	0.01	0.01
TiO_2	%	0.85	0.75	0.59		0.24		0.29	0.18		0.49	0.84	0.29	0.82
MnO	%	0.02	0.08	0.03		0.09		0.07	0.01		0.06	0.12	0.06	0.08
P_2O_5	%	0.28	0.23	0.24		0.08		0.10	0.02		0.18	0.31	0.13	0.28
SrO	%	0.05	0.06	0.05		0.04		0.03	0.01		0.04	0.06	0.02	0.08
BaO	%	0.14	0.14	0.15		0.15		0.09	0.15		0.14	0.17	0.13	0.17
LOI		1.51	3.18	1.87		3.22		0.79	2.35		1.19	1.29	1.74	2.81
Ag	ppm	<0.5	<0.5	<0.5		<0.5		<0.5	<0.5	0.5	<0.5	<0.5	<0.5	0.6
Al	%									0.31				
As	ppm	4.3	0.9	5.8		5.1		2	46.1	358	21.9	15.3	32.3	10.7
Au	ppm									0.016				
B	ppm									<10				
Ba	ppm	1210	1215	1270		1215		707	1255	340	1225	1330	1075	1350
Be	ppm									0.13				
Bi	ppm	0.13	0.05	0.14		0.03		0.09	0.76	0.93	0.12	0.14	0.31	0.29
C	%	0.05	0.19	0.05		0.3		0.06	0.04		0.02	0.02	0.03	0.03
Ca	%									0.18				
Cd	ppm	<0.5	<0.5	<0.5		0.5		<0.5	<0.5	0.12	0.6	0.8	1.1	<0.5
Ce	ppm	112.5	105.5	92.8		90		59.1	46	15.2	82.3	107.5	66.9	92.7
Co	ppm	9	11	4		3		4	20	0.4	7	12	3	9
Cr	ppm	30	30	20		20		30	20	11	40	60	30	40
Cs	ppm	6.38	2.95	4.12		2.28		3.36	4.19	0.75	2.24	2.76	2.45	1.66
Cu	ppm	22	9	32		4		9	3	22.8	14	12	23	4
Dy	ppm	4.84	3.47	3.69		2.81		3.1	1.52		3.47	4.33	2.92	3.61
Er	ppm	2.51	2.03	2.01		1.65		1.69	1.12		1.85	2.47	1.53	1.66
Eu	ppm	1.83	1.43	1.4		0.9		0.8	0.48		1.18	1.47	0.92	1.8
Fe	%									1.51				
Ga	ppm	21.6	20.4	19.6		17.8		18.7	16.4	2.24	19.6	19.9	18.2	22.5
Gd	ppm	5.61	4.59	4.45		3.89		3.67	1.77		4.63	5.49	3.56	4.73
Ge	ppm	<5	<5	<5		<5		<5	<5	<0.05	<5	<5	<5	<5
Hf	ppm	6.7	6.4	5.8		3.8		3.9	3.4	0.05	5.4	7.2	4.2	5.5
Hg	ppm	0.006	<0.005	<0.005		<0.005		<0.005	0.013	0.24	0.015	0.008	<0.005	<0.005
Ho	ppm	0.91	0.72	0.71		0.54		0.61	0.32		0.67	0.81	0.53	0.63
In	ppm	0.03	0.017	0.045		0.025		0.021	<0.005	0.02	0.014	0.013	0.042	0.008
K	%									0.22				
La	ppm	55.2	57.6	51.4		50.2		30.7	25.2	6.9	43.3	56.3	36.2	49.1
Li	ppm	30	20	20		10		10	20	3	10	10	10	10
Lu	ppm	0.37	0.29	0.31		0.22		0.25	0.16		0.3	0.33	0.24	0.26
Mg	%									0.07				
Mn	ppm									49				
Mo	ppm	1	1	2		1		3	1	5.04	1	1	2	<1
Na	%									0.01				
Nb	ppm	16.6	16.1	15.1		14.6		16.1	13.9	0.11	16.9	17.3	15.5	14.4
Nd	ppm	44.2	38.7	34.8		31.8		23.7	14.4		32.5	42.6	26.1	36.7
Ni	ppm	3	8	5		3		2	2	2.5	9	12	6	6
P	ppm									440				
Pb	ppm	9	19	20		24		23	23	72.7	18	20	80	38
Pr	ppm	13.1	11.75	10.65		10.05		6.63	4.78		9.54	12.3	7.71	10.75
Rb	ppm	129.5	152.5	117.5		178		168.5	193.5	11.4	223	159.5	178.5	112
Re	ppm	<0.001	<0.001	<0.001		<0.001		<0.001	<0.001	0.001	0.003	<0.001	0.001	<0.001
S	%	0.01	0.05	0.01		0.01		0.02	0.04	0.17	0.01	0.01	0.01	0.01
Sb	ppm	1.45	0.35	0.5		0.43		0.23	0.3	5.39	1.25	0.91	0.75	0.95
Sc	ppm	12	7	8		4		5	4	3.5	7	10	5	8
Se	ppm	0.2	<0.2	0.4		0.3		0.3	0.7	1.4	<0.2	0.3	0.4	0.2
Sm	ppm	7.86	6.52	6.33		5.6		4.9	2.57		6.41	7.84	5.1	6.79
Sn	ppm	12	2	5		3		3	2	0.3	2	2	3	3
Sr	ppm	475	513	417		335		260	97.1	31.6	371	549	247	749
Ta	ppm	1.1	1.2	1		1.2		1.3	1.1		1.3	1.1	1.2	0.8
Tb	ppm	0.83	0.66	0.65		0.54		0.59	0.31		0.67	0.78	0.56	0.65
Te	ppm	<0.01	0.01	0.06		0.01		<0.01	0.02	0.41	0.02	0.01	<0.01	0.18
Th	ppm	21.6	23.7	22.4		18.95		16.3	14.7	1.8	18.6	21.7	17.3	14.4
Ti	%									<0.005				
Tl	ppm	0.66	0.07	0.18		0.13		0.21	0.58	0.76	0.15	0.1	0.14	0.07
Tm	ppm	0.38	0.27	0.3		0.23		0.24	0.17		0.3	0.35	0.22	0.28
U	ppm	4.33	4.93	4.57		4.55		5.34	4.31	0.64	4.8	3.34	4.74	2.79
V	ppm	113	90	84		24		33	19	43	71	112	54	101
W	ppm	1	1	3		2		1	2	0.91	2	2	2	1
Y	ppm	26.5	20.4	21		16.1		17.5	10.3	1.63	20.5	23.4	16.1	19.1
Yb	ppm	2.56	2.06	2.05		1.44		1.68	1.23		1.83	2.04	1.47	1.63
Zn	ppm	26	66	55		108		62	7	11	43	140	231	82
Zr	ppm	265	256	219		132		134	102	1.9	203	293	141	231

Major oxides are reported in weight percent normalized to 100% anhydrous. Abbreviations are same as map units in geologic map (Plate 1).
Samples "KS###" collected by Gabriel Aliaga. Samples "KTC###" and "Key XXXX" collected by Tom Chapin for U.S. Gold Corp.
[1]Whole-rock geochemistry not submitted for outcrops previously sampled to avoid repeat analyses. Equivalent sample indicated.

Table A1. Multi-element geochemistry of unaltered and altered rocks.

Sample ID		KS105	KS106	KS107	KS108	KS109	KS110	KS111	KS112	KS113	KS114A	KS114B	KS115	KS116
UTM East		539569	539544	539971	539939	539892	539514	539524	539489	540035	536139	536139	539011	539365
NAD27 North		4417387	4417347	4417387	4417327	4417345	4417280	4417283	4417242	4417547	4416180	4416180	4416621	4416737
Unit		Twp	Tmp	Tmd	Twp	Twp	Tmp	Tmd	Twp	Tmd	Tgd	Tgd	Twp	Tda?
Comment/Alteration					chlorite	chlorite				chlorite				mixed/altered
Whole-rock[1]		Y			Y	KTC419	KTC426	Y	Y	Y	Y	Y	Y	Y
Ore chemistry Thin Section		Y			Y	Y		Y	Y	Y	Y	Y	Y	Y
SiO₂	%	64.73			71.12			62.21	63.74	64.41	62.46	60.20	60.88	77.85
Al₂O₃	%	15.89			14.74			15.97	16.12	15.35	17.09	17.39	16.48	13.36
FeO*	%	4.59			3.06			5.63	4.91	4.98	5.27	5.62	6.09	0.43
CaO	%	4.06			1.54			5.29	4.29	4.60	5.05	5.53	5.14	3.18
MgO	%	2.06			1.42			3.00	2.37	2.50	2.25	2.78	3.36	0.38
Na₂O	%	3.01			2.11			2.53	3.06	2.87	3.55	3.88	2.71	3.83
K₂O	%	4.37			5.19			3.80	4.11	3.84	2.91	3.08	3.74	0.65
Cr₂O₃	%	0.01			0.01			0.01	0.01	0.02	0.01	0.01	0.01	0.01
TiO₂	%	0.78			0.44			0.93	0.86	0.83	0.83	0.87	0.98	0.13
MnO	%	0.08			0.08			0.10	0.08	0.10	0.09	0.09	0.11	0.03
P₂O₅	%	0.21			0.15			0.30	0.24	0.28	0.28	0.31	0.30	0.04
SrO	%	0.06			0.03			0.07	0.07	0.07	0.07	0.09	0.07	0.07
BaO	%	0.14			0.11			0.16	0.14	0.14	0.14	0.15	0.13	0.04
LOI		3.2			3.13			1.58	4	1.63	0.83	0.76	4.14	2.19
Ag	ppm	<0.5			<0.5			<0.5	<0.5	<0.5	<0.5	<0.5	<0.5	<0.5
Al	%													
As	ppm	2			4.3			21.8	1.2	2.1	0.6	0.6	7.7	1.7
Au	ppm													
B	ppm													
Ba	ppm	1145			965			1280	1085	1335	1290	1270	1265	343
Be	ppm													
Bi	ppm	0.02			0.04			0.2	0.03	0.01	0.02	0.01	0.01	<0.01
C	%	0.25			0.07			0.02	0.26	0.08	0.06	0.03	0.28	0.03
Ca	%													
Cd	ppm	<0.5			<0.5			<0.5	<0.5	0.7	<0.5	<0.5	<0.5	<0.5
Ce	ppm	102			74.1			100.5	103.5	99.8	78	64.4	86.4	21.4
Co	ppm	11			6			15	13	12	10	14	14	
Cr	ppm	30			30			60	20	110	20	50	20	10
Cs	ppm	2.29			3.97			1.92	1.96	2.89	3.86	2.86	4.03	6.52
Cu	ppm	12			6			8	12	20	7	12	10	3
Dy	ppm	3.48			3.43			4.26	3.75	4.15	3.67	2.88	4.31	2.22
Er	ppm	1.94			1.9			2.3	1.99	2.32	1.88	1.58	2.35	1.22
Eu	ppm	1.37			0.97			1.6	1.58	1.44	1.6	1.45	1.64	0.28
Fe	%													
Ga	ppm	19.9			19.7			20.5	19.8	20.7	22.1	20.5	21.5	17.1
Gd	ppm	4.78			4.11			5.72	4.79	5.58	5.24	4.22	5.53	3.17
Ge	ppm	<5			<5			<5	<5	<5	<5	<5	<5	<5
Hf	ppm	6.3			4.8			7.2	6.1	7.4	6	5.4	6.2	4.8
Hg	ppm	<0.005			0.012			<0.005	<0.005	<0.005	<0.005	<0.005	0.007	<0.005
Ho	ppm	0.7			0.66			0.82	0.74	0.77	0.72	0.59	0.86	0.42
In	ppm	0.02			0.019			0.014	0.019	0.055	0.022	0.016	0.027	<0.005
K	%													
La	ppm	55.5			37.7			51.7	55.1	55.6	43.6	35.9	47.4	7.8
Li	ppm	20			30			10	20	20	10	30	20	10
Lu	ppm	0.29			0.26			0.32	0.29	0.33	0.22	0.23	0.34	0.17
Mg	%													
Mn	ppm													
Mo	ppm	1			1			1	<1	4	3	1	1	1
Na	%													
Nb	ppm	15.5			16.5			16.4	15.9	19	13	10	14.6	11.9
Nd	ppm	37.3			29			40.4	38.8	41.3	34.4	29	38.3	17.3
Ni	ppm	9			5			8	10	7	5	11	5	
P	ppm													
Pb	ppm	14			25			13	19	36	22	12	5	16
Pr	ppm	11.3			8.6			11.7	11.65	11.4	9.02	7.57	10.1	3.7
Rb	ppm	149			185.5			104	135.5	128	84.8	83.6	118.5	17.5
Re	ppm	<0.001			0.001			<0.001	0.001	<0.001	0.002	0.001	0.001	<0.001
S	%	0.01			0.01			0.09	0.02	0.02	0.42	0.01	0.06	0.01
Sb	ppm	0.22			0.7			1.24	0.32	0.67	0.27	0.11	2.8	0.22
Sc	ppm	8			6			11	8	9	8	9	13	2
Se	ppm	0.2			<0.2			<0.2	<0.2	0.6	0.2	<0.2	<0.2	<0.2
Sm	ppm	6.41			5.74			7.6	6.84	7.56	6.63	5.53	7.13	4.18
Sn	ppm	2			3			1	2	2	1	1	2	<1
Sr	ppm	501			301			581	552	583	611	683	633	656
Ta	ppm	1.2			1.3			0.9	1.1	1	0.7	0.6	0.9	1
Tb	ppm	0.62			0.6			0.79	0.67	0.76	0.69	0.54	0.77	0.39
Te	ppm	<0.01			<0.01			<0.01	0.01	<0.01	0.03	<0.01	<0.01	<0.01
Th	ppm	22.8			17.95			17.15	21.7	19.2	13.35	10.7	17.05	17
Ti	%													
Tl	ppm	0.06			0.13			0.05	0.04	0.05	0.51	0.33	0.08	0.07
Tm	ppm	0.28			0.27			0.37	0.29	0.32	0.27	0.22	0.35	0.15
U	ppm	4.46			4.59			3.64	4.34	3.92	2.87	2.27	3.93	2.35
V	ppm	95			51			118	106	103	86	114	177	
W	ppm	2			2			1	1	1	1	2	2	1
Y	ppm	19.9			18.7			23.8	20.2	22.5	20.1	16	24	12
Yb	ppm	1.95			1.82			2.22	1.99	2.08	1.79	1.43	2.17	1.19
Zn	ppm	68			63			48	75	125	149	83	54	11
Zr	ppm	241			176			288	248	303	242	245	241	172

Major oxides are reported in weight percent normalized to 100% anhydrous. Abbreviations are same as map units in geologic map (Plate 1).
Samples "KS###" collected by Gabriel Aliaga. Samples "KTC###" and "Key XXXX" collected by Tom Chapin for U.S. Gold Corp.
[1]Whole-rock geochemistry not submitted for outcrops previously sampled to avoid repeat analyses. Equivalent sample indicated.

Table A1. Multi-element geochemistry of unaltered and altered rocks.

Sample ID		KS117	KS118	KS119	KS120	KS121	KS122	KS123	KS124	KS125	KS126	KS127	KS128	KS129
UTM East		539428	539426	539433	539658	539501	539504	540620	540204	540148	540073	539943	540608	538449
NAD27 North		4416762	4416791	4416806	4416832	4416726	4416702	4416954	4417170	4417117	4417170	4416870	4416796	4417026
Unit		Tda	Tda	Tda	ODul	Tda?	Tda?	ODul	Tmd	Tmd	Twp	Tmd	Tmp	Ov
Comment/Alteration		clay			marble	mixed/altered	mixed/altered	marble			chlorite	sodic-calcic		lim bx
Whole-rock[1]			Y	Y		Y			Y		Y	Y	Y	
Ore chemistry							Y		Y					Y
Thin Section			Y	Y	Y	Y		Y	Y	Y	Y	Y	Y	
SiO$_2$	%	70.19	65.39	64.80		63.54			65.26		71.16	61.80	74.45	
Al$_2$O$_3$	%	17.27	17.79	18.11		16.90			15.85		14.31	16.12	14.74	
FeO*	%	0.85	1.64	2.87		2.11			4.83		3.10	3.93	1.27	
CaO	%	5.44	5.18	4.96		9.83			2.54		2.02	6.12	0.44	
MgO	%	0.71	1.23	0.91		2.24			2.54		1.39	1.62	0.35	
Na$_2$O	%	4.36	4.03	3.55		3.94			2.84		1.84	3.85	2.65	
K$_2$O	%	0.45	3.69	3.84		0.16			4.67		5.37	4.94	5.58	
Cr$_2$O$_3$	%	0.01	0.01	0.01		0.01			0.01		0.01	0.01	0.01	
TiO$_2$	%	0.45	0.49	0.49		0.78			0.88		0.43	0.84	0.15	
MnO	%	0.07	0.07	0.05		0.11			0.08		0.04	0.09	0.01	
P$_2$O$_5$	%	0.07	0.18	0.16		0.26			0.31		0.15	0.29	0.10	
SrO	%	0.10	0.08	0.08		0.07			0.05		0.04	0.09	0.04	
BaO	%	0.03	0.22	0.17		0.03			0.15		0.13	0.29	0.21	
LOI		2.56	2.09	0.83		5.27			4.03		3.38	2.19	1.86	
Ag	ppm	<0.5	<0.5	<0.5		<0.5	0.08		<0.5		<0.5	<0.5	<0.5	0.11
Al	%						0.04							0.56
As	ppm	6	8.3	3.7		18	11.5		17.8		2.7	1.9	1.2	363
Au	ppm						<0.005		<0.005					<0.005
B	ppm						<10							<10
Ba	ppm	325	2080	1655		283	20		1330		1190	2480	2020	2730
Be	ppm						0.26							0.23
Bi	ppm	0.01	0.02	0.01		0.01	0.91		0.29		0.1	0.02	0.01	2.13
C	%	0.34	0.14	0.03		1.01			0.28		0.23	0.26	0.02	
Ca	%						22.9							0.34
Cd	ppm	<0.5	<0.5	<0.5		<0.5	0.07		<0.5		<0.5	<0.5	<0.5	0.3
Ce	ppm	59.2	76.8	96.6		125.5	2.13		101.5		71.8	53.1	97.2	28.2
Co	ppm	1	4	5		2	0.4		13		7	5	1	2.3
Cr	ppm	10	10	10		20			40		30	10	10	20
Cs	ppm	0.89	0.77	0.97		1.48			2.54		3.79	0.93	1.4	0.46
Cu	ppm	2	6	2		5	8.9		8		6	6	3	15.6
Dy	ppm	3.63	6.15	3.9		8.6			4		3.42	3.24	2.18	
Er	ppm	2.08	3.34	2.13		4.5			2.13		1.92	1.79	0.75	
Eu	ppm	1.01	1.84	1.71		1.08			1.53		1.15	1.5	1.23	
Fe	%						0.24							1.11
Ga	ppm	22.9	23.5	24.1		22.1	0.13		21.5		18.6	18.1	24.1	1.77
Gd	ppm	4.57	7.22	5.01		12.15			5.93		4.06	4.02	4.08	
Ge	ppm	<5	<5	<5		<5	<0.05		<5		<5	<5	<5	0.05
Hf	ppm	7.7	7.8	7.9		5.6			7.9		4.8	7.4	3.4	0.06
Hg	ppm	0.012	<0.005	<0.005		0.015	0.09		0.009		<0.005	<0.005	<0.005	0.37
Ho	ppm	0.71	1.22	0.71		1.62			0.85		0.64	0.61	0.29	
In	ppm	0.007	0.006	0.012		0.045	0.007		0.024		0.029	0.039	0.022	0.084
K	%						0.01							0.05
La	ppm	26.5	42.4	54.8		43.1	1.1		59.6		40.8	29.7	55.7	17.6
Li	ppm	10	<10	<10		10	0.4		30		20	10	<10	4.2
Lu	ppm	0.31	0.41	0.3		0.49			0.28		0.28	0.26	0.07	
Mg	%						12.7							0.05
Mn	ppm						1580							87
Mo	ppm	<1	1	2		<1	0.31		1		<1	1	1	7.62
Na	%						0.01							<0.01
Nb	ppm	14.3	13.1	14.3		19.2	0.07		19.8		17.8	14.6	6.9	0.14
Nd	ppm	29.6	38.2	40.3		83			45.6		30.4	24.6	39.2	
Ni	ppm	1		1		3	130		4		6		2	22.3
P	ppm						980							980
Pb	ppm	5	3	14		5	15.1		39		10	9	18	38.2
Pr	ppm	7.63	9.52	10.9		19.45			13.25		8.4	6.34	10.95	
Rb	ppm	10.6	68.1	105		2.8	0.3		168.5		181.5	100.5	148.5	2.4
Re	ppm	<0.001	<0.001	<0.001		<0.001	<0.001		<0.001		<0.001	<0.001	<0.001	0.001
S	%	0.03	0.02	0.04		0.04	<0.01		0.01		0.01	0.01	<0.01	0.07
Sb	ppm	0.53	0.39	0.53		0.68	0.73		0.59		0.61	0.51	0.05	26.7
Sc	ppm	4	4	4		10	0.2		10		6	7	2	3.2
Se	ppm	<0.2	<0.2	0.7		0.2	0.3		0.8		<0.2	0.2	0.2	0.3
Sm	ppm	5.89	8.23	7.15		16.95			7.94		5.94	4.8	7.09	
Sn	ppm	2	2	1		1	<0.2		2		3	4	2	2.2
Sr	ppm	863	746	750		646	60.7		513		344	707	377	66
Ta	ppm	0.9	0.7	0.8		0.8			1.1		1.3	0.9	0.1	
Tb	ppm	0.6	1.14	0.71		1.61			0.71		0.64	0.58	0.5	
Te	ppm	<0.01	<0.01	<0.01		0.01	0.24		0.03		<0.01	<0.01	<0.01	0.76
Th	ppm	18.4	15.05	17.15		12			21.1		18.15	15.5	14.85	3.2
Ti	%						<0.005							<0.005
Tl	ppm	0.04	0.03	0.08		0.02	0.04		0.07		0.21	0.04	0.1	0.23
Tm	ppm	0.28	0.46	0.3		0.52			0.29		0.27	0.25	0.08	
U	ppm	2.37	2.55	3.37		2.69	0.1		3.94		4.32	3.6	1.85	0.87
V	ppm	37	48	43		108	3		99		49	82	5	42
W	ppm	1	1	1		1	0.43		1		1	1	1	1.27
Y	ppm	19.6	34.7	21		41.7	2.17		21.5		19.1	18.1	8.6	13.9
Yb	ppm	2.02	2.82	1.96		3.45			1.94		1.79	1.72	0.49	
Zn	ppm	20	33	41		62	24		99		46	56	40	60
Zr	ppm	325	327	334		228			320		180	297	111	1.8

Major oxides are reported in weight percent normalized to 100% anhydrous. Abbreviations are same as map units in geologic map (Plate 1).

Samples "KS###" collected by Gabriel Aliaga. Samples "KTC###" and "Key XXXX" collected by Tom Chapin for U.S. Gold Corp.

[1]Whole-rock geochemistry not submitted for outcrops previously sampled to avoid repeat analyses. Equivalent sample indicated.

Table A1. Multi-element geochemistry of unaltered and altered rocks.

Sample ID		KS130	KS131	KS132	KS133	KS134	KS135	KS136	KS137	KS138	KS139	KS140	KS141	KS142
UTM	East	538351	538384	538910	541366	541747	541388	540847	537931	539354	539354	539354	540054	539354
NAD27	North	4417071	4417196	4418000	4416857	4416881	4417035	4417719	4419755	4419536	4419536	4419536	4417754	4419536
Unit		gossan	Twd	Twq	Ta	Tvc	Ta	Tvc	Twq	COcb	Ta	Ta	Tda	Ta
Comment/Alteration		gossan	sodic-calcic	endo-skarn	float	float	oxidized	clay	@530m	@222m clay	@330m clay	@376m clay	@16m, clay	@412m clay
Whole-rock[1]			Y	Y	Y	Y	Y	Y	Y	Y			Y	Y
Ore chemistry		Y												
Thin Section			Y	Y	Y	Y	Y	Y	Y	Y	Y	Y	Y	Y
SiO2	%		62.60	67.48	64.38	84.16	64.52	81.82	68.12	48.67			70.33	63.44
Al2O3	%		15.88	15.92	16.64	9.98	16.92	11.31	15.25	15.55			18.03	16.77
FeO*	%		4.38	1.04	5.00	0.80	4.83	1.07	3.49	13.04			2.35	4.22
CaO	%		4.34	5.60	4.52	0.17	4.77	0.08	2.75	1.04			0.45	1.91
MgO	%		1.58	1.52	2.14	0.50	1.53	0.44	1.63	13.37			1.23	2.62
Na2O	%		3.93	3.57	2.74	0.34	3.18	0.09	3.34	0.06			0.54	0.19
K2O	%		5.71	3.69	3.14	3.64	2.77	4.78	4.46	2.89			5.97	9.31
Cr2O3	%		0.01	0.01	0.01	0.01	0.01	0.01	0.01	0.07			0.01	0.01
TiO2	%		0.84	0.64	0.75	0.22	0.75	0.11	0.55	3.95			0.42	0.82
MnO	%		0.08	0.03	0.20	0.02	0.08	0.02	0.07	0.10			0.02	0.02
P2O5	%		0.32	0.24	0.27	0.02	0.25	0.04	0.15	0.67			0.12	0.29
SrO	%		0.10	0.09	0.07	0.01	0.12	0.01	0.05	0.01			0.04	0.04
BaO	%		0.22	0.18	0.14	0.13	0.28	0.22	0.13	0.58			0.49	0.35
LOI			0.87	1.02	2.51	2.26	2.89	2.55	0.84	8.25			5.47	5.83
Ag	ppm	0.8	<0.5	<0.5	<0.5	1.4	<0.5	<0.5	<0.5	<0.5			<0.5	<0.5
Al	%	0.37												
As	ppm	637	1.5	10.8	1.1	21.4	4.9	11.1	0.9	121			10.6	51.1
Au	ppm	0.017												
B	ppm	<10												
Ba	ppm	1090	2080	1750	1350	1215	2530	2070	1275	4670			4660	3260
Be	ppm	0.07												
Bi	ppm	1.3	0.17	0.04	0.03	0.26	0.02	0.16	0.02	0.01			0.09	0.03
C	%		0.05	0.04	0.17	0.03	0.06	0.02	0.05	0.04			0.01	0.25
Ca	%	0.44												
Cd	ppm	1.18	0.5	<0.5	<0.5	<0.5	<0.5	<0.5	<0.5	<0.5			<0.5	<0.5
Ce	ppm	35.3	139	76.1	83.2	21.1	81.2	84.3	106.5	88.7			108	71.2
Co	ppm	1.5	8	3	10	1	11	1	9	54			9	12
Cr	ppm	14	20	20	20	40	20	10	30	450			10	20
Cs	ppm	0.18	5.63	1.69	1.47	5.12	38.6	3.06	8.52	6.43			6.7	14.25
Cu	ppm	73.4	6	5	13	4	9	3	6	67			120	4
Dy	ppm		5.22	3.69	3.66	1.64	3.34	2.58	3.28	5.75			4.15	3.02
Er	ppm		2.63	2.2	2	1.39	1.91	1.64	1.62	2.69			2.22	1.95
Eu	ppm		1.79	1.43	1.48	0.28	1.43	0.81	1.35	2.8			1.75	1.34
Fe	%	1.18												
Ga	ppm	1.85	22.3	21.3	22	14.5	20.5	16.3	21.7	21.7			22.6	17.5
Gd	ppm		6.26	4.93	4.82	1.45	4.3	3.25	4.37	7.22			5.41	4.16
Ge	ppm	0.05	<5	<5	<5	<5	<5	<5	<5	<5			<5	<5
Hf	ppm	0.22	7.5	6.1	5.8	4.3	6	3.9	5.6	6.7			8.7	5.6
Hg	ppm	0.47	<0.005	0.011	0.01	0.01	0.012	0.03	0.005	0.015			0.012	0.007
Ho	ppm		0.94	0.75	0.76	0.4	0.71	0.58	0.6	1.06			0.83	0.66
In	ppm	0.151	0.021	0.01	0.037	0.012	0.028	0.006	0.022	0.074			0.017	0.008
K	%	0.02												
La	ppm	28.4	86.4	37.2	46.5	18.6	46	48.7	62.2	45.8			63.9	39.4
Li	ppm	1.9	10	10	20	20	20	10	30	60			30	20
Lu	ppm		0.38	0.29	0.3	0.28	0.32	0.26	0.26	0.32			0.34	0.32
Mg	%	0.12												
Mn	ppm	129												
Mo	ppm	10.3	9	1	2	3	2	2	4	<1			4	2
Na	%	0.01												
Nb	ppm	0.11	20	15.7	12.8	13.2	12.7	16.2	17.3	53.6			16	12.6
Nd	ppm		52.5	36.6	36	11.6	33.9	31	38.8	44.1			45	31
Ni	ppm	9.2	6	4	4	3	4	1	7	198			15	5
P	ppm	680												
Pb	ppm	56.9	29	11	16	5	22	8	23	4			11	14
Pr	ppm		15.25	9.35	9.58	3.34	8.99	9.23	11.4	10.9			12.6	8.22
Rb	ppm	1	207	98.4	76.8	133.5	102	166.5	172.5	60.8			124	314
Re	ppm	0.001	0.001	<0.001	<0.001	<0.001	<0.001	<0.001	<0.001	0.025			0.06	<0.001
S	%	0.09	0.02	0.03	0.03	0.08	0.04	0.18	0.03	1.89			0.29	2.12
Sb	ppm	137.5	0.15	4.49	0.6	1.22	0.72	0.32	0.12	0.92			1	1.97
Sc	ppm	1.1	7	8	10	5	10	3	6	25			5	10
Se	ppm	1.3	0.2	0.2	<0.2	0.2	<0.2	0.6	<0.2	2.2			1.7	1.4
Sm	ppm		9.01	7	6.57	1.86	6.04	5.33	6.66	8.75			7.88	5.42
Sn	ppm	1.2	2	4	2	3	2	2	2	2			2	2
Sr	ppm	74	826	785	628	82.7	916	87.6	514	70.7			380	407
Ta	ppm		1.2	1.1	0.7	0.8	0.7	1	1.3	3.3			1	0.7
Tb	ppm		0.91	0.67	0.67	0.21	0.61	0.45	0.59	1.05			0.73	0.53
Te	ppm	0.46	<0.01	0.31	<0.01	0.33	0.01	0.02	<0.01	<0.01			<0.01	0.02
Th	ppm	4.6	25.9	23.1	12.15	7.86	12.5	13.2	27.7	5.47			21.2	12.05
Ti	%	<0.005												
Tl	ppm	1.77	0.08	0.14	0.06	0.26	0.06	0.33	0.28	0.31			0.35	0.31
Tm	ppm		0.39	0.28	0.28	0.24	0.27	0.25	0.25	0.34			0.3	0.29
U	ppm	2.65	6.25	4.14	2.72	3.67	2.77	3.56	5.71	9.59			4.96	2.83
V	ppm	48	80	89	110	73	107	13	67	290			34	118
W	ppm	2.31	4	4	1	2	1	1	1	17			10	4
Y	ppm	14.2	27	21.1	19.9	12.8	19.5	15.6	18.2	28.1			23.9	17.6
Yb	ppm		2.47	2.2	1.84	1.76	2	1.64	1.77	2.28			2.2	1.87
Zn	ppm	55	83	22	104	9	90	6	69	177			51	22
Zr	ppm	3	312	238	241	161	244	138	213	275			359	236

Major oxides are reported in weight percent normalized to 100% anhydrous. Abbreviations are same as map units in geologic map (Plate 1).
Samples "KS###" collected by Gabriel Aliaga. Samples "KTC###" and "Key XXXX" collected by Tom Chapin for U.S. Gold Corp.
[1]Whole-rock geochemistry not submitted for outcrops previously sampled to avoid repeat analyses. Equivalent sample indicated.

Table A1. Multi-element geochemistry of unaltered and altered rocks.

Sample ID		KS143	KS144	KTC 002	KTC 005	KTC 007	KTC 011	KTC 012	KTC 013	KTC 015	KTC 016	KTC 017	KTC 019	KTC 021
UTM	East	536833	540610	539799	540182	540023	539715	539756	539788	539907	540198	540147	539910	540469
NAD27	North	4418073	4414578	4416596	4416769	4416663	4416227	4416273	4416292	4416194	4416435	4416431	4415825	4416316
Unit		Ovb	Ta	Tda	Tmd	Ta	Tvc	Tda	Tda	Tda	Ta	Tda	Ta	Tda
Comment/Alteration														
Whole-rock[1]		KTC345		Y	Y	Y	Y	Y	Y	Y	Y	Y	Y	Y
Ore chemistry														
Thin Section		Y	Y											
SiO2	%			66.80	58.96	60.87	75.64	71.42	71.29	67.80	63.28	64.53	62.29	67.54
Al2O3	%			17.09	15.78	16.46	14.10	14.84	15.80	17.13	17.34	18.15	16.88	17.38
FeO*	%			1.43	6.87	5.98	2.08	3.07	3.08	3.21	5.32	3.65	5.00	2.59
CaO	%			4.21	6.48	5.36	0.41	3.00	1.55	2.56	3.46	4.50	5.39	2.90
MgO	%			1.56	3.53	3.40	0.46	1.19	0.95	0.79	2.47	1.08	2.70	0.86
Na2O	%			3.66	2.97	3.11	2.12	2.52	2.78	3.10	3.63	3.69	3.14	3.27
K2O	%			4.38	3.91	3.17	4.29	3.03	3.66	4.48	2.97	3.35	3.15	4.27
Cr2O3	%			0.01	0.01	0.01	0.01	0.01	0.01	0.01	0.01	0.01	0.01	0.01
TiO2	%			0.40	0.86	0.85	0.23	0.43	0.42	0.43	0.81	0.53	0.83	0.43
MnO	%			0.02	0.08	0.23	0.02	0.08	0.06	0.07	0.13	0.06	0.13	0.06
P2O5	%			0.13	0.31	0.27	0.10	0.18	0.18	0.14	0.28	0.21	0.29	0.17
SrO	%			0.07	0.07	0.09	0.05	0.06	0.05	0.06	0.08	0.08	0.05	0.07
BaO	%			0.24	0.17	0.21	0.49	0.18	0.17	0.22	0.22	0.17	0.15	0.46
LOI				0.23	0.16	0.19	0.47	0.17	0.16	0.21	0.21	0.17	0.14	0.44
Ag	ppm			0.25	0.25	0.25	0.25	0.25	0.25	0.25	0.25	0.25	0.25	0.25
Al	%													
As	ppm			7	13	7	11	6	13	2.5	23	2.5	2.5	11
Au	ppm													
B	ppm													
Ba	ppm			2250	1550	1840	4740	1665	1540	2080	2020	1650	1305	4030
Be	ppm													
Bi	ppm													
C	%													
Ca	%													
Cd	ppm			0.25	0.25	0.25	0.25	0.25	0.25	0.25	0.25	0.25	0.25	0.25
Ce	ppm			112	82.8	74.4	85.2	75.5	72.2	103	82.2	96.2	75.8	101
Co	ppm			1	11	10	2	5	4	5	10	7	11	4
Cr	ppm			10	20	20	10	10	10	10	20	10	20	10
Cs	ppm			4.25	1.8	3.03	4.79	3.72	3.29	6.27	1.41	1.94	6.83	1.38
Cu	ppm			7	3	4	4	4	4	5	4	6	9	5
Dy	ppm			3.29	4.29	3.5	2.86	3.03	2.72	3.89	3.71	3.92	3.28	3.74
Er	ppm			1.82	2.4	2.05	1.6	1.64	1.63	2.19	2.02	1.98	1.98	2.13
Eu	ppm			1.58	1.82	1.69	1.03	1.27	1.27	1.61	1.59	1.86	1.38	1.52
Fe	%													
Ga	ppm			21.4	20.4	19.2	15	18.7	19.1	22.9	20.6	23.6	21	21.9
Gd	ppm			5.19	5.48	4.62	4.02	3.84	3.98	5.26	4.9	5.35	4.48	5.28
Ge	ppm													
Hf	ppm			7.7	5.6	4.6	4.7	4.8	4.8	7.9	5.5	7.5	5.2	7.8
Hg	ppm													
Ho	ppm			0.58	0.82	0.71	0.57	0.59	0.52	0.79	0.7	0.78	0.65	0.69
In	ppm													
K	%													
La	ppm			60.5	42.8	39	45	39.2	38.8	54.2	45	50.9	38.5	56.3
Li	ppm			10	20	40	20	10	10	20	30	10	20	10
Lu	ppm			0.25	0.34	0.29	0.26	0.26	0.24	0.34	0.3	0.3	0.3	0.29
Mg	%													
Mn	ppm													
Mo	ppm			1	2	3	0.5	1	1	2	1	1	1	3
Na	%													
Nb	ppm			13.9	13.6	10.8	14.7	12	11.7	14.6	11.6	14.1	11.5	14.9
Nd	ppm			45.2	37	32.1	33.1	30.8	30.1	41.6	36.2	39.7	32.2	43.4
Ni	ppm			4	2	5	2	1	4	2	7	2	7	2
P	ppm													
Pb	ppm			12	7	24	24	18	16	18	14	19	11	15
Pr	ppm			12.4	9.7	8.38	9.16	8.22	7.95	11.2	9.32	10.6	8.48	11.6
Rb	ppm			91	95	68.7	119	85.9	99.3	135.5	72.4	103.5	87	119.5
Re	ppm													
S	%													
Sb	ppm													
Sc	ppm			4	10	12	4	5	5	4	10	5	10	4
Se	ppm													
Sm	ppm			7.91	7.61	6.03	6.04	5.73	5.03	7.81	6.6	7.44	6.02	7.54
Sn	ppm			2	5	2	2	1	2	2	2	2	1	2
Sr	ppm			605	619	650	433	524	461	571	720	721	487	603
Ta	ppm			0.9	0.9	0.6	1	0.8	0.7	1	1.1	0.9	0.7	1
Tb	ppm			0.66	0.86	0.67	0.56	0.54	0.55	0.81	0.69	0.76	0.6	0.72
Te	ppm													
Th	ppm			18.45	13.55	9.58	14.05	11.45	10.6	19.1	11.75	16.05	10.25	18.3
Ti	%													
Tl	ppm			5	5	5	5	5	5	5	5	5	5	5
Tm	ppm			0.26	0.35	0.31	0.26	0.24	0.22	0.35	0.29	0.32	0.27	0.28
U	ppm			3.65	3.25	2.17	3.39	2.79	2.58	3.93	2.51	3.29	2.39	3.65
V	ppm			19	96	124	8	33	30	26	107	44	113	26
W	ppm			1	1	1	2	1	1	2	2	2	1	2
Y	ppm			16.7	22.6	18.6	15.6	15.7	14.6	21.3	20.4	20.8	19	21.7
Yb	ppm			1.75	2.36	1.82	1.67	1.67	1.59	2.07	2.07	2.17	1.87	2.07
Zn	ppm			24	38	154	49	73	59	64	77	74	77	65
Zr	ppm			328	238	194	176	199	203	342	226	325	212	335

Major oxides are reported in weight percent normalized to 100% anhydrous. Abbreviations are same as map units in geologic map (Plate 1).
Samples "KS###" collected by Gabriel Aliaga. Samples "KTC###" and "Key XXXX" collected by Tom Chapin for U.S. Gold Corp.

[1] Whole-rock geochemistry not submitted for outcrops previously sampled to avoid repeat analyses. Equivalent sample indicated.

Table A1. Multi-element geochemistry of unaltered and altered rocks.

Sample ID		KTC 023	KTC 024	KTC 028	KTC 039	KTC 040	KTC 042	KTC 043	KTC 046	KTC 049	KTC 051	KTC 052	KTC 054	KTC 055
UTM NAD27	East	540554	540595	540931	540285	540449	540500	540351	540205	540192	540807	540655	540653	540705
	North	4416377	4416574	4415808	4415946	4415814	4415302	4415141	4415325	4415681	4417420	4417504	4414911	4414790
Unit		Ta	Tda	Tvc	Ta	Tda	Ta	Ta	Ta	Ta	Tda	Tvc	Ta	Ta
Comment/Alteration														
Whole-rock[1]		Y	Y	Y	Y	Y	Y	Y	Y	Y	Y	Y	Y	Y
Ore chemistry														
Thin Section														
SiO$_2$	%	63.48	74.14	78.59	65.09	66.05	64.42	63.37	62.60	62.78	69.95	77.71	62.76	61.42
Al$_2$O$_3$	%	16.51	17.72	13.39	15.39	18.01	17.60	17.14	17.12	16.72	16.33	13.48	17.36	17.86
FeO*	%	5.30	0.71	0.71	6.68	3.36	5.10	4.84	5.17	5.37	3.73	1.11	5.26	5.40
CaO	%	5.14	0.14	0.31	3.45	3.41	4.25	4.93	5.46	4.54	1.35	0.12	5.07	5.40
MgO	%	2.28	1.40	0.39	3.38	0.89	0.80	1.96	2.63	2.44	1.61	0.39	2.28	2.13
Na$_2$O	%	2.83	0.14	1.64	1.80	3.31	3.42	3.39	3.44	3.75	1.89	0.19	3.32	3.41
K$_2$O	%	2.86	4.84	4.55	2.83	3.96	3.05	2.98	2.16	3.02	4.09	6.52	2.54	2.78
Cr$_2$O$_3$	%	0.01	0.01	0.01	0.01	0.01	0.01	0.01	0.01	0.01	0.01	0.01	0.01	0.01
TiO$_2$	%	0.92	0.53	0.12	0.75	0.51	0.80	0.83	0.81	0.80	0.46	0.15	0.80	0.89
MnO	%	0.10	0.01	0.02	0.19	0.04	0.05	0.06	0.10	0.10	0.16	0.03	0.09	0.09
P$_2$O$_5$	%	0.33	0.14	0.06	0.25	0.20	0.29	0.26	0.26	0.27	0.19	0.03	0.29	0.35
SrO	%	0.08	0.03	0.03	0.05	0.07	0.07	0.07	0.08	0.07	0.05	0.03	0.08	0.08
BaO	%	0.16	0.19	0.17	0.14	0.19	0.14	0.14	0.15	0.13	0.18	0.22	0.14	0.17
LOI		0.16	0.19	0.16	6.75	3.05	2.57	2.05	2.25	2.28	4.35	2.13	2.57	2.06
Ag	ppm	0.25	0.25	0.25	<0.5	<0.5	<0.5	<0.5	<0.5	<0.5	<0.5	<0.5	<0.5	<0.5
Al	%													
As	ppm	2.5	18	15	20	7	<5	6	<5	6	23	48	<5	<5
Au	ppm													
B	ppm													
Ba	ppm	1425	1765	1480	1160	1640	1230	1185	1320	1180	1540	1985	1190	1455
Be	ppm													
Bi	ppm													
C	%													
Ca	%													
Cd	ppm	0.25	0.25	0.25	<0.5	<0.5	<0.5	<0.5	<0.5	<0.5	<0.5	<0.5	<0.5	<0.5
Ce	ppm	95.2	115	77.1	63.5	95.7	74.8	76	76	75	77.6	91.3	77.1	82.7
Co	ppm	11	0.5	0.5	11	5	8	9	11	12	3	1	9	9
Cr	ppm	10	10	5	10	10	20	20	20	20			10	10
Cs	ppm	0.66	1.02	2.6	0.35	1.31	1.22	1.35	8.65	0.69	4.63	4.31	1.65	1.75
Cu	ppm	9	1	3	9	9	6	8	9	9	4	6	10	11
Dy	ppm	3.81	3.2	2.46	2.93	3.97	3.93	3.24	3.98	3.85	3.6	2.78	3.64	5.61
Er	ppm	2.07	1.76	1.47	1.72	2.15	2.25	1.92	1.94	2.02	1.78	1.51	1.94	2.99
Eu	ppm	1.59	1.73	0.7	1.15	1.72	1.35	1.37	1.42	1.39	1.58	1.06	1.38	1.81
Fe	%													
Ga	ppm	21.8	24.1	16.4	17.1	23.3	20.9	20.5	21.5	20.5	20.2	16.3	20.7	21.6
Gd	ppm	5.18	5.19	3.08	3.66	5.22	4.48	4.74	4.44	4.29	4.99	3.61	4.58	6.92
Ge	ppm													
Hf	ppm	6.8	8.5	4.2	5	8.6	5.7	5.8	5.5	5.4	5.5	4.7	5.6	6.1
Hg	ppm													
Ho	ppm	0.72	0.61	0.48	0.6	0.68	0.74	0.71	0.66	0.66	0.63	0.53	0.66	1.08
In	ppm													
K	%													
La	ppm	49.1	61.1	44.1	33.9	53.1	40.4	40.9	40.4	39.6	53.9	47.2	41.1	54.5
Li	ppm	5	5	20	10	10	10	10	10	10	20	10	10	10
Lu	ppm	0.27	0.31	0.26	0.23	0.33	0.31	0.24	0.3	0.3	0.24	0.23	0.26	0.4
Mg	%													
Mn	ppm													
Mo	ppm	2	1	1	1	2	1	1	2	1	1	1	1	2
Na	%													
Nb	ppm	15.5	16.3	15.9	10	13.6	11.9	11.6	11.4	11.5	12.9	14.5	11.8	12.3
Nd	ppm	41	46.2	29.1	29.2	42.8	34.3	34.6	34.4	33.9	43.5	38.3	35.1	50.5
Ni	ppm	4	3	3	2	2	4	3	4	4		1	5	2
P	ppm													
Pb	ppm	19	7	4	9	19	13	12	15	15	13	20	19	14
Pr	ppm	10.65	12.1	8.38	7.5	11.35	9.12	9.09	9.11	8.76	11.8	10.35	9.02	12.7
Rb	ppm	68.7	157	132.5	61.3	114.5	86.3	83.6	146	85.1	119.5	236	85.7	75.7
Re	ppm													
S	%													
Sb	ppm													
Sc	ppm	8	4	3	10	5	9	11	11	12	5	3	11	11
Se	ppm													
Sm	ppm	7	7.86	4.18	5.34	7.74	6.3	6.45	6.36	6.38	7.34	6.12	6.65	8.83
Sn	ppm	2	5	2	2	2	1	2	2	2	3	2	2	2
Sr	ppm	673	211	224	388	588	599	618	689	606	408	203	631	659
Ta	ppm	1	1.1	1.1	0.6	0.9	0.8	0.8	0.7	0.7	0.9	1	0.7	0.8
Tb	ppm	0.75	0.65	0.43	0.56	0.73	0.6	0.62	0.7	0.64	0.67	0.55	0.62	0.99
Te	ppm													
Th	ppm	15.3	18.4	14.55	10.1	16.85	12.2	11.5	11.7	11.55	12.75	15.55	12.2	11.45
Ti	%													
Tl	ppm	5	5	5	<10	<10	<10	10	<10	<10	10	10	<10	<10
Tm	ppm	0.3	0.29	0.24	0.29	0.26	0.31	0.28	0.27	0.31	0.26	0.24	0.31	0.43
U	ppm	3.11	3.63	3.52	2.11	3.25	2.66	2.66	2.62	2.49	3.06	3.35	2.43	2.54
V	ppm	95	37	9	103	38	85	121	118	121	38		93	114
W	ppm	2	2	2	<1	1	1	1	1	1	4	1	1	1
Y	ppm	22	18.5	15	16	20.4	20.4	19.7	19.3	18.9	19.6	14.5	18.7	29.3
Yb	ppm	2.02	2.13	1.7	1.62	2.11	1.95	2	1.72	1.94	1.85	1.5	1.83	2.67
Zn	ppm	90	5	12	173	76	75	82	89	85	73	51	89	100
Zr	ppm	285	369	148	194	334	234	228	219	217	232	158	221	242

Major oxides are reported in weight percent normalized to 100% anhydrous. Abbreviations are same as map units in geologic map (Plate 1).
Samples "KS###" collected by Gabriel Aliaga. Samples "KTC###" and "Key XXXX" collected by Tom Chapin for U.S. Gold Corp.

[1]Whole-rock geochemistry not submitted for outcrops previously sampled to avoid repeat analyses. Equivalent sample indicated.

Table A1. Multi-element geochemistry of unaltered and altered rocks.

Sample ID		KTC 224	KTC 227	KTC 234	KTC 238	KTC 240	KTC 247	KTC 265	KTC 268	KTC 269	KTC 281	KTC 282	KTC 293	KTC 297
UTM	East	537245	537373	537458	536048	536048	538067	538609	537665	538363	539086	539024	539822	539001
NAD27	North	4416123	4415648	4415971	4416209	4416209	4420595	4419431	4419132	4419095	4418591	4418501	4418326	4418076
Unit		Tgd	Ovb	Ovb	Tgd	Tgd	Ta	Twp	Twq	Twd	Twd	Twd	Ta	Twd
Comment/Alteration														
Whole-rock[1]		Y	Y	Y	Y	Y	Y	Y	Y	Y	Y	Y	Y	Y
Ore chemistry													Y	
Thin Section		Y	Y	Y	Y	Y	Y	Y	Y	Y	Y	Y	Y	Y
SiO2	%	63.03	51.01	44.26	62.38	60.50	70.56	64.71	68.05	60.05	61.12	63.93	70.89	64.63
Al2O3	%	17.01	16.64	16.31	17.50	16.90	16.08	19.38	15.50	16.19	16.88	16.09	16.72	16.44
FeO*	%	5.30	10.82	12.85	5.46	6.04	7.79	5.19	3.36	3.29	6.18	4.30	2.72	1.49
CaO	%	4.18	5.21	8.89	4.70	5.89	0.39	8.71	3.25	8.35	5.60	5.21	0.16	6.93
MgO	%	2.45	5.13	5.39	2.17	3.01	0.60	0.22	1.64	2.71	2.43	1.98	0.70	1.44
Na2O	%	3.40	6.22	2.25	3.51	3.46	0.11	0.01	3.14	4.31	3.18	2.63	0.11	2.83
K2O	%	3.10	0.35	3.96	2.85	2.66	2.98	0.07	4.06	3.50	2.92	4.45	7.07	4.83
Cr2O3	%	0.01	0.01	0.01	0.01	0.01	0.01	0.01	0.01	0.01	0.01	0.01	0.01	0.01
TiO2	%	0.88	3.31	4.48	0.84	0.89	0.65	1.11	0.59	0.98	0.99	0.71	0.85	0.73
MnO	%	0.07	0.17	0.22	0.03	0.10	0.01	0.05	0.03	0.10	0.12	0.06	0.01	0.04
P2O5	%	0.36	0.89	0.96	0.33	0.32	0.47	0.41	0.18	0.29	0.35	0.32	0.14	0.31
SrO	%	0.07	0.09	0.13	0.08	0.08	0.03	0.01	0.06	0.10	0.08	0.08	0.02	0.07
BaO	%	0.15	0.15	0.30	0.13	0.13	0.33	0.14	0.14	0.13	0.14	0.24	0.62	0.24
LOI		2.25	4.98	6.51	1.95	4.46	10.9	12.3	1.34	1.13	0.41	2.36	4.23	2.46
Ag	ppm	<0.5	<0.5	<0.5	<0.5	<0.5	<0.5	<0.5	<0.5	<0.5	<0.5	<0.5	<0.5	<0.5
Al	%													
As	ppm	34	<5	5	<5	<5	90	189	22	8	<5	9	2150	8
Au	ppm												0.006	
B	ppm													
Ba	ppm	1340	1350	2480	1195	1165	2580	1025	1245	1140	1280	2140	5240	2060
Be	ppm													
Bi	ppm													
C	%													
Ca	%													
Cd	ppm	0.6	<0.5	<0.5	<0.5	<0.5	<0.5	<0.5	<0.5	<0.5	<0.5	<0.5	<0.5	<0.5
Ce	ppm	81.9	122.5	137.5	80.1	74.2	73.6	76.9	100.5	89.4	84.4	84.3	76.2	74
Co	ppm	9	28	39	9	12	1	14	9	10	9	8	1	3
Cr	ppm	20	70	10	10	30	20	10	30	20	20	10	10	10
Cs	ppm	4.76	1.9	5	6.34	6.01	2.05	1.12	4.21	1.8	2.82	5.03	7.63	3.22
Cu	ppm	13	23	122	6	9	7	20	6	16	7	17	47	3
Dy	ppm	4.05	6.7	5.95	3.53	4.01	1.23	3.78	3.1	3.79	4.38	3.36	2.83	3.51
Er	ppm	2.05	3.06	2.73	1.88	1.97	0.79	1.92	1.5	2.09	2.43	1.96	1.64	1.9
Eu	ppm	1.56	3.23	3.35	1.64	1.59	1.28	1.34	1.3	1.55	1.64	1.56	1.06	1.17
Fe	%													
Ga	ppm	21	23.6	22	21.5	21.1	19.3	18.7	21.6	20	30.6	29.1	21.5	19.3
Gd	ppm	5.58	9.33	9.59	5.04	5.33	2.9	4.82	4.14	5.46	5.62	4.29	3.46	4.57
Ge	ppm													
Hf	ppm	6.1	8.5	8.3	5.8	5.4	4.2	5.3	6	6.8	6	5.9	5.5	5.1
Hg	ppm													
Ho	ppm	0.79	1.26	1.12	0.73	0.82	0.28	0.74	0.61	0.73	0.94	0.67	0.57	0.7
In	ppm													
K	%													
La	ppm	42	60.1	67.4	41.8	37.8	37.3	38.1	54	46.1	42.7	46.3	42.1	36.6
Li	ppm	30	40	40	30	10	<10	30	10	10	10	20	10	10
Lu	ppm	0.25	0.3	0.3	0.25	0.26	0.2	0.32	0.27	0.28	0.37	0.29	0.32	0.27
Mg	%													
Mn	ppm													
Mo	ppm	3	1	2	1	2	2	6	1	1	3	3	4	5
Na	%													
Nb	ppm	13.2	58.2	82.1	13.5	11	8.8	14	16.2	15.8	13.9	14.4	12.6	14.9
Nd	ppm	36.3	58.7	64.4	35.1	34.9	32.8	34.2	36.6	36.9	39.4	36.6	29.8	32.2
Ni	ppm	7	39	54	4	9	2	4	8	8	2	1	6	25
P	ppm													
Pb	ppm	6	6	5	10	12	9	11	12	12	16	9	42	12
Pr	ppm	9.67	14.9	16.55	9.34	8.86	8.44	9.4	10.75	10.25	9.92	9.63	8.36	8.95
Rb	ppm	96.7	7.8	80.4	101	80.8	49.2	2.7	137.5	105.5	91	143.5	256	128.5
Re	ppm													
S	%													
Sb	ppm													
Sc	ppm	10	16	18	8	13	11	9	7	9	13	7	12	7
Se	ppm													
Sm	ppm	6.53	10.7	10.75	6.37	6.35	6.5	6.06	5.82	6.15	7.01	6.15	5.52	5.83
Sn	ppm	2	3	2	2	1	1	2	3	1	2	1	1	1
Sr	ppm	623	724	1050	661	713	265	39.4	496	833	676	753	176.5	624
Ta	ppm	0.8	3.7	5.7	0.9	0.7	0.5	0.8	1.1	1.1	1.1	1	0.6	0.9
Tb	ppm	0.74	1.22	1.24	0.66	0.77	0.3	0.63	0.59	0.7	0.88	0.67	0.48	0.6
Te	ppm													
Th	ppm	13.35	7.58	7.42	11.5	11	7.33	11.1	21	14.65	14.15	13.9	11.2	15.45
Ti	%													
Tl	ppm	<10	10	<10	<10	<10	<10	<10	<10	<10	<10	<10	10	<10
Tm	ppm	0.25	0.36	0.35	0.25	0.32	0.13	0.28	0.26	0.32	0.37	0.26	0.26	0.27
U	ppm	3.26	1.87	1.95	2.89	2.4	2.01	3.63	3.4	3.06	2.62	2.93	2.74	4.07
V	ppm	116	237	337	80	142	136	196	76	144	178	79	107	114
W	ppm	2	1	1	2	1	7	29	1	4	1	4	5	2
Y	ppm	22	31.3	29.4	19.8	22.3	7.2	19.1	16.3	21.2	24.6	19.7	14.2	19
Yb	ppm	2.02	2.41	2.1	1.8	2.05	1.16	1.92	1.5	1.95	2.4	1.77	2.05	1.77
Zn	ppm	83	117	114	36	92	12	32	22	37	101	30	14	37
Zr	ppm	229	349	343	243	209	170	214	237	274	214	232	222	195

Major oxides are reported in weight percent normalized to 100% anhydrous. Abbreviations are same as map units in geologic map (Plate 1).
Samples "KS###" collected by Gabriel Aliaga. Samples "KTC###" and "Key XXXX" collected by Tom Chapin for U.S. Gold Corp.

[1]Whole-rock geochemistry not submitted for outcrops previously sampled to avoid repeat analyses. Equivalent sample indicated.

Table A1. Multi-element geochemistry of unaltered and altered rocks.

Sample ID		KTC 307	KTC 311	KTC 312	KTC 313	KTC 318	KTC 319	KTC 337	KTC 338	KTC 339	KTC 344	KTC 345	KTC 348	KTC 350
UTM	East	538354	541498	540890	541050	540371	540221	536949	536935	536892	536752	536842	536658	536671
NAD27	North	4416849	4416978	4416922	4416906	4416312	4415878	4418099	4418343	4418236	4418139	4418067	4418684	4418682
Unit		Ovb	Tvc	Tda	Tmp	Tda	Tda	Twd	Tvc	Tta	Tta	Ovb	Tvc	Ovb
Comment/Alteration														
Whole-rock[1]		Y	Y	Y	Y	Y	Y	Y	Y	Y	Y	Y	Y	Y
Ore chemistry														
Thin Section		Y	Y	Y	Y	Y	Y	Y	Y	Y	Y	Y	Y	Y
SiO_2	%	50.84	76.71	67.26	74.39	65.81	65.39	59.96	75.91	57.37	53.64	45.72	78.25	45.12
Al_2O_3	%	17.46	14.11	17.43	14.66	17.97	18.09	18.04	14.54	17.89	18.97	18.06	13.98	18.37
FeO*	%	8.61	0.32	2.97	1.08	3.55	3.58	5.29	1.65	6.91	9.26	12.50	1.61	12.55
CaO	%	7.68	0.29	3.11	1.01	3.28	3.66	3.98	0.20	0.92	1.41	7.28	0.30	7.16
MgO	%	4.21	0.51	0.75	0.26	1.29	1.13	2.43	0.32	2.68	4.94	5.94	0.50	5.88
Na_2O	%	3.62	2.05	3.37	2.85	3.36	3.41	4.86	0.13	0.21	0.21	4.47	0.12	4.68
K_2O	%	2.67	5.48	4.24	5.31	3.71	3.58	3.70	6.86	11.26	9.44	0.66	4.84	0.69
Cr_2O_3	%	0.01	0.01	0.01	0.01	0.01	0.01	0.01	0.01	0.01	0.01	0.01	0.01	0.01
TiO_2	%	3.45	0.15	0.42	0.03	0.53	0.54	0.88	0.11	1.13	1.23	3.88	0.14	3.97
MnO	%	0.07	0.03	0.04	0.16	0.06	0.07	0.04	0.03	0.09	0.09	0.14	0.03	0.15
P_2O_5	%	1.18	0.03	0.14	0.05	0.20	0.21	0.55	0.05	0.46	0.43	1.03	0.04	1.07
SrO	%	0.05	0.04	0.06	0.03	0.07	0.08	0.10	0.01	0.09	0.02	0.13	0.01	0.14
BaO	%	0.14	0.27	0.19	0.16	0.17	0.25	0.16	0.16	0.97	0.36	0.18	0.15	0.20
LOI		3.73	2.79	2.34	1.69	4.11	3.18	2.34	2.7	4.71	6.62	9.86	3.32	9.82
Ag	ppm	<0.5	<0.5	<0.5	<0.5	<0.5	<0.5	<0.5	<0.5	1.6	<0.5	<0.5	<0.5	<0.5
Al	%													
As	ppm	93	<5	<5	14	19	<5	<5	52	92	26	7	12	9
Au	ppm													
B	ppm													
Ba	ppm	1110	2330	1780	1355	1530	2150	1265	1430	8000	2960	1495	1305	1575
Be	ppm													
Bi	ppm													
C	%													
Ca	%													
Cd	ppm	<0.5	<0.5	<0.5	<0.5	<0.5	<0.5	<0.5	<0.5	<0.5	0.5	<0.5	<0.5	0.8
Ce	ppm	134.5	50.2	103	22.3	91.6	86.1	95.6	57.5	98	63.6	138	32.3	144.5
Co	ppm	17	2	4	1	5	5	11	1	10	18	28		29
Cr	ppm		10		20	10	10				20	70		70
Cs	ppm	2.27	2.51	1.81	2.51	3.26	3.31	4.86	2.37	6.03	1.86	1.79	2.43	1.85
Cu	ppm	25	2	3	1	5	4	7	2	26	10	39	2	39
Dy	ppm	7.18	2.02	3.74	3.41	3.78	3.54	3.04	2.85	6.82	5.02	5.95	1.63	6
Er	ppm	3.43	1.11	1.88	3.64	1.98	1.86	1.28	1.75	3.12	2.95	2.69	1.28	2.7
Eu	ppm	3.29	0.65	1.5	0.49	1.55	1.51	1.54	0.83	2.03	1.42	3.1	0.27	3.02
Fe	%													
Ga	ppm	21.4	16.9	21.4	23.5	21.9	21.6	22.1	20.6	15.4	20.1	20.4	18.4	21.3
Gd	ppm	9.23	2.56	4.92	1.89	4.96	4.7	5.26	3.27	8.56	5.45	7.92	1.19	8.1
Ge	ppm													
Hf	ppm	6.7	4.8	8.2	1.4	7.2	7	5.3	3.9	5.2	4.5	8.2	4.2	8.2
Hg	ppm													
Ho	ppm	1.35	0.4	0.7	0.89	0.69	0.68	0.52	0.56	1.25	1.03	1.07	0.38	1.08
In	ppm													
K	%													
La	ppm	65.5	29.6	54.6	11.7	48.4	46.1	49.4	37.5	53.7	31.3	71.3	22.4	72.1
Li	ppm	30	10	10	<10	10	10	20	20	30	20	60	10	60
Lu	ppm	0.39	0.21	0.31	0.84	0.27	0.27	0.15	0.26	0.38	0.44	0.35	0.23	0.33
Mg	%													
Mn	ppm													
Mo	ppm	1	<1	2	1	2	2	<1	<1	11	3	3	1	3
Na	%													
Nb	ppm	94.4	14.5	15.3	2.9	13.9	13.4	13.4	14	11.8	10.9	94.4	18.3	95.6
Nd	ppm	57.5	23.1	39.8	8.6	36.9	35.1	40	27.8	51.9	32.9	60.2	8.3	61.1
Ni	ppm	8	2					6	2	7	8	39		40
P	ppm													
Pb	ppm		6	17	23	11	14	10	6	10	9	18	30	18
Pr	ppm	15.1	6.98	11.4	2.51	10.5	9.91	11.3	8.15	13.55	8.37	16.05	2.84	16.5
Rb	ppm	84.1	154	120.5	151	95.4	104	134.5	198	347	206	17.6	155.5	18.3
Re	ppm													
S	%													
Sb	ppm													
Sc	ppm	9	2	4	1	4	5	5	3	6	19	16	3	15
Se	ppm													
Sm	ppm	10.9	3.91	7.11	2.2	6.59	6.18	7.18	4.57	10.2	6.78	10.35	1.41	10.65
Sn	ppm	3	2	2	1	2	2	5	2	1	1	2	2	2
Sr	ppm	403	331	549	266	578	642	855	82.7	768	201	940	129.5	969
Ta	ppm	5.4	1	0.9		0.8	0.8	0.7	1	0.6	0.5	5.9	1.1	6
Tb	ppm	1.29	0.36	0.65	0.4	0.7	0.66	0.64	0.51	1.25	0.83	1.11	0.23	1.09
Te	ppm													
Th	ppm	7.48	15.25	18.15	3.85	15.15	14.3	11.65	14.05	7.84	7.73	8.26	12	8.31
Ti	%													
Tl	ppm	<10	<10	<10	<10	<10	<10	<10	<10	10	<10	<10	<10	<10
Tm	ppm	0.45	0.2	0.29	0.7	0.27	0.27	0.18	0.24	0.41	0.44	0.38	0.22	0.4
U	ppm	1.92	3.03	3.51	5.71	3.07	2.91	2.39	3.9	7.49	4.31	3.16	3.41	3.16
V	ppm	168		28		45	50	117	6	171	225	237	11	241
W	ppm	15	1	1	<1	1	1	2	20	25	18	4	51	4
Y	ppm	32.2	11	19.5	25.4	19.9	19.2	14.9	16.9	34	28.5	27.9	11.2	28.4
Yb	ppm	2.68	1.36	1.94	5.37	1.84	1.84	1.02	1.73	2.54	2.86	2.37	1.48	2.38
Zn	ppm	47	12	148	17	51	76	31	55	80	89	151	13	151
Zr	ppm	310	169	327	32	306	294	232	134	219	181	397	140	408

Major oxides are reported in weight percent normalized to 100% anhydrous. Abbreviations are same as map units in geologic map (Plate 1).
Samples "KS###" collected by Gabriel Aliaga. Samples "KTC###" and "Key XXXX" collected by Tom Chapin for U.S. Gold Corp.

[1]Whole-rock geochemistry not submitted for outcrops previously sampled to avoid repeat analyses. Equivalent sample indicated.

Table A1. Multi-element geochemistry of unaltered and altered rocks.

Sample ID		KTC 351	KTC 352	KTC 353	KTC 357	KTC 359	KTC 361	KTC 365	KTC 370	KTC 371	KTC 372	KTC 375	KTC 377	KTC 382
UTM NAD27	East	536931	536936	536287	537242	537301	537237	537314	540556	540560	540675	540167	540326	536305
	North	44 18540	44 18499	44 18539	44 18874	44 18786	44 18763	44 18906	44 16763	44 16757	44 17021	44 16898	44 16650	44 16625
Unit		Tvc	Tvc	Tta	Twq	Twq	Twq	Tmp	Tmp	Tmd	Tmd	Twp	Tmd	Tgd
Comment/Alteration														
Whole-rock[1]		Y	Y	Y	Y	Y	Y	Y	Y	Y	Y	Y	Y	Y
Ore chemistry														
Thin Section		Y	Y	Y	Y	Y	Y	Y	Y	Y	Y	Y	Y	Y
SiO_2	%	79.86	77.58	54.90	68.54	68.07	67.63	78.83	75.04	61.11	62.49	60.67	61.47	59.80
Al_2O_3	%	10.43	12.62	19.03	16.06	16.10	15.35	11.32	14.53	16.48	15.75	16.72	16.23	17.58
FeO*	%	1.84	1.02	7.89	1.07	0.94	3.29	0.86	0.78	5.52	5.33	5.91	5.61	2.10
CaO	%	0.39	0.34	1.27	5.52	5.32	3.15	0.31	0.75	5.67	4.93	4.16	3.75	5.55
MgO	%	0.36	0.45	5.68	1.66	0.93	1.50	0.17	0.27	3.02	2.68	4.01	3.33	3.20
Na_2O	%	0.14	0.89	0.43	5.37	4.23	3.15	2.61	2.88	2.74	2.80	3.15	3.60	3.44
K_2O	%	6.07	6.54	8.30	0.88	3.49	4.95	5.76	5.53	3.79	4.51	3.66	4.32	6.61
Cr_2O_3	%	0.01	0.01	0.01	0.01	0.01	0.01	0.00	0.01	0.01	0.01	0.01	0.01	0.01
TiO_2	%	0.22	0.11	1.46	0.57	0.57	0.57	0.11	0.03	0.98	0.87	1.08	0.95	0.96
MnO	%	0.03	0.03	0.07	0.03	0.02	0.04	0.01	0.06	0.10	0.09	0.10	0.12	0.02
P_2O_5	%	0.17	0.05	0.42	0.18	0.16	0.17	0.00	0.06	0.34	0.31	0.33	0.34	0.30
SrO	%	0.02	0.03	0.02	0.07	0.06	0.06	0.01	0.03	0.07	0.07	0.06	0.08	0.07
BaO	%	0.45	0.33	0.53	0.03	0.09	0.14	0.01	0.05	0.16	0.16	0.13	0.19	0.35
LOI		2.47	3.16	7.17	2.11	2.3	0.92	0.86	1.16	2.69	1.47	4.42	3.97	2.37
Ag	ppm	0.7	<0.5	<0.5	0.25	0.25	0.25	0.5	0.25	0.25	0.25	0.25	0.25	0.25
Al	%													
As	ppm	85	20	44	8	2.5	2.5	9	2.5	5	2.5	2.5	2.5	13
Au	ppm													
B	ppm													
Ba	ppm	3930	2920	4290	248	751	1185	113.5	469	1390	1460	1020	1565	3080
Be	ppm													
Bi	ppm													
C	%													
Ca	%													
Cd	ppm	<0.5	<0.5	<0.5	0.25	0.25	0.25	0.25	0.25	0.25	0.25	0.25	0.25	0.25
Ce	ppm	45.3	47.7	71	71.6	55.6	101.5	61.7	10.8	93.6	98.8	85.9	95.7	72.9
Co	ppm		1	20	2	1	7	1	1	16	14	17	15	3
Cr	ppm	30		30	20	20	20	10	10	60	560	20	60	20
Cs	ppm	9.79	10.25	3.86	7.22	2.54	6	4.9	0.82	2.85	1.99	2.19	1.47	10.9
Cu	ppm	17	1	9	1	2	2	1	1	7	5	14	8	1
Dy	ppm	2.59	2.64	5.2	2.97	3.59	2.91	1.8	1.65	4.31	4.36	3.59	4.11	4.2
Er	ppm	1.54	1.48	2.84	1.61	1.94	1.48	1.28	1.74	2.2	2.27	1.88	2.3	2.22
Eu	ppm	0.65	0.75	1.43	0.98	1.16	1.23	0.13	0.48	1.6	1.61	1.55	1.66	1.52
Fe	%													
Ga	ppm	12.2	13.2	20.8	19.5	19.7	19.2	16.3	22.9	20.1	21.2	18.8	19.1	18.9
Gd	ppm	2.99	3.23	5.57	4.12	4.47	3.85	1.71	0.99	5.32	5.61	4.75	5.71	5.05
Ge	ppm													
Hf	ppm	3.4	3.7	5.1	6.1	6.1	5.2	5.1	0.9	7.2	7.4	5.6	6.9	5.2
Hg	ppm													
Ho	ppm	0.56	0.51	1.03	0.58	0.7	0.54	0.36	0.43	0.82	0.86	0.69	0.86	0.84
In	ppm													
K	%													
La	ppm	24.6	39	36.4	31.6	25.9	60.1	44.9	6.3	51.1	55.2	47.6	53	40.6
Li	ppm	10	10	40	10	10	10	10	5	10	10	30	10	10
Lu	ppm	0.25	0.2	0.39	0.22	0.27	0.25	0.25	0.43	0.33	0.35	0.29	0.34	0.35
Mg	%													
Mn	ppm													
Mo	ppm	2	1	2	0.5	0.5	1	1	0.5	2	2	2	0.5	1
Na	%													
Nb	ppm	12.2	15.3	16.5	19.7	15.9	14.4	12.8	3.5	17.7	18.8	15.2	17.2	11.3
Nd	ppm	19.6	27.4	32.5	34.3	33.1	40.1	17.6	4.8	41.9	44.7	37.7	42.5	34.5
Ni	ppm	3		13	10	6	12	1	1	9	9	18	9	6
P	ppm													
Pb	ppm	11	8	7	7	14	22	8	26	18	32	13	15	5
Pr	ppm	5.59	8.1	8.53	9.11	8.11	11.65	6.34	1.38	11.5	12.1	10.3	11.8	9.1
Rb	ppm	149.5	163	158.5	30.4	75.5	166.5	331	143.5	113.5	157	111.5	130.5	156
Re	ppm													
S	%													
Sb	ppm													
Sc	ppm	4	2	14	5	4	6	0.5	1	11	10	10	11	12
Se	ppm													
Sm	ppm	3.79	4.79	6.37	5.85	6.38	6.53	2.46	0.99	7.46	7.58	6.45	7.85	6.58
Sn	ppm	2	2	1	1	1	2	3	1	2	2	2	2	1
Sr	ppm	180	225	165	583	534	486	63.3	297	589	612	474	709	606
Ta	ppm	0.8	1	0.9	1.2	1.3	1.1	1.3	0.1	1.1	1.1	1	1.1	0.7
Tb	ppm	0.46	0.45	0.83	0.58	0.63	0.56	0.29	0.2	0.81	0.81	0.66	0.8	0.74
Te	ppm													
Th	ppm	10.15	12.75	8.6	25.1	25.3	25.5	52.6	2.14	17.2	19.15	16.45	17.95	11.7
Ti	%													
Tl	ppm	<10	<10	<10	5	5	5	5	5	5	5	5	5	5
Tm	ppm	0.22	0.19	0.44	0.24	0.3	0.22	0.23	0.34	0.34	0.35	0.27	0.35	0.33
U	ppm	7.19	3.13	1.8	4.45	4.17	4.12	8.44	1.27	3.52	3.99	3.59	3.62	2.86
V	ppm	80	5	190	50	48	62	5	2.5	117	112	123	113	122
W	ppm	4	10	29	1	1	1	4	0.5	1	1	1	1	2
Y	ppm	16.6	14.5	28.8	16.3	19.1	15.7	12.8	12.5	23	23.4	18.8	23.1	22.2
Yb	ppm	1.49	1.46	2.71	1.49	1.84	1.57	1.75	2.67	2.17	2.21	1.75	2.11	2.13
Zn	ppm	41	30	92	17	17	35	16	15	75	136	86	87	16
Zr	ppm	124	123	217	226	228	197	152	21	283	300	218	277	206

Major oxides are reported in weight percent normalized to 100% anhydrous. Abbreviations are same as map units in geologic map (Plate 1).
Samples "KS###" collected by Gabriel Aliaga. Samples "KTC###" and "Key XXXX" collected by Tom Chapin for U.S. Gold Corp.

[1]Whole-rock geochemistry not submitted for outcrops previously sampled to avoid repeat analyses. Equivalent sample indicated.

Table A1. Multi-element geochemistry of unaltered and altered rocks.

Sample ID		KTC 392	KTC 398	KTC 400	KTC 401	KTC 407	KTC 412	KTC 415	KTC 418	KTC 419	KTC 421	KTC 423	KTC 426
UTM	East	540676	540003	539972	539800	540692	540558	540033	539855	539884	539812	539569	539478
NAD27	North	4416959	4417710	4417948	4417800	4417896	4418224	4417979	4417500	4417366	4417174	4417179	4417233
Unit		Tgd	Trp	Trp	Trp	Tvc	Tvc	Tmd	Trp	Twp	Tmd	Twp	Tmp
Comment/Alteration													
Whole-rock[1]		Y	Y	Y	Y	Y	Y	Y	Y	Y	Y	Y	Y
Ore chemistry													
Thin Section		Y											
SiO$_2$	%	57.05	79.98	79.90	75.71	81.93	81.45	64.25	74.66	70.73	65.49	61.49	75.51
Al$_2$O$_3$	%	18.21	12.50	12.94	13.32	13.53	13.20	15.91	13.39	14.14	15.48	16.60	14.11
FeO*	%	6.27	0.73	0.77	1.58	0.67	1.28	4.74	2.21	2.93	4.88	6.01	0.74
CaO	%	7.22	0.17	0.11	0.86	0.11	0.10	4.70	1.35	2.80	3.63	4.29	1.05
MgO	%	3.50	0.33	0.22	0.47	0.31	0.35	2.12	0.89	1.61	2.14	3.23	0.10
Na$_2$O	%	3.66	0.17	0.15	2.71	0.07	0.05	2.72	2.13	2.45	2.75	2.98	3.49
K$_2$O	%	2.40	5.65	5.68	4.94	3.08	3.09	4.17	4.82	4.57	4.15	3.67	4.74
Cr$_2$O$_3$	%	0.01	0.01	0.01	0.01	0.01	0.01	0.01	0.01	0.01	0.01	0.01	0.01
TiO$_2$	%	1.03	0.22	0.09	0.17	0.12	0.12	0.83	0.23	0.40	0.89	1.09	0.05
MnO	%	0.07	0.01	0.01	0.02	0.01	0.02	0.07	0.07	0.08	0.08	0.09	0.04
P$_2$O$_5$	%	0.38	0.01	0.03	0.07	0.05	0.07	0.28	0.09	0.15	0.31	0.34	0.09
SrO	%	0.09	0.01	0.01	0.02	0.01	0.01	0.06	0.02	0.03	0.06	0.05	0.02
BaO	%	0.11	0.22	0.08	0.12	0.12	0.25	0.14	0.12	0.11	0.14	0.16	0.05
LOI		1.62	2.85	2.65	1.99	3.44	3.44	1.36	3.53	4.63	1.65	5.25	0.82
Ag	ppm	0.25	0.5	0.25	0.25	0.25	0.25	0.25	0.25	0.25	0.25	0.25	0.25
Al	%												
As	ppm	2.5	10	50	15	2.5	35	9	6	5	7	13	5
Au	ppm												
B	ppm												
Ba	ppm	980	1990	740	1045	980	2300	1320	1075	1010	1265	1350	432
Be	ppm												
Bi	ppm												
C	%												
Ca	%												
Cd	ppm	0.25	0.25	0.25	0.25	0.25	0.25	0.25	0.25	0.5	0.25	0.25	0.25
Ce	ppm	70.6	36.5	35.8	57.4	80.2	79.3	105.5	64.5	64.1	104	96.6	27.9
Co	ppm	12	0.5	0.5	1	0.5	1	11	2	5	12	17	0.5
Cr	ppm	30	20	10	10	10	10	50	20	30	50	30	10
Cs	ppm	11.2	2.67	2.91	6.32	2.82	3.68	5.14	3.7	2.78	2.67	1.97	0.83
Cu	ppm	6	6	2	21	1	1	9	7	13	7	16	2
Dy	ppm	3.99	2.08	2.22	2.55	2.41	2.18	4.04	2.7	3.44	4.31	4.06	1.96
Er	ppm	2.05	1.19	1.12	1.4	1.42	1.22	2.09	1.38	1.73	2.08	1.84	1.63
Eu	ppm	1.69	0.55	0.47	0.73	0.73	0.76	1.62	0.77	1.06	1.55	1.7	0.5
Fe	%												
Ga	ppm	21.7	17.3	17.7	17.3	18.5	21.4	22	18.5	18.5	21.5	21.3	28.1
Gd	ppm	4.94	2.44	2.33	3.13	3.07	3.27	5.4	3.42	4.55	5.65	5.49	1.96
Ge	ppm												
Hf	ppm	5	4	3.2	3.6	4.1	4.6	8	4	5.1	7.9	5.8	2.3
Hg	ppm												
Ho	ppm	0.8	0.42	0.42	0.47	0.52	0.42	0.79	0.5	0.66	0.87	0.78	0.45
In	ppm												
K	%												
La	ppm	38.3	18.8	20.3	31.8	39.3	42.8	55.5	34.6	39.6	55	54.2	14.8
Li	ppm	30	10	10	20	20	20	20	20	20	20	20	10
Lu	ppm	0.3	0.22	0.2	0.22	0.25	0.25	0.3	0.24	0.28	0.34	0.29	0.35
Mg	%												
Mn	ppm												
Mo	ppm	5	3	1	2	2	2	2	1	1	1	1	0.5
Na	%												
Nb	ppm	11.4	14.4	12.6	14	15.8	17.4	18.6	15.5	15.8	18.2	16.3	4.5
Nd	ppm	34.4	15.5	14.9	23.2	29.4	29.9	43.4	25.8	30.8	44.6	41.9	11.7
Ni	ppm	9	0.5	1	1	0.5	1	8	2	3	6	15	1
P	ppm												
Pb	ppm	11	37	72	26	9	9	17	20	25	23	15	22
Pr	ppm	8.93	4.11	4.22	6.52	8.81	8.5	11.7	7.32	8.27	11.8	11.15	3.14
Rb	ppm	99.5	185	219	161.5	122	122.5	157	176	171.5	135.5	121.5	124
Re	ppm												
S	%												
Sb	ppm												
Sc	ppm	11	3	3	3	3	3	10	4	5	10	11	1
Se	ppm												
Sm	ppm	6.69	3.31	3.08	4.29	4.44	4.98	7.51	4.66	5.58	7.78	7.3	2.42
Sn	ppm	1	2	3	3	2	1	2	3	5	2	2	1
Sr	ppm	820	110.5	106	199.5	80.9	74	589	209	287	554	516	257
Ta	ppm	0.7	1.3	1.4	1.2	1.1	1.2	1.2	1.3	1.2	1.1	1.1	0.2
Tb	ppm	0.7	0.36	0.36	0.43	0.41	0.39	0.72	0.45	0.61	0.78	0.72	0.29
Te	ppm												
Th	ppm	9.53	17.55	16.75	16.9	15.1	15.3	21.3	18.1	17.25	21.2	17.15	4.06
Ti	%												
Tl	ppm	5	5	5	5	5	5	5	5	5	5	5	5
Tm	ppm	0.29	0.18	0.16	0.2	0.21	0.23	0.29	0.2	0.26	0.31	0.28	0.26
U	ppm	1.9	4.99	4.65	4.29	4.54	4.03	4.02	5.35	4.52	4.09	3.74	5.54
V	ppm	142	17	9	14	2.5	2.5	102	22	44	101	147	6
W	ppm	3	2	2	2	1	2	2	2	2	1	2	1
Y	ppm	20.6	12.2	13.1	14.5	13.4	12.9	22.6	15	20.4	23.9	22.5	13.2
Yb	ppm	1.82	1.25	1.21	1.33	1.62	1.48	2.01	1.45	1.7	2.18	1.91	2.2
Zn	ppm	44	15	17	63	16	11	80	59	93	89	86	34
Zr	ppm	199	120	79	103	129	149	305	125	169	304	227	55

Major oxides are reported in weight percent normalized to 100% anhydrous. Abbreviations are same as map units in geologic map (Plate 1).
Samples "KS###" collected by Gabriel Aliaga. Samples "KTC###" and "Key XXXX" collected by Tom Chapin for U.S. Gold Corp.

[1]Whole-rock geochemistry not submitted for outcrops previously sampled to avoid repeat analyses. Equivalent sample indicated.

Table A1. Multi-element geochemistry of unaltered and altered rocks.

Sample ID		KTC 427	KTC 429	KTC 437	KTC 438	KTC 439	KTC 440	KTC 441	KTC 446	KTC 448	KTC 453
UTM	East	540682	541095	540611	540542	540187	540062	540083	540188	539994	540292
NAD27	North	4419092	4418868	4419160	4418983	4418604	4418568	4418786	4418937	4418776	4419243
Unit		Tmd	COcb	COcb	Tad	Tad	Tdad	Tad	Tdad	Tad	Tdad
Comment/Alteration											
Whole-rock[1]		Y	Y	Y	Y	Y	Y	Y	Y	Y	Y
Ore chemistry											
Thin Section											
SiO$_2$	%	63.10	41.38	49.51	76.53	74.53	69.78	63.54	69.56	66.10	71.33
Al$_2$O$_3$	%	15.67	13.08	19.56	18.71	17.96	17.70	17.29	17.34	18.09	17.76
FeO*	%	5.22	6.11	8.04	1.48	1.23	2.65	4.63	2.92	4.78	1.90
CaO	%	4.48	26.16	8.69	0.21	0.30	0.13	5.71	0.33	1.30	0.52
MgO	%	2.97	2.74	5.34	0.37	0.61	0.83	1.98	0.61	2.14	0.49
Na$_2$O	%	3.20	3.53	1.63	0.02	0.06	0.12	0.09	0.09	0.08	2.22
K$_2$O	%	3.91	1.82	3.35	1.66	3.96	7.71	5.35	8.14	5.79	4.94
Cr$_2$O$_3$	%	0.01	0.03	0.03	0.01	0.01	0.01	0.01	0.01	0.01	0.01
TiO$_2$	%	0.87	3.58	2.32	0.77	0.79	0.39	0.73	0.38	0.76	0.39
MnO	%	0.07	0.18	0.10	0.01	0.01	0.01	0.09	0.01	0.06	0.03
P$_2$O$_5$	%	0.30	0.74	0.32	0.14	0.19	0.13	0.25	0.13	0.28	0.14
SrO	%	0.06	0.05	0.08	0.01	0.01	0.01	0.02	0.01	0.01	0.03
BaO	%	0.14	0.58	1.02	0.09	0.34	0.52	0.31	0.48	0.59	0.24
LOI		2.09	18.2	11.65	6.45	4.29	3.09	8.06	3.05	5.1	3.42
Ag	ppm	0.25	0.25	<0.5	<0.5	<0.5	<0.5	<0.5	<0.5	<0.5	<0.5
Al	%										
As	ppm	2.5	13	7	22	78	17	10	19	33	5
Au	ppm										
B	ppm										
Ba	ppm	1185	4240	8050	859	3060	4670	2690	4290	5230	2280
Be	ppm										
Bi	ppm										
C	%										
Ca	%										
Cd	ppm	0.25	0.25	0.6	<0.5	<0.5	<0.5	<0.5	<0.5	<0.5	<0.5
Ce	ppm	93.1	68.6	44	82.2	68.8	97	76.3	109.5	82.7	109
Co	ppm	13	57	27		1	1	8	3	9	2
Cr	ppm	60	130	230	10	10		10		10	
Cs	ppm	2.06	1.64	6.2	4.17	8.98	10.25	12.25	21.1	10.4	11.9
Cu	ppm	2	43	57	30	34	3	8	3	2	3
Dy	ppm	3.95	5.02	3.51	3.34	2.08	3.49	3.04	3.81	3.76	4.02
Er	ppm	2.04	2.41	1.69	1.89	1.51	1.93	1.83	2.3	2.04	2.09
Eu	ppm	1.55	2.42	1.61	0.99	1.13	1.26	1.31	1.69	1.34	1.38
Fe	%										
Ga	ppm	20.3	15	17.9	20.1	20.3	21	18.6	21.5	20.1	20.8
Gd	ppm	5.36	7.29	4.25	3.77	3.19	4.16	4.11	5.42	4.63	5.14
Ge	ppm										
Hf	ppm	6.6	5.8	3.4	6	6.2	7.9	5.3	8.2	5.9	8.2
Hg	ppm										
Ho	ppm	0.8	0.97	0.64	0.68	0.47	0.65	0.66	0.81	0.73	0.77
In	ppm										
K	%										
La	ppm	48.7	32.3	21.5	44	36.5	49.3	40.6	58.2	43.7	55.5
Li	ppm	20	30	50	60	10	10	20	10	20	10
Lu	ppm	0.31	0.28	0.21	0.29	0.3	0.29	0.27	0.32	0.29	0.3
Mg	%										
Mn	ppm										
Mo	ppm	1	1	<1	2	2	4	1	4	2	2
Na	%										
Nb	ppm	16.1	43.6	24.6	12.7	13.1	14.4	11.1	14.7	12.5	14.4
Nd	ppm	40.4	37.9	22	30.6	27.2	35.2	30.7	41.7	33.5	40.6
Ni	ppm	5	137	70	5	4	2	2	1	4	2
P	ppm										
Pb	ppm	10	1	2	6	14		6	9	7	17
Pr	ppm	10.6	8.64	5.61	8.92	7.62	10.45	8.42	11.9	9.32	11.65
Rb	ppm	122	21.3	94.3	63	120.5	275	165.5	278	191	156
Re	ppm										
S	%										
Sb	ppm										
Sc	ppm	11	15	32	6	8	3	8	3	9	3
Se	ppm										
Sm	ppm	6.76	8.23	5.01	5.3	5.48	5.9	5.5	7.43	5.88	7.15
Sn	ppm	1	2	1	2	1	1	1	2	1	2
Sr	ppm	527	376	625	41.5	63.5	130	179.5	76.3	113	245
Ta	ppm	1	2.8	1.5	0.8	0.8	1	0.7	1	0.8	1
Tb	ppm	0.7	0.93	0.64	0.6	0.37	0.63	0.58	0.75	0.64	0.73
Te	ppm										
Th	ppm	17.25	3.74	2.51	12.15	12.75	18.85	10.75	19.5	12.05	19
Ti	%										
Tl	ppm	5	5	<10	<10	10	10	<10	<10	10	<10
Tm	ppm	0.29	0.3	0.23	0.28	0.24	0.3	0.27	0.31	0.3	0.32
U	ppm	3.27	1.4	0.66	3.05	2.86	3.72	2.3	3.87	2.66	3.6
V	ppm	101	207	260	83	78	24	96	24	103	24
W	ppm	1	1	2	11	4	2	2	2	1	2
Y	ppm	21.9	25.3	16.3	17.9	13.3	18.7	17.5	21.1	19.2	20.3
Yb	ppm	1.97	1.87	1.43	1.83	1.62	1.94	1.75	1.97	1.74	1.92
Zn	ppm	52	87	63	11	6	10	88	45	97	55
Zr	ppm	265	229	130	247	263	325	220	343	246	348

Major oxides are reported in weight percent normalized to 100% anhydrous. Abbreviations are same as map units in geologic map (Plate 1).
Samples "KS###" collected by Gabriel Aliaga. Samples "KTC###" and "Key XXXX" collected by Tom Chapin for U.S. Gold Corp.
[1]Whole-rock geochemistry not submitted for outcrops previously sampled to avoid repeat analyses. Equivalent sample indicated.

Table A1. Multi-element geochemistry of unaltered and altered rocks.

Sample ID		KTC 457	KTC 458	KTC 460	KTC 463	KTC 465	KTC 467	KTC 468	KTC 469	KTC 472	KTC 473
UTM	East	540169	540297	540526	540416	541235	539830	539848	539718	538841	538520
NAD27	North	4419352	4419674	4419674	4420291	4420031	4421064	4421245	4421277	4421646	4420882
Unit		COcb	COcb	COcb	Tdad	Ta	Ta	Ta	Ta	Ta	Ta
Comment/Alteration											
Whole-rock[1]		Y	Y	Y	Y	Y	Y	Y	Y	Y	Y
Ore chemistry											
Thin Section											
SiO2	%	51.19	49.81	48.31	81.09	63.00	65.76	65.23	66.23	64.38	69.47
Al2O3	%	18.22	16.79	14.74	14.73	16.99	17.60	19.12	17.68	17.12	17.52
FeO*	%	9.53	10.27	8.65	1.48	5.05	3.33	3.36	2.92	4.30	2.47
CaO	%	3.38	8.25	12.94	0.40	5.33	4.41	4.27	4.63	4.79	0.80
MgO	%	4.24	4.32	4.63	0.29	2.63	0.76	1.07	0.37	1.75	0.96
Na2O	%	2.33	2.82	3.78	0.04	3.32	3.63	3.27	3.68	3.25	2.72
K2O	%	5.61	2.83	2.40	1.04	2.26	3.24	2.22	3.08	3.12	4.52
Cr2O3	%	0.01	0.01	0.03	0.01	0.01	0.01	0.01	0.01	0.01	0.01
TiO2	%	2.53	3.06	3.27	0.33	0.81	0.75	0.95	0.84	0.72	0.87
MnO	%	0.16	0.12	0.16	0.01	0.10	0.03	0.03	0.02	0.07	0.02
P2O5	%	0.81	1.01	0.58	0.22	0.28	0.26	0.24	0.35	0.27	0.32
SrO	%	0.06	0.06	0.05	0.01	0.08	0.07	0.09	0.07	0.07	0.03
BaO	%	1.93	0.66	0.45	0.35	0.14	0.16	0.15	0.15	0.14	0.29
LOI		5.42	10.2	12.5	5.75	2.15	1.79	6.02	1.7	2.3	3.97
Ag	ppm	<0.5	<0.5	<0.5	<0.5	<0.5	0.25	0.25	0.25	0.25	0.25
Al	%										
As	ppm	5	<5	<5	26	<5	10	2.5	2.5	2.5	2.5
Au	ppm										
B	ppm										
Ba	ppm		5530	3550	3110	1275	1315	1305	1415	1255	2510
Be	ppm										
Bi	ppm										
C	%										
Ca	%										
Cd	ppm	0.5	0.5	<0.5	<0.5	<0.5	0.25	0.25	0.25	0.25	0.25
Ce	ppm	196	164	82.8	95.4	79.1	87.1	109.5	88.3	82.8	76.7
Co	ppm	23	24	34		11	5	4	3	8	4
Cr	ppm	10	30	240	30	10	20	30	10	30
Cs	ppm	2.87	9.27	4.06	6.74	26.6	1.24	1.8	1.52	1.94	3.04
Cu	ppm	38	34	60	6	8	5	11	6	6	8
Dy	ppm	7.03	6.9	4.69	3.19	3.66	3.36	4.37	3.73	3.25	3.58
Er	ppm	3.19	2.95	2.3	1.63	2.1	1.88	2.02	2.25	1.98	2.02
Eu	ppm	3.8	3.46	2.37	1.34	1.41	1.35	1.88	1.62	1.27	1.29
Fe	%										
Ga	ppm	25.9	23.9	15.9	15.9	19.5	20.7	22.5	22.3	20.1	19.5
Gd	ppm	10.05	9.62	6.37	4.07	4.52	4.2	6.21	5.21	4.32	4.79
Ge	ppm										
Hf	ppm	9.5	8.7	5.6	6.6	5.3	6	6	5.9	5.9	5.6
Hg	ppm										
Ho	ppm	1.26	1.25	0.88	0.6	0.71	0.66	0.79	0.78	0.66	0.72
In	ppm										
K	%										
La	ppm	106.5	88.6	40.1	52.5	41.7	47.3	56.4	49.2	44.6	40.4
Li	ppm	60	70	60	50	10	10	10	10	10	10
Lu	ppm	0.35	0.3	0.25	0.26	0.28	0.24	0.24	0.34	0.28	0.27
Mg	%										
Mn	ppm										
Mo	ppm	3	3	<1	3	2	1	2	2	2	1
Na	%										
Nb	ppm	156.5	120.5	47.1	12.5	12.2	11.8	14	12.9	11.2	12.1
Nd	ppm	72.9	66.7	38.8	34.7	32.3	36	44.6	38	34.8	34.5
Ni	ppm	4	27	99	12	6	3	6	2	2	3
P	ppm										
Pb	ppm	6	2		15	14	12	15	13	12	11
Pr	ppm	20.3	18.2	9.93	10.3	9.04	9.79	12.6	10.05	9.55	9.04
Rb	ppm	124.5	67.2	33	38.9	78.2	89.1	83	86.5	91.8	101.5
Re	ppm										
S	%										
Sb	ppm										
Sc	ppm	5	15	20	3	11	8	12	9	10	11
Se	ppm										
Sm	ppm	13.1	12.3	7.52	5.86	5.94	6.19	8.09	6.15	5.74	5.48
Sn	ppm	3	3	2	2	2	2	2	2	2	1
Sr	ppm	574	422	361	131	683	625	779	698	658	300
Ta	ppm	8.7	6.8	3	0.9	0.7	0.7	0.8	0.7	0.7	0.7
Tb	ppm	1.39	1.34	0.91	0.58	0.61	0.57	0.83	0.72	0.63	0.65
Te	ppm										
Th	ppm	15.8	12.35	4.48	15.75	10.65	12.3	12.75	12.65	12.05	11.45
Ti	%										
Tl	ppm	<10	<10	<10	<10	<10	5	5	5	5	5
Tm	ppm	0.43	0.38	0.31	0.22	0.29	0.25	0.28	0.27	0.27	0.27
U	ppm	3.44	2.82	1.24	3.96	2.47	2.69	3.25	2.86	2.48	2.25
V	ppm	101	208	248	30	122	99	125	104	96	110
W	ppm	4	3	2	8	1	1	2	2	2	5
Y	ppm	31.3	29.7	21.5	16.7	19	17.5	18.5	22.6	18.4	18.7
Yb	ppm	2.43	1.97	1.79	1.62	1.95	1.82	1.81	2.16	1.82	1.89
Zn	ppm	116	104	77	22	86	82	82	55	89	59
Zr	ppm	487	412	247	268	220	240	248	243	231	223

Major oxides are reported in weight percent normalized to 100% anhydrous. Abbreviations are same as map units in geologic map (Plate 1).
Samples "KS###" collected by Gabriel Aliaga. Samples "KTC###" and "Key XXXX" collected by Tom Chapin for U.S. Gold Corp.
[1]Whole-rock geochemistry not submitted for outcrops previously sampled to avoid repeat analyses. Equivalent sample indicated.

Table A1. Multi-element geochemistry of unaltered and altered rocks.

Sample ID		KTC 475	KTC 478	KTC 479	KTC 485	KTC 486	KTC 489	KTC 490	KTC 492	KTC 496	KTC 500
UTM	East	538726	538869	538954	539150	539092	538964	539348	539363	539688	539727
NAD27	North	4417232	4417369	4417819	4417525	4417422	4416609	4417022	4416795	4416492	4416818
Unit		Twd	Twd	COcb	Ovb	Twp	Twp	Tmp	Tda	Tda	Tda
Comment/Alteration											
Whole-rock[1]		Y	Y	Y	Y	Y	Y	Y	Y	Y	Y
Ore chemistry											
Thin Section											
SiO_2	%	65.43	71.95	49.87	45.45	65.22	59.38	73.39	65.00	68.12	65.37
Al_2O_3	%	15.81	12.85	15.68	14.98	15.71	16.78	14.14	21.15	16.41	17.17
FeO*	%	4.33	3.48	5.83	10.85	4.56	6.47	1.15	0.39	3.57	3.71
CaO	%	3.95	2.97	17.82	8.45	3.88	5.39	2.10	6.56	2.69	4.67
MgO	%	1.83	2.19	4.11	9.05	1.87	3.79	0.46	0.64	0.88	0.98
Na_2O	%	3.09	2.60	1.47	1.71	3.25	2.81	3.56	4.90	2.72	3.86
K_2O	%	4.27	2.88	1.93	4.45	4.19	3.70	4.71	0.44	4.60	3.24
Cr_2O_3	%	0.01	0.01	0.01	0.05	0.01	0.01	0.01	0.01	0.01	0.00
TiO_2	%	0.75	0.61	2.45	4.02	0.79	1.05	0.16	0.60	0.54	0.50
MnO	%	0.04	0.03	0.09	0.05	0.08	0.12	0.03	0.02	0.03	0.07
P_2O_5	%	0.24	0.27	0.60	0.70	0.26	0.31	0.07	0.17	0.20	0.16
SrO	%	0.08	0.04	0.05	0.04	0.06	0.06	0.05	0.10	0.06	0.08
BaO	%	0.17	0.12	0.09	0.19	0.13	0.13	0.17	0.02	0.19	0.19
LOI		2.42	1.65	0.45	1.44	1.73	4.88	0.89	4.43	4.25	1.02
Ag	ppm	0.25	0.25	0.25	0.25	0.25	0.25	0.25	0.25	0.25	0.25
Al	%										
As	ppm	68	2.5	18	194	2.5	2.5	10	9	10	8
Au	ppm										
B	ppm										
Ba	ppm	1560	1030	772	1615	1235	1085	1520	203	1775	1745
Be	ppm										
Bi	ppm										
C	%										
Ca	%										
Cd	ppm	0.8	0.25	0.5	0.7	0.25	0.25	0.25	0.25	0.25	0.25
Ce	ppm	111.5	79.2	116.5	106	102.5	77.7	52.2	89.7	103	105
Co	ppm	7	6	16	47	12	16	1	0.5	4	5
Cr	ppm	5	40	60	390	30	10	5	5	5	10
Cs	ppm	5.11	11	9.77	65.9	2.59	6.99	0.56	29.4	3.16	1.04
Cu	ppm	31	31	97	8	6	2	2	0.5	2	2
Dy	ppm	4.14	3.17	5.77	6.04	3.85	4.28	3.16	3.92	4.09	4.28
Er	ppm	2.39	1.68	3.23	2.8	2.24	2.34	1.77	2.13	2.12	2.23
Eu	ppm	1.42	1	2.65	3.11	1.44	1.44	0.99	0.82	1.57	1.63
Fe	%										
Ga	ppm	18.5	17.3	19.7	23	21.3	20.1	15.5	19.2	19.5	20.5
Gd	ppm	5.33	4.44	7.6	8.19	5.18	5.24	3.88	5.09	5.64	5.31
Ge	ppm										
Hf	ppm	6.1	5.5	6.9	7.7	6.6	5.1	4.7	8.6	8.7	7.4
Hg	ppm										
Ho	ppm	0.78	0.63	1.19	1.13	0.78	0.89	0.64	0.79	0.8	0.79
In	ppm										
K	%										
La	ppm	57.7	41.1	56.2	53.4	57.6	41.4	26.5	36.7	60.7	60.6
Li	ppm	20	40	20	20	30	30	5	20	10	10
Lu	ppm	0.31	0.27	0.4	0.3	0.3	0.34	0.27	0.32	0.33	0.32
Mg	%										
Mn	ppm										
Mo	ppm	2	14	47	1	0.5	1	1	0.5	1	1
Na	%										
Nb	ppm	15.1	17.5	85.2	62	17.9	13.5	15.5	13.2	15.6	13.6
Nd	ppm	44.2	32	53	52.9	41.8	35.6	25.2	41.4	46.6	42.7
Ni	ppm	1	11	38	193	11	2	0.5	0.5	0.5	1
P	ppm										
Pb	ppm	16	13	1	2	20	5	5	1	2	28
Pr	ppm	12.05	9.03	13.95	12.45	11.3	9.23	6.29	11	12.35	11.6
Rb	ppm	116	97.6	63.9	372	149	108.5	127	10.6	149.5	72.8
Re	ppm										
S	%										
Sb	ppm										
Sc	ppm	10	7	16	25	9	16	3	5	6	5
Se	ppm										
Sm	ppm	7.7	5.42	9.52	11.05	7.34	7.14	5.19	7.47	8.21	7.74
Sn	ppm	3	2	23	2	2	2	1	0.5	2	1
Sr	ppm	595	308	381	310	530	554	412	846	508	690
Ta	ppm	1	1.1	5.3	3.6	1.3	0.9	1	0.9	1	0.8
Tb	ppm	0.72	0.59	1.05	1.16	0.73	0.78	0.54	0.71	0.72	0.77
Te	ppm										
Th	ppm	19.35	18.9	7.96	5.88	23.5	14.35	15.75	18.05	17.7	16.05
Ti	%										
Tl	ppm	5	5	5	5	5	10	5	5	5	5
Tm	ppm	0.32	0.25	0.42	0.39	0.32	0.35	0.28	0.33	0.32	0.32
U	ppm	3.92	4.52	3.79	1.69	4.83	3.19	3.35	2.31	3.07	2.4
V	ppm	95	83	186	330	103	196	2.5	41	41	49
W	ppm	2	3	3	4	2	3	1	2	2	1
Y	ppm	20.2	18.3	30.5	27.2	20.5	21.2	16.7	19.7	20.9	20.1
Yb	ppm	2.13	1.78	2.76	2.24	2.07	2.04	1.66	2.14	1.96	1.97
Zn	ppm	57	37	123	49	73	74	23	9	32	72
Zr	ppm	231	217	322	324	251	192	162	338	344	296

Major oxides are reported in weight percent normalized to 100% anhydrous. Abbreviations are same as map units in geologic map (Plate 1).

Samples "KS###" collected by Gabriel Aliaga. Samples "KTC###" and "Key XXXX" collected by Tom Chapin for U.S. Gold Corp.

[1] Whole-rock geochemistry not submitted for outcrops previously sampled to avoid repeat analyses. Equivalent sample indicated.

Table A1. Multi-element geochemistry of unaltered and altered rocks.

Sample ID		Key 1601-1090	Key 1601-1234	Key 1601-1269	Key 1601-921.5	Key 1605-1167	Key 1605-1262
UTM	East	539354	539354	539354	539354	538297	538297
NAD27	North	4419536	4419536	4419536	4419536	4420595	4420595
Unit		Tad	Tad	Tad	COcb	COcb	COcb
Comment/Alteration							
Whole-rock[1]		Y	Y	Y	Y	Y	Y
Ore chemistry							
Thin Section							
SiO$_2$	%	66.90	67.41	63.12	58.38	44.49	53.48
Al$_2$O$_3$	%	18.21	15.51	17.41	20.84	19.13	14.42
FeO*	%	3.98	4.99	5.61	5.52	10.83	6.89
CaO	%	0.58	3.87	3.80	0.66	10.15	10.10
MgO	%	2.62	1.92	2.99	6.08	6.27	4.07
Na$_2$O	%	0.10	0.92	2.04	0.06	0.11	3.33
K$_2$O	%	6.16	3.65	3.39	5.27	3.58	2.84
Cr$_2$O$_3$	%	0.01	0.01	0.01	0.09	0.02	0.01
TiO$_2$	%	0.85	0.74	0.81	2.64	3.94	2.73
MnO	%	0.03	0.05	0.03	0.03	0.12	0.12
P$_2$O$_5$	%	0.28	0.24	0.27	0.31	0.66	0.57
SrO	%	0.03	0.03	0.08	0.01	0.01	0.03
BaO	%	0.25	0.64	0.44	0.11	0.68	1.40
LOI		5.34	8.02	7.25	7.18	16.8	9.18
Ag	ppm	<0.5	0.5	<0.5	<0.5	<0.5	<0.5
Al	%						
As	ppm	22	926	123	981	99	7
Au	ppm						
B	ppm						
Ba	ppm	2250	5470	3790	946	5160	
Be	ppm						
Bi	ppm						
C	%						
Ca	%						
Cd	ppm	<0.5	<0.5	1.1	<0.5	<0.5	<0.5
Ce	ppm	79	65.5	78.8	42.1	87.8	78.9
Co	ppm	6	7	7	46	21	20
Cr	ppm	20	20	20	650	150	90
Cs	ppm	19.1	19.2	26.4	16.3	8.7	6.81
Cu	ppm	18	10	2	173	40	24
Dy	ppm	3.66	3.13	3.73	3.4	5.6	4.73
Er	ppm	2.09	1.7	2.01	1.89	2.56	2.19
Eu	ppm	1.11	0.94	1.6	0.98	2.44	2.37
Fe	%						
Ga	ppm	22.8	18.8	21	23.8	23.9	16.9
Gd	ppm	4.19	3.98	4.65	4.13	7.48	6.12
Ge	ppm						
Hf	ppm	6	4.9	5.5	4	6.7	5.8
Hg	ppm						
Ho	ppm	0.7	0.61	0.71	0.71	0.99	0.86
In	ppm						
K	%						
La	ppm	40.3	34	41.4	20.7	41.2	38.4
Li	ppm	30	10	50	20	30	40
Lu	ppm	0.33	0.26	0.3	0.24	0.27	0.26
Mg	%						
Mn	ppm						
Mo	ppm	2	3	3	1	1	1
Na	%						
Nb	ppm	12.7	11	11.8	30.7	49.1	39.5
Nd	ppm	32.6	27.1	32.9	21.2	41	35.7
Ni	ppm	8	15	1	130	120	73
P	ppm						
Pb	ppm		7	3	2	3	5
Pr	ppm	8.86	7.3	9	5.22	10.25	9.13
Rb	ppm	198.5	114	96.8	177	93.9	59.5
Re	ppm						
S	%						
Sb	ppm						
Sc	ppm	10	8	10	41	18	13
Se	ppm						
Sm	ppm	5.76	4.95	6.14	4.46	8.35	7.31
Sn	ppm	2	1	2	2	2	2
Sr	ppm	256	237	584	27.1	112	280
Ta	ppm	0.8	0.8	0.7	1.9	2.8	2.4
Tb	ppm	0.6	0.53	0.64	0.56	0.99	0.82
Te	ppm						
Th	ppm	12.7	10.35	11.45	3.11	5.22	4.7
Ti	%						
Tl	ppm	10	<10	<10	<10	<10	<10
Tm	ppm	0.33	0.24	0.3	0.26	0.33	0.26
U	ppm	3.43	2.23	2.38	1.66	1.5	1.75
V	ppm	146	116	132	371	252	194
W	ppm	10	1	1	7	9	1
Y	ppm	20.6	16.5	20	17.7	24.7	22.6
Yb	ppm	2.14	1.73	1.89	1.66	1.97	1.73
Zn	ppm	66	35	40	26	36	132
Zr	ppm	246	204	228	149	291	251

Major oxides are reported in weight percent normalized to 100% anhydrous. Abbreviations are same as map units in geologic map (Plate 1).
Samples "KS###" collected by Gabriel Aliaga. Samples "KTC###" and "Key XXXX" collected by Tom Chapin for U.S. Gold Corp.
[1] Whole-rock geochemistry not submitted for outcrops previously sampled to avoid repeat analyses. Equivalent sample indicated.

Appendix B – U-Pb Zircon Results

Table B1. U-Pb zircon analyses.

Analysis	U (ppm)	206Pb/204Pb	U/Th	206Pb*/207Pb*	± (%)	207Pb*/235U*	± (%)	206Pb*/238U	± (%)	error corr.	206Pb*/238U* (Ma)	± (Ma)	207Pb*/235U (Ma)	± (Ma)	206Pb*/207Pb* (Ma)	± (Ma)	Best age (Ma)	± (Ma)	Conc (%)
Sample KS014 - Walti quartz monzonite (Twq)																			
Spot 11	154	304	2.1	1298.8683	26.6	0.0005	26.6	0.0051	1.1	0.04	32.8	0.4	0.6	0.1	NA	NA	32.8	0.4	NA
Spot 20	123	674	1.9	33.7686	38.3	0.0212	38.4	0.0052	1.6	0.04	33.3	0.5	21.3	8.1	NA	NA	33.3	0.5	NA
Spot 26	69	297	2.4	156.2076	381.1	0.0046	381.1	0.0052	1.7	0.00	33.5	0.6	4.7	17.7	NA	NA	33.5	0.6	NA
Spot 12	77	583	2.2	46.6904	19.1	0.0155	19.2	0.0052	1.3	0.07	33.7	0.4	15.6	3.0	NA	NA	33.7	0.4	NA
Spot 27	182	912	1.8	32.7762	4.5	0.0220	4.8	0.0052	1.6	0.33	33.7	0.5	22.1	1.1	NA	NA	33.7	0.5	NA
Spot 1	168	2435	1.8	22.6937	6.1	0.0322	6.3	0.0053	1.3	0.20	34.0	0.4	32.1	2.0	NA	NA	34.0	0.4	NA
Spot 2	136	961	1.7	27.5482	11.4	0.0267	11.5	0.0053	1.3	0.11	34.3	0.4	26.7	3.0	NA	NA	34.3	0.4	NA
Spot 29	266	2974	2.1	17.7836	5.4	0.0413	5.5	0.0053	1.2	0.22	34.3	0.4	41.1	2.2	460.5	118.8	34.3	0.4	NA
Spot 28	170	953	1.9	32.6063	14.7	0.0226	14.8	0.0053	1.4	0.09	34.4	0.5	22.7	3.3	NA	NA	34.4	0.5	NA
Spot 22	163	4035	1.7	22.3234	4.4	0.0330	4.6	0.0053	1.2	0.27	34.4	0.4	33.0	1.5	NA	NA	34.4	0.4	NA
Spot 5	135	1070	1.8	23.6619	3.3	0.0312	3.6	0.0054	1.4	0.39	34.4	0.5	31.2	1.1	NA	NA	34.4	0.5	NA
Spot 32	158	4448	2.0	20.6818	2.8	0.0359	3.1	0.0054	1.1	0.38	34.7	0.4	35.8	1.1	115.5	66.9	34.7	0.4	NA
Spot 17	141	757	1.8	27.3030	5.6	0.0272	5.7	0.0054	1.3	0.22	34.7	0.4	27.3	1.5	NA	NA	34.7	0.4	NA
Spot 10	211	1104	1.8	26.4018	6.2	0.0282	6.3	0.0054	1.3	0.20	34.7	0.4	28.2	1.7	NA	NA	34.7	0.4	NA
Spot 33	130	5571	1.9	20.8912	3.6	0.0358	3.9	0.0054	1.3	0.33	34.8	0.4	35.7	1.4	91.7	86.3	34.8	0.4	NA
Spot 6	149	1067	1.9	25.7051	12.0	0.0291	12.1	0.0054	1.4	0.12	34.8	0.5	29.1	3.5	NA	NA	34.8	0.5	NA
Spot 23	289	1200	1.8	27.5245	8.1	0.0272	8.1	0.0054	1.2	0.15	34.9	0.4	27.2	2.2	NA	NA	34.9	0.4	NA
Spot 18	370	2337	2.3	22.7134	5.4	0.0330	5.5	0.0054	1.1	0.21	35.0	0.4	33.0	1.8	NA	NA	35.0	0.4	NA
Spot 30	110	873	2.1	32.2128	6.5	0.0233	6.6	0.0054	1.1	0.17	35.0	0.4	23.4	1.5	NA	NA	35.0	0.4	NA
Spot 4	185	372	2.0	133.2132	34.1	0.0056	34.1	0.0055	1.2	0.04	35.0	0.4	5.7	1.9	NA	NA	35.0	0.4	NA
Spot 14	145	864	1.9	22.1899	19.7	0.0341	19.7	0.0055	1.1	0.06	35.3	0.4	34.0	6.6	NA	NA	35.3	0.4	NA
Spot 24	100	22560	2.0	20.0614	3.3	0.0379	3.5	0.0055	1.3	0.37	35.5	0.5	37.8	1.3	186.8	76.6	35.5	0.5	NA
Spot 31	150	303283	1.9	19.6830	2.7	0.0387	3.0	0.0055	1.3	0.43	35.5	0.5	38.5	1.1	231.0	62.6	35.5	0.5	NA
Spot 8	155	819	1.5	15.0277	2.8	0.0507	3.1	0.0055	1.3	0.43	35.5	0.5	50.2	1.5	822.6	59.3	35.5	0.5	NA
Spot 19	150	27288	2.1	18.9859	2.9	0.0402	3.2	0.0055	1.3	0.40	35.6	0.5	40.0	1.2	313.7	65.6	35.6	0.5	NA
Spot 21	114	5866	1.9	22.7037	3.5	0.0337	3.8	0.0056	1.4	0.38	35.7	0.5	33.7	1.2	NA	NA	35.7	0.5	NA
Spot 7	72	1958	2.2	23.5876	4.4	0.0325	4.7	0.0056	1.5	0.33	35.8	0.6	32.5	1.5	NA	NA	35.8	0.6	NA
Spot 13	216	11477	1.7	17.9565	2.2	0.0430	2.4	0.0056	1.0	0.43	36.0	0.4	42.8	1.0	439.0	47.9	36.0	0.4	NA
Spot 25	187	596	1.6	12.8949	5.4	0.0602	5.5	0.0056	1.2	0.21	36.2	0.4	59.4	3.2	1134.5	107.0	36.2	0.4	NA
Spot 15	84	9084	2.1	19.5858	4.3	0.0397	4.6	0.0056	1.8	0.38	36.3	0.6	39.6	1.8	242.4	98.2	36.3	0.6	NA
Spot 35	164	410	1.8	19.7072	6.3	0.0395	6.5	0.0057	1.3	0.20	36.3	0.5	39.4	2.5	228.2	146.2	36.3	0.5	NA
Spot 9	261	48442	1.7	15.8098	3.3	0.0500	3.4	0.0057	0.8	0.25	36.8	0.3	49.5	1.6	715.8	69.1	36.8	0.3	NA
Spot 16	165	1219	1.7	17.1067	3.7	0.0472	4.0	0.0059	1.4	0.36	37.7	0.5	46.9	1.8	545.9	81.6	37.7	0.5	NA
Spot 34	134	497	1.6	5.3919	6.7	0.1667	7.0	0.0065	1.9	0.27	41.9	0.8	156.5	10.1	2701.6	111.0	41.9	0.8	NA
Spot 3	235	499	1.6	7.3978	3.1	0.1343	3.6	0.0072	1.8	0.49	46.3	0.8	128.0	4.3	2165.5	54.5	46.3	0.8	NA
Sample KS025 - Trachyandesite dikes (Tta)																			
Spot 39	208	386	1.7	124.0158	253.7	0.0057	253.7	0.0052	1.6	0.01	33.2	0.5	5.8	14.7	NA	NA	33.2	0.5	NA
Spot 64	155	561	1.7	35.3957	15.1	0.0202	15.2	0.0052	1.4	0.09	33.3	0.4	20.3	3.0	NA	NA	33.3	0.4	NA
Spot 41	100	422	2.0	83.1034	25.4	0.0087	25.4	0.0052	1.5	0.06	33.6	0.5	8.8	2.2	NA	NA	33.6	0.5	NA
Spot 63	158	631	1.7	40.3005	35.6	0.0179	35.6	0.0052	1.1	0.03	33.7	0.4	18.0	6.4	NA	NA	33.7	0.4	NA
Spot 55	107	381	1.9	113.6155	44.7	0.0064	44.7	0.0052	1.6	0.04	33.7	0.5	6.4	2.9	NA	NA	33.7	0.5	NA
Spot 49	219	692	1.5	29.9614	2.0	0.0242	2.3	0.0053	1.2	0.51	33.8	0.4	24.3	0.6	NA	NA	33.8	0.4	NA
Spot 59	146	1710	1.7	23.9371	7.2	0.0304	7.2	0.0053	0.9	0.13	33.9	0.3	30.4	2.2	NA	NA	33.9	0.3	NA
Spot 65	185	34363	1.5	19.4967	3.0	0.0374	3.1	0.0053	1.0	0.33	34.0	0.4	37.3	1.2	252.9	68.4	34.0	0.4	NA
Spot 56	218	491	1.8	57.0985	11.9	0.0128	11.9	0.0053	1.0	0.09	34.0	0.4	12.9	1.5	NA	NA	34.0	0.4	NA
Spot 36	82	789	2.2	28.8175	12.9	0.0254	13.0	0.0053	1.7	0.13	34.2	0.6	25.5	3.3	NA	NA	34.2	0.6	NA
Spot 53	240	1748	1.5	24.3619	5.4	0.0302	5.5	0.0053	1.2	0.21	34.3	0.4	30.2	1.6	NA	NA	34.3	0.4	NA
Spot 68	102	343	1.7	33.6414	10.6	0.0219	10.7	0.0053	1.4	0.13	34.4	0.5	22.0	2.3	NA	NA	34.4	0.5	NA
Spot 43	82	761	2.2	33.9598	20.7	0.0217	20.7	0.0053	1.4	0.07	34.4	0.5	21.8	4.5	NA	NA	34.4	0.5	NA
Spot 42	142	2848	1.7	21.2642	4.0	0.0347	4.2	0.0053	1.3	0.32	34.4	0.5	34.6	1.4	49.6	94.7	34.4	0.5	NA
Spot 48	147	1230	1.8	23.4906	3.7	0.0314	3.9	0.0054	1.2	0.31	34.4	0.4	31.4	1.2	NA	NA	34.4	0.4	NA
Spot 61	124	721	1.7	26.5967	6.3	0.0278	6.4	0.0054	1.3	0.20	34.5	0.5	27.8	1.8	NA	NA	34.5	0.5	NA
Spot 38	74	742	2.2	24.6829	5.4	0.0302	5.5	0.0054	1.2	0.22	34.7	0.4	30.2	1.6	NA	NA	34.7	0.4	NA
Spot 62	138	1796	1.5	23.2865	6.8	0.0320	7.0	0.0054	1.3	0.19	34.8	0.5	32.0	2.2	NA	NA	34.8	0.5	NA
Spot 52	241	4301	1.6	21.1940	2.5	0.0353	2.8	0.0054	1.3	0.45	34.9	0.4	35.2	1.0	57.4	60.1	34.9	0.4	NA
Spot 44	195	780	1.9	33.3918	15.5	0.0225	15.5	0.0054	1.2	0.08	35.0	0.4	22.6	3.5	NA	NA	35.0	0.4	NA
Spot 47	108	828	1.9	16.9659	16.8	0.0442	16.9	0.0054	1.5	0.09	35.0	0.5	43.9	7.3	564.0	368.3	35.0	0.5	NA
Spot 54	148	645	1.6	20.0752	7.5	0.0374	7.7	0.0055	1.5	0.19	35.1	0.5	37.3	2.8	185.2	175.8	35.1	0.5	NA
Spot 58	175	913	1.8	22.0689	16.6	0.0341	16.7	0.0055	1.5	0.09	35.1	0.5	34.1	5.6	NA	NA	35.1	0.5	NA
Spot 67	160	766	1.8	33.7000	19.7	0.0224	19.8	0.0055	1.1	0.05	35.2	0.4	22.5	4.4	NA	NA	35.2	0.4	NA
Spot 60	115	2518	2.3	25.4381	3.7	0.0297	3.9	0.0055	1.1	0.29	35.3	0.4	29.7	1.1	NA	NA	35.3	0.4	NA
Spot 70	216	1949	1.4	20.6907	8.3	0.0367	8.4	0.0055	0.9	0.11	35.4	0.3	36.6	3.0	114.4	196.7	35.4	0.3	NA
Spot 51	254	14259	1.6	18.8116	2.8	0.0404	3.0	0.0055	0.9	0.29	35.4	0.3	40.2	1.2	334.6	64.0	35.4	0.3	NA
Spot 37	206	3007	1.9	22.3122	3.0	0.0343	3.3	0.0055	1.2	0.37	35.6	0.4	34.2	1.1	NA	NA	35.6	0.4	NA
Spot 69	198	803	1.8	16.1687	3.3	0.0475	3.5	0.0056	1.1	0.32	35.8	0.4	47.1	1.6	667.9	71.7	35.8	0.4	NA
Spot 46	222	2493	1.4	21.9912	4.0	0.0352	4.1	0.0056	1.1	0.26	36.1	0.4	35.1	1.4	NA	NA	36.1	0.4	NA
Spot 66	119	6336	2.1	22.0849	3.5	0.0353	3.8	0.0057	1.5	0.40	36.4	0.5	35.2	1.3	NA	NA	36.4	0.5	NA
Spot 57	191	18340	1.6	14.6072	4.5	0.0537	4.7	0.0057	1.5	0.32	36.6	0.5	53.2	2.4	881.6	92.1	36.6	0.5	NA
Spot 45	212	959	1.6	15.1879	8.3	0.0518	8.3	0.0057	1.0	0.12	36.7	0.4	51.2	4.2	800.4	173.4	36.7	0.4	NA
Spot 40	355	3830	1.7	20.3805	1.8	0.0392	2.1	0.0058	1.0	0.46	37.2	0.4	39.0	0.8	150.0	43.0	37.2	0.4	NA
Spot 50	168	331	1.5	8.6170	13.9	0.0947	14.7	0.0059	4.8	0.33	38.0	1.8	91.9	12.9	1895.4	250.6	38.0	1.8	NA
Sample KS044 - Rhyolite porphyry (Trp)																			
Spot 29	2130	4336	1.9	20.3030	1.5	0.0357	1.8	0.0053	1.0	0.54	33.9	0.3	35.7	0.6	158.9	36.2	33.9	0.3	NA
Spot 27	3217	138058	2.9	20.3343	0.7	0.0370	1.1	0.0055	0.8	0.74	35.1	0.3	36.9	0.4	155.3	17.4	35.1	0.3	NA
Spot 33	2586	7570	3.1	21.1728	0.7	0.0355	1.1	0.0055	0.8	0.73	35.1	0.3	35.4	0.4	59.9	17.3	35.1	0.3	NA
Spot 5	147	2058	1.9	21.8590	3.5	0.0344	3.7	0.0055	1.1	0.29	35.1	0.4	34.4	1.2	NA	NA	35.1	0.4	NA
Spot 9	3440	24040	3.8	21.1583	0.8	0.0360	1.1	0.0055	0.8	0.70	35.6	0.3	35.9	0.4	61.5	18.5	35.6	0.3	NA
Spot 26	1409	24348	3.7	20.9622	1.0	0.0364	1.2	0.0055	0.6	0.52	35.6	0.2	36.3	0.4	83.6	23.9	35.6	0.2	NA
Spot 19	581	15999	1.8	20.0677	1.5	0.0380	1.8	0.0055	1.0	0.54	35.6	0.3	37.9	0.7	186.1	35.3	35.6	0.3	NA
Spot 14	3593	17350	3.1	21.1106	1.0	0.0362	1.3	0.0055	0.9	0.67	35.6	0.3	36.1	0.5	66.8	23.5	35.6	0.3	NA
Spot 6	4228	17633	2.0	21.4136	0.6	0.0360	1.0	0.0056	0.7	0.77	35.9	0.3	35.9	0.3	32.8	14.8	35.9	0.3	NA
Spot 28	3297	22007	3.1	21.3024	1.1	0.0362	1.5	0.0056	1.0	0.67	36.0	0.4	36.1	0.5	45.3	27.3	36.0	0.4	NA
Spot 16	2119	49228	3.8	20.5787	1.0	0.0375	1.4	0.0056	0.9	0.67	36.0	0.3	37.4	0.5	127.3	24.2	36.0	0.3	NA
Spot 30	2398	12947	3.3	20.6188	1.0	0.0375	1.4	0.0056	1.0	0.73	36.0	0.4	37.3	0.5	122.7	22.9	36.0	0.4	NA
Spot 34	3254	13047	2.2	21.1353	1.2	0.0366	1.4	0.0056	0.8	0.58	36.1	0.3	36.5	0.5	64.1	27.5	36.1	0.3	NA
Spot 10	4916	30596	3.6	21.3035	0.9	0.0364	1.2	0.0056	0.8	0.68	36.1	0.3	36.3	0.4	45.1	21.7	36.1	0.3	NA
Spot 35	3979	13172	2.7	21.4586	0.8	0.0361	1.1	0.0056	0.8	0.74	36.2	0.3	36.0	0.4	27.8	18.3	36.2	0.3	NA
Spot 11	3945	11202	2.4	21.6946	0.8	0.0357	1.1	0.0056	0.8	0.71	36.2	0.3	35.7	0.4	1.5	18.2	36.2	0.3	NA
Spot 23	3419	30307	3.2	21.1165	0.9	0.0367	1.2	0.0056	0.8	0.69	36.2	0.3	36.6	0.4	66.2	20.9	36.2	0.3	NA
Spot 13	3658	41387	2.6	21.0770	0.8	0.0369	1.2	0.0056	0.9	0.75	36.2	0.3	36.7	0.4	70.7	19.5	36.2	0.3	NA
Spot 18	2902	236709	3.2	20.9100	0.7	0.0372	1.1	0.0056	0.8	0.73	36.3	0.3	37.1	0.4	89.6	17.6	36.3	0.3	NA
Spot 25	3115	50491	3.8	21.0912	0.9	0.0369	1.3	0.0057	1.0	0.74	36.3	0.4	36.8	0.5	69.1	20.8	36.3	0.4	NA
Spot 24	1889	42947	2.7	21.2745	0.9	0.0366	1.3	0.0057	0.9	0.71	36.3	0.3	36.5	0.5	48.4	21.0	36.3	0.3	NA

Table B1. U-Pb zircon analyses.

Analysis	U (ppm)	206Pb/204Pb	U/Th	206Pb*/207Pb*	± (%)	Isotope ratios 207Pb*/235U*	± (%)	206Pb*/238U	± (%)	error corr.	Apparent ages (Ma) 206Pb*/238U*	± (Ma)	207Pb*/235U	± (Ma)	206Pb*/207Pb*	± (Ma)	Best age (Ma)	± (Ma)	Conc (%)
Spot 17	2406	40271	3.2	21.2089	1.0	0.0368	1.3	0.0057	0.9	0.66	36.4	0.3	36.7	0.5	55.8	23.4	36.4	0.3	NA
Spot 8	4121	7001	2.4	20.9396	1.1	0.0374	1.4	0.0057	1.0	0.68	36.6	0.4	37.3	0.5	86.2	25.3	36.6	0.4	NA
Spot 7	1648	13516	3.5	20.8818	1.2	0.0376	1.4	0.0057	0.7	0.48	36.7	0.2	37.5	0.5	92.7	29.2	36.7	0.2	NA
Spot 4	1563	130552	3.4	20.9628	1.0	0.0376	1.4	0.0057	0.9	0.69	36.7	0.3	37.5	0.5	83.5	23.4	36.7	0.3	NA
Spot 31	208	4086	2.3	20.8241	2.5	0.0379	2.7	0.0057	1.0	0.38	36.8	0.4	37.7	1.0	99.3	58.5	36.8	0.4	NA
Spot 12	1132	16020	4.2	19.6395	1.5	0.0402	1.9	0.0057	1.2	0.65	36.8	0.5	40.0	0.8	236.1	33.6	36.8	0.5	NA
Spot 3	2816	61401	2.8	20.8414	0.8	0.0379	1.1	0.0057	0.8	0.71	36.9	0.3	37.8	0.4	97.3	19.0	36.9	0.3	NA
Spot 15	1694	5587	2.5	21.9587	1.0	0.0360	1.4	0.0057	0.9	0.68	36.9	0.3	35.9	0.5	NA	NA	36.9	0.3	NA
Spot 32	2551	8654	3.5	21.1195	1.5	0.0374	1.7	0.0057	0.8	0.48	36.9	0.3	37.3	0.6	65.9	35.4	36.9	0.3	NA
Spot 22	193	654	2.1	13.3840	10.5	0.0592	10.6	0.0057	1.5	0.14	37.0	0.5	58.4	6.0	1060.0	211.6	37.0	0.5	NA
Spot 1	3279	7866	2.9	22.0347	0.8	0.0360	1.3	0.0058	1.0	0.77	37.0	0.4	35.9	0.5	NA	NA	37.0	0.4	NA
Spot 20	1455	10297	3.6	21.4431	1.5	0.0373	1.7	0.0058	0.8	0.48	37.3	0.3	37.2	0.6	29.6	35.5	37.3	0.3	NA
Spot 21	320	29226	2.9	20.5326	2.1	0.0391	2.5	0.0058	1.4	0.55	37.5	0.5	39.0	1.0	132.5	50.1	37.5	0.5	NA
Spot 2	379	30968	3.1	20.9540	2.0	0.0387	2.2	0.0059	1.0	0.44	37.8	0.4	38.6	0.8	84.5	48.0	37.8	0.4	NA
Sample KS050 - Aphyric rhyolite (Tvc)																			
Spot 122	248	602	2.2	44.0838	56.3	0.0165	56.3	0.0053	1.3	0.02	34.0	0.4	16.6	9.3	NA	NA	34.0	0.4	NA
Spot 118	242	506	2.6	42.7517	65.2	0.0172	65.2	0.0054	1.3	0.02	34.4	0.4	17.4	11.2	NA	NA	34.4	0.4	NA
Spot 110	323	1438	1.7	22.5066	4.6	0.0328	4.8	0.0054	1.3	0.27	34.5	0.4	32.8	1.5	NA	NA	34.5	0.4	NA
Spot 123	219	2105	3.1	24.4529	4.1	0.0304	4.3	0.0054	1.2	0.29	34.7	0.4	30.4	1.3	NA	NA	34.7	0.4	NA
Spot 128	243	786	3.0	31.1818	4.3	0.0239	4.5	0.0054	1.3	0.29	34.7	0.5	24.0	1.1	NA	NA	34.7	0.5	NA
Spot 127	222	772	2.6	34.9889	4.3	0.0213	4.5	0.0054	1.4	0.31	34.7	0.5	21.4	0.9	NA	NA	34.7	0.5	NA
Spot 101	236	418	2.9	39.9913	29.5	0.0187	29.5	0.0054	1.2	0.04	34.9	0.4	18.8	5.5	NA	NA	34.9	0.4	NA
Spot 121	418	2441	0.9	22.9710	6.4	0.0327	6.7	0.0054	1.8	0.28	35.0	0.6	32.7	2.1	NA	NA	35.0	0.6	NA
Spot 117	362	2581	2.8	23.4869	3.4	0.0320	3.5	0.0055	1.0	0.28	35.1	0.3	32.0	1.1	NA	NA	35.1	0.3	NA
Spot 103	333	2057	2.6	22.4256	2.5	0.0335	2.7	0.0055	1.1	0.40	35.1	0.4	33.5	0.9	NA	NA	35.1	0.4	NA
Spot 116	514	1415	0.9	27.0642	1.7	0.0280	2.0	0.0055	1.1	0.56	35.3	0.4	28.0	0.6	NA	NA	35.3	0.4	NA
Spot 133	247	1622	2.8	23.1116	4.6	0.0328	4.7	0.0055	1.3	0.27	35.4	0.4	32.8	1.5	NA	NA	35.4	0.4	NA
Spot 108	237	4614	2.7	21.6167	2.8	0.0351	2.9	0.0055	1.0	0.34	35.4	0.4	35.0	1.0	10.2	66.4	35.4	0.4	NA
Spot 102	164	961	2.1	30.7782	3.2	0.0248	3.9	0.0055	2.1	0.54	35.7	0.7	24.9	1.0	NA	NA	35.7	0.7	NA
Spot 130	470	1174	2.8	25.4036	16.3	0.0302	16.4	0.0056	1.3	0.08	35.8	0.5	30.2	4.9	NA	NA	35.8	0.5	NA
Spot 126	259	2293	2.9	25.1764	2.5	0.0305	2.8	0.0056	1.1	0.40	35.8	0.4	30.5	0.8	NA	NA	35.8	0.4	NA
Spot 131	312	2302	1.6	23.6863	7.9	0.0325	8.0	0.0056	1.0	0.12	35.9	0.4	32.4	2.5	NA	NA	35.9	0.4	NA
Spot 135	243	835	3.0	33.5712	19.6	0.0229	19.6	0.0056	1.1	0.06	35.9	0.4	23.0	4.5	NA	NA	35.9	0.4	NA
Spot 112	271	1740	2.2	24.8409	5.9	0.0310	6.0	0.0056	1.1	0.18	35.9	0.4	31.0	1.8	NA	NA	35.9	0.4	NA
Spot 104	153	2104	2.4	21.3224	3.7	0.0361	4.2	0.0056	1.8	0.44	35.9	0.7	36.0	1.5	43.0	89.1	35.9	0.7	NA
Spot 132	219	22159	1.5	20.2726	2.3	0.0381	2.7	0.0056	1.3	0.49	36.0	0.5	37.9	1.0	162.4	54.6	36.0	0.5	NA
Spot 107	262	3704	2.7	23.1217	2.6	0.0334	2.9	0.0056	1.2	0.41	36.1	0.4	33.4	0.9	NA	NA	36.1	0.4	NA
Spot 109	229	9350	2.0	21.6762	3.0	0.0358	3.2	0.0056	1.2	0.37	36.1	0.4	35.7	1.1	3.5	72.7	36.1	0.4	NA
Spot 105	220	39975	1.4	20.1856	2.6	0.0385	2.9	0.0056	1.3	0.45	36.2	0.5	38.4	1.1	172.4	60.4	36.2	0.5	NA
Spot 114	319	2575	3.0	20.2751	4.2	0.0385	4.4	0.0057	1.1	0.25	36.4	0.4	38.4	1.7	162.1	99.2	36.4	0.4	NA
Spot 120	192	3696	2.9	17.6230	3.2	0.0443	3.4	0.0057	1.2	0.35	36.4	0.4	44.0	1.5	480.6	70.6	36.4	0.4	NA
Spot 119	274	1340	2.9	28.8651	2.5	0.0271	2.9	0.0057	1.4	0.48	36.4	0.5	27.1	0.8	NA	NA	36.4	0.5	NA
Spot 106	185	1996	2.2	25.1874	3.1	0.0312	3.3	0.0057	1.2	0.36	36.6	0.4	31.2	1.0	NA	NA	36.6	0.4	NA
Spot 115	323	8106	3.3	21.6435	2.3	0.0365	2.7	0.0057	1.3	0.49	36.8	0.5	36.4	1.0	7.2	56.3	36.8	0.5	NA
Spot 125	481	5732	1.7	19.8014	3.0	0.0402	3.4	0.0058	1.6	0.46	37.1	0.6	40.0	1.3	217.1	69.5	37.1	0.6	NA
Spot 124	194	1736	1.9	14.7380	5.6	0.0545	5.8	0.0058	1.5	0.27	37.4	0.6	53.8	3.0	863.2	116.2	37.4	0.6	NA
Spot 111	244	5017	2.4	17.5398	2.5	0.0464	2.9	0.0059	1.5	0.50	38.0	0.6	46.1	1.3	491.1	55.7	38.0	0.6	NA
Spot 129	1308	35283	3.4	21.2539	1.0	0.0827	1.4	0.0127	0.9	0.68	81.7	0.7	80.6	1.0	50.7	23.7	81.7	0.7	NA
Spot 113	79	1738	2.8	10.6435	2.7	0.6553	4.4	0.0506	3.4	0.79	318.3	10.7	511.8	17.6	1506.4	50.9	318.3	10.7	NA
Spot 134	226	8593	3.2	9.8956	1.1	0.9555	1.9	0.0686	1.5	0.80	427.7	6.2	681.0	9.4	1642.8	21.1	1642.8	21.1	26.0
Sample KS051 - Dacite agglomerate (Tda)																			
Spot 52	57	135	1.9	14.239	7.14	0.04525	7.40	0.00468	1.94	0.26	30.1	0.6	44.9	3.3	934.2	146.7	30.1	0.6	NA
Spot 54	56	170	2.1	23.718	13.26	0.02817	13.44	0.00485	2.18	0.16	31.2	0.7	28.2	3.7	-217.9	334.7	31.2	0.7	NA
Spot 68	47	157	2.4	18.912	5.90	0.03598	6.15	0.00494	1.71	0.28	31.7	0.5	35.9	2.2	322.5	134.2	31.7	0.5	NA
Spot 39	39	141	2.0	16.825	37.84	0.04097	37.88	0.00500	1.72	0.05	32.2	0.6	40.8	15.1	582.2	850.5	32.2	0.6	NA
Spot 36	58	245	1.5	107.7096	19.1	0.0065	19.2	0.0051	1.9	0.10	32.5	0.6	6.5	1.3	NA	NA	32.5	0.6	NA
Spot 51	40	190	2.0	57.390	39.72	0.01215	39.77	0.00506	2.06	0.05	32.5	0.7	12.3	4.8	0.0	NA	32.5	0.7	NA
Spot 62	56	247	1.8	785.3285	124.3	0.0009	124.3	0.0051	1.5	0.01	32.7	0.5	0.9	1.1	NA	NA	32.7	0.5	NA
Spot 65	52	266	2.0	5936.8440	3597.1	0.0001	3597.1	0.0052	1.7	0.00	33.3	0.5	0.1	4.4	NA	NA	33.3	0.5	NA
Spot 66	42	607	1.9	32.0726	8.9	0.0225	9.1	0.0052	2.0	0.22	33.7	0.7	22.6	2.0	NA	NA	33.7	0.7	NA
Spot 63	51	218	1.7	257.2167	6.3	0.0028	6.5	0.0052	1.5	0.23	33.7	0.5	2.9	0.2	NA	NA	33.7	0.5	NA
Spot 37	58	394	2.3	44.0557	12.6	0.0165	12.8	0.0053	1.9	0.15	33.9	0.6	16.6	2.1	NA	NA	33.9	0.6	NA
Spot 70	51	440	2.0	84.3056	12.0	0.0086	12.2	0.0053	2.0	0.17	34.0	0.7	8.7	1.1	NA	NA	34.0	0.7	NA
Spot 67	44	302	1.6	52.3428	91.2	0.0140	91.3	0.0053	2.0	0.02	34.2	0.7	14.1	12.8	NA	NA	34.2	0.7	NA
Spot 41	50	621	1.9	38.0871	9.6	0.0193	9.8	0.0053	1.7	0.18	34.4	0.6	19.5	1.9	NA	NA	34.4	0.6	NA
Spot 64	50	621	2.1	32.9393	5.5	0.0224	5.7	0.0054	1.5	0.27	34.4	0.5	22.5	1.3	NA	NA	34.4	0.5	NA
Spot 56	60	856	2.0	21.5279	16.0	0.0343	16.1	0.0054	1.7	0.10	34.4	0.6	34.2	5.4	20.1	387.0	34.4	0.6	NA
Spot 57	48	584	1.9	29.1668	16.3	0.0253	16.4	0.0054	1.6	0.10	34.4	0.6	25.4	4.1	NA	NA	34.4	0.6	NA
Spot 42	56	360	1.5	60.8370	68.5	0.0122	68.6	0.0054	1.4	0.02	34.6	0.5	12.3	8.4	NA	NA	34.6	0.5	NA
Spot 60	46	2663	2.2	20.9378	3.8	0.0356	4.1	0.0054	1.4	0.35	34.7	0.5	35.5	1.4	86.4	91.2	34.7	0.5	NA
Spot 58	50	1465	1.6	23.2539	7.1	0.0321	7.3	0.0054	1.9	0.27	34.8	0.7	32.0	2.3	NA	NA	34.8	0.7	NA
Spot 55	228	38593	1.2	20.4266	2.4	0.0365	2.7	0.0054	1.1	0.40	34.8	0.4	36.4	1.0	144.7	57.2	34.8	0.4	NA
Spot 40	47	319	1.6	233.9748	281.1	0.0032	281.1	0.0054	2.1	0.01	34.9	0.7	3.2	9.1	NA	NA	34.9	0.7	NA
Spot 53	61	591	1.6	27.0782	16.7	0.0279	16.8	0.0055	1.5	0.09	35.2	0.5	27.9	4.6	NA	NA	35.2	0.5	NA
Spot 44	47	685	1.8	28.7798	10.0	0.0263	10.1	0.0055	1.8	0.18	35.3	0.6	26.4	2.6	NA	NA	35.3	0.6	NA
Spot 69	58	17086	2.0	18.3214	5.9	0.0416	6.2	0.0055	1.8	0.30	35.5	0.7	41.4	2.5	394.1	131.8	35.5	0.7	NA
Spot 43	57	19724	1.6	17.7949	5.5	0.0432	5.8	0.0056	1.8	0.31	35.8	0.7	42.9	2.5	459.2	122.9	35.8	0.7	NA
Spot 47	54	3489	2.1	21.0440	4.2	0.0366	4.6	0.0056	1.7	0.37	35.9	0.6	36.5	1.6	74.4	100.9	35.9	0.6	NA
Spot 45	58	2565	1.9	19.0779	6.9	0.0406	7.0	0.0056	1.6	0.22	36.2	0.6	40.5	2.8	302.7	156.6	36.2	0.6	NA
Spot 61	49	2546	2.4	26.5399	4.3	0.0299	4.6	0.0058	1.8	0.39	37.0	0.7	29.9	1.4	NA	NA	37.0	0.7	NA
Spot 48	46	1967	2.2	24.8245	5.1	0.0320	5.4	0.0058	1.8	0.33	37.1	0.7	32.0	1.7	NA	NA	37.1	0.7	NA
Spot 49	58	803	1.6	15.1954	6.4	0.0527	6.7	0.0058	2.0	0.29	37.3	0.7	52.1	3.4	799.4	135.1	37.3	0.7	NA
Spot 46	50	285	1.1	8.7051	8.2	0.0949	8.6	0.0060	2.5	0.29	38.5	1.0	92.0	7.6	1877.1	148.1	38.5	1.0	NA
Spot 50	29	90	2.1	3.999	18.23	0.26871	18.61	0.00780	3.77	0.20	50.1	1.9	241.7	40.0	3184.5	291.3	50.1	1.9	NA
Spot 38	55	1696	2.3	17.9720	5.2	0.0624	6.5	0.0081	4.0	0.61	52.2	2.1	61.5	3.9	437.1	115.4	52.2	2.1	NA
Spot 59	55	244	1.6	2.8817	3.6	0.4121	4.9	0.0086	3.2	0.66	55.3	1.8	350.4	14.4	3693.3	55.6	55.3	1.8	NA
Sample KS126 - Walti intermediate porphyritic dikes (Twp)																			
Spot 84	6941	29996	2.6	21.3908	0.8	0.0310	1.1	0.0048	0.8	0.68	31.0	0.2	31.0	0.3	35.4	20.0	31.0	0.2	NA
Spot 59	6625	11105	2.8	21.3796	0.9	0.0313	1.4	0.0049	1.1	0.75	31.3	0.3	31.3	0.4	36.6	22.1	31.3	0.3	NA
Spot 71	5963	25419	2.8	21.2463	0.9	0.0323	1.5	0.0050	1.1	0.79	32.0	0.3	32.3	0.5	51.6	21.4	32.0	0.4	NA
Spot 79	6248	35009	3.2	21.2802	0.8	0.0325	1.3	0.0050	1.1	0.79	32.3	0.3	32.5	0.4	47.8	19.2	32.3	0.3	NA
Spot 56	5801	12969	3.0	21.4652	0.8	0.0324	1.0	0.0051	0.7	0.65	32.5	0.2	32.4	0.3	27.0	18.8	32.5	0.2	NA
Spot 63	5533	35206	2.6	21.7286	0.9	0.0321	1.4	0.0051	1.1	0.78	32.6	0.4	32.1	0.5	NA	NA	32.6	0.4	NA
Spot 51	4878	9134	3.0	21.8071	1.6	0.0323	2.0	0.0051	1.1	0.55	32.9	0.4	32.3	0.6	NA	NA	32.9	0.4	NA
Spot 60	4986	10395	2.4	21.8194	0.8	0.0324	1.5	0.0051	1.3	0.84	33.0	0.4	32.4	0.5	NA	NA	33.0	0.4	NA
Spot 68	4259	32164	3.3	21.1737	0.9	0.0337	1.2	0.0052	0.9	0.75	33.3	0.3	33.6	0.4	59.8	18.6	33.3	0.3	NA
Spot 83	4624	15990	3.6	21.7009	1.0	0.0329	1.4	0.0052	1.0	0.69	33.3	0.3	32.9	0.5	NA	NA	33.3	0.3	NA
Spot 64	4301	11715	3.4	21.7561	0.9	0.0329	1.4	0.0052	1.1	0.78	33.4	0.4	32.9	0.5	NA	NA	33.4	0.4	NA
Spot 75	4308	38348	2.1	21.3369	0.8	0.0337	1.2	0.0052	0.9	0.75	33.6	0.3	33.7	0.4	41.4	19.5	33.6	0.3	NA
Spot 58	3226	21517	3.3	21.3800	1.0	0.0338	1.5	0.0052	1.1	0.75	33.7	0.4	33.8	0.5	36.6	23.8	33.7	0.4	NA

Table B1. U-Pb zircon analyses.

Analysis	U (ppm)	206Pb/204Pb	U/Th	206Pb*/207Pb*	±(%)	207Pb*/235U*	±(%)	206Pb*/238U	±(%)	error corr.	206Pb*/238U* (Ma)	±(Ma)	207Pb*/235U (Ma)	±(Ma)	206Pb*/207Pb* (Ma)	±(Ma)	Best age (Ma)	±(Ma)	Conc (%)
Spot 62	4076	13440	3.2	21.6825	0.7	0.0335	1.2	0.0053	1.0	0.82	33.9	0.3	33.5	0.4	2.8	17.1	33.9	0.3	NA
Spot 78	4180	65197	2.0	21.2294	0.8	0.0343	1.3	0.0053	1.1	0.80	33.9	0.4	34.2	0.5	53.5	19.3	33.9	0.4	NA
Spot 55	141	1237	0.9	23.0520	5.5	0.0316	5.6	0.0053	1.2	0.22	34.0	0.4	31.6	1.8	NA	NA	34.0	0.4	NA
Spot 57	4067	133043	2.5	21.3462	1.0	0.0343	1.5	0.0053	1.1	0.76	34.1	0.4	34.2	0.5	40.4	23.0	34.1	0.4	NA
Spot 80	3456	1090466	3.3	21.2812	0.7	0.0348	1.2	0.0054	1.0	0.82	34.5	0.4	34.7	0.4	47.7	16.8	34.5	0.4	NA
Spot 81	3408	17086	2.4	21.0879	1.1	0.0351	1.7	0.0054	1.3	0.76	34.5	0.4	35.0	0.6	69.4	25.7	34.5	0.4	NA
Spot 67	2739	17496	3.2	21.3086	1.2	0.0348	1.6	0.0054	1.0	0.64	34.6	0.3	34.7	0.6	44.6	29.0	34.6	0.3	NA
Spot 65	2409	233807	2.6	21.2572	0.9	0.0349	1.3	0.0054	0.9	0.70	34.6	0.3	34.8	0.4	50.3	21.8	34.6	0.3	NA
Spot 61	3650	19783	2.4	21.4470	0.9	0.0346	1.2	0.0054	0.9	0.70	34.7	0.3	34.6	0.4	29.1	21.1	34.7	0.3	NA
Spot 70	3061	25251	2.7	21.3371	0.9	0.0348	1.4	0.0054	1.1	0.80	34.7	0.4	34.8	0.5	41.4	20.7	34.7	0.4	NA
Spot 72	3496	23262	2.7	21.4838	1.2	0.0348	1.6	0.0054	1.1	0.67	34.9	0.4	34.7	0.5	25.0	28.3	34.9	0.4	NA
Spot 74	2064	16369	2.4	19.7888	1.4	0.0379	1.7	0.0054	1.0	0.60	34.9	0.4	37.7	0.6	218.6	31.7	34.9	0.4	NA
Spot 85	140	771	0.9	36.7093	6.6	0.0204	6.8	0.0054	1.5	0.22	35.0	0.3	20.6	1.4	NA	NA	35.0	0.5	NA
Spot 54	2076	13010	3.2	21.0263	0.9	0.0357	1.3	0.0055	1.0	0.71	35.0	0.3	35.6	0.5	76.4	22.3	35.0	0.3	NA
Spot 77	2705	34889	3.1	21.4281	1.2	0.0353	1.4	0.0055	0.8	0.58	35.2	0.3	35.2	0.5	31.2	28.4	35.2	0.3	NA
Spot 82	2505	15559	2.9	21.6467	1.0	0.0349	1.4	0.0055	0.9	0.68	35.3	0.3	34.9	0.5	6.8	24.7	35.3	0.3	NA
Spot 69	173	5640	1.5	19.0050	3.5	0.0399	3.7	0.0055	1.2	0.31	35.4	0.4	39.7	1.5	311.4	80.8	35.4	0.4	NA
Spot 53	1795	33219	3.3	21.1980	1.0	0.0360	1.7	0.0055	1.3	0.78	35.6	0.5	35.9	0.6	57.0	24.7	35.6	0.5	NA
Spot 52	1965	25537	3.6	21.1134	1.1	0.0363	1.5	0.0056	1.0	0.68	35.8	0.4	36.2	0.5	66.5	25.6	35.8	0.4	NA
Spot 73	2298	37725	3.4	20.8830	1.0	0.0370	1.3	0.0056	0.9	0.70	36.0	0.3	36.9	0.5	92.6	22.7	36.0	0.3	NA
Spot 76	269	1026	1.7	12.0417	4.6	0.0658	4.7	0.0057	1.2	0.25	36.9	0.4	64.7	2.9	1269.4	88.9	36.9	0.4	NA
Spot 66	89	1004	0.8	12.0853	9.3	0.0655	9.5	0.0057	1.9	0.20	36.9	0.7	64.5	5.9	1262.3	182.7	36.9	0.7	NA
Sample KS048 - Tertiary Conglomerate (Tcg)																			
Spot 180	292	3136	1.7	20.7358	4.4	0.0271	4.7	0.0041	1.7	0.36	26.2	0.4	27.1	1.3	109.4	102.9	26.2	0.4	NA
Spot 40	13028	23054	4.3	21.3817	0.8	0.0290	1.2	0.0045	0.9	0.76	29.0	0.3	29.1	0.3	36.4	18.9	29.0	0.3	NA
Spot 35	12156	365892	4.9	21.0992	0.7	0.0302	1.7	0.0046	1.5	0.90	29.8	0.4	30.2	0.5	68.2	17.8	29.8	0.4	NA
Spot 0	388	864	1.7	10.4557	14.1	0.0640	14.3	0.0049	2.5	0.17	31.2	0.8	63.0	8.8	1539.9	266.9	31.2	0.8	NA
Spot 132	8858	27358	4.3	21.3410	0.8	0.0319	1.6	0.0049	1.4	0.86	31.8	0.4	31.9	0.5	41.0	20.0	31.8	0.4	NA
Spot 12	6659	40693	4.0	21.1749	0.8	0.0333	1.2	0.0051	0.8	0.68	32.9	0.3	33.3	0.4	59.6	20.2	32.9	0.3	NA
Spot 15	163	1943	0.7	23.2104	4.1	0.0312	4.4	0.0053	1.4	0.32	33.8	0.5	31.2	1.3	NA	NA	33.8	0.5	NA
Spot 170	3333	8374	3.6	21.9539	1.3	0.0332	1.8	0.0053	1.2	0.69	34.0	0.4	33.1	0.6	NA	NA	34.0	0.4	NA
Spot 133	737	1989	2.6	22.6901	8.7	0.0321	8.8	0.0053	1.5	0.17	34.0	0.5	32.1	2.8	NA	NA	34.0	0.5	NA
Spot 42	4411	16589	3.3	21.6826	0.9	0.0337	1.5	0.0053	1.1	0.77	34.1	0.4	33.6	0.5	2.8	22.7	34.1	0.4	NA
Spot 153	513	2109	1.1	24.1397	3.5	0.0303	3.8	0.0053	1.6	0.41	34.2	0.5	30.3	1.1	NA	NA	34.2	0.5	NA
Spot 75	2231	59912	4.8	21.2246	1.2	0.0345	1.7	0.0053	1.2	0.70	34.2	0.4	34.4	0.6	54.0	28.6	34.2	0.4	NA
Spot 195	2848	9097	3.0	21.3033	0.9	0.0344	1.4	0.0053	1.0	0.75	34.2	0.3	34.4	0.5	45.2	21.4	34.2	0.3	NA
Spot 159	2771	19102	4.7	21.1600	1.1	0.0347	1.6	0.0053	1.1	0.71	34.3	0.4	34.6	0.6	61.3	27.3	34.3	0.4	NA
Spot 81	622	1426	2.6	30.2406	3.6	0.0244	3.8	0.0053	1.4	0.38	34.4	0.5	24.4	0.9	NA	NA	34.4	0.5	NA
Spot 61	503	1048	1.9	20.5758	6.5	0.0358	6.8	0.0053	1.8	0.27	34.4	0.6	35.7	2.4	127.6	154.1	34.4	0.6	NA
Spot 96	2872	8122	3.4	21.7313	1.6	0.0339	2.0	0.0054	1.2	0.60	34.4	0.4	33.9	0.7	NA	NA	34.4	0.4	NA
Spot 25	252	478	2.9	60.7021	5.4	0.0122	5.6	0.0054	1.2	0.21	34.4	0.4	12.3	0.7	NA	NA	34.4	0.4	NA
Spot 82	725	6421	0.7	21.8758	2.5	0.0338	2.8	0.0054	1.2	0.42	34.5	0.4	33.7	0.9	NA	NA	34.5	0.4	NA
Spot 107	3729	27103	3.1	21.0124	1.0	0.0352	1.4	0.0054	1.0	0.73	34.5	0.4	35.1	0.5	77.9	23.3	34.5	0.4	NA
Spot 196	3017	13442	3.3	20.5404	1.2	0.0360	1.6	0.0054	1.1	0.69	34.5	0.4	35.9	0.6	131.7	27.8	34.5	0.4	NA
Spot 176	352	1183	2.8	27.1002	12.5	0.0273	12.6	0.0054	1.4	0.11	34.5	0.5	27.4	3.4	NA	NA	34.5	0.5	NA
Spot 93	814	2350	2.2	23.8108	7.8	0.0312	7.9	0.0054	1.0	0.13	34.6	0.4	31.2	2.4	NA	NA	34.6	0.4	NA
Spot 37	2806	8413	2.9	21.7621	1.9	0.0341	2.3	0.0054	1.3	0.55	34.6	0.4	34.1	0.8	NA	NA	34.6	0.4	NA
Spot 9	543	11982	1.3	21.6346	2.1	0.0344	2.5	0.0054	1.3	0.54	34.7	0.5	34.3	0.8	8.2	50.1	34.7	0.5	NA
Spot 32	3823	35826	2.9	21.3066	1.0	0.0349	1.5	0.0054	1.1	0.75	34.7	0.4	34.8	0.5	44.8	24.3	34.7	0.4	NA
Spot 8	604	1483	2.0	26.8153	2.5	0.0277	2.9	0.0054	1.4	0.49	34.7	0.4	27.8	0.8	NA	NA	34.7	0.4	NA
Spot 198	386	1220	2.5	27.5371	2.9	0.0270	3.2	0.0054	1.3	0.40	34.7	0.4	27.1	0.8	NA	NA	34.7	0.4	NA
Spot 85	233	789	5.0	26.6373	7.1	0.0279	7.2	0.0054	1.3	0.19	34.7	0.5	28.0	2.0	NA	NA	34.7	0.5	NA
Spot 83	3430	6930	5.0	22.3174	1.0	0.0334	1.5	0.0054	1.2	0.77	34.7	0.4	33.3	0.5	NA	NA	34.7	0.4	NA
Spot 90	761	7806	2.6	22.1051	1.8	0.0337	2.1	0.0054	1.1	0.54	34.7	0.4	33.6	0.7	NA	NA	34.7	0.4	NA
Spot 173	3706	12659	4.4	21.8328	1.0	0.0341	1.5	0.0054	1.1	0.74	34.7	0.4	34.1	0.5	NA	NA	34.7	0.4	NA
Spot 157	3305	13610	3.4	21.6053	0.8	0.0345	1.4	0.0054	1.1	0.81	34.8	0.4	34.4	0.5	11.4	20.1	34.8	0.4	NA
Spot 155	872	8928	1.0	21.9738	1.9	0.0340	2.5	0.0054	1.7	0.67	34.8	0.6	33.9	0.8	NA	NA	34.8	0.6	NA
Spot 136	2720	5473	4.4	21.9899	1.1	0.0340	1.7	0.0054	1.2	0.74	34.9	0.4	33.9	0.6	NA	NA	34.9	0.4	NA
Spot 192	1468	41555	3.7	20.8076	1.3	0.0359	1.8	0.0054	1.3	0.71	34.9	0.4	35.8	0.6	101.1	30.4	34.9	0.4	NA
Spot 67	1070	9633	1.2	20.0183	2.5	0.0374	2.7	0.0054	1.1	0.41	34.9	0.4	37.3	1.0	191.9	58.2	34.9	0.4	NA
Spot 191	331	675	3.1	33.9040	3.7	0.0221	4.0	0.0054	1.6	0.40	34.9	0.6	22.2	0.9	NA	NA	34.9	0.6	NA
Spot 193	90	496	1.3	66.2656	7.1	0.0113	7.4	0.0054	2.1	0.29	34.9	0.7	11.4	0.8	NA	NA	34.9	0.7	NA
Spot 51	2661	12434	4.3	21.7625	1.0	0.0345	1.5	0.0054	1.0	0.71	35.0	0.4	34.4	0.5	NA	NA	35.0	0.4	NA
Spot 34	360	838	2.6	35.0724	6.2	0.0214	6.4	0.0055	1.3	0.20	35.1	0.4	21.5	1.4	NA	NA	35.1	0.4	NA
Spot 28	664	1341	0.9	27.1536	4.5	0.0277	4.8	0.0055	1.5	0.31	35.1	0.5	27.7	1.3	NA	NA	35.1	0.5	NA
Spot 156	440	1461	2.2	20.2548	4.6	0.0371	4.8	0.0055	1.4	0.28	35.1	0.5	37.0	1.7	164.4	107.5	35.1	0.5	NA
Spot 186	2440	71489	3.2	21.1076	1.0	0.0356	1.3	0.0055	0.9	0.66	35.1	0.3	35.6	0.5	67.2	23.3	35.1	0.3	NA
Spot 163	555	1616	2.9	25.2637	6.2	0.0298	6.4	0.0055	1.6	0.26	35.1	0.6	29.8	1.9	NA	NA	35.1	0.6	NA
Spot 143	4233	10177	5.0	21.7108	1.5	0.0347	1.9	0.0055	1.1	0.59	35.1	0.4	34.6	0.6	NA	NA	35.1	0.4	NA
Spot 118	404	942	2.0	31.0180	25.2	0.0243	25.3	0.0055	1.3	0.05	35.1	0.5	24.4	6.1	NA	NA	35.1	0.5	NA
Spot 187	537	977	2.0	31.6906	2.1	0.0238	2.8	0.0055	1.8	0.63	35.1	0.6	23.9	0.7	NA	NA	35.1	0.6	NA
Spot 188	294	1122367	2.7	20.6363	2.9	0.0365	3.2	0.0055	1.3	0.42	35.1	0.5	36.4	1.1	120.7	68.0	35.1	0.5	NA
Spot 89	2866	145466	3.7	20.9470	0.9	0.0360	1.6	0.0055	1.3	0.82	35.2	0.4	35.9	0.5	85.4	21.3	35.2	0.4	NA
Spot 70	869	14117	1.4	21.4957	1.5	0.0351	2.2	0.0055	1.6	0.73	35.2	0.6	35.0	0.7	23.6	35.5	35.2	0.6	NA
Spot 104	2375	25817	4.9	20.8065	1.1	0.0363	1.6	0.0055	1.1	0.68	35.2	0.4	36.2	0.6	101.3	27.1	35.2	0.4	NA
Spot 74	598	29154	1.2	21.8935	1.4	0.0345	1.9	0.0055	1.3	0.68	35.2	0.5	34.5	0.7	NA	NA	35.2	0.5	NA
Spot 194	338	1356	3.1	28.0332	15.9	0.0270	16.0	0.0055	1.7	0.11	35.3	0.6	27.0	4.3	NA	NA	35.3	0.6	NA
Spot 130	1065	9261	3.3	21.9582	1.8	0.0345	2.2	0.0055	1.3	0.58	35.3	0.4	34.4	0.7	NA	NA	35.3	0.4	NA
Spot 47	3795	24565	3.1	21.4872	1.0	0.0353	1.5	0.0055	1.1	0.72	35.4	0.4	35.2	0.5	24.6	24.9	35.4	0.4	NA
Spot 44	133	2140	1.9	24.3291	3.5	0.0312	3.8	0.0055	1.5	0.40	35.4	0.5	31.2	1.2	NA	NA	35.4	0.5	NA
Spot 103	527	4232	0.8	21.9711	1.7	0.0345	2.2	0.0055	1.4	0.63	35.4	0.5	34.5	0.7	NA	NA	35.4	0.5	NA
Spot 120	2138	9316	4.3	21.8666	1.4	0.0347	1.8	0.0055	1.2	0.64	35.4	0.4	34.6	0.6	NA	NA	35.4	0.4	NA
Spot 49	618	2297	1.6	24.5954	8.2	0.0309	8.3	0.0055	1.3	0.16	35.4	0.5	30.9	2.5	NA	NA	35.4	0.5	NA
Spot 55	423	1734	1.8	21.9451	2.4	0.0346	2.7	0.0055	1.2	0.43	35.4	0.4	34.6	0.9	NA	NA	35.4	0.4	NA
Spot 19	460	2878	2.5	18.9083	4.2	0.0402	4.3	0.0055	1.0	0.22	35.5	0.3	40.0	1.7	323.0	95.7	35.5	0.3	NA
Spot 116	2053	18029	4.3	20.5844	1.1	0.0369	1.5	0.0055	1.0	0.65	35.5	0.3	36.8	0.5	126.6	26.5	35.5	0.3	NA
Spot 135	813	3790	3.1	22.8416	3.7	0.0333	3.8	0.0055	1.0	0.26	35.5	0.4	33.3	1.3	NA	NA	35.5	0.4	NA
Spot 167	90	580	2.6	48.8498	66.1	0.0156	66.1	0.0055	2.2	0.03	35.5	0.8	15.7	10.3	NA	NA	35.5	0.8	NA
Spot 11	542	4155	1.7	20.2763	2.1	0.0375	2.5	0.0055	1.4	0.57	35.5	0.5	37.4	0.9	162.0	48.3	35.5	0.5	NA
Spot 66	332	2779	2.6	23.7151	2.8	0.0321	3.1	0.0055	1.4	0.45	35.5	0.5	32.1	1.0	NA	NA	35.5	0.5	NA
Spot 18	156	5450	2.5	21.7544	3.7	0.0350	4.1	0.0055	1.8	0.43	35.5	0.6	35.0	1.4	NA	NA	35.5	0.6	NA
Spot 100	779	12893	1.8	18.3122	1.8	0.0416	2.2	0.0055	1.3	0.58	35.5	0.5	41.4	0.9	395.2	40.6	35.5	0.5	NA
Spot 20	225	8029	1.4	19.1646	3.0	0.0398	3.4	0.0055	1.7	0.49	35.6	0.6	39.6	1.3	292.3	67.8	35.6	0.6	NA
Spot 105	385	2258	3.2	22.8660	7.6	0.0333	7.7	0.0055	1.3	0.17	35.6	0.5	33.3	2.5	NA	NA	35.6	0.5	NA
Spot 30	360	1434	2.1	24.2484	2.7	0.0314	2.8	0.0055	0.8	0.30	35.6	0.3	31.4	0.9	NA	NA	35.6	0.3	NA
Spot 57	503	1470	1.0	25.8597	3.9	0.0295	4.2	0.0055	1.3	0.32	35.6	0.5	29.5	1.2	NA	NA	35.6	0.5	NA
Spot 106	785	5473	2.7	22.1255	2.9	0.0345	3.3	0.0055	1.5	0.45	35.6	0.5	34.4	1.1	NA	NA	35.6	0.5	NA
Spot 46	190	986	2.9	31.6430	22.5	0.0241	22.5	0.0055	1.4	0.06	35.6	0.5	24.2	5.4	NA	NA	35.6	0.5	NA
Spot 65	88	619	2.3	33.4029	25.8	0.0229	25.9	0.0055	1.9	0.07	35.6	0.7	23.0	5.9	NA	NA	35.6	0.7	NA
Spot 91	218	1926	1.4	13.9357	4.2	0.0548	4.4	0.0055	1.3	0.30	35.6	0.5	54.2	2.3	978.2	85.9	35.6	0.5	NA
Spot 45	415	1691	0.9	24.7084	7.6	0.0309	7.6	0.0055	1.1	0.15	35.7	0.4	30.9	2.3	NA	NA	35.7	0.4	NA
Spot 148	678	31489	3.1	21.2802	1.7	0.0359	2.2	0.0056	1.4	0.62	35.7	0.5	35.9	0.8	47.8	41.8	35.7	0.5	NA

Table B1. U-Pb zircon analyses.

Analysis	U (ppm)	206Pb 204Pb	U/Th	206Pb* 207Pb*	± (%)	207Pb* 235U*	± (%)	206Pb* 238U	± (%)	error corr.	206Pb* 238U* (Ma)	± (Ma)	207Pb* 235U (Ma)	± (Ma)	206Pb* 207Pb* (Ma)	± (Ma)	Best age (Ma)	± (Ma)	Conc (%)
Spot 144	1676	13702	4.4	21.5084	1.4	0.0356	1.8	0.0056	1.2	0.64	35.7	0.4	35.5	0.6	22.2	34.0	35.7	0.4	NA
Spot 50	434	1108	2.5	20.0579	14.1	0.0382	14.2	0.0056	1.1	0.08	35.7	0.4	38.0	5.3	187.2	330.8	35.7	0.4	NA
Spot 92	804	2354	2.2	23.2408	2.2	0.0330	2.7	0.0056	1.4	0.54	35.7	0.5	32.9	0.9	NA	NA	35.7	0.5	NA
Spot 121	1865	5424	5.1	22.5705	1.4	0.0340	1.9	0.0056	1.3	0.68	35.8	0.5	34.0	0.6	NA	NA	35.8	0.5	NA
Spot 27	2537	14451	4.2	21.6455	1.2	0.0355	1.7	0.0056	1.2	0.70	35.8	0.4	35.4	0.6	7.0	29.3	35.8	0.4	NA
Spot 59	161	2856	1.4	23.9731	5.2	0.0321	5.5	0.0056	1.9	0.33	35.9	0.7	32.1	1.8	NA	NA	35.9	0.7	NA
Spot 175	865	2386	4.0	22.2430	3.4	0.0346	3.7	0.0056	1.2	0.33	35.9	0.4	34.6	1.2	NA	NA	35.9	0.4	NA
Spot 150	2105	14432	4.1	21.4244	1.3	0.0360	1.6	0.0056	1.0	0.62	36.0	0.4	35.9	0.6	31.6	30.1	36.0	0.4	NA
Spot 162	357	922	3.7	29.2625	13.4	0.0263	13.4	0.0056	1.4	0.10	36.0	0.5	26.4	3.5	NA	NA	36.0	0.5	NA
Spot 110	267	2415	2.7	23.0976	7.7	0.0334	7.8	0.0056	1.5	0.19	36.0	0.5	33.3	2.6	NA	NA	36.0	0.5	NA
Spot 189	558	11595	2.5	21.4434	1.9	0.0360	2.3	0.0056	1.3	0.57	36.0	0.5	35.9	0.8	29.5	45.0	36.0	0.5	NA
Spot 154	216	1903	1.3	22.5961	3.2	0.0341	3.5	0.0056	1.3	0.38	36.0	0.5	34.1	1.2	NA	NA	36.0	0.5	NA
Spot 137	462	7988	2.8	21.8500	2.4	0.0353	2.8	0.0056	1.4	0.51	36.0	0.5	35.2	1.0	NA	NA	36.0	0.5	NA
Spot 29	1159	8279	1.5	21.4888	1.5	0.0359	1.8	0.0056	1.0	0.54	36.0	0.3	35.8	0.6	24.4	35.9	36.0	0.3	NA
Spot 31	1939	15340	4.3	21.6224	1.5	0.0357	2.3	0.0056	1.8	0.78	36.0	0.7	35.6	0.8	9.5	34.9	36.0	0.7	NA
Spot 161	444	16781	1.4	20.5636	2.2	0.0376	2.7	0.0056	1.5	0.55	36.1	0.5	37.5	1.0	129.0	52.5	36.1	0.5	NA
Spot 86	611	26647	3.7	20.7597	2.4	0.0373	2.8	0.0056	1.4	0.49	36.1	0.5	37.2	1.0	106.6	56.9	36.1	0.5	NA
Spot 38	252	1811	2.8	21.4536	2.8	0.0361	3.0	0.0056	1.0	0.33	36.1	0.4	36.0	1.1	28.4	67.7	36.1	0.4	NA
Spot 126	238	1779899	3.2	18.4695	3.3	0.0419	3.7	0.0056	1.6	0.43	36.1	0.6	41.7	1.5	376.0	74.3	36.1	0.6	NA
Spot 199	394	2670	2.3	23.7514	2.4	0.0326	2.6	0.0056	1.2	0.44	36.2	0.4	32.6	0.8	NA	NA	36.2	0.4	NA
Spot 141	323	1838	3.8	25.2419	3.0	0.0307	3.2	0.0056	1.2	0.36	36.2	0.4	30.7	1.0	NA	NA	36.2	0.4	NA
Spot 72	366	7996	3.1	19.1790	2.2	0.0404	2.6	0.0056	1.4	0.53	36.2	0.5	40.3	1.0	290.6	50.2	36.2	0.5	NA
Spot 23	423	3231	2.6	22.4942	3.7	0.0345	4.0	0.0056	1.5	0.38	36.2	0.5	34.4	1.3	NA	NA	36.2	0.5	NA
Spot 64	445	2142	3.5	24.2638	1.9	0.0320	2.4	0.0056	1.4	0.60	36.2	0.5	32.0	0.7	NA	NA	36.2	0.5	NA
Spot 95	539	351635	2.7	21.1933	2.3	0.0366	2.7	0.0056	1.3	0.50	36.2	0.5	36.5	1.0	57.5	54.8	36.2	0.5	NA
Spot 24	342	861	3.8	32.0728	3.1	0.0242	3.3	0.0056	1.4	0.41	36.2	0.5	24.3	0.8	NA	NA	36.2	0.5	NA
Spot 6	443	3648	1.9	19.6367	2.2	0.0396	2.4	0.0056	1.1	0.43	36.3	0.4	39.4	0.9	236.4	51.0	36.3	0.4	NA
Spot 5	349	4814	3.0	19.7102	4.3	0.0395	4.4	0.0056	1.1	0.25	36.3	0.4	39.3	1.7	227.8	99.0	36.3	0.4	NA
Spot 183	595	4666	2.4	22.5495	2.1	0.0345	2.4	0.0056	1.3	0.53	36.3	0.5	34.4	0.8	NA	NA	36.3	0.5	NA
Spot 71	467	4594	1.7	24.3425	4.1	0.0320	4.3	0.0056	1.3	0.31	36.3	0.5	32.0	1.3	NA	NA	36.3	0.5	NA
Spot 53	207	2130	1.6	21.4175	3.6	0.0364	3.8	0.0057	1.4	0.36	36.3	0.5	36.3	1.4	32.4	85.5	36.3	0.5	NA
Spot 79	293	6288	2.2	20.9797	2.7	0.0371	3.0	0.0057	1.1	0.38	36.3	0.4	37.0	1.1	81.6	64.8	36.3	0.4	NA
Spot 16	575	3245	2.3	18.7768	2.3	0.0415	2.7	0.0057	1.4	0.53	36.4	0.5	41.3	1.1	338.8	51.2	36.4	0.5	NA
Spot 123	2073	19626	3.6	21.0644	1.1	0.0371	1.6	0.0057	1.1	0.72	36.4	0.4	37.0	0.6	72.1	26.4	36.4	0.4	NA
Spot 131	300	1786	2.7	18.1810	3.5	0.0430	3.8	0.0057	1.4	0.36	36.4	0.5	42.7	1.6	411.3	78.9	36.4	0.5	NA
Spot 134	2249	6507	4.1	21.8460	1.0	0.0358	1.4	0.0057	1.0	0.69	36.5	0.4	35.7	0.5	NA	NA	36.5	0.4	NA
Spot 160	275	3581	2.9	16.9082	2.5	0.0463	2.7	0.0057	1.1	0.40	36.5	0.4	45.9	1.2	571.4	54.4	36.5	0.4	NA
Spot 168	628	3646	1.0	20.7820	2.8	0.0377	3.1	0.0057	1.2	0.39	36.5	0.4	37.5	1.1	104.1	66.4	36.5	0.4	NA
Spot 33	324	782	2.2	17.7921	10.5	0.0441	10.6	0.0057	1.4	0.13	36.6	0.5	43.9	4.6	459.5	234.0	36.6	0.5	NA
Spot 84	115	2952	2.2	27.2771	4.1	0.0288	4.4	0.0057	1.6	0.36	36.6	0.6	28.8	1.3	NA	NA	36.6	0.6	NA
Spot 68	215	20477	1.7	17.8012	5.5	0.0441	5.8	0.0057	1.8	0.32	36.7	0.7	43.9	2.5	458.3	121.1	36.7	0.7	NA
Spot 177	274	1311	2.7	27.7186	8.2	0.0284	8.4	0.0057	2.1	0.25	36.7	0.8	28.4	2.4	NA	NA	36.7	0.8	NA
Spot 125	227	8747	3.1	21.1481	3.1	0.0373	3.3	0.0057	1.2	0.35	36.8	0.4	37.1	1.2	62.6	73.7	36.8	0.4	NA
Spot 87	377	2590	2.1	25.8534	2.9	0.0305	3.2	0.0057	1.3	0.41	36.8	0.5	30.5	1.0	NA	NA	36.8	0.5	NA
Spot 4	619	1589	1.8	25.1318	2.2	0.0315	2.4	0.0057	1.0	0.40	36.9	0.4	31.4	0.8	NA	NA	36.9	0.4	NA
Spot 124	297	3310	2.4	15.4244	5.0	0.0513	5.1	0.0057	1.1	0.22	36.9	0.4	50.8	2.5	768.0	105.8	36.9	0.4	NA
Spot 14	79	1942	0.9	16.6151	5.5	0.0476	5.8	0.0057	1.9	0.33	36.9	0.7	47.2	2.7	609.3	118.4	36.9	0.7	NA
Spot 119	377	6179	1.5	15.7641	4.7	0.0502	4.9	0.0057	1.4	0.29	36.9	0.5	49.7	2.4	721.9	100.7	36.9	0.5	NA
Spot 117	396	3684	0.8	22.7980	2.6	0.0347	2.8	0.0057	1.2	0.41	36.9	0.4	34.7	1.0	NA	NA	36.9	0.4	NA
Spot 99	218	4118	3.4	21.8754	3.3	0.0362	3.5	0.0058	1.2	0.33	37.0	0.4	36.1	1.2	NA	NA	37.0	0.4	NA
Spot 111	588	1305	1.1	19.4805	4.4	0.0407	4.6	0.0058	1.2	0.26	37.0	0.4	40.5	1.8	254.8	102.0	37.0	0.4	NA
Spot 17	1855	146314	2.6	21.0459	1.2	0.0377	1.6	0.0058	1.1	0.67	37.0	0.4	37.6	0.6	74.2	28.6	37.0	0.4	NA
Spot 78	193	1170	1.0	24.6049	3.6	0.0322	3.9	0.0058	1.4	0.37	37.0	0.5	32.2	1.2	NA	NA	37.0	0.5	NA
Spot 108	76	1006	0.9	27.6581	4.4	0.0288	4.9	0.0058	2.0	0.42	37.2	0.8	28.8	1.4	NA	NA	37.2	0.8	NA
Spot 164	322	6454	2.5	17.1539	3.3	0.0465	3.5	0.0058	1.1	0.33	37.2	0.4	46.1	1.6	539.9	72.1	37.2	0.4	NA
Spot 43	254	2136	2.3	20.1359	2.9	0.0396	3.2	0.0058	1.3	0.41	37.2	0.5	39.5	1.2	178.2	67.8	37.2	0.5	NA
Spot 102	1143	6555	2.5	22.8900	2.3	0.0349	2.6	0.0058	1.2	0.48	37.3	0.5	34.8	0.9	NA	NA	37.3	0.5	NA
Spot 2	477	1397	3.3	25.6118	4.4	0.0313	4.6	0.0058	1.3	0.28	37.4	0.5	31.3	1.4	NA	NA	37.4	0.5	NA
Spot 149	358	178636	2.8	20.6514	2.0	0.0389	2.3	0.0058	1.2	0.52	37.4	0.5	38.7	0.9	118.9	46.9	37.4	0.5	NA
Spot 151	171	629	2.6	18.8448	8.0	0.0426	8.2	0.0058	1.5	0.18	37.5	0.5	42.4	3.4	330.6	182.6	37.5	0.5	NA
Spot 60	425	932	3.0	12.4121	3.5	0.0650	3.8	0.0059	1.4	0.36	37.6	0.5	63.9	2.4	1210.1	69.6	37.6	0.5	NA
Spot 145	289	1244	2.1	21.9217	2.8	0.0369	3.1	0.0059	1.3	0.43	37.7	0.5	36.8	1.1	NA	NA	37.7	0.5	NA
Spot 88	1159	204949	6.8	20.3369	1.8	0.0398	2.2	0.0059	1.3	0.60	37.8	0.5	39.6	0.9	155.0	41.9	37.8	0.5	NA
Spot 138	317	966	1.1	17.5993	10.8	0.0464	10.8	0.0059	1.1	0.10	38.1	0.4	46.0	4.9	483.6	238.3	38.1	0.4	NA
Spot 113	325	6686	2.5	14.9360	3.9	0.0548	4.2	0.0059	1.4	0.34	38.2	0.5	54.2	2.2	835.4	82.2	38.2	0.5	NA
Spot 101	1089	4941	3.8	22.6493	3.8	0.0363	4.0	0.0060	1.3	0.33	38.4	0.5	36.2	1.4	NA	NA	38.4	0.5	NA
Spot 165	269	3496	2.7	18.9849	2.5	0.0438	2.8	0.0060	1.3	0.48	38.8	0.5	43.5	1.2	313.8	56.5	38.8	0.5	NA
Spot 128	89	1540	0.8	13.0067	5.3	0.0641	5.6	0.0060	1.8	0.32	38.9	0.7	63.1	3.4	1117.3	106.6	38.9	0.7	NA
Spot 26	222	2911	2.5	15.5203	3.3	0.0541	3.7	0.0061	1.7	0.45	39.1	0.7	53.5	2.0	754.9	70.7	39.1	0.7	NA
Spot 174	1066	18213	4.4	20.1955	1.4	0.0419	1.8	0.0061	1.2	0.64	39.4	0.5	41.7	0.7	171.3	32.8	39.4	0.5	NA
Spot 142	129	1087	1.4	7.1190	22.7	0.1228	22.9	0.0063	2.7	0.12	40.8	1.1	117.6	25.4	2232.2	398.6	40.8	1.1	NA
Spot 94	431	372	2.0	5.2894	6.3	0.1827	6.5	0.0070	1.6	0.25	45.0	0.7	170.4	10.2	2733.3	104.1	45.0	0.7	NA
Spot 171	293	3191	1.9	13.6463	2.6	0.0944	3.4	0.0093	2.2	0.64	59.9	1.3	91.6	3.0	1020.8	53.2	59.9	1.3	NA
Spot 22	364	8501	5.4	21.6091	1.5	0.0962	2.0	0.0151	1.4	0.68	96.5	1.3	93.3	1.8	11.0	35.9	96.5	1.3	NA
Spot 129	609	6710	3.4	14.5670	2.6	0.2118	4.4	0.0224	3.6	0.82	142.7	5.1	195.1	7.9	887.3	52.9	142.7	5.1	NA
Spot 73	351	7899	2.3	20.8314	2.0	0.1717	2.5	0.0260	1.5	0.60	165.2	2.5	160.9	3.7	98.5	47.4	165.2	2.5	NA
Spot 69	423	13994	3.4	10.4798	1.3	0.7916	2.5	0.0602	2.2	0.87	376.8	7.9	592.1	11.2	1535.6	23.6	376.8	7.9	NA
Spot 41	273	31115	2.9	13.3999	0.9	1.8155	1.6	0.1765	1.3	0.82	1047.9	12.8	1051.1	10.5	1057.6	18.3	1057.6	18.3	99.1
Spot 114	258	22236	3.6	13.1961	0.8	1.9603	1.3	0.1877	1.0	0.78	1108.9	10.6	1102.0	8.9	1088.4	16.7	1088.4	16.7	101.9
Spot 139	101	71516	2.2	13.1591	1.1	1.9114	1.7	0.1825	1.3	0.77	1080.6	13.0	1085.1	11.3	1094.0	21.9	1094.0	21.9	98.8
Spot 76	305	36665	2.7	13.1322	0.6	1.9139	1.2	0.1824	1.0	0.86	1079.9	10.0	1085.9	7.8	1098.1	12.0	1098.1	12.0	98.3
Spot 178	293	43592	2.6	13.0742	0.9	1.7860	1.7	0.1694	1.5	0.89	1008.9	14.2	1040.4	11.4	1106.9	17.1	1106.9	17.1	91.1
Spot 122	104	70496	2.4	12.5496	1.3	1.9994	1.7	0.1821	1.0	0.62	1078.2	10.2	1115.3	11.3	1188.3	26.0	1188.3	26.0	90.7
Spot 36	74	93523	1.1	11.7999	0.8	2.1503	3.0	0.1841	2.9	0.97	1089.4	29.1	1165.2	20.9	1308.9	16.3	1308.9	16.3	83.2
Spot 52	137	30270	1.6	11.7736	0.9	2.6278	1.4	0.2245	1.1	0.77	1305.5	12.8	1308.5	10.3	1313.2	17.1	1313.2	17.1	99.4
Spot 3	85	18988	1.6	11.5486	1.1	2.8169	1.7	0.2360	1.4	0.79	1366.1	16.6	1360.1	12.8	1350.5	20.3	1350.5	20.3	101.2
Spot 127	60	12955	2.4	11.5300	0.8	2.7886	2.1	0.2333	1.9	0.92	1351.8	23.1	1352.5	15.4	1353.7	15.2	1353.7	15.2	99.9
Spot 197	90	36890	1.6	11.3513	0.9	2.9308	1.5	0.2414	1.2	0.81	1393.9	14.6	1389.9	11.0	1383.7	16.5	1383.7	16.5	100.7
Spot 62	296	28862	4.8	11.3378	0.7	2.4809	1.9	0.2041	1.8	0.93	1197.3	19.6	1266.5	14.0	1386.0	13.7	1386.0	13.7	86.4
Spot 48	151	92721	2.8	10.9977	0.9	2.9987	1.4	0.2393	1.1	0.78	1383.0	13.5	1407.3	10.6	1444.3	16.7	1444.3	16.7	95.8
Spot 146	150	37109	1.9	10.9840	0.7	3.0915	1.2	0.2464	1.0	0.83	1419.8	13.0	1430.6	9.5	1446.6	13.1	1446.6	13.1	98.1
Spot 147	178	53551	3.0	9.6044	0.6	4.0763	1.1	0.2841	0.9	0.83	1611.8	13.4	1649.6	9.3	1698.0	11.8	1698.0	11.8	94.9
Spot 166	135	24431	3.6	9.5554	0.8	4.1326	1.4	0.2865	1.2	0.85	1624.1	17.6	1660.8	11.8	1707.4	14.1	1707.4	14.1	95.1
Spot 112	185	57419	2.3	9.2845	0.7	4.3178	1.6	0.2909	1.5	0.90	1645.9	21.3	1696.8	13.5	1760.2	13.1	1760.2	13.1	93.5
Spot 39	90	8031	2.5	9.0201	1.0	5.1267	1.5	0.3355	1.1	0.76	1865.2	18.3	1840.5	12.6	1812.8	17.5	1812.8	17.5	102.9
Spot 172	182	63685	1.6	8.9540	1.0	5.0053	1.5	0.3252	1.2	0.77	1815.0	18.6	1820.2	13.0	1826.2	17.9	1826.2	17.9	99.4
Spot 152	128	33565	1.9	8.9348	0.8	5.1423	1.6	0.3334	1.4	0.88	1854.7	23.2	1843.1	13.9	1830.1	14.2	1830.1	14.2	101.3
Spot 181	113	183582	2.9	8.8461	0.8	5.1445	1.9	0.3302	1.1	0.82	1839.4	17.8	1843.5	11.5	1848.1	14.0	1848.1	14.0	99.5
Spot 190	65	92040	1.7	8.7451	0.8	5.2748	1.5	0.3347	1.2	0.82	1861.1	19.4	1864.8	12.5	1868.9	15.2	1868.9	15.2	99.6
Spot 109	93	8639	1.7	8.7012	0.8	5.4953	1.3	0.3469	1.0	0.79	1920.0	16.8	1899.9	11.1	1877.9	14.3	1877.9	14.3	102.2
Spot 7	164	60485	1.0	8.6932	0.9	4.8994	1.3	0.3090	1.0	0.76	1736.0	15.6	1802.1	11.3	1879.6	15.5	1879.6	15.5	92.4
Spot 13	112	36969	0.9	8.5791	0.9	5.5465	1.6	0.3453	1.3	0.81	1911.9	21.4	1907.8	13.7	1903.4	16.7	1903.4	16.7	100.4
Spot 56	78	26132	1.0	8.4730	0.9	5.5261	1.3	0.3397	0.9	0.73	1885.4	15.0	1904.7	10.8	1925.7	15.3	1925.7	15.3	97.9

Table B1. U-Pb zircon analyses.

Analysis	U (ppm)	206Pb 204Pb	U/Th	206Pb* 207Pb*	± (%)	Isotope ratios					Apparent ages (Ma)						Best age (Ma)	± (Ma)	Conc (%)
						207Pb* 235U*	± (%)	206Pb* 238U	± (%)	error corr.	206Pb* 238U*	± (Ma)	207Pb* 235U	± (Ma)	206Pb* 207Pb*	± (Ma)			
Spot 184	255	1003287	1.7	7.8840	0.9	6.1711	1.4	0.3530	1.1	0.79	1949.0	19.3	2000.4	12.7	2053.8	15.6	2053.8	15.6	94.9
Spot 63	134	183514	2.8	6.2732	0.8	10.1576	1.3	0.4623	1.1	0.82	2449.9	21.9	2449.2	12.1	2448.6	12.8	2448.6	12.8	100.1
Spot 179	122	467501	1.3	5.4860	0.9	12.6930	1.3	0.5053	1.0	0.74	2636.3	21.0	2657.1	12.4	2673.0	14.7	2673.0	14.7	98.6
Spot 98	57	21373	2.1	5.4754	1.1	13.2750	1.6	0.5274	1.2	0.75	2730.5	27.5	2699.4	15.5	2676.2	17.9	2676.2	17.9	102.0
Spot 21	33	75824	3.4	5.4370	1.0	11.8918	3.1	0.4691	2.9	0.94	2479.8	59.4	2595.9	28.7	2687.8	17.0	2687.8	17.0	92.3
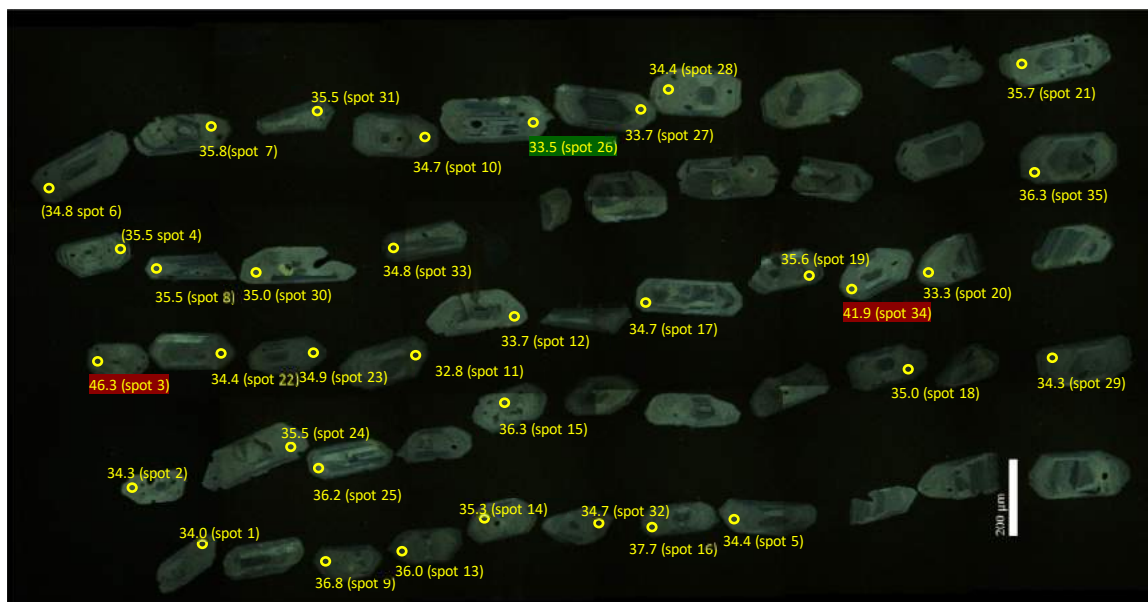
Figure B1. Sample KS014 (Walti quartz monzonite) zircon SEM-CL images and spot analyses in Ma.
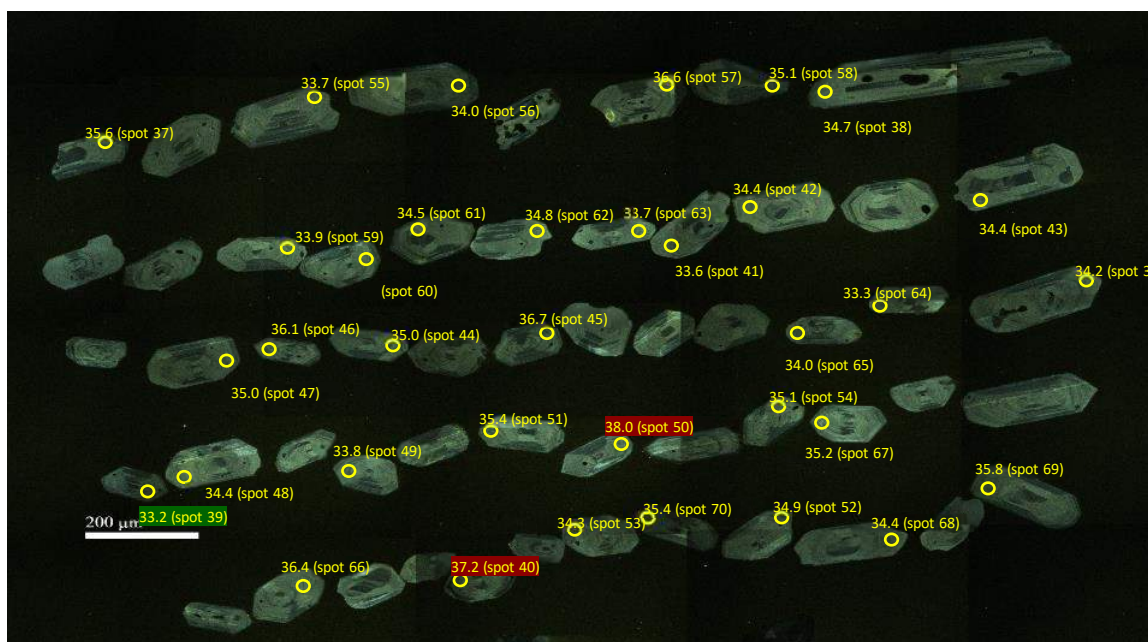
Figure B2. Sample KS025 (Trachyandesite) zircon SEM-CL images and spot analyses in Ma.
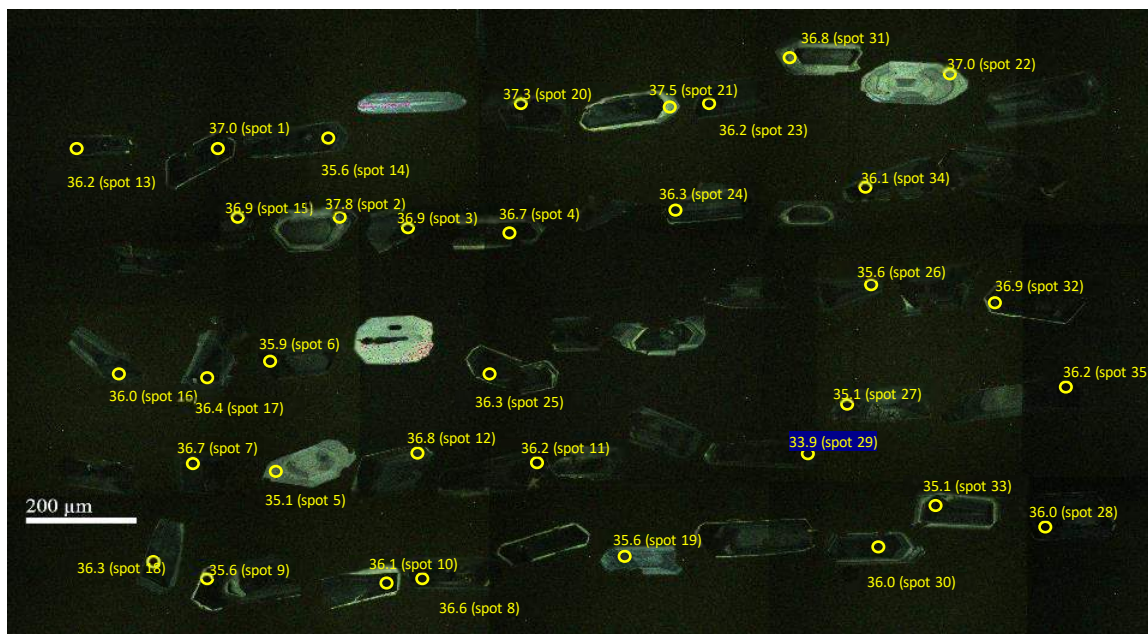
Figure B3. Sample KS044 (rhyolite porphyry) zircon SEM-CL images and spot analyses in Ma.
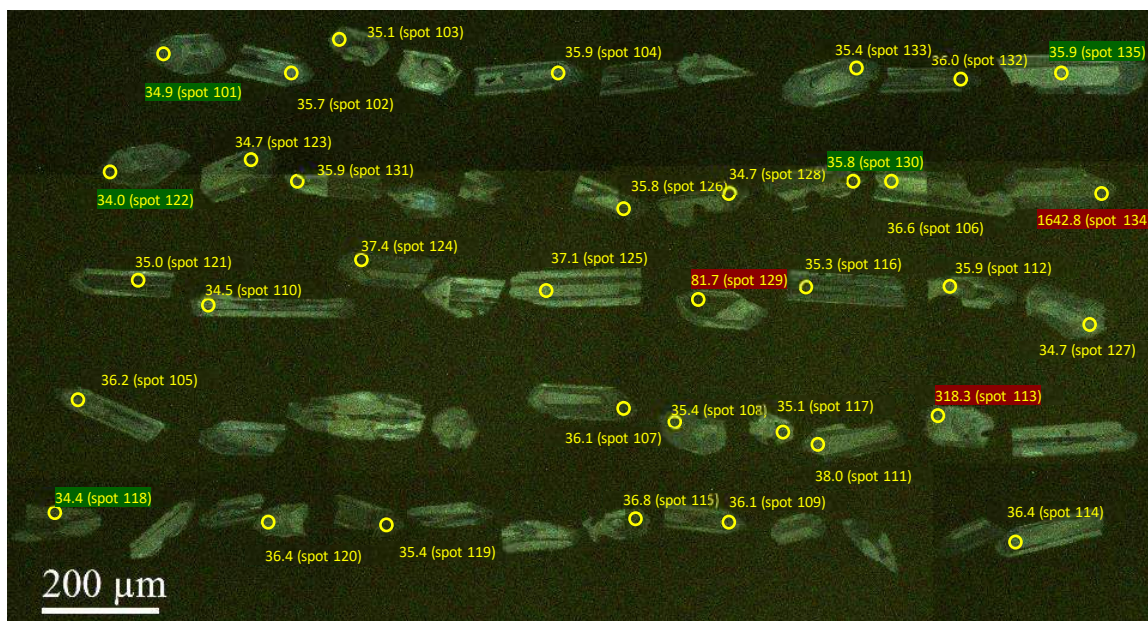
Figure B4. Sample KS050 (aphyric rhyolite) zircon SEM-CL images and spot analysis in Ma.
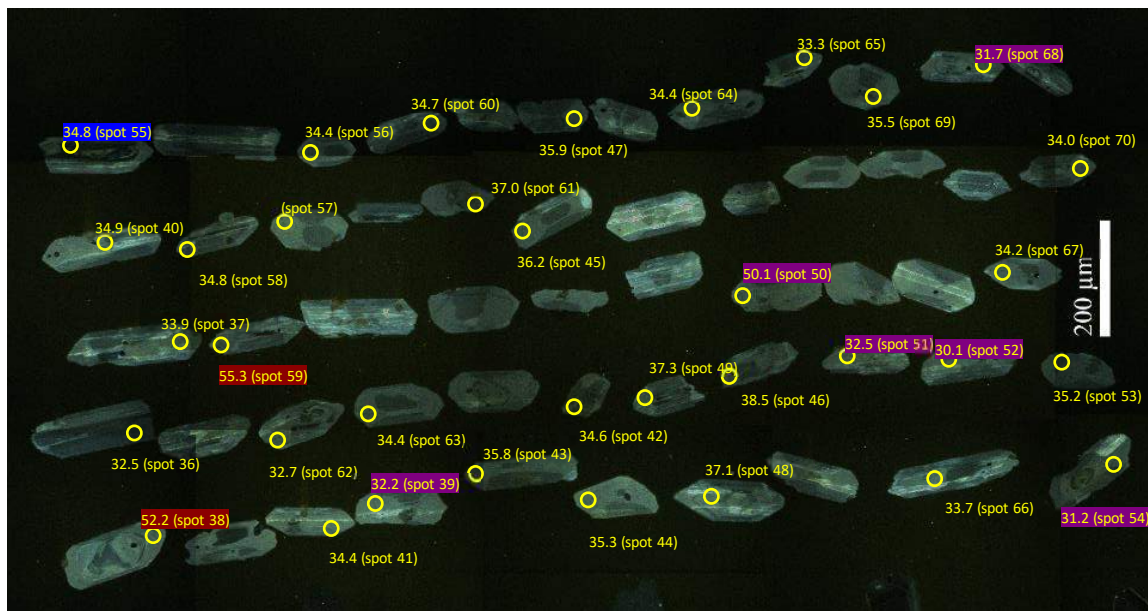
Figure B5. Sample KS051 (dacite agglomerate) zircon SEM-CL images and spot analyses in Ma.
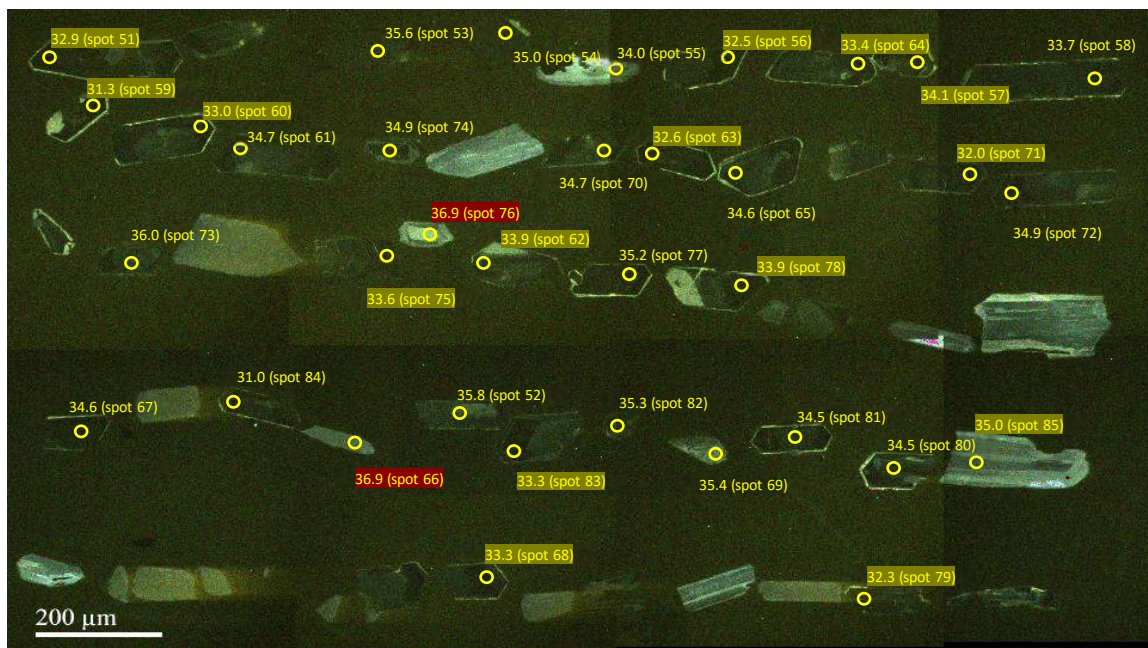
Figure B6. Sample KS126 (Walti intermediate porphyritic dikes) zircon SEM-CL images and spot analyses in Ma.

Figure B7. Sample KS048 (Tertiary conglomerate) zircon SEM-CL images and spot analyses in Ma.

Appendix C – ^{40}Ar/^{39}Ar Results

Table C1. ^{40}Ar/^{39}Ar analytical data, bulk grain step heating results.

ID		Power (Watts)	^{40}Ar/^{39}Ar	^{37}Ar/^{39}Ar	^{36}Ar/^{39}Ar (x 10^{-3})	^{39}Ar$_K$ (x 10^{-15} mol)	K/Ca	^{40}Ar* (%)	^{39}Ar (%)	Age (Ma)	±1σ (Ma)
KS 001, Illite, 5.54 mg, J=0.0019528±0.02%, IC=1.019395±0.0025272, NM-297B, Lab#=66439-01, Argus VI										
Xi	A	0.4	13.52	0.0167	5.412	12.7	30.6	88.2	5.5	42.116	0.049
Xi	B	0.6	13.02	0.0164	1.664	20.0	31.2	96.2	14.2	44.239	0.029
Xi	C	0.8	12.20	0.0164	0.4629	35.2	31.0	98.9	29.5	42.614	0.015
Xi	D	1.0	12.15	0.0167	0.2832	43.6	30.5	99.3	48.4	42.598	0.012
Xi	E	1.2	12.00	0.0158	0.2515	49.2	32.3	99.4	69.8	42.131	0.011
Xi	F	1.5	11.73	0.0154	0.3003	49.5	33.2	99.3	91.3	41.112	0.011
Xi	G	2.0	11.49	0.0149	0.5438	19.2	34.2	98.6	99.7	40.032	0.025
Xi	H	3.0	12.44	-0.0044	6.395	0.8	-	84.8	100.0	37.29	0.52
		Integrated age ± 1σ		n=8		230.2	32.0		K2O=8.17%	42.066	0.010
		Plateau ± 1σ	no plateau	n=0	MSWD=0.00	0.000			0.0	0.00	0.000
		Isochron±2σ	no isochron	n=0	MSWD=1.00		^{40}Ar/^{36}Ar=		0.0±0.0	0.000	0.000
KS 019, Illite, 5.15 mg, J=0.0019513±0.02%, IC=1.018498±0.002561, NM-297B, Lab#=66437-02, Argus VI										
Xi	A	0.2	22.39	0.0158	69.83	0.6	32.3	7.8	0.2	6.25	0.83
Xi	B	0.4	21.43	0.0107	38.78	1.9	47.6	46.5	1.0	35.25	0.33
Xi	C	0.6	15.71	0.0110	16.80	3.9	46.4	68.4	2.5	37.97	0.16
Xi	D	0.8	11.90	0.0072	4.532	14.7	71.3	88.7	8.1	37.322	0.043
Xi	E	1.0	11.15	0.0061	2.084	22.8	83.7	94.5	16.8	37.214	0.025
Xi	F	1.2	10.97	0.0044	1.678	26.7	114.7	95.5	27.0	36.996	0.022
Xi	G	1.5	10.73	0.0038	1.113	34.2	132.7	96.9	40.0	36.771	0.017
Xi	H	2.0	10.51	0.0034	0.6916	38.0	150.6	98.1	54.6	36.419	0.015
Xi	I	3.0	10.42	0.0029	0.7458	33.4	174.4	97.9	67.3	36.060	0.016
Xi	J	4.0	10.45	0.0032	0.8306	29.5	159.0	97.7	78.6	36.075	0.017
Xi	K	5.0	10.48	0.0214	0.9360	19.1	23.8	97.4	85.9	36.085	0.027
	L	6.0	10.47	0.0115	1.073	11.1	44.5	97.0	90.2	35.900	0.040
	M	7.0	10.54	0.0038	1.391	8.0	133.8	96.1	93.2	35.797	0.054
	N	15.0	11.16	0.0024	3.760	17.7	215.1	90.0	100.0	35.533	0.034
		Integrated age ± 1σ		n=14		261.6	89.1		K2O=10.00%	36.380	0.011
		Plateau ± 1σ	steps L-N	n=3	MSWD=26.56	36.824			14.1	35.71	0.120
		Isochron±2σ	steps L-N	n=3	MSWD=1.02		^{40}Ar/^{36}Ar=		258.4±4.7	36.020	0.046
KS 029, Illite, 4.96 mg, J=0.0019571±0.02%, IC=1.019427±0.0025354, NM-297C, Lab#=66447-01, Argus VI										
Xi	A	0.4	7.764	0.0061	6.193	2.2	84.2	76.4	0.8	21.11	0.18
Xi	B	0.6	11.78	0.0029	1.789	4.5	177.8	95.5	2.5	39.83	0.10
Xi	C	0.8	10.96	0.0026	0.4773	10.7	193.1	98.7	6.6	38.329	0.038
Xi	D	1.0	10.80	0.0035	0.2539	18.1	145.6	99.3	13.4	38.000	0.024
Xi	E	1.2	10.61	0.0033	0.1712	25.8	156.2	99.5	23.2	37.435	0.019
Xi	F	1.5	10.43	0.0039	0.1283	39.1	130.8	99.6	38.1	36.847	0.012
Xi	G	2.0	10.38	0.0034	0.1089	62.2	151.5	99.7	61.7	36.664	0.009
i	H	3.0	10.30	0.0034	0.1716	70.1	150.5	99.5	88.3	36.324	0.008
i	I	4.0	10.29	0.0038	0.3708	30.9	135.8	98.9	100.0	36.076	0.016

Table C1. $^{40}Ar/^{39}Ar$ analytical data, bulk grain step heating results.

ID		Power (Watts)	$^{40}Ar/^{39}Ar$	$^{37}Ar/^{39}Ar$	$^{36}Ar/^{39}Ar$ (x 10^{-3})	$^{39}Ar_K$ (x 10^{-15} mol)	K/Ca	$^{40}Ar^*$ (%)	^{39}Ar (%)	Age (Ma)	±1σ (Ma)
Integrated age ± 1σ			n=9			263.3	146.5		K2O=10.42%	36.693	0.009
Plateau ± 1σ		steps H-I	n=2	MSWD=183.48	100.972				38.3	36.27	0.101
Isochron±2σ		no isochron	n=0	MSWD=1.00			$^{40}Ar/^{36}Ar=$	0.0±0.0		0.00	0.00

KS 099, Illite, 4.41 mg, J=0.0019371±0.02%, IC=1.037222±0.0024034, NM-297B, Lab#=66430-01, Argus VI

ID		Power (Watts)	$^{40}Ar/^{39}Ar$	$^{37}Ar/^{39}Ar$	$^{36}Ar/^{39}Ar$ (x 10^{-3})	$^{39}Ar_K$ (x 10^{-15} mol)	K/Ca	$^{40}Ar^*$ (%)	^{39}Ar (%)	Age (Ma)	±1σ (Ma)
Xi	D	1.0	337.2	0.0401	1104.3	1.7	12.7	3.2	1.9	38.2	2.9
Xi	E	1.2	96.62	0.0186	295.1	1.8	27.5	9.7	3.8	33.08	0.97
Xi	F	1.5	47.24	0.0561	131.9	2.0	9.1	17.5	6.0	29.08	0.46
Xi	G	2.0	24.55	0.0447	52.69	3.2	11.4	36.6	9.6	31.55	0.24
Xi	H	3.0	15.80	0.0378	17.19	6.9	13.5	67.9	17.1	37.62	0.10
Xi	I	4.0	13.11	0.0215	3.637	19.6	23.8	91.8	38.7	42.155	0.031
Xi	J	5.0	12.00	0.0186	0.7316	44.6	27.4	98.2	87.7	41.279	0.055
Xi	K	6.0	10.37	0.0299	0.9158	10.5	17.0	97.4	99.2	35.452	0.042
Xi	L	7.0	8.935	0.0180	1.899	0.7	28.4	93.7	100.0	29.43	0.60
Integrated age ± 1σ			n=9			91.1	21.1		K2O=4.09%	39.600	0.067
Plateau ± 1σ		no plateau	n=0	MSWD=0.00	0.000				0.0	0.00	0.000
Isochron±2σ		no isochron	n=0	MSWD=1.00			$^{40}Ar/^{36}Ar=$	0.0±0.0		0.000	0.000

KS 099, Illite, 4.92 mg, J=0.0019517±0.02%, IC=1.034801±0.003132, NM-297B, Lab#=66431-01, Argus VI

ID		Power (Watts)	$^{40}Ar/^{39}Ar$	$^{37}Ar/^{39}Ar$	$^{36}Ar/^{39}Ar$ (x 10^{-3})	$^{39}Ar_K$ (x 10^{-15} mol)	K/Ca	$^{40}Ar^*$ (%)	^{39}Ar (%)	Age (Ma)	±1σ (Ma)
Xi	A	1.0	181.8	0.0068	608.5	5.0	75.0	1.1	3.0	7.1	2.2
Xi	B	2.0	44.20	0.0129	118.1	14.4	39.6	21.0	11.7	32.87	0.40
Xi	C	2.5	15.85	0.0111	15.33	18.2	46.2	71.4	22.8	39.986	0.073
Xi	D	3.0	12.18	0.0100	2.328	39.4	50.9	94.4	46.6	40.579	0.020
Xi	E	3.5	11.38	0.0092	0.5188	52.6	55.5	98.7	78.4	39.668	0.013
Xi	F	3.6	10.98	0.0094	0.1964	25.5	54.5	99.5	93.9	38.599	0.022
Xi	G	3.8	10.71	0.0024	0.1602	8.2	210.3	99.6	98.8	37.689	0.060
Xi	H	3.9	10.40	-0.0097	0.1048	1.9	-	99.7	100.0	36.63	0.24
Integrated age ± 1σ			n=8			165.1	54.8		K2O=6.61%	38.061	0.075
Plateau ± 1σ		no plateau	n=0	MSWD=0.00	0.000				0.0	0.00	0.000
Isochron±2σ		no isochron	n=0	MSWD=1.00			$^{40}Ar/^{36}Ar=$	0.0±0.0		0.000	0.000

KS 139, Illite, 4.74 mg, J=0.0019575±0.02%, IC=1.019414±0.0025289, NM-297C, Lab#=66444-01, Argus VI

ID		Power (Watts)	$^{40}Ar/^{39}Ar$	$^{37}Ar/^{39}Ar$	$^{36}Ar/^{39}Ar$ (x 10^{-3})	$^{39}Ar_K$ (x 10^{-15} mol)	K/Ca	$^{40}Ar^*$ (%)	^{39}Ar (%)	Age (Ma)	±1σ (Ma)
Xi	B	0.4	56.20	0.0062	170.3	0.9	82.3	10.4	0.4	20.85	0.90
Xi	C	0.5	43.42	0.0336	115.8	1.0	15.2	21.2	0.8	32.66	0.74
Xi	D	0.6	24.03	0.0270	50.38	2.0	18.9	38.0	1.7	32.46	0.36
Xi	E	0.7	16.34	0.1081	23.33	3.1	4.7	57.8	3.0	33.54	0.20
Xi	F	0.8	13.92	0.1884	13.69	4.3	2.7	71.0	4.9	35.09	0.13
Xi	G	1.0	12.75	0.1608	8.974	7.1	3.2	79.3	7.9	35.855	0.085
Xi	H	1.2	11.69	0.0247	4.990	12.2	20.7	87.4	13.1	36.239	0.047
Xi	J	1.8	11.00	0.0069	2.423	23.9	74.1	93.5	23.4	36.462	0.026
Xi	K	2.0	10.78	0.0053	1.827	25.9	96.3	95.0	34.6	36.322	0.022
Xi	L	3.0	10.68	0.0054	1.727	33.3	94.3	95.2	48.9	36.047	0.018
Xi	M	4.0	10.57	0.0026	1.514	28.6	194.8	95.8	61.2	35.893	0.020
Xi	N	5.0	10.57	0.0036	1.666	22.0	141.3	95.3	70.7	35.736	0.025
	O	6.0	10.81	0.0052	2.549	16.3	98.2	93.0	77.7	35.659	0.035
	P	7.0	10.86	0.0070	2.832	11.6	72.4	92.3	82.7	35.554	0.046

Table C1. ^{40}Ar/^{39}Ar analytical data, bulk grain step heating results.

	ID	Power	^{40}Ar/^{39}Ar	^{37}Ar/^{39}Ar	^{36}Ar/^{39}Ar	^{39}Ar$_K$	K/Ca	^{40}Ar*	^{39}Ar	Age	±1σ
		(Watts)			(x 10^{-3})	(x 10^{-15} mol)		(%)	(%)	(Ma)	(Ma)
	Q	8.0	11.28	0.0067	4.261	10.3	76.3	88.8	87.1	35.540	0.051
	R	10.0	11.74	0.0100	5.853	12.7	51.3	85.3	92.6	35.495	0.053
	S	15.0	12.62	0.0117	8.993	17.2	43.6	78.9	100.0	35.318	0.049
	Integrated age ± 1σ		n=17			232.2	30.6		K2O=9.61%	35.762	0.013
	Plateau ± 1σ	steps O-S	n=5	MSWD=8.30	68.038				29.3	35.54	0.058
	Isochron±2σ	steps O-S	n=5	MSWD=1.00			^{40}Ar/^{36}Ar=		282.1±2.4	35.748	0.042

KS023, Hornblende, 8.17 mg, J=0.0019533±0.02%, IC=1.019151±0.0025435, NM-297B, Lab#=66429-01, Argus VI

	ID	Power	^{40}Ar/^{39}Ar	^{37}Ar/^{39}Ar	^{36}Ar/^{39}Ar	^{39}Ar$_K$	K/Ca	^{40}Ar*	^{39}Ar	Age	±1σ
Xi	A	1.5	64.94	2.119	193.4	1.0	0.24	12.2	2.3	28.21	0.92
Xi	B	2.0	18.92	1.770	35.43	0.7	0.29	45.4	3.8	30.48	0.67
Xi	C	2.5	15.62	1.057	25.00	0.6	0.48	53.2	5.2	29.51	0.67
Xi	D	3.0	14.38	1.239	21.77	0.6	0.41	56.0	6.6	28.56	0.69
Xi	E	3.5	13.97	2.769	17.68	1.1	0.18	64.2	9.0	31.83	0.41
Xi	F	4.0	11.30	4.661	6.828	4.1	0.11	85.5	18.2	34.34	0.12
	G	4.5	10.76	5.042	4.265	6.8	0.10	92.1	33.5	35.207	0.071
	H	5.0	10.81	4.920	4.642	4.5	0.10	91.0	43.7	34.96	0.10
	I	5.5	10.96	4.721	5.554	3.2	0.11	88.5	50.9	34.47	0.15
	J	6.0	10.80	4.794	5.022	3.3	0.11	89.9	58.3	34.50	0.13
	K	7.0	10.59	5.052	3.488	9.5	0.10	94.2	79.7	35.415	0.055
	L	15.0	10.42	4.134	3.979	9.0	0.12	92.0	100.0	34.030	0.056
	Integrated age ± 1σ		n=12			44.4	0.11		K2O=1.07%	34.317	0.041
	Plateau ± 1σ	steps G-L	n=6	MSWD=71.04	36.324				81.8	34.82	0.262
	Isochron±2σ	steps G-L	n=6	MSWD=81.78			^{40}Ar/^{36}Ar=		443.8±32.9	33.387	0.197

KS095, Hornblende, 4.2 mg, J=0.0019508±0.02%, IC=1.01921±0.0025394, NM-297B, Lab#=66436-01, Argus VI

	ID	Power	^{40}Ar/^{39}Ar	^{37}Ar/^{39}Ar	^{36}Ar/^{39}Ar	^{39}Ar$_K$	K/Ca	^{40}Ar*	^{39}Ar	Age	±1σ
Xi	A	1.5	56.80	0.8961	170.8	0.6	0.57	11.3	1.8	22.7	1.2
Xi	B	2.0	23.63	1.404	52.35	0.4	0.36	35.0	3.0	29.3	1.1
Xi	C	2.5	18.71	3.280	32.47	0.9	0.16	50.2	5.7	33.29	0.52
Xi	D	3.0	13.01	3.204	11.22	4.3	0.16	76.5	18.0	35.30	0.13
i	E	3.5	11.47	3.110	5.624	11.3	0.16	87.7	50.1	35.654	0.054
i	F	4.0	10.97	3.168	3.883	10.2	0.16	91.9	79.2	35.736	0.054
Xi	G	4.5	11.16	3.555	5.018	5.2	0.14	89.3	94.0	35.343	0.095
Xi	H	5.0	10.89	3.601	5.175	1.0	0.14	88.7	96.8	34.22	0.41
Xi	L	15.0	9.107	1.874	2.515	1.1	0.27	93.5	100.0	30.18	0.33
	Integrated age ± 1σ		n=9			35.0	0.16		K2O=1.64%	35.003	0.046
	Plateau ± 1σ	steps E-F	n=2	MSWD=1.12	21.439				61.2	35.70	0.041
	Isochron±2σ	no isochron	n=0	MSWD=1.28			^{40}Ar/^{36}Ar=		0.0±0.0	0.000	0.000

KS114A, Hornblende, 2.33 mg, J=0.0019555±0.02%, IC=1.019262±0.0025354, NM-297C, Lab#=66449-01, Argus VI

	ID	Power	^{40}Ar/^{39}Ar	^{37}Ar/^{39}Ar	^{36}Ar/^{39}Ar	^{39}Ar$_K$	K/Ca	^{40}Ar*	^{39}Ar	Age	±1σ
Xi	A	1.5	51.55	1.096	142.7	0.9	0.47	18.4	5.2	33.61	0.87
	B	2.5	14.02	0.6337	13.20	1.7	0.81	72.5	14.4	36.05	0.28
	C	3.5	13.02	3.175	10.21	3.3	0.16	78.8	32.6	36.43	0.16
	D	4.0	11.38	4.216	5.582	4.2	0.12	88.5	55.9	35.80	0.11
	E	4.5	11.61	4.563	6.293	3.2	0.11	87.2	73.7	36.00	0.14
	F	5.0	11.88	4.469	7.299	2.0	0.11	84.9	84.9	35.85	0.22
	G	6.0	11.85	3.049	7.320	0.8	0.17	83.8	89.4	35.29	0.46

Table C1. ^{40}Ar/^{39}Ar analytical data, bulk grain step heating results.

	ID	Power (Watts)	^{40}Ar/^{39}Ar	^{37}Ar/^{39}Ar	^{36}Ar/^{39}Ar (x 10^{-3})	^{39}Ar$_K$ (x 10^{-15} mol)	K/Ca	^{40}Ar* (%)	^{39}Ar (%)	Age (Ma)	±1σ (Ma)
	H	7.0	11.23	1.567	3.914	0.8	0.33	90.8	93.8	36.18	0.51
	I	15.0	10.79	1.265	2.841	1.1	0.40	93.2	100.0	35.64	0.33
	Integrated age ± 1σ		n=9			18.0	0.16		K2O=1.52%	35.849	0.083
	Plateau ± 1σ	steps B-I	n=8	MSWD=2.12		17.1			94.8	35.97	0.10
	Isochron±2σ	steps B-I	n=8	MSWD=1.28			^{40}Ar/^{36}Ar=		315.3±7.8	35.55	0.18

KS135, Hornblende, 8.08 mg, J=0.0019537±0.02%, IC=1.016167±0.0026298, NM-297B, Lab#=66424-01, Argus VI

	ID	Power	^{40}Ar/^{39}Ar	^{37}Ar/^{39}Ar	^{36}Ar/^{39}Ar	^{39}Ar$_K$	K/Ca	^{40}Ar*	^{39}Ar	Age	±1σ
Xi	A	2.0	24.99	3.866	52.88	5.9	0.13	38.7	18.2	34.38	0.23
Xi	B	4.0	11.80	4.517	7.822	7.4	0.11	83.5	41.2	35.031	0.078
i	C	4.5	10.92	4.952	4.216	10.9	0.10	92.3	75.0	35.816	0.047
i	E	5.0	10.99	4.957	4.277	8.1	0.10	92.2	100.0	35.988	0.061
	Integrated age ± 1σ		n=4			32.3	0.11		K2O=0.79%	35.418	0.052
	Plateau ± 1σ	steps C-E	n=2	MSWD=4.98		19.017			58.8	35.88	0.083
	Isochron±2σ	no isochron	n=0	MSWD=1.12			^{40}Ar/^{36}Ar=		0.0±0.0	0.000	0.000

KS144, Hornblende, 6.07 mg, J=0.0019542±0.01%, IC=1.019086±0.0025474, NM-297B, Lab#=66427-01, Argus VI

	ID	Power	^{40}Ar/^{39}Ar	^{37}Ar/^{39}Ar	^{36}Ar/^{39}Ar	^{39}Ar$_K$	K/Ca	^{40}Ar*	^{39}Ar	Age	±1σ
Xi	A	1.5	107.4	2.069	328.2	0.2	0.25	9.8	0.7	37.4	3.1
Xi	B	2.0	32.29	2.058	79.79	0.1	0.25	27.5	0.9	31.5	7.0
Xi	C	3.0	20.12	4.234	36.84	0.2	0.12	47.6	1.4	34.0	2.6
	D	3.5	14.86	4.906	18.35	1.2	0.10	66.2	5.5	34.96	0.39
	E	4.0	12.39	5.058	9.117	5.4	0.10	81.6	24.1	35.92	0.10
	F	4.5	11.43	5.085	5.717	8.9	0.10	88.9	54.7	36.089	0.065
	G	5.0	11.10	5.110	4.722	7.6	0.100	91.2	80.8	35.978	0.069
	H	5.5	11.10	5.117	4.668	3.8	0.100	91.4	94.0	36.04	0.11
	I	6.0	11.59	5.162	6.473	0.8	0.099	87.1	96.9	35.88	0.48
	J	7.0	11.71	5.091	7.041	0.6	0.10	85.8	99.1	35.71	0.61
	K	15.0	11.73	5.074	8.639	0.3	0.10	81.8	100.0	34.1	1.4
	Integrated age ± 1σ		n=11			29.1	0.10		K2O=0.94%	35.935	0.055
	Plateau ± 1σ	steps D-K	n=8	MSWD=1.70		28.7			98.6	36.005	0.052
	Isochron±2σ	steps D-K	n=8	MSWD=1.12			^{40}Ar/^{36}Ar=		282.5±5.6	36.210	0.096

KS137, Biotite, 3.64 mg, J=0.0019575±0.02%, IC=1.016453±0.0026031, NM-297C, Lab#=66446-01, Argus VI

	ID	Power	^{40}Ar/^{39}Ar	^{37}Ar/^{39}Ar	^{36}Ar/^{39}Ar	^{39}Ar$_K$	K/Ca	^{40}Ar*	^{39}Ar	Age	±1σ
Xi	A	1.0	27.42	0.0488	63.52	6.1	10.5	31.5	4.2	30.73	0.26
Xi	B	2.0	12.19	0.0110	7.689	12.4	46.2	81.4	12.7	35.180	0.054
Xi	C	2.5	10.71	0.0051	1.834	15.3	100.3	94.9	23.2	36.039	0.031
Xi	D	3.0	10.48	0.0083	1.144	16.6	61.4	96.8	34.6	35.968	0.028
Xi	E	4.0	10.54	0.0193	1.305	30.2	26.4	96.4	55.3	36.005	0.018
Xi	F	4.5	10.64	0.0343	1.894	22.8	14.9	94.8	70.9	35.758	0.028
	H	5.0	10.90	0.0470	2.998	16.8	10.9	91.9	82.4	35.537	0.033
	I	5.5	10.50	0.0190	1.813	2.7	26.8	94.9	84.3	35.35	0.14
	J	6.0	10.56	0.0268	1.817	4.3	19.0	94.9	87.2	35.562	0.097
	L	10.0	10.49	0.0353	1.616	18.7	14.5	95.5	100.0	35.533	0.029
	Integrated age ± 1σ		n=10			145.9	20.5		K2O=7.87%	35.537	0.017
	Plateau ± 1σ	steps H-L	n=4	MSWD=0.57		42.426			29.1	35.53	0.022
	Isochron±2σ	steps H-L	n=4	MSWD=0.83			^{40}Ar/^{36}Ar=		297.2±9.0	35.519	0.072

Table C1. ^{40}Ar/^{39}Ar analytical data, bulk grain step heating results.

	ID	Power	^{40}Ar/^{39}Ar	^{37}Ar/^{39}Ar	^{36}Ar/^{39}Ar	^{39}Ar$_K$	K/Ca	^{40}Ar*	^{39}Ar	Age	±1σ
		(Watts)			(x 10^{-3})	(x 10^{-15} mol)		(%)	(%)	(Ma)	(Ma)
			KS 143, Biotite, .91 mg, J=0.0019502±0.02%, IC=1.0193±0.0025325, NM-297B, Lab#=66434-01, Argus VI								
Xi	A	1.0	70.99	1.807	73.40	0.9	0.28	69.7	5.4	168.7	1.1
Xi	B	1.5	116.3	0.9135	31.56	1.3	0.56	92.0	12.5	347.2	1.5
Xi	C	2.0	142.1	0.4051	14.09	2.0	1.3	97.1	23.7	436.4	1.0
Xi	D	2.5	151.2	0.2115	8.209	2.1	2.4	98.4	35.8	466.3	1.1
Xi	E	3.0	153.0	0.1744	5.944	1.9	2.9	98.9	46.4	473.2	1.1
i	F	3.5	149.5	0.2242	5.170	1.7	2.3	99.0	56.3	464.2	1.3
i	G	4.0	150.2	0.2015	3.746	1.9	2.5	99.3	67.1	467.3	1.0
i	H	4.3	150.3	0.1464	3.408	1.3	3.5	99.3	74.8	467.9	1.6
i	I	4.5	149.3	0.1453	4.154	1.1	3.5	99.2	80.8	464.5	2.0
i	J	5.0	148.8	0.1946	4.207	1.1	2.6	99.2	87.2	463.2	2.0
i	K	6.0	149.9	0.1426	3.594	2.3	3.6	99.3	100.0	466.6	1.0
	Integrated age ± 1σ		n=11			17.6	1.5		K2O=3.81%	440.36	0.41
	Plateau ± 1σ	steps F-K	n=6	MSWD=1.59	9.4			53.6	466.10	0.69
	Isochron±2σ	no isochron	n=0	MSWD=1.02		^{40}Ar/^{36}Ar=	0.0±0.0	0.0	0.0

Notes:
Isotopic ratios corrected for blank, radioactive decay, and mass discrimination, not corrected for interfering reactions.
Errors quoted for individual analyses include analytical error only, without interfering reaction or J uncertainties.
Integrated age calculated by summing isotopic measurements of all steps.
Integrated age error calculated by quadratically combining errors of isotopic measurements of all steps.
Plateau age is inverse-variance-weighted mean of selected steps.
Plateau age error is inverse-variance-weighted mean error (Taylor, 1982) times root MSWD where MSWD>1.
Plateau error is weighted error of Taylor (1982).
Decay constants and isotopic abundances after Steiger and Jäger (1977).
symbol preceding sample ID denotes analyses excluded from plateau age calculations.
Weight percent K$_2$O calculated from ^{39}Ar signal, sample weight, and instrument sensitivity.
Ages calculated relative to FC-2 Fish Canyon Tuff sanidine interlaboratory standard at 28.201 Ma
Decay Constant (LambdaK (total))= 5.463e-10/a
Correction factors:
(^{39}Ar/^{37}Ar)$_{Ca}$ = 0.0007593 ± 0.000008
(^{36}Ar/^{37}Ar)$_{Ca}$ = 0.0002772 ± 0.0000010
(^{38}Ar/^{39}Ar)$_K$ = 0.01271
(^{40}Ar/^{39}Ar)$_K$ = 0.007204 ± 0.00046

Table C2. ^{40}Ar/^{39}Ar analytical data, single crystal step heating results.

ID		Power (Watts)	^{40}Ar/^{39}Ar	^{37}Ar/^{39}Ar	^{36}Ar/^{39}Ar (x 10^{-3})	^{39}Ar$_K$ (x 10^{-15} mol)	K/Ca	^{40}Ar* (%)	^{39}Ar (%)	Age (Ma)	±1σ (Ma)
			KS 003, Plagioclase, J=0.0019577±0.02%, IC=1.000371±0.0009714, NM-297C, Lab#=66445-01, Argus VI								
Xi	A	0.2	66.96	4.511	196.4	0.114	0.11	13.8	11.6	33.04	0.94
	B	0.3	20.40	2.945	36.28	0.089	0.17	48.6	20.6	35.27	0.56
	C	0.4	17.61	1.804	26.05	0.052	0.28	57.1	25.9	35.72	0.79
	D	3.0	17.32	5.032	25.81	0.728	0.10	58.3	100.0	35.97	0.13
	Integrated age ± 1σ			n=4		0.983	0.11			35.55	0.16
	Plateau ± 1σ	steps B-D		n=3	MSWD=0.79	0.869			88.4	35.93	0.12
	Isochron±2σ	steps B-D		n=3	MSWD=0.05		^{40}Ar/^{36}Ar=	277.3±14.3		37.5	1.3
			KS 003, Plagioclase, J=0.0019577±0.02%, IC=1.000371±0.0009714, NM-297C, Lab#=66445-02, Argus VI								
	A	0.2	53.89	3.629	150.0	0.136	0.14	18.3	14.1	35.14	0.79
	B	0.3	17.58	2.976	25.95	0.118	0.17	57.7	26.3	36.08	0.44
	C	0.4	15.99	3.405	21.33	0.447	0.15	62.3	72.5	35.42	0.16
	D	3.0	12.89	4.968	10.54	0.266	0.10	79.0	100.0	36.25	0.17
	Integrated age ± 1σ			n=4		0.967	0.13			35.69	0.15
	Plateau ± 1σ	steps A-D		n=4	MSWD=4.59	0.967			100.0	35.83	0.24
	Isochron±2σ	steps A-D		n=4	MSWD=5.43		^{40}Ar/^{36}Ar=	292.7±1.6		36.01	0.15
			KS 003, Plagioclase, J=0.0019577±0.02%, IC=1.000371±0.0009714, NM-297C, Lab#=66445-03, Argus VI								
Xi	A	0.2	96.12	4.523	297.4	0.078	0.11	9.0	7.2	30.7	1.3
	B	0.3	25.99	5.093	55.45	0.108	0.10	38.5	17.2	35.68	0.50
	C	0.4	19.70	3.719	34.00	0.033	0.14	50.5	20.2	35.4	1.2
	D	3.0	18.55	5.007	30.01	0.865	0.10	54.4	100.0	35.93	0.12
	Integrated age ± 1σ			n=4		1.085	0.10			35.51	0.15
	Plateau ± 1σ	steps B-D		n=3	MSWD=0.20	1.007			92.8	35.91	0.12
	Isochron±2σ	steps B-D		n=3	MSWD=0.15		^{40}Ar/^{36}Ar=	292.6±5.8		36.21	0.62
			KS 003, Plagioclase, J=0.0019577±0.02%, IC=1.000371±0.0009714, NM-297C, Lab#=66445-04, Argus VI								
	A	0.2	53.17	5.448	148.6	0.047	0.094	18.3	17.5	34.6	1.4
	B	0.3	23.36	3.104	48.22	0.045	0.16	40.1	34.5	33.32	0.96
	C	0.4	20.07	3.224	36.60	0.024	0.16	47.4	43.6	33.9	1.5
	D	3.0	15.89	6.118	21.66	0.150	0.083	62.9	100.0	35.58	0.32
	Integrated age ± 1σ			n=4		0.267	0.098			34.87	0.37
	Plateau ± 1σ	steps A-D		n=4	MSWD=2.09	0.267			100.0	35.27	0.42
	Isochron±2σ	steps A-D		n=4	MSWD=2.34		^{40}Ar/^{36}Ar=	291.8±3.1		35.66	0.42
			KS 003, Plagioclase, J=0.0019577±0.02%, IC=1.000371±0.0009714, NM-297C, Lab#=66445-05, Argus VI								
	A	0.2	75.87	4.009	224.8	0.072	0.13	12.9	12.5	34.8	1.2
	B	0.3	27.17	2.648	60.18	0.051	0.19	35.3	21.4	34.12	0.90
	C	0.4	23.61	2.137	47.16	0.092	0.24	41.7	37.4	34.99	0.57
	D	3.0	19.38	5.375	33.43	0.360	0.095	51.3	100.0	35.41	0.21
	Integrated age ± 1σ			n=4		0.575	0.11			35.15	0.23
	Plateau ± 1σ	steps A-D		n=4	MSWD=0.83	0.575			100.0	35.29	0.19

Table C2. ^{40}Ar/^{39}Ar analytical data, single crystal step heating results.

ID	Power (Watts)	^{40}Ar/^{39}Ar	^{37}Ar/^{39}Ar	^{36}Ar/^{39}Ar (x 10^{-3})	^{39}Ar$_K$ (x 10^{-15} mol)	K/Ca	^{40}Ar* (%)	^{39}Ar (%)	Age (Ma)	±1σ (Ma)
Isochron±2σ	steps A-D	n=4	MSWD=0.93			^{40}Ar/^{36}Ar=	294.1±1.8		35.49	0.31

KS 003, Plagioclase, J=0.0019577±0.02%, IC=1.000371±0.0009714, NM-297C, Lab#=66445-06, Argus VI

ID	Power (Watts)	^{40}Ar/^{39}Ar	^{37}Ar/^{39}Ar	^{36}Ar/^{39}Ar (x 10^{-3})	^{39}Ar$_K$ (x 10^{-15} mol)	K/Ca	^{40}Ar* (%)	^{39}Ar (%)	Age (Ma)	±1σ (Ma)
A	0.2	50.68	7.666	140.0	0.036	0.067	19.6	14.7	35.4	1.5
B	0.3	27.69	8.508	56.17	0.008	0.060	42.6	18.0	42.0	4.8
C	0.4	28.53	11.38	38.61	0.002	0.045	63.3	18.7	64.1	31.9
D	3.0	14.59	6.869	17.27	0.200	0.074	68.9	100.0	35.82	0.25
Integrated age ± 1σ		n=4			0.247	0.072			36.15	0.36
Plateau ± 1σ	steps A-D	n=4	MSWD=0.83	0.247				100.0	35.83	0.25
Isochron±2σ	steps A-D	n=4	MSWD=2.03			^{40}Ar/^{36}Ar=	295.1±3.5		35.86	0.34

KS 003, Plagioclase, J=0.0019577±0.02%, IC=1.000371±0.0009714, NM-297C, Lab#=66445-07, Argus VI

ID	Power (Watts)	^{40}Ar/^{39}Ar	^{37}Ar/^{39}Ar	^{36}Ar/^{39}Ar (x 10^{-3})	^{39}Ar$_K$ (x 10^{-15} mol)	K/Ca	^{40}Ar* (%)	^{39}Ar (%)	Age (Ma)	±1σ (Ma)
A	0.2	45.87	8.306	124.9	0.044	0.061	21.0	10.5	34.5	1.3
B	0.3	26.99	5.866	60.11	0.028	0.087	35.9	17.2	34.6	1.4
C	0.4	15.41	6.030	20.38	0.037	0.085	64.1	26.2	35.2	1.0
D	3.0	12.46	7.694	10.16	0.306	0.066	80.9	100.0	35.97	0.17
Integrated age ± 1σ		n=4			0.414	0.068			35.65	0.23
Plateau ± 1σ	steps A-D	n=4	MSWD=0.89	0.414				100.0	35.91	0.16
Isochron±2σ	steps A-D	n=4	MSWD=0.28			^{40}Ar/^{36}Ar=	291.1±3.0		36.08	0.20

KS 003, Plagioclase, J=0.0019577±0.02%, IC=1.000371±0.0009714, NM-297C, Lab#=66445-08, Argus VI

ID	Power (Watts)	^{40}Ar/^{39}Ar	^{37}Ar/^{39}Ar	^{36}Ar/^{39}Ar (x 10^{-3})	^{39}Ar$_K$ (x 10^{-15} mol)	K/Ca	^{40}Ar* (%)	^{39}Ar (%)	Age (Ma)	±1σ (Ma)
A	0.2	130.3	4.590	408.8	0.117	0.11	7.6	6.3	35.2	1.3
B	0.3	30.92	3.618	72.04	0.140	0.14	32.1	13.8	35.32	0.49
C	0.4	20.14	2.588	35.14	0.072	0.20	49.5	17.7	35.43	0.66
D	3.0	19.08	3.985	31.80	1.53	0.13	52.4	100.0	35.597	0.093
Integrated age ± 1σ		n=4			1.86	0.13			35.54	0.12
Plateau ± 1σ	steps A-D	n=4	MSWD=0.15	1.86				100.0	35.582	0.090
Isochron±2σ	steps A-D	n=4	MSWD=0.13			^{40}Ar/^{36}Ar=	295.1±0.9		35.63	0.14

KS 003, Plagioclase, J=0.0019577±0.02%, IC=1.000371±0.0009714, NM-297C, Lab#=66445-09, Argus VI

	ID	Power (Watts)	^{40}Ar/^{39}Ar	^{37}Ar/^{39}Ar	^{36}Ar/^{39}Ar (x 10^{-3})	^{39}Ar$_K$ (x 10^{-15} mol)	K/Ca	^{40}Ar* (%)	^{39}Ar (%)	Age (Ma)	±1σ (Ma)
Xi	A	0.2	64.53	3.936	187.7	0.101	0.13	14.6	11.2	33.46	0.95
i	B	0.3	23.11	3.830	42.90)	0.060	0.13	46.5	18.0	38.18	0.77
i	C	3.0	14.33	4.441	15.68	0.736	0.11	70.2	100.0	35.81	0.10
	Integrated age ± 1σ		n=3			0.897	0.12			35.71	0.15
	Plateau ± 1σ	steps B-C	n=2	MSWD=9.34	0.797				88.8	35.85	0.311
	Isochron±2σ	no isochron	n=0	MSWD=0.05			^{40}Ar/^{36}Ar=	0.0±0.0		0.00	0.00

KS 003, Plagioclase, J=0.0019577±0.02%, IC=1.000371±0.0009714, NM-297C, Lab#=66445-10, Argus VI

	ID	Power (Watts)	^{40}Ar/^{39}Ar	^{37}Ar/^{39}Ar	^{36}Ar/^{39}Ar (x 10^{-3})	^{39}Ar$_K$ (x 10^{-15} mol)	K/Ca	^{40}Ar* (%)	^{39}Ar (%)	Age (Ma)	±1σ (Ma)
i	A	0.4	20.38	3.675	36.11	0.419	0.14	49.1	66.8	35.58	0.20
i	B	3.0	11.38	5.316	5.581	0.208	0.096	89.3	100.0	36.21	0.18
	Integrated age ± 1σ		n=2			0.627	0.12			35.79	0.15
	Plateau ± 1σ	steps A-B	n=2	MSWD=5.39	0.627				100.0	35.92	0.313
	Isochron±2σ	no isochron	n=0	MSWD=0.00			^{40}Ar/^{36}Ar=	0.0±0.0		0.00	0.00

Table C2. ^{40}Ar/^{39}Ar analytical data, single crystal step heating results.

	ID	Power (Watts)	^{40}Ar/^{39}Ar	^{37}Ar/^{39}Ar	^{36}Ar/^{39}Ar (x 10^{-3})	^{39}Ar$_K$ (x 10^{-15} mol)	K/Ca	^{40}Ar* (%)	^{39}Ar (%)	Age (Ma)	±1σ (Ma)
			KS 003, Plagioclase, J=0.0019577±0.02%, IC=1.000371±0.0009714, NM-297C, Lab#=66445-11, Argus VI								
i	A	0.4	29.57	3.163	68.48	0.153	0.16	32.4	32.6	34.12	0.49
i	B	3.0	15.05	4.641	18.39	0.316	0.11	66.4	100.0	35.58	0.19
		Integrated age ± 1σ		n=2		0.469	0.12			35.11	0.20
		Plateau ± 1σ	steps A-B	n=2	MSWD=7.86	0.469			100.0	35.40	0.490
		Isochron±2σ	no isochron	n=0	MSWD=0.00		^{40}Ar/^{36}Ar=	0.0±0.0		0.00	0.00
			KS 003, Plagioclase, J=0.0019577±0.02%, IC=1.000371±0.0009714, NM-297C, Lab#=66445-12, Argus VI								
i	A	0.4	40.16	6.135	104.0	0.116	0.083	24.7	25.9	35.42	0.67
i	B	3.0	14.32	8.159	16.92	0.333	0.063	69.8	100.0	35.66	0.18
		Integrated age ± 1σ		n=2		0.449	0.067			35.60	0.22
		Plateau ± 1σ	steps A-B	n=2	MSWD=0.12	0.449			100.0	35.64	0.173
		Isochron±2σ	no isochron	n=0	MSWD=0.00		^{40}Ar/^{36}Ar=	0.0±0.0		0.00	0.00
			KS 003, Plagioclase, J=0.0019577±0.02%, IC=1.000371±0.0009714, NM-297C, Lab#=66445-13, Argus VI								
i	A	0.4	29.45	3.756	67.86	0.206	0.14	32.9	30.4	34.52	0.39
i	B	3.0	14.52	5.663	17.03	0.472	0.090	68.5	100.0	35.45	0.14
		Integrated age ± 1σ		n=2		0.679	0.10			35.16	0.15
		Plateau ± 1σ	steps A-B	n=2	MSWD=5.11	0.679			100.0	35.34	0.289
		Isochron±2σ	no isochron	n=0	MSWD=0.00		^{40}Ar/^{36}Ar=	0.0±0.0		0.00	0.00
			KS 003, Plagioclase, J=0.0019577±0.02%, IC=1.000371±0.0009714, NM-297C, Lab#=66445-14, Argus VI								
i	A	0.4	28.57	5.570	64.68	0.192	0.092	34.7	34.6	35.31	0.39
i	B	3.0	12.61	6.506	10.74	0.362	0.078	79.0	100.0	35.52	0.14
		Integrated age ± 1σ		n=2		0.553	0.083			35.45	0.16
		Plateau ± 1σ	steps A-B	n=2	MSWD=0.26	0.553			100.0	35.50	0.132
		Isochron±2σ	no isochron	n=0	MSWD=0.00		^{40}Ar/^{36}Ar=	0.0±0.0		0.00	0.00
			KS 003, Plagioclase, J=0.0019577±0.02%, IC=1.000371±0.0009714, NM-297C, Lab#=66445-15, Argus VI								
i	A	0.4	30.75	3.215	71.92	0.262	0.16	31.7	48.1	34.69	0.35
i	B	3.0	15.68	5.808	20.80	0.282	0.088	63.8	100.0	35.65	0.20
		Integrated age ± 1σ		n=2		0.544	0.11			35.19	0.20
		Plateau ± 1σ	steps A-B	n=2	MSWD=5.50	0.544			100.0	35.41	0.415
		Isochron±2σ	no isochron	n=0	MSWD=0.00		^{40}Ar/^{36}Ar=	0.0±0.0		0.00	0.00
			KS 041, Plagioclase, J=0.001954±0.02%, IC=0.9975058±0.0007907, NM-297B, Lab#=66425-01, Argus VI								
Xi	A	0.2	401.3	1.672	1342.1	0.044	0.31	1.2	2.8	17.3	2.6
Xi	B	0.2	26.12	2.649	59.98	0.108	0.19	33.0	9.8	30.58	0.84
Xi	C	0.4	12.65	2.892	12.28	0.391	0.18	73.2	34.8	32.864	0.099
Xi	D	3.0	14.61	3.369	17.82	1.018	0.15	65.8	100.0	34.150	0.055
		Integrated age ± 1σ		n=4		1.56	0.16			33.10	0.10

Table C2. ^{40}Ar/^{39}Ar analytical data, single crystal step heating results.

	ID	Power (Watts)	^{40}Ar/^{39}Ar	^{37}Ar/^{39}Ar	^{36}Ar/^{39}Ar (x 10^{-3})	^{39}Ar$_K$ (x 10^{-15} mol)	K/Ca	^{40}Ar* (%)	^{39}Ar (%)	Age (Ma)	±1σ (Ma)
Plateau ± 1σ		no plateau	n=0	MSWD=0.00	0.000			0.0	0.00	0.000
Isochron±2σ		no isochron	n=0	MSWD=0.00		^{40}Ar/^{36}Ar=	0.0±0.0		0.000	0.000

KS 041, Plagioclase, J=0.001954±0.02%, IC=0.9975058±0.0007907, NM-297B, Lab#=66425-02, Argus VI

	ID	Power	^{40}Ar/^{39}Ar	^{37}Ar/^{39}Ar	^{36}Ar/^{39}Ar	^{39}Ar$_K$	K/Ca	^{40}Ar*	^{39}Ar	Age	±1σ
Xi	A	0.3	42.89	2.990	116.6	0.295	0.17	20.2	26.8	30.82	0.42
Xi	B	0.4	17.66	2.486	29.23	0.452	0.21	52.2	67.7	32.76	0.18
i	C	0.5	17.68	4.162	28.59	0.194	0.12	54.1	85.3	33.98	0.29
i	D	3.0	17.81	5.699	28.59	0.162	0.090	55.2	100.0	34.96	0.31
Integrated age ± 1σ			n=4			1.103	0.15			32.78	0.15
Plateau ± 1σ		steps C-D	n=2	MSWD=5.35	0.356			32.3		34.44	0.485
Isochron±2σ		no isochron	n=0	MSWD=0.00		^{40}Ar/^{36}Ar=	0.0±0.0		0.00	0.00

KS 041, Plagioclase, J=0.001954±0.02%, IC=0.9975058±0.0007907, NM-297B, Lab#=66425-03, Argus VI

	ID	Power	^{40}Ar/^{39}Ar	^{37}Ar/^{39}Ar	^{36}Ar/^{39}Ar	^{39}Ar$_K$	K/Ca	^{40}Ar*	^{39}Ar	Age	±1σ
Xi	A	0.3	67.34	2.644	197.7	0.550	0.19	13.5	61.6	32.41	0.44
i	B	0.4	13.84	3.971	13.76	0.050	0.13	73.0	67.3	35.85	0.71
i	C	0.5	11.73	4.151	7.291	0.061	0.12	84.5	74.1	35.20	0.54
i	D	3.0	13.21	4.113	12.17	0.231	0.12	75.3	100.0	35.33	0.20
Integrated age ± 1σ			n=4			0.892	0.16			33.55	0.28
Plateau ± 1σ		steps B-D	n=3	MSWD=0.29	0.342			38.4		35.35	0.178
Isochron±2σ		no isochron	n=0	MSWD=0.00		^{40}Ar/^{36}Ar=	0.0±0.0		0.00	0.00

KS 041, Plagioclase, J=0.001954±0.02%, IC=0.9975058±0.0007907, NM-297B, Lab#=66425-04, Argus VI

	ID	Power	^{40}Ar/^{39}Ar	^{37}Ar/^{39}Ar	^{36}Ar/^{39}Ar	^{39}Ar$_K$	K/Ca	^{40}Ar*	^{39}Ar	Age	±1σ
Xi	A	0.3	27.71	4.268	65.79	0.226	0.12	31.1	33.0	30.64	0.37
Xi	B	0.4	17.20	4.594	28.04	0.188	0.11	54.0	60.5	33.02	0.28
i	C	0.5	14.45	6.332	17.42	0.070	0.081	68.0	70.7	34.94	0.56
i	D	3.0	12.81	6.916	11.75	0.200	0.074	77.3	100.0	35.25	0.22
Integrated age ± 1σ			n=4			0.683	0.095			33.08	0.17
Plateau ± 1σ		steps C-D	n=2	MSWD=0.26	0.270			39.5		35.21	0.203
Isochron±2σ		no isochron	n=0	MSWD=0.00		^{40}Ar/^{36}Ar=	0.0±0.0		0.00	0.00

KS 041, Plagioclase, J=0.001954±0.02%, IC=0.9975058±0.0007907, NM-297B, Lab#=66425-05, Argus VI

	ID	Power	^{40}Ar/^{39}Ar	^{37}Ar/^{39}Ar	^{36}Ar/^{39}Ar	^{39}Ar$_K$	K/Ca	^{40}Ar*	^{39}Ar	Age	±1σ
Xi	A	0.3	105.9	3.845	331.7	0.331	0.13	7.7	38.3	29.21	0.68
Xi	B	0.4	22.82	4.670	46.47	0.278	0.11	41.5	70.6	33.64	0.28
i	C	0.5	14.76	4.698	17.40	0.044	0.11	67.8	75.6	35.55	0.82
i	D	3.0	22.29	5.360	42.66	0.210	0.095	45.4	100.0	35.99	0.32
Integrated age ± 1σ			n=4			0.863	0.11			32.61	0.29
Plateau ± 1σ		steps C-D	n=2	MSWD=0.24	0.254			29.4		35.93	0.302
Isochron±2σ		no isochron	n=0	MSWD=0.00		^{40}Ar/^{36}Ar=	0.0±0.0		0.00	0.00

KS 041, Plagioclase, J=0.001954±0.02%, IC=0.9975058±0.0007907, NM-297B, Lab#=66425-06, Argus VI

	ID	Power	^{40}Ar/^{39}Ar	^{37}Ar/^{39}Ar	^{36}Ar/^{39}Ar	^{39}Ar$_K$	K/Ca	^{40}Ar*	^{39}Ar	Age	±1σ
Xi	A	0.3	39.23	3.457	102.5	0.316	0.15	23.5	55.5	32.78	0.35
Xi	B	0.4	16.18	5.394	24.34	0.016	0.095	58.3	58.4	33.5	2.1
i	C	0.5	13.33	5.055	12.08	0.081	0.10	76.3	72.7	36.15	0.49

Table C2. ^{40}Ar/^{39}Ar analytical data, single crystal step heating results.

	ID	Power (Watts)	^{40}Ar/^{39}Ar	^{37}Ar/^{39}Ar	^{36}Ar/^{39}Ar (x 10^{-3})	^{39}Ar$_K$ (x 10^{-15} mol)	K/Ca	^{40}Ar* (%)	^{39}Ar (%)	Age (Ma)	±1σ (Ma)
i	D	3.0	12.40	5.207	9.866	0.155	0.098	79.9	100.0	35.22	0.26
	Integrated age ± 1σ			n=4		0.569				33.95	0.23
	Plateau ± 1σ	steps C-D		n=2	MSWD=2.79	0.237	0.099±0.002		41.6	35.43	0.387
	Isochron±2σ	no isochron		n=0	MSWD=0.00		^{40}Ar/^{36}Ar=	0.0±0.0		0.00	0.00

KS 041, Plagioclase, J=0.001954±0.02%, IC=0.9975058±0.0007907, NM-297B, Lab#=66425-07, Argus VI

	ID	Power (Watts)	^{40}Ar/^{39}Ar	^{37}Ar/^{39}Ar	^{36}Ar/^{39}Ar (x 10^{-3})	^{39}Ar$_K$ (x 10^{-15} mol)	K/Ca	^{40}Ar* (%)	^{39}Ar (%)	Age (Ma)	±1σ (Ma)
Xi	A	0.3	19.52	3.346	34.94	0.220	0.15	48.5	47.5	33.61	0.30
	B	0.4	16.35	4.394	22.72	0.039	0.12	61.1	55.8	35.51	0.99
	C	0.5	12.41	4.424	9.278	0.038	0.12	80.8	63.9	35.63	0.93
	D	3.0	12.95	4.218	11.01	0.167	0.12	77.5	100.0	35.66	0.25
	Integrated age ± 1σ			n=4		0.464	0.13			34.67	0.20
	Plateau ± 1σ	steps B-D		n=3	MSWD=0.01	0.243			52.5	35.65	0.23
	Isochron±2σ	steps B-D		n=3	MSWD=0.00		^{40}Ar/^{36}Ar=	292.2±24.2		35.8	0.9

KS 041, Plagioclase, J=0.001954±0.02%, IC=0.9975058±0.0007907, NM-297B, Lab#=66425-08, Argus VI

	ID	Power (Watts)	^{40}Ar/^{39}Ar	^{37}Ar/^{39}Ar	^{36}Ar/^{39}Ar (x 10^{-3})	^{39}Ar$_K$ (x 10^{-15} mol)	K/Ca	^{40}Ar* (%)	^{39}Ar (%)	Age (Ma)	±1σ (Ma)
	A	0.3	126.4	3.703	397.2	0.088	0.14	7.4	9.6	33.0	1.4
	B	0.4	12.64	4.209	10.81	0.072	0.12	77.4	17.4	34.76	0.48
	C	0.5	11.54	3.800	7.195	0.085	0.13	84.3	26.6	34.54	0.42
	D	3.0	16.31	3.756	22.91	0.678	0.14	60.4	100.0	34.97	0.12
	Integrated age ± 1σ			n=4		0.923	0.13			34.73	0.17
	Plateau ± 1σ	steps A-D		n=4	MSWD=0.95	0.923			100.0	34.92	0.11
	Isochron±2σ	steps A-D		n=4	MSWD=0.76		^{40}Ar/^{36}Ar=	294.3±1.1		35.01	0.14

KS 041, Plagioclase, J=0.001954±0.02%, IC=0.9975058±0.0007907, NM-297B, Lab#=66425-09, Argus VI

	ID	Power (Watts)	^{40}Ar/^{39}Ar	^{37}Ar/^{39}Ar	^{36}Ar/^{39}Ar (x 10^{-3})	^{39}Ar$_K$ (x 10^{-15} mol)	K/Ca	^{40}Ar* (%)	^{39}Ar (%)	Age (Ma)	±1σ (Ma)
Xi	A	0.3	55.44	3.329	161.0	0.401	0.15	14.7	28.4	28.94	0.40
Xi	B	0.4	17.34	2.833	30.42	0.349	0.18	49.5	53.2	30.50	0.21
Xi	C	0.5	21.04	3.741	41.39	0.431	0.14	43.3	83.8	32.39	0.21
Xi	D	3.0	15.40	5.061	20.04	0.227	0.10	64.2	100.0	35.15	0.22
	Integrated age ± 1σ			n=4		1.41	0.14			31.39	0.15
	Plateau ± 1σ	no plateau		n=0	MSWD=0.00	0.000			0.0	0.00	0.000
	Isochron±2σ	no isochron		n=0	MSWD=5.35		^{40}Ar/^{36}Ar=	0.0±0.0		0.00	0.00

KS 041, Plagioclase, J=0.001954±0.02%, IC=0.9975058±0.0007907, NM-297B, Lab#=66425-10, Argus VI

	ID	Power (Watts)	^{40}Ar/^{39}Ar	^{37}Ar/^{39}Ar	^{36}Ar/^{39}Ar (x 10^{-3})	^{39}Ar$_K$ (x 10^{-15} mol)	K/Ca	^{40}Ar* (%)	^{39}Ar (%)	Age (Ma)	±1σ (Ma)
Xi	A	0.3	31.95	3.004	76.58	0.220	0.17	29.9	27.5	33.95	0.37
	B	0.4	12.46	3.573	9.814	0.165	0.14	79.1	48.1	34.99	0.23
	C	0.5	15.54	4.155	15.57	0.013	0.12	72.6	49.7	40.0	2.8
	D	3.0	11.60	4.015	6.502	0.403	0.13	86.3	100.0	35.54	0.11
	Integrated age ± 1σ			n=4		0.802	0.14			35.06	0.13
	Plateau ± 1σ	steps B-D		n=3	MSWD=3.58	0.582			72.5	35.44	0.19
	Isochron±2σ	steps B-D		n=3	MSWD=5.35		^{40}Ar/^{36}Ar=	263.6±19.9		36.12	0.43

KS 041, Plagioclase, J=0.001954±0.02%, IC=0.9975058±0.0007907, NM-297B, Lab#=66425-11, Argus VI

	ID	Power (Watts)	^{40}Ar/^{39}Ar	^{37}Ar/^{39}Ar	^{36}Ar/^{39}Ar (x 10^{-3})	^{39}Ar$_K$ (x 10^{-15} mol)	K/Ca	^{40}Ar* (%)	^{39}Ar (%)	Age (Ma)	±1σ (Ma)
Xi	A	0.3	94.84	3.622	295.6	0.291	0.14	8.2	17.2	27.65	0.68

Table C2. ^{40}Ar/^{39}Ar analytical data, single crystal step heating results.

	ID	Power (Watts)	^{40}Ar/^{39}Ar	^{37}Ar/^{39}Ar	^{36}Ar/^{39}Ar (x 10^{-3})	^{39}Ar$_K$ (x 10^{-15} mol)	K/Ca	^{40}Ar* (%)	^{39}Ar (%)	Age (Ma)	±1σ (Ma)
Xi	B	0.4	12.18	3.943	11.70	0.198	0.13	74.2	28.9	32.14	0.22
i	C	0.5	13.04	3.371	14.19	0.121	0.15	70.0	36.1	32.41	0.34
i	D	3.0	16.24	4.853	24.66	1.082	0.11	57.6	100.0	33.246	0.096
	Integrated age ± 1σ			n=4		1.69	0.12			32.10	0.14
	Plateau ± 1σ	steps C-D		n=2	MSWD=5.46	1.203			71.1	33.19	0.216
	Isochron±2σ	no isochron		n=0	MSWD=4.08		^{40}Ar/^{36}Ar=	0.0±0.0		0.00	0.00

KS 041, Plagioclase, J=0.001954±0.02%, IC=0.9975058±0.0007907, NM-297B, Lab#=66425-12, Argus VI

	ID	Power (Watts)	^{40}Ar/^{39}Ar	^{37}Ar/^{39}Ar	^{36}Ar/^{39}Ar (x 10^{-3})	^{39}Ar$_K$ (x 10^{-15} mol)	K/Ca	^{40}Ar* (%)	^{39}Ar (%)	Age (Ma)	±1σ (Ma)
	A	0.3	19.63	3.334	35.08	0.228	0.15	48.6	31.8	33.86	0.29
	B	0.4	13.30	4.875	10.81	0.024	0.10	79.0	35.2	37.3	1.4
	C	0.5	14.22	5.423	14.42	0.019	0.094	73.1	37.7	37.0	1.9
	D	3.0	27.45	4.524	61.69	0.446	0.11	34.9	100.0	34.08	0.23
	Integrated age ± 1σ			n=4		0.716	0.12			34.19	0.18
	Plateau ± 1σ	steps A-D		n=4	MSWD=2.63	0.716			100.0	34.07	0.29
	Isochron±2σ	steps A-D		n=4	MSWD=4.08		^{40}Ar/^{36}Ar=	292.8±3.6		34.54	0.64

KS 041, Plagioclase, J=0.001954±0.02%, IC=0.9975058±0.0007907, NM-297B, Lab#=66425-13, Argus VI

	ID	Power (Watts)	^{40}Ar/^{39}Ar	^{37}Ar/^{39}Ar	^{36}Ar/^{39}Ar (x 10^{-3})	^{39}Ar$_K$ (x 10^{-15} mol)	K/Ca	^{40}Ar* (%)	^{39}Ar (%)	Age (Ma)	±1σ (Ma)
	A	0.3	17.20	5.590	19.56	0.007	0.091	69.0	1.5	42.1	5.2
	B	0.4	13.52	5.224	11.00	0.024	0.098	79.1	6.4	38.0	1.5
	C	0.5	12.39	5.233	7.559	0.027	0.097	85.4	11.9	37.6	1.3
	D	3.0	11.13	4.916	4.984	0.429	0.10	90.4	100.0	35.74	0.10
	Integrated age ± 1σ			n=4		0.487	0.10			36.05	0.15
	Plateau ± 1σ	steps A-D		n=4	MSWD=1.92	0.487			100.0	35.77	0.14
	Isochron±2σ	steps A-D		n=4	MSWD=0.16		^{40}Ar/^{36}Ar=	424.7±60.1		34.10	0.79

KS 041, Plagioclase, J=0.001954±0.02%, IC=0.9975058±0.0007907, NM-297B, Lab#=66425-14, Argus VI

	ID	Power (Watts)	^{40}Ar/^{39}Ar	^{37}Ar/^{39}Ar	^{36}Ar/^{39}Ar (x 10^{-3})	^{39}Ar$_K$ (x 10^{-15} mol)	K/Ca	^{40}Ar* (%)	^{39}Ar (%)	Age (Ma)	±1σ (Ma)
Xi	A	0.3	60.23	2.497	176.6	0.383	0.20	13.7	29.9	29.29	0.46
Xi	B	0.4	18.17	2.599	32.58	0.469	0.20	48.2	66.6	31.08	0.18
i	C	0.5	13.32	3.647	12.18	0.048	0.14	75.2	70.3	35.58	0.77
i	D	3.0	13.64	3.348	13.81	0.380	0.15	72.1	100.0	34.90	0.15
	Integrated age ± 1σ			n=4		1.28	0.18			31.85	0.16
	Plateau ± 1σ	steps C-D		n=2	MSWD=0.75	0.428			33.4	34.93	0.147
	Isochron±2σ	no isochron		n=0	MSWD=0.27		^{40}Ar/^{36}Ar=	0.0±0.0		0.00	0.00

KS 041, Plagioclase, J=0.001954±0.02%, IC=0.9975058±0.0007907, NM-297B, Lab#=66425-15, Argus VI

	ID	Power (Watts)	^{40}Ar/^{39}Ar	^{37}Ar/^{39}Ar	^{36}Ar/^{39}Ar (x 10^{-3})	^{39}Ar$_K$ (x 10^{-15} mol)	K/Ca	^{40}Ar* (%)	^{39}Ar (%)	Age (Ma)	±1σ (Ma)
Xi	A	0.3	37.25	2.504	97.60	0.395	0.20	23.1	38.7	30.57	0.34
Xi	B	0.4	18.47	2.943	32.32	0.384	0.17	49.6	76.3	32.51	0.19
i	C	0.5	15.07	5.164	19.97	0.069	0.099	63.7	83.1	34.12	0.54
i	D	3.0	14.35	5.494	16.05	0.172	0.093	70.1	100.0	35.74	0.27
	Integrated age ± 1σ			n=4		1.020	0.15			32.42	0.16
	Plateau ± 1σ	steps C-D		n=2	MSWD=7.22	0.242			23.7	35.43	0.645
	Isochron±2σ	no isochron		n=0	MSWD=0.05		^{40}Ar/^{36}Ar=	0.0±0.0		0.00	0.00

Table C2. ^{40}Ar/^{39}Ar analytical data, single crystal step heating results.

	ID	Power (Watts)	^{40}Ar/^{39}Ar	^{37}Ar/^{39}Ar	^{36}Ar/^{39}Ar (x 10^{-3})	^{39}Ar$_K$ (x 10^{-15} mol)	K/Ca	^{40}Ar* (%)	^{39}Ar (%)	Age (Ma)	±1σ (Ma)
		KS 063, Plagioclase, J=0.0019562±0.02%, IC=1.000371±0.0009714, NM-297C, Lab#=66448-01, Argus VI									
Xi	A	0.2	92.89	0.0468	262.2	0.016	10.9	16.6	18.5	54.4	4.1
Xi	B	0.2	41.78	0.4862	26.27	0.004	1.0	81.5	23.0	118.1	23.4
Xi	C	3.0	31.26	0.0934	56.42	0.067	5.5	46.7	100.0	51.50	0.84
	Integrated age ± 1σ		n=3			0.087	5.0			55.1	1.1
	Plateau ± 1σ	no plateau	n=0	MSWD=0.00	0.000				0.0	0.00	0.000
	Isochron±2σ	no isochron	n=0	MSWD=0.27			^{40}Ar/^{36}Ar=	0.0±0.0		0.0	0.0
		KS 063, Plagioclase, J=0.0019562±0.02%, IC=1.000371±0.0009714, NM-297C, Lab#=66448-02, Argus VI									
Xi	A	0.2	827.1	0.2523	2752.1	0.007	2.0	1.7	13.7	49.1	13.9
Xi	B	0.2	170.6	1.334	463.3	0.001	0.38	19.8	16.5	117.3	62.6
Xi	C	3.0	139.4	0.1692	374.7	0.040	3.0	20.6	100.0	100.0	2.7
	Integrated age ± 1σ		n=3			0.048	2.4			93.6	3.5
	Plateau ± 1σ	no plateau	n=0	MSWD=0.00	0.000				0.0	0.00	0.000
	Isochron±2σ	no isochron	n=0	MSWD=0.27			^{40}Ar/^{36}Ar=	0.0±0.0		0.0	0.0
		KS 063, Plagioclase, J=0.0019562±0.02%, IC=1.000371±0.0009714, NM-297C, Lab#=66448-03, Argus VI									
Xi	A	0.3	293.6	0.5942	883.7	0.016	0.86	11.1	24.1	112.7	6.7
Xi	B	3.0	109.2	0.1957	239.9	0.052	2.6	35.1	100.0	132.3	2.4
	Integrated age ± 1σ		n=2			0.068	1.7			127.6	2.5
	Plateau ± 1σ	no plateau	n=0	MSWD=0.00	0.000				0.0	0.00	0.000
	Isochron±2σ	no isochron	n=0	MSWD=0.27			^{40}Ar/^{36}Ar=	0.0±0.0		0.0	0.0
		KS 063, Plagioclase, J=0.0019562±0.02%, IC=1.000371±0.0009714, NM-297C, Lab#=66448-04, Argus VI									
Xi	A	0.3	145.1	2.432	422.4	0.007	0.21	14.1	28.1	72.2	9.5
Xi	B	3.0	76.06	0.3497	179.6	0.017	1.5	30.3	100.0	80.6	4.1
	Integrated age ± 1σ		n=2			0.024	0.55			78.3	4.1
	Plateau ± 1σ	no plateau	n=0	MSWD=0.00	0.000				0.0	0.00	0.000
	Isochron±2σ	no isochron	n=0	MSWD=0.27			^{40}Ar/^{36}Ar=	0.0±0.0		0.0	0.0
		KS 063, Plagioclase, J=0.0019562±0.02%, IC=1.000371±0.0009714, NM-297C, Lab#=66448-11, Argus VI									
Xi	A	0.3	153.9	0.8787	454.7	0.105	0.58	12.7	22.0	68.7	1.5
Xi	B	3.0	45.76	0.4136	82.56	0.372	1.2	46.8	100.0	75.06	0.34
	Integrated age ± 1σ		n=2			0.477	0.99			73.67	0.42
	Plateau ± 1σ	no plateau	n=0	MSWD=0.00	0.000				0.0	0.00	0.000
	Isochron±2σ	no isochron	n=0	MSWD=0.27			^{40}Ar/^{36}Ar=	0.0±0.0		0.00	0.00
		KS 063, Plagioclase, J=0.0019562±0.02%, IC=1.000371±0.0009714, NM-297C, Lab#=66448-14, Argus VI									
Xi	A	0.3	100.5	0.4344	280.7	0.157	1.2	17.5	32.7	61.87	0.89
Xi	B	3.0	37.84	0.1976	71.49	0.324	2.6	44.2	100.0	58.92	0.32
	Integrated age ± 1σ		n=2			0.481	1.9			59.89	0.36
	Plateau ± 1σ	no plateau	n=0	MSWD=0.00	0.000				0.0	0.00	0.000

Table C2. ^{40}Ar/^{39}Ar analytical data, single crystal step heating results.

	ID	Power (Watts)	^{40}Ar/^{39}Ar	^{37}Ar/^{39}Ar	^{36}Ar/^{39}Ar (x 10^{-3})	^{39}Ar$_K$ (x 10^{-15} mol)	K/Ca	^{40}Ar* (%)	^{39}Ar (%)	Age (Ma)	±1σ (Ma)
Isochron±2σ		no isochron	n=0	MSWD=0.27			^{40}Ar/^{36}Ar=	0.0±0.0		0.00	0.00

KS 068, Plagioclase, J=0.0019478±0.02%, IC=0.9975058±0.0007907, NM-297B, Lab#=66433-01, Argus VI

	ID	Power	^{40}Ar/^{39}Ar	^{37}Ar/^{39}Ar	^{36}Ar/^{39}Ar	^{39}Ar$_K$	K/Ca	^{40}Ar*	^{39}Ar	Age	±1σ
	A	0.2	13.80	4.382	13.26	0.037	0.12	74.2	43.4	36.26	0.65
	B	0.3	18.30	4.475	27.26	0.022	0.11	58.0	69.4	37.6	1.3
	C	0.4	58.20	4.097	157.9	0.001	0.12	20.4	70.6	41.9	40.0
	D	3.0	13.40	4.972	11.13	0.025	0.10	78.5	100.0	37.2	1.4
Integrated age ± 1σ			n=4			0.086	0.11			36.95	0.75
Plateau ± 1σ		steps A-D	n=4	MSWD=0.33	0.086				100.0	36.62	0.54
Isochron±2σ		steps A-D	n=4	MSWD=0.27			^{40}Ar/^{36}Ar=	313.7±26.8		35.7	1.4

KS 068, Plagioclase, J=0.0019478±0.02%, IC=1.000371±0.0009714, NM-297B, Lab#=66433-10, Argus VI

	ID	Power	^{40}Ar/^{39}Ar	^{37}Ar/^{39}Ar	^{36}Ar/^{39}Ar	^{39}Ar$_K$	K/Ca	^{40}Ar*	^{39}Ar	Age	±1σ
Xi	A	0.2	39.79	3.372	105.4	0.158	0.15	22.4	8.7	31.57	0.54
Xi	B	0.2	19.93	4.400	38.98	0.201	0.12	44.0	19.8	31.08	0.33
Xi	C	0.3	20.40	3.913	40.25	0.370	0.13	43.2	40.2	31.26	0.25
Xi	D	3.0	14.92	3.811	18.28	1.082	0.13	65.9	100.0	34.793	0.088
Integrated age ± 1σ			n=4			1.81	0.13			33.379	0.095
Plateau ± 1σ		no plateau	n=0	MSWD=0.00	0.000				0.0	0.00	0.000
Isochron±2σ		no isochron	n=0	MSWD=0.39			^{40}Ar/^{36}Ar=	0.0±0.0		0.00	0.00

KS 068, Plagioclase, J=0.0019478±0.02%, IC=1.000371±0.0009714, NM-297B, Lab#=66433-11, Argus VI

	ID	Power	^{40}Ar/^{39}Ar	^{37}Ar/^{39}Ar	^{36}Ar/^{39}Ar	^{39}Ar$_K$	K/Ca	^{40}Ar*	^{39}Ar	Age	±1σ
Xi	A	0.2	18.96	4.624	32.78	0.202	0.11	50.9	15.2	34.19	0.30
	B	0.2	12.07	4.089	8.704	0.232	0.12	81.5	32.8	34.80	0.19
	C	0.3	13.68	3.478	13.77	0.456	0.15	72.3	67.3	35.03	0.13
	D	3.0	13.02	4.186	11.74	0.433	0.12	76.0	100.0	35.04	0.12
Integrated age ± 1σ			n=4			1.32	0.13			34.865	0.082
Plateau ± 1σ		steps B-D	n=3	MSWD=0.65	1.122				84.8	34.99	0.08
Isochron±2σ		steps B-D	n=3	MSWD=0.39			^{40}Ar/^{36}Ar=	307.0±12.4		34.55	0.48

KS 068, Plagioclase, J=0.0019478±0.02%, IC=1.000371±0.0009714, NM-297B, Lab#=66433-12, Argus VI

	ID	Power	^{40}Ar/^{39}Ar	^{37}Ar/^{39}Ar	^{36}Ar/^{39}Ar	^{39}Ar$_K$	K/Ca	^{40}Ar*	^{39}Ar	Age	±1σ
Xi	A	0.2	30.95	3.610	74.30	0.204	0.14	30.0	9.7	32.89	0.42
	B	0.2	12.53	2.787	10.41	0.206	0.18	77.3	19.6	34.26	0.22
	C	0.3	13.23	2.979	12.42	0.502	0.17	74.1	43.6	34.68	0.12
	D	3.0	13.80	3.662	14.50	1.180	0.14	71.1	100.0	34.756	0.078
Integrated age ± 1σ			n=4			2.09	0.15			34.508	0.071
Plateau ± 1σ		steps B-D	n=3	MSWD=2.20	1.89				90.3	34.696	0.094
Isochron±2σ		steps B-D	n=3	MSWD=0.85			^{40}Ar/^{36}Ar=	323.6±15.7		33.45	0.70

KS 079, Plagioclase, J=0.0019522±0.02%, IC=0.9975058±0.0007907, NM-297B, Lab#=66438-01, Argus VI

	ID	Power	^{40}Ar/^{39}Ar	^{37}Ar/^{39}Ar	^{36}Ar/^{39}Ar	^{39}Ar$_K$	K/Ca	^{40}Ar*	^{39}Ar	Age	±1σ
Xi	A	0.2	17.80	0.0877	29.13	0.911	5.8	51.7	47.9	32.55	0.12
i	B	0.3	13.60	0.0362	14.21	0.845	14.1	69.1	92.3	33.26	0.10
i	C	3.0	18.81	0.0080	32.03	0.147	64.0	49.7	100.0	33.07	0.37
Integrated age ± 1σ			n=3			1.90	8.7			32.907	0.079

Table C2. ^{40}Ar/^{39}Ar analytical data, single crystal step heating results.

	ID	Power (Watts)	^{40}Ar/^{39}Ar	^{37}Ar/^{39}Ar	^{36}Ar/^{39}Ar (x 10^{-3})	^{39}Ar$_K$ (x 10^{-15} mol)	K/Ca	^{40}Ar* (%)	^{39}Ar (%)	Age (Ma)	±1σ (Ma)
	Plateau ± 1σ	steps B-C	n=2		MSWD=0.24	0.992			52.1	33.25	0.097
	Isochron±2σ	no isochron	n=0		MSWD=8.21		^{40}Ar/^{36}Ar=	0.0±0.0		0.00	0.00

KS 079, Plagioclase, J=0.0019522±0.02%, IC=0.9975058±0.0007907, NM-297B, Lab#=66438-02, Argus VI

	ID	Power (Watts)	^{40}Ar/^{39}Ar	^{37}Ar/^{39}Ar	^{36}Ar/^{39}Ar (x 10^{-3})	^{39}Ar$_K$ (x 10^{-15} mol)	K/Ca	^{40}Ar* (%)	^{39}Ar (%)	Age (Ma)	±1σ (Ma)
Xi	A	0.2	19.40	0.2361	34.99	0.150	2.2	46.8	29.4	32.13	0.37
i	B	0.2	11.65	0.0570	7.561	0.204	8.9	80.8	69.4	33.32	0.19
i	C	3.0	14.66	0.0622	18.22	0.156	8.2	63.3	100.0	32.86	0.29
	Integrated age ± 1σ		n=3			0.511	4.6			32.83	0.16
	Plateau ± 1σ	steps B-C	n=2		MSWD=1.76	0.360			70.6	33.18	0.207
	Isochron±2σ	no isochron	n=0		MSWD=8.21		^{40}Ar/^{36}Ar=	0.0±0.0		0.00	0.00

KS 079, Plagioclase, J=0.0019522±0.02%, IC=0.9975058±0.0007907, NM-297B, Lab#=66438-03, Argus VI

	ID	Power (Watts)	^{40}Ar/^{39}Ar	^{37}Ar/^{39}Ar	^{36}Ar/^{39}Ar (x 10^{-3})	^{39}Ar$_K$ (x 10^{-15} mol)	K/Ca	^{40}Ar* (%)	^{39}Ar (%)	Age (Ma)	±1σ (Ma)
i	A	0.2	26.81	0.1555	60.83	0.045	3.3	33.0	15.8	31.32	1.00
i	B	0.2	11.64	0.0563	8.457	0.056	9.1	78.6	35.5	32.37	0.60
i	C	3.0	11.89	0.0422	9.443	0.182	12.1	76.5	100.0	32.21	0.23
	Integrated age ± 1σ		n=3			0.283	8.1			32.10	0.25
	Plateau ± 1σ	steps A-C	n=3		MSWD=0.43	0.283			100.0	32.19	0.21
	Isochron±2σ	no isochron	n=0		MSWD=8.21		^{40}Ar/^{36}Ar=	0.0±0.0		0.00	0.00

KS 079, Plagioclase, J=0.0019522±0.02%, IC=0.9975058±0.0007907, NM-297B, Lab#=66438-04, Argus VI

	ID	Power (Watts)	^{40}Ar/^{39}Ar	^{37}Ar/^{39}Ar	^{36}Ar/^{39}Ar (x 10^{-3})	^{39}Ar$_K$ (x 10^{-15} mol)	K/Ca	^{40}Ar* (%)	^{39}Ar (%)	Age (Ma)	±1σ (Ma)
i	A	0.2	96.47	-1.5355	364.3	0.000	-	-11.7	0.0	-41	123
i	B	0.2	-135.7081	4.922	-601.0680	0.000	0.10	-31.2	0.0	146	564
i	C	3.0	1.397	0.0105	2.124	1.20	48.7	54.9	100.0	2.726	0.033
	Integrated age ± 1σ		n=3			1.20	54.7			2.692	0.041
	Plateau ± 1σ	steps A-C	n=3		MSWD=0.09	1.20			100.0	2.726	0.033
	Isochron±2σ	no isochron	n=0		MSWD=8.21		^{40}Ar/^{36}Ar=	0.0±0.0		0.00	0.00

KS 079, Plagioclase, J=0.0019522±0.02%, IC=0.9975058±0.0007907, NM-297B, Lab#=66438-05, Argus VI

	ID	Power (Watts)	^{40}Ar/^{39}Ar	^{37}Ar/^{39}Ar	^{36}Ar/^{39}Ar (x 10^{-3})	^{39}Ar$_K$ (x 10^{-15} mol)	K/Ca	^{40}Ar* (%)	^{39}Ar (%)	Age (Ma)	±1σ (Ma)
Xi	A	0.2	2.528	0.0096	2.581	0.033	53.0	69.8	3.3	6.27	0.63
i	B	0.2	1.257	-0.0305	1.006	0.072	-	76.0	10.6	3.39	0.28
i	C	3.0	3.548	0.0152	9.394	0.884	33.7	21.6	100.0	2.736	0.065
	Integrated age ± 1σ		n=3			0.989	43.9			2.901	0.065
	Plateau ± 1σ	steps B-C	n=2		MSWD=5.22	0.956			96.7	2.77	0.144
	Isochron±2σ	no isochron	n=0		MSWD=8.21		^{40}Ar/^{36}Ar=	0.0±0.0		0.00	0.00

KS 079, Plagioclase, J=0.0019522±0.02%, IC=0.9975058±0.0007907, NM-297B, Lab#=66438-06, Argus VI

	ID	Power (Watts)	^{40}Ar/^{39}Ar	^{37}Ar/^{39}Ar	^{36}Ar/^{39}Ar (x 10^{-3})	^{39}Ar$_K$ (x 10^{-15} mol)	K/Ca	^{40}Ar* (%)	^{39}Ar (%)	Age (Ma)	±1σ (Ma)
i	A	0.2	48.50	7.105	146.6	0.018	0.072	11.8	14.3	20.5	2.3
i	B	0.2	31.49	7.492	75.88	0.006	0.068	30.7	19.3	34.5	5.6
i	C	3.0	34.03	4.308	92.86	0.099	0.12	20.4	100.0	24.71	0.61
	Integrated age ± 1σ		n=3			0.123	0.10			24.60	0.64
	Plateau ± 1σ	steps A-C	n=3		MSWD=3.14	0.123			100.0	24.5	1.0
	Isochron±2σ	no isochron	n=0		MSWD=8.21		^{40}Ar/^{36}Ar=	0.0±0.0		0.0	0.0

Table C2. ^{40}Ar/^{39}Ar analytical data, single crystal step heating results.

	ID	Power (Watts)	^{40}Ar/^{39}Ar	^{37}Ar/^{39}Ar	^{36}Ar/^{39}Ar (x 10^{-3})	^{39}Ar$_K$ (x 10^{-15} mol)	K/Ca	^{40}Ar* (%)	^{39}Ar (%)	Age (Ma)	±1σ (Ma)
			KS 079, Plagioclase, J=0.0019522±0.02%, IC=0.9975058±0.0007907, NM-297B, Lab#=66438-07, Argus VI								
Xi	A	0.2	26.37	0.5421	57.74	0.103	0.94	35.4	12.9	33.09	0.54
i	B	0.2	11.28	0.2825	7.810	0.072	1.8	79.7	21.9	31.85	0.46
i	C	3.0	11.39	0.2974	8.283	0.626	1.7	78.7	100.0	31.748	0.086
	Integrated age ± 1σ		n=3			0.801	1.6			31.93	0.11
	Plateau ± 1σ	steps B-C	n=2	MSWD=0.05		0.698			87.1	31.75	0.084
	Isochron±2σ	no isochron	n=0	MSWD=8.21			^{40}Ar/^{36}Ar=	0.0±0.0		0.00	0.00
			KS 079, Plagioclase, J=0.0019522±0.02%, IC=0.9975058±0.0007907, NM-297B, Lab#=66438-08, Argus VI								
Xi	A	0.2	26.43	1.265	60.06	0.069	0.40	33.2	23.5	31.13	0.76
i	B	0.2	13.80	0.0851	15.45	0.065	6.0	67.0	45.6	32.71	0.60
i	C	3.0	13.77	0.0981	14.83	0.161	5.2	68.2	100.0	33.27	0.27
	Integrated age ± 1σ		n=3			0.295	1.4			32.64	0.27
	Plateau ± 1σ	steps B-C	n=2	MSWD=0.71		0.226			76.5	33.17	0.248
	Isochron±2σ	no isochron	n=0	MSWD=8.21			^{40}Ar/^{36}Ar=	0.0±0.0		0.00	0.00
			KS 079, Plagioclase, J=0.0019522±0.02%, IC=0.9975058±0.0007907, NM-297B, Lab#=66438-09, Argus VI								
i	A	0.2	139.3	2.533	454.3	0.014	0.20	3.8	17.6	18.6	4.0
i	B	0.2	44.52	0.6675	138.6	0.018	0.76	8.1	40.5	12.8	2.0
i	C	3.0	48.05	0.6313	151.3	0.047	0.81	7.0	100.0	12.1	1.2
	Integrated age ± 1σ		n=3			0.079	0.52			13.4	1.1
	Plateau ± 1σ	steps A-C	n=3	MSWD=1.25		0.079			100.0	12.7	1.1
	Isochron±2σ	no isochron	n=0	MSWD=8.21			^{40}Ar/^{36}Ar=	0.0±0.0		0.0	0.0
			KS 079, Plagioclase, J=0.0019522±0.02%, IC=0.9975058±0.0007907, NM-297B, Lab#=66438-10, Argus VI								
i	A	0.2	36.20	1.874	90.60	0.072	0.27	26.5	28.0	33.97	0.77
i	B	0.2	12.81	0.8058	10.77	0.028	0.63	75.7	38.9	34.3	1.2
i	C	3.0	15.93	1.741	20.78	0.158	0.29	62.3	100.0	35.17	0.30
	Integrated age ± 1σ		n=3			0.258	0.30			34.74	0.31
	Plateau ± 1σ	steps A-C	n=3	MSWD=1.25		0.258			100.0	34.98	0.30
	Isochron±2σ	no isochron	n=0	MSWD=8.21			^{40}Ar/^{36}Ar=	0.0±0.0		0.00	0.00
			KS 079, Plagioclase, J=0.0019522±0.02%, IC=0.9975058±0.0007907, NM-297B, Lab#=66438-11, Argus VI								
i	A	0.2	12.33	0.0427	11.80	0.230	11.9	71.7	73.6	31.32	0.20
i	B	0.2	11.32	0.0241	7.746	0.042	21.2	79.8	87.1	31.96	0.78
Xi	C	3.0	13.66	-0.0159	13.18	0.040	-	71.5	100.0	34.53	0.86
	Integrated age ± 1σ		n=3			0.312	15.6			31.82	0.21
	Plateau ± 1σ	steps A-B	n=2	MSWD=0.64		0.272			87.1	31.36	0.190
	Isochron±2σ	no isochron	n=0	MSWD=8.21			^{40}Ar/^{36}Ar=	0.0±0.0		0.0	0.0
			KS 079, Plagioclase, J=0.0019522±0.02%, IC=0.9975058±0.0007907, NM-297B, Lab#=66438-12, Argus VI								
i	A	0.2	28.63	0.5647	64.40	0.113	0.90	33.7	27.1	34.13	0.52

Table C2. ^{40}Ar/^{39}Ar analytical data, single crystal step heating results.

	ID	Power (Watts)	^{40}Ar/^{39}Ar	^{37}Ar/^{39}Ar	^{36}Ar/^{39}Ar (x 10^{-3})	^{39}Ar$_K$ (x 10^{-15} mol)	K/Ca	^{40}Ar* (%)	^{39}Ar (%)	Age (Ma)	±1σ (Ma)
i	B	0.2	12.13	0.2134	9.770	0.102	2.4	76.3	51.6	32.78	0.35
i	C	3.0	14.16	0.4818	15.81	0.202	1.1	67.3	100.0	33.74	0.22
	Integrated age ± 1σ			n=3		0.418	1.2			33.61	0.20
	Plateau ± 1σ	steps A-C	n=3	MSWD=3.40	0.418				100.0	33.54	0.32
	Isochron±2σ	no isochron	n=0	MSWD=8.21			^{40}Ar/^{36}Ar=	0.0±0.0		0.00	0.00

KS 079, Plagioclase, J=0.0019522±0.02%, IC=0.9975058±0.0007907, NM-297B, Lab#=66438-13, Argus VI

	ID	Power	^{40}Ar/^{39}Ar	^{37}Ar/^{39}Ar	^{36}Ar/^{39}Ar	^{39}Ar$_K$	K/Ca	^{40}Ar*	^{39}Ar	Age	±1σ
i	A	0.2	18.23	0.0611	31.24	0.112	8.3	49.4	22.2	31.88	0.44
i	B	0.2	10.49	0.0238	5.673	0.140	21.5	84.0	50.1	31.22	0.26
i	C	3.0	13.81	0.3256	15.54	0.252	1.6	66.9	100.0	32.72	0.20
	Integrated age ± 1σ			n=3		0.504	2.8			32.12	0.16
	Plateau ± 1σ	steps A-C	n=3	MSWD=10.91	0.504				100.0	32.13	0.487
	Isochron±2σ	no isochron	n=0	MSWD=8.21			^{40}Ar/^{36}Ar=	0.0±0.0		0.00	0.00

KS 079, Plagioclase, J=0.0019522±0.02%, IC=0.9975058±0.0007907, NM-297B, Lab#=66438-14, Argus VI

	ID	Power	^{40}Ar/^{39}Ar	^{37}Ar/^{39}Ar	^{36}Ar/^{39}Ar	^{39}Ar$_K$	K/Ca	^{40}Ar*	^{39}Ar	Age	±1σ
i	A	0.2	-28.9737	-0.2552	-93.4731	-0.001	-	4.8	-1.2	-4.9	18.7
i	B	0.2	29.51	-0.2588	96.51	0.001	-	3.2	-0.2	3.4	22.7
i	C	3.0	22.87	3.412	47.72	0.098	0.15	39.6	100.0	32.12	0.56
	Integrated age ± 1σ			n=3		0.098	0.15			32.29	0.72
	Plateau ± 1σ	steps A-C	n=3	MSWD=2.76	0.098				100.0	32.07	0.93
	Isochron±2σ	no isochron	n=0	MSWD=8.21			^{40}Ar/^{36}Ar=	0.0±0.0		0.0	0.0

KS 079, Plagioclase, J=0.0019522±0.02%, IC=0.9975058±0.0007907, NM-297B, Lab#=66438-15, Argus VI

	ID	Power	^{40}Ar/^{39}Ar	^{37}Ar/^{39}Ar	^{36}Ar/^{39}Ar	^{39}Ar$_K$	K/Ca	^{40}Ar*	^{39}Ar	Age	±1σ
Xi	A	0.2	12.57	0.0977	12.91	0.024	5.2	69.7	23.0	31.0	1.2
i	B	0.2	12.61	0.0597	11.43	0.034	8.5	73.2	54.7	32.69	0.95
i	C	3.0	14.90	0.0464	16.51	0.048	11.0	67.3	100.0	35.45	0.79
	Integrated age ± 1σ			n=3		0.106	8.2			33.56	0.55
	Plateau ± 1σ	steps B-C	n=2	MSWD=5.02	0.082				77.0	34.33	1.359
	Isochron±2σ	no isochron	n=0	MSWD=8.21			^{40}Ar/^{36}Ar=	0.0±0.0		0.0	0.0

KS 098, Sanidine, J=0.0019483±0.02%, IC=1.000371±0.0009714, NM-297B, Lab#=66432-16, Argus VI

	ID	Power	^{40}Ar/^{39}Ar	^{37}Ar/^{39}Ar	^{36}Ar/^{39}Ar	^{39}Ar$_K$	K/Ca	^{40}Ar*	^{39}Ar	Age	±1σ
i	A	0.2	52.80	0.0152	143.9	0.274	33.5	19.4	2.3	36.23	0.49
i	B	0.2	11.22	0.0087	4.174	0.303	58.7	89.0	4.8	35.25	0.13
i	C	3.0	12.40	0.0129	7.931	11.53	39.7	81.1	100.0	35.493	0.019
	Integrated age ± 1σ			n=3		12.1	39.8			35.504	0.023
	Plateau ± 1σ	steps A-C	n=3	MSWD=2.80	12.1				100.0	35.490	0.032
	Isochron±2σ	no isochron	n=0	MSWD=8.21			^{40}Ar/^{36}Ar=	0.0±0.0		0.000	0.000

KS 098, Sanidine, J=0.0019483±0.02%, IC=1.000371±0.0009714, NM-297B, Lab#=66432-17, Argus VI

	ID	Power	^{40}Ar/^{39}Ar	^{37}Ar/^{39}Ar	^{36}Ar/^{39}Ar	^{39}Ar$_K$	K/Ca	^{40}Ar*	^{39}Ar	Age	±1σ
i	A	0.2	10.96	0.0102	3.281	0.190	50.0	91.2	4.7	35.25	0.19
i	B	0.2	11.28	0.0117	4.320	0.401	43.5	88.7	14.6	35.31	0.11
i	C	3.0	12.28	0.0078	7.787	3.47	65.5	81.3	100.0	35.237	0.032
	Integrated age ± 1σ			n=3		4.06	61.5			35.245	0.032

Table C2. ^{40}Ar/^{39}Ar analytical data, single crystal step heating results.

	ID	Power (Watts)	^{40}Ar/^{39}Ar	^{37}Ar/^{39}Ar	^{36}Ar/^{39}Ar (x 10^{-3})	^{39}Ar$_K$ (x 10^{-15} mol)	K/Ca	^{40}Ar* (%)	^{39}Ar (%)	Age (Ma)	±1σ (Ma)
Plateau ± 1σ		steps A-C	n=3	MSWD=0.21		4.06			100.0	35.243	0.031
Isochron±2σ		no isochron	n=0	MSWD=8.21			^{40}Ar/^{36}Ar=	0.0±0.0		0.00	0.00

KS 098, Sanidine, J=0.0019483±0.02%, IC=1.000371±0.0009714, NM-297B, Lab#=66432-18, Argus VI

	ID	Power	^{40}Ar/^{39}Ar	^{37}Ar/^{39}Ar	^{36}Ar/^{39}Ar	^{39}Ar$_K$	K/Ca	^{40}Ar*	^{39}Ar	Age	±1σ
Xi	A	0.2	78.74	0.0293	236.6	0.301	17.4	11.2	5.9	31.18	0.60
i	B	0.2	12.55	0.0151	9.607	0.360	33.8	77.4	13.0	34.30	0.13
i	C	3.0	13.74	0.0075	13.64	4.44	68.2	70.6	100.0	34.268	0.038
Integrated age ± 1σ			n=3			5.10	54.8			34.088	0.050
Plateau ± 1σ		steps B-C	n=2	MSWD=0.07		4.800			94.1	34.27	0.037
Isochron±2σ		no isochron	n=0	MSWD=8.21			^{40}Ar/^{36}Ar=	0.0±0.0		0.000	0.000

KS 098, Sanidine, J=0.0019483±0.02%, IC=1.000371±0.0009714, NM-297B, Lab#=66432-19, Argus VI

	ID	Power	^{40}Ar/^{39}Ar	^{37}Ar/^{39}Ar	^{36}Ar/^{39}Ar	^{39}Ar$_K$	K/Ca	^{40}Ar*	^{39}Ar	Age	±1σ
Xi	A	0.2	407.0	0.1876	1358.5	0.082	2.7	1.4	1.4	19.7	2.8
Xi	B	0.2	23.57	0.1080	48.31	0.421	4.7	39.4	8.6	32.84	0.23
Xi	C	3.0	15.18	0.0110	18.87	5.34	46.5	63.3	100.0	33.928	0.040
Integrated age ± 1σ			n=3			5.85	25.0			33.650	0.057
Plateau ± 1σ		no plateau	n=0	MSWD=0.00		0.000			0.0	0.00	0.000
Isochron±2σ		no isochron	n=0	MSWD=8.21			^{40}Ar/^{36}Ar=	0.0±0.0		0.000	0.000

KS 098, Sanidine, J=0.0019483±0.02%, IC=1.000371±0.0009714, NM-297B, Lab#=66432-20, Argus VI

	ID	Power	^{40}Ar/^{39}Ar	^{37}Ar/^{39}Ar	^{36}Ar/^{39}Ar	^{39}Ar$_K$	K/Ca	^{40}Ar*	^{39}Ar	Age	±1σ
Xi	A	0.2	718.2	0.0653	2430.2	0.132	7.8	0.0	0.9	0.2	3.8
Xi	B	0.2	38.76	0.0274	101.5	0.832	18.6	22.6	6.3	30.93	0.24
Xi	C	3.0	18.10	0.0073	29.31	14.4	70.0	52.1	100.0	33.342	0.041
Integrated age ± 1σ			n=3			15.4	57.5			32.929	0.053
Plateau ± 1σ		no plateau	n=0	MSWD=0.00		0.000			0.0	0.00	0.000
Isochron±2σ		no isochron	n=0	MSWD=8.21			^{40}Ar/^{36}Ar=	0.0±0.0		0.000	0.000

KS 098, Sanidine, J=0.0019483±0.02%, IC=1.000371±0.0009714, NM-297B, Lab#=66432-21, Argus VI

	ID	Power	^{40}Ar/^{39}Ar	^{37}Ar/^{39}Ar	^{36}Ar/^{39}Ar	^{39}Ar$_K$	K/Ca	^{40}Ar*	^{39}Ar	Age	±1σ
Xi	A	0.2	18.00	0.0092	27.47	0.862	55.2	54.9	10.7	34.88	0.12
i	B	0.2	10.73	0.0078	2.447	0.886	65.4	93.3	21.7	35.321	0.055
i	C	3.0	11.12	0.0079	3.751	6.32	64.4	90.0	100.0	35.341	0.019
Integrated age ± 1σ			n=3			8.06	63.4			35.289	0.022
Plateau ± 1σ		steps B-C	n=2	MSWD=0.12		7.201			89.3	35.34	0.020
Isochron±2σ		no isochron	n=0	MSWD=8.21			^{40}Ar/^{36}Ar=	0.0±0.0		0.000	0.000

KS 098, Sanidine, J=0.0019483±0.02%, IC=1.000371±0.0009714, NM-297B, Lab#=66432-22, Argus VI

	ID	Power	^{40}Ar/^{39}Ar	^{37}Ar/^{39}Ar	^{36}Ar/^{39}Ar	^{39}Ar$_K$	K/Ca	^{40}Ar*	^{39}Ar	Age	±1σ
i	A	0.2	21.53	0.0169	38.57	0.355	30.1	47.1	4.5	35.78	0.22
i	B	0.2	10.42	0.0075	1.392	0.360	68.5	96.1	9.1	35.312	0.098
i	C	3.0	10.57	0.0084	1.783	7.11	60.7	95.0	100.0	35.462	0.013
Integrated age ± 1σ			n=3			7.82	58.3			35.469	0.018
Plateau ± 1σ		steps A-C	n=3	MSWD=2.24		7.82			100.0	35.460	0.020
Isochron±2σ		no isochron	n=0	MSWD=8.21			^{40}Ar/^{36}Ar=	0.0±0.0		0.000	0.000

Table C2. ^{40}Ar/^{39}Ar analytical data, single crystal step heating results.

ID		Power (Watts)	^{40}Ar/^{39}Ar	^{37}Ar/^{39}Ar	^{36}Ar/^{39}Ar (x 10^{-3})	^{39}Ar$_K$ (x 10^{-15} mol)	K/Ca	^{40}Ar* (%)	^{39}Ar (%)	Age (Ma)	±1σ (Ma)
		KS 098, Sanidine, J=0.0019483±0.02%, IC=1.000371±0.0009714, NM-297B, Lab#=66432-23, Argus VI									
i	A	0.2	-4.2666	0.5265	-47.6246	-0.001	0.97	-230.4	-0.9	34.8	29.7
i	B	0.2	14.84	-0.0321	7.702	0.003	-	84.6	1.9	44.2	10.7
i	C	3.0	10.37	0.0087	1.415	0.120	58.9	96.0	100.0	35.12	0.29
	Integrated age ± 1σ		n=3			0.123	171.8			35.38	0.46
	Plateau ± 1σ	steps A-C	n=3	MSWD=0.36	0.123				100.0	35.13	0.29
	Isochron±2σ	no isochron	n=0	MSWD=8.21			^{40}Ar/^{36}Ar=	0.0±0.0		0.0	0.0
		KS 098, Sanidine, J=0.0019483±0.02%, IC=1.000371±0.0009714, NM-297B, Lab#=66432-24, Argus VI									
i	A	0.2	10.97	0.0162	3.490	0.196	31.4	90.6	7.9	35.10	0.18
i	B	0.2	10.29	0.0201	1.508	0.113	25.3	95.7	12.4	34.77	0.29
i	C	3.0	10.71	0.0088	2.493	2.18	58.0	93.1	100.0	35.214	0.027
	Integrated age ± 1σ		n=3			2.49	51.6			35.185	0.032
	Plateau ± 1σ	steps A-C	n=3	MSWD=1.30	2.49				100.0	35.208	0.031
	Isochron±2σ	no isochron	n=0	MSWD=8.21			^{40}Ar/^{36}Ar=	0.0±0.0		0.00	0.00
		KS 098, Sanidine, J=0.0019483±0.02%, IC=1.000371±0.0009714, NM-297B, Lab#=66432-25, Argus VI									
Xi	A	0.2	35.65	0.0223	87.83	0.398	22.9	27.2	1.9	34.24	0.32
i	B	0.2	10.54	0.0135	2.027	0.911	37.7	94.3	6.3	35.100	0.050
i	C	3.0	11.10	0.0090	3.960	19.6	57.0	89.5	100.0	35.051	0.010
	Integrated age ± 1σ		n=3			20.9	54.2			35.037	0.014
	Plateau ± 1σ	steps B-C	n=2	MSWD=0.92	20.472				98.1	35.05	0.012
	Isochron±2σ	no isochron	n=0	MSWD=8.21			^{40}Ar/^{36}Ar=	0.0±0.0		0.000	0.000
		KS 098, Sanidine, J=0.0019483±0.02%, IC=1.000371±0.0009714, NM-297B, Lab#=66432-26, Argus VI									
i	A	0.2	29.63	0.0489	66.71	0.655	10.4	33.5	8.0	35.04	0.22
i	B	0.2	10.58	0.0093	1.917	0.440	54.7	94.7	13.4	35.355	0.088
i	C	3.0	11.56	0.0085	5.323	7.09	60.3	86.4	100.0	35.249	0.019
	Integrated age ± 1σ		n=3			8.19	43.5			35.238	0.026
	Plateau ± 1σ	steps A-C	n=3	MSWD=1.16	8.19				100.0	35.252	0.021
	Isochron±2σ	no isochron	n=0	MSWD=8.21			^{40}Ar/^{36}Ar=	0.0±0.0		0.000	0.000
		KS 098, Sanidine, J=0.0019483±0.02%, IC=1.000371±0.0009714, NM-297B, Lab#=66432-27, Argus VI									
Xi	A	0.2	33.00	0.0259	77.09	0.145	19.7	31.0	3.3	36.08	0.51
i	B	0.2	10.38	0.0116	1.103	0.306	44.2	96.9	10.2	35.48	0.12
i	C	3.0	10.80	0.0089	2.792	3.98	57.2	92.4	100.0	35.195	0.020
	Integrated age ± 1σ		n=3			4.43	52.9			35.243	0.027
	Plateau ± 1σ	steps B-C	n=2	MSWD=5.76	4.282				96.7	35.20	0.048
	Isochron±2σ	no isochron	n=0	MSWD=8.21			^{40}Ar/^{36}Ar=	0.0±0.0		0.000	0.000
		KS 098, Sanidine, J=0.0019483±0.02%, IC=1.000371±0.0009714, NM-297B, Lab#=66432-28, Argus VI									
i	A	0.2	18.98	0.0151	30.38	0.084	33.8	52.7	2.7	35.33	0.53

Table C2. ^{40}Ar/^{39}Ar analytical data, single crystal step heating results.

	ID	Power (Watts)	^{40}Ar/^{39}Ar	^{37}Ar/^{39}Ar	^{36}Ar/^{39}Ar (x 10^{-3})	^{39}Ar$_K$ (x 10^{-15} mol)	K/Ca	^{40}Ar* (%)	^{39}Ar (%)	Age (Ma)	±1σ (Ma)
i	B	0.2	10.42	0.0036	1.218	0.242	142.7	96.5	10.7	35.49	0.14
i	C	3.0	11.23	0.0077	4.059	2.73	66.1	89.3	100.0	35.418	0.028
		Integrated age ± 1σ		n=3		3.06	67.2			35.422	0.032
	Plateau ± 1σ	steps A-C		n=3	MSWD=0.14	3.06			100.0	35.420	0.028
	Isochron±2σ	no isochron		n=0	MSWD=8.21		^{40}Ar/^{36}Ar=	0.0±0.0		0.000	0.000

KS 098, Sanidine, J=0.0019483±0.02%, IC=1.000371±0.0009714, NM-297B, Lab#=66432-29, Argus VI

	ID	Power (Watts)	^{40}Ar/^{39}Ar	^{37}Ar/^{39}Ar	^{36}Ar/^{39}Ar (x 10^{-3})	^{39}Ar$_K$ (x 10^{-15} mol)	K/Ca	^{40}Ar* (%)	^{39}Ar (%)	Age (Ma)	±1σ (Ma)
i	A	0.2	34.02	0.0311	81.13	0.108	16.4	29.5	3.1	35.46	0.61
i	B	0.2	10.64	0.0195	2.203	0.182	26.2	93.9	8.4	35.27	0.19
i	C	3.0	10.64	0.0096	1.937	3.19	53.0	94.6	100.0	35.529	0.018
		Integrated age ± 1σ		n=3		3.48	47.2			35.513	0.028
	Plateau ± 1σ	steps A-C		n=3	MSWD=0.97	3.48			100.0	35.526	0.020
	Isochron±2σ	no isochron		n=0	MSWD=8.21		^{40}Ar/^{36}Ar=	0.0±0.0		0.000	0.000

KS 098, Sanidine, J=0.0019483±0.02%, IC=1.000371±0.0009714, NM-297B, Lab#=66432-30, Argus VI

	ID	Power (Watts)	^{40}Ar/^{39}Ar	^{37}Ar/^{39}Ar	^{36}Ar/^{39}Ar (x 10^{-3})	^{39}Ar$_K$ (x 10^{-15} mol)	K/Ca	^{40}Ar* (%)	^{39}Ar (%)	Age (Ma)	±1σ (Ma)
Xi	A	0.2	127.4	0.0280	403.6	0.114	18.2	6.4	3.1	28.6	1.3
i	B	0.2	14.77	0.0235	16.54	0.164	21.7	66.9	7.7	34.90	0.28
i	C	3.0	14.08	0.0074	14.43	3.35	68.8	69.7	100.0	34.663	0.043
		Integrated age ± 1σ		n=3		3.63	58.1			34.485	0.058
	Plateau ± 1σ	steps B-C		n=2	MSWD=0.71	3.513			96.9	34.67	0.043
	Isochron±2σ	no isochron		n=0	MSWD=8.21		^{40}Ar/^{36}Ar=	0.0±0.0		0.000	0.000

KS 110, Orthoclase, J=0.0019503±0.02%, IC=0.9975058±0.0007907, NM-297B, Lab#=66435-01, Argus VI

	ID	Power (Watts)	^{40}Ar/^{39}Ar	^{37}Ar/^{39}Ar	^{36}Ar/^{39}Ar (x 10^{-3})	^{39}Ar$_K$ (x 10^{-15} mol)	K/Ca	^{40}Ar* (%)	^{39}Ar (%)	Age (Ma)	±1σ (Ma)
i	A	0.4	17.76	0.1223	26.79	0.942	4.2	55.5	23.3	34.81	0.12
i	B	0.5	18.02	0.1303	27.47	1.40	3.9	55.0	57.7	35.015	0.086
i	C	0.6	17.59	0.1093	26.45	1.71	4.7	55.6	100.0	34.561	0.086
		Integrated age ± 1σ		n=3		4.05	4.3			34.774	0.055
	Plateau ± 1σ	steps A-C		n=3	MSWD=6.93	4.052			100.0	34.79	0.144
	Isochron±2σ	no isochron		n=0	MSWD=8.21		^{40}Ar/^{36}Ar=	0.0±0.0		0.0	0.0

KS 110, Orthoclase, J=0.0019503±0.02%, IC=0.9975058±0.0007907, NM-297B, Lab#=66435-02, Argus VI

	ID	Power (Watts)	^{40}Ar/^{39}Ar	^{37}Ar/^{39}Ar	^{36}Ar/^{39}Ar (x 10^{-3})	^{39}Ar$_K$ (x 10^{-15} mol)	K/Ca	^{40}Ar* (%)	^{39}Ar (%)	Age (Ma)	±1σ (Ma)
Xi	D	0.4	10.62	0.0161	1.859	0.297	31.7	94.8	0.9	35.59	0.21
Xi	E	0.5	10.57	0.0212	1.686	1.30	24.0	95.3	4.7	35.581	0.070
Xi	F	0.6	11.06	0.0204	1.561	12.6	25.0	95.8	41.7	37.433	0.018
	G	0.7	10.82	0.0190	1.688	6.31	26.8	95.4	60.2	36.456	0.027
	H	0.7	10.57	0.0198	0.9891	3.83	25.7	97.2	71.5	36.304	0.031
	I	0.8	10.57	0.0198	0.9941	5.36	25.8	97.2	87.2	36.299	0.027
	J	0.8	10.63	0.0194	1.363	2.31	26.2	96.2	93.9	36.126	0.046
	K	0.9	10.54	0.0197	1.002	2.06	25.9	97.2	100.0	36.183	0.048
		Integrated age ± 1σ		n=8		34.1	25.7			36.697	0.014
	Plateau ± 1σ	steps G-K		n=5	MSWD=13.26	19.862			58.3	36.32	0.053
	Isochron±2σ	steps G-K		n=5	MSWD=8.21		^{40}Ar/^{36}Ar=	365.8±15.4		36.02	0.07

Table C2. ^{40}Ar/^{39}Ar analytical data, single crystal step heating results.

ID	Power	^{40}Ar/^{39}Ar	^{37}Ar/^{39}Ar	^{36}Ar/^{39}Ar	^{39}Ar$_K$	K/Ca	^{40}Ar*	^{39}Ar	Age	±1σ
	(Watts)			(x 10^{-3})	(x 10^{-15} mol)		(%)	(%)	(Ma)	(Ma)

Notes:

Isotopic ratios corrected for blank, radioactive decay, and mass discrimination, not corrected for interfering reactions.

Errors quoted for individual analyses include analytical error only, without interfering reaction or J uncertainties.

Integrated age calculated by summing isotopic measurements of all steps.

Integrated age error calculated by quadratically combining errors of isotopic measurements of all steps.

Plateau age is inverse-variance-weighted mean of selected steps.

Plateau age error is inverse-variance-weighted mean error (Taylor, 1982) times root MSWD where MSWD>1.

Plateau error is weighted error of Taylor (1982).

Decay constants and isotopic abundances after Steiger and Jäger (1977).

\# symbol preceding sample ID denotes analyses excluded from plateau age calculations.

Ages calculated relative to FC-2 Fish Canyon Tuff sanidine interlaboratory standard at 28.201 Ma

Decay Constant (LambdaK (total)) = 5.463e-10/a

Correction factors:

$(^{39}$Ar/^{37}Ar)$_{Ca}$ = 0.0007593 ± 0.000008

$(^{36}$Ar/^{37}Ar)$_{Ca}$ = 0.0002772 ± 0.0000010

$(^{38}$Ar/^{39}Ar)$_K$ = 0.01271

$(^{40}$Ar/^{39}Ar)$_K$ = 0.007204 ± 0.00046

Table C3. ^{40}Ar/^{39}Ar analytical data, total fusion results.

	ID	Power	^{40}Ar/^{39}Ar	^{37}Ar/^{39}Ar	^{36}Ar/^{39}Ar	^{39}Ar$_K$	K/Ca	^{40}Ar*	Age	±1σ
		(watts)			(x 10^{-3})	(x 10^{-15} mol)		(%)	(Ma)	(Ma)

KS 068, Plagioclase, J=0.0019478±0.02%, IC=0.9975058±0.0007907, NM-297B, Lab#=66433, Argus VI

	ID	Power	^{40}Ar/^{39}Ar	^{37}Ar/^{39}Ar	^{36}Ar/^{39}Ar	^{39}Ar$_K$	K/Ca	^{40}Ar*	Age	±1σ
	06	3	73.19	5.128	217.4	0.012	0.099	12.8	33.2	3.8
	09	3	38.14	4.965	98.66	0.014	0.10	24.6	33.3	2.8
	04	3	14.37	4.811	16.87	0.153	0.11	68.0	34.65	0.28
	02	3	17.90	4.050	28.45	0.054	0.13	54.9	34.79	0.76
	08	3	18.57	0.0658	29.28	0.032	7.8	53.4	35.0	1.1
	03	3	18.63	3.968	30.64	0.096	0.13	53.1	35.06	0.46
	05	3	13.11	4.376	12.00	0.055	0.12	75.7	35.13	0.66
	07	3	15.46	6.121	17.96	0.011	0.083	68.9	37.7	3.0
	Mean age ± 1σ		n=8		MSWD=0.33		1.1 ±5.4		34.81	0.21

KS 098, Sanidine, J=0.0019483±0.02%, IC=0.9975058±0.0007907, NM-297B, Lab#=66432, Argus VI

	ID	Power	^{40}Ar/^{39}Ar	^{37}Ar/^{39}Ar	^{36}Ar/^{39}Ar	^{39}Ar$_K$	K/Ca	^{40}Ar*	Age	±1σ
x	04	3	10.45	0.0079	4.772	29.296	64.9	86.5	31.923	0.017
x	15	3	13.59	0.0164	12.95	6.222	31.0	71.8	34.487	0.028
x	14	3	16.04	0.0134	20.83	10.057	38.2	61.6	34.894	0.036
x	02	3	13.06	0.0102	10.67	10.109	50.0	75.9	34.986	0.020
x	13	3	13.08	0.0082	10.67	5.928	62.4	75.9	35.034	0.030
x	08	3	13.26	0.0109	11.27	9.259	47.0	74.9	35.049	0.023
x	11	3	12.24	0.0101	7.741	9.976	50.3	81.3	35.144	0.019
	05	3	11.58	0.0091	5.317	5.841	55.9	86.4	35.326	0.022
	12	3	11.70	0.0087	5.711	9.600	58.8	85.6	35.355	0.017
	10	3	12.32	0.0110	7.804	3.297	46.5	81.3	35.357	0.035
	06	3	11.38	0.0096	4.585	4.233	53.0	88.1	35.391	0.023
	01	3	12.31	0.0109	7.712	10.175	46.9	81.5	35.423	0.019
	03	3	12.89	0.0089	9.596	6.182	57.2	78.0	35.473	0.026
	07	3	11.55	0.0100	5.082	8.881	51.0	87.0	35.477	0.016
	09	3	11.67	0.0138	5.438	11.933	37.1	86.2	35.505	0.015
	Mean age ± 1σ		n=8		MSWD=11.90		50.8 ±14.3		35.43	0.03

Notes:

Isotopic ratios corrected for blank, radioactive decay, and mass discrimination, not corrected for interfering reactions.

Errors quoted for individual analyses include analytical error only, without interfering reaction or J uncertainties.

Mean age is weighted mean age of Taylor (1982). Mean age error is weighted error

of the mean (Taylor, 1982), multiplied by the root of the MSWD where MSWD>1, and also

incorporates uncertainty in J factors and irradiation correction uncertainties.

Decay constants and isotopic abundances after Steiger and Jäger (1977).

symbol preceding sample ID denotes analyses excluded from mean age calculations.

Ages calculated relative to FC-2 Fish Canyon Tuff sanidine interlaboratory standard at 28.201 Ma

Decay Constant (LambdaK (total)) = 5.543e-10/a

Correction factors:

$(^{39}$Ar/^{37}Ar$)_{Ca}$ = 0.0007593 ± 0.000008

$(^{36}$Ar/^{37}Ar$)_{Ca}$ = 0.0002772 ± 0.0000010

$(^{38}$Ar/^{39}Ar$)_K$ = 0.01271

$(^{40}$Ar/^{39}Ar$)_K$ = 0.007204 ± 0.00046

Explanation

Map symbols

- Contact
- Approximate Contact
- Thrust Fault
- Normal Fault
- Quaternary Fault
- U.S. Gold Corp Drill
- Conodant Fossil Sample + Age[2]
- Radiolaria Fossil Sample + Age[2]
- U–Pb Zircon Sample + Age[1]

- Strike and Dip of Bedding
- Strike and Dip of Foliation
- Strike and Dip of Jointing
- Mines and Workings
- $^{40}Ar/^{39}Ar$ Plagioclase Sample + Age[1]
- $^{40}Ar/^{39}Ar$ Sanidine Sample + Age[1]
- $^{40}Ar/^{39}Ar$ Biotite Sample + Age[1]
- $^{40}Ar/^{39}Ar$ Hornblende Sample + Age[1]
- $^{40}Ar/^{39}Ar$ Illite Sample + Age[1]

Quaternary
- Qal — Alluvium
- Qaf — Alluvial Fan
- QToa — Older Alluvium

Tertiary
- Tda — Dacite Agglomerate
- Tdad — Dacite Dikes
- Tta — Trachyandesite Dikes
- Trp — Rhyolite Porphyry
- Twq — Walti Quartz Monzonite
- Twd — Walti Diorite
- Twp — Walti Intermediate Porphyritic Dikes
- Tgd — Gund Diorite
- Tmd — Mud Springs Diorite
- Tmp — Mud Springs Pegmatite
- Ta — Andesite of McClusky Creek
- Tad — Andesite Dikes
- Tcg — Tertiary Conglomerate
- Tvc — Aphyric Rhyolite + Volcaniclastics

Unconformity
Antler Orogeny

Basin Domain (Upper Plate)
- Devonian
- Silurian: Se — Elder Sandstone
- Ordovician: Ov — Valmy Formation; Ovq — Valmy Quartzite; Ovb — Valmy Basalts
- Cambrian: COc — Comus Formation; COcb — Comus Basalts

Slope Domain (Lower Plate)
- Dhc — Horse Canyon Unit
- Dw — Wenban Formation
- Srm — Roberts Mountains Formation
- ODul — Undifferentiated Limestone/Marble

Plate 1. Geologic Map of the Keystone Project, Cortez Trend, Eureka Co., Nevada

By
Gabriel E. Aliaga
2018

[1]Isotopic dating by Gabriel Aliaga

[2]Biostratigraphy by Tom Chapin, U.S. Gold Corp., and Pierre Zippi, Biostratigraphy.com

Mapping of igneous rocks by Gabriel Aliaga, conducted over summers 2017 and 2018

Mapping of Paleozoic rocks contributed by Tom Chapin, 2017, unpublished report for U.S. Gold Corp.

Scale 1:10,000
Datum UTM NAD27 Zone 11
Contour Interval 200 feet

Scale bars: 250, 500, 1,000, 1,500, 2,000 Meters
500, 1,000, 2,000, 3,000, 4,000 Feet